1-1-2013

The Scope of the Bis-Urea Macrocycle Assembly Motif

Michael F. Geer
University of South Carolina

THE SCOPE OF THE *BIS*-UREA MACROCYCLE ASEMBLY MOTIF

by

Michael F. Geer

Bachelor of Science
Clarion University of Pennsylvania, 2008

Submitted in Partial Fulfillment of the Requirements

For the Degree of Doctor of Philosophy in

Chemistry

College of Arts and Sciences

University of South Carolina

2013

Accepted by:

Linda S. Shimizu, Major Professor

Brian Benicewicz, Chairman, Examining Committee

Stanley Angel, Committee Member

Christopher Williams, Committee Member

Lacy Ford, Vice Provost and Dean of Graduate Studies

DEDICATION

This work is dedicated to my wife Dee and my three children, Schuyler, Devon and Alexis, without whose unwavering support this could not have been possible.

ACKNOWLEDGEMENTS

I would like to take the opportunity to thank all those who contributed and helped me in my path to this thesis. First to Dr. Linda Shimizu whose leadership and teaching helped me to become the scientist I am today. Also, whose patience and compassion proved invaluable during my growth. Also, to the Shimizu group members who proved to be great friends and peers, including Yeuwen, Sandipan, and Kinkini, who's involved debates I will miss. To Weiwei and Sahan who have proven to be good friend I wish all the luck with their futures.

I would also like to thank the University of South Carolina's Dean's Dissertation Fellowship and the NSF (CHE-1012298, CHE-0718171 and CHE-1048629 (computational center)) for their financial support.

I would like to thank my Family, my mom and dad who have been great support and inspiration to strive to be great at all I do. Finally and most importantly to my wife and children who have sacrificed a lot to allow me to follow my dream and allow me the time I needed to be successful.

ABSTRACT

From the formation of rock candy crystals, to the functionality of DNA in the cell, to the cosmic dust throughout the universe, supramolecular chemistry has a great impact and importance in the world around us. In this thesis, we explore the supramolecular interactions and self-assembly of *bis*-urea macrocyclic systems and investigate how their structure and assembly influences bulk properties and functionality. Specifically, in chapter one, we review the factors that guide, limit, and define supramolecular structures from the atomic to the centimeter scale.

In chapter two, we investigate the incorporation of benzophenone, a well known triplet sensitizer, within a *bis*-urea macrocycle and its effects on the photophysical properties. *Bis*-urea macrocycles consist of two urea groups and two C-shaped spacers. We observe upon self-assembly that the benzophenone *bis*-urea macrocycle generates a host with an unusually stable radical, which was detected by Electron Paramagnetic Resonance spectroscopy (EPR). The host crystals are porous structures that are able to absorb guests including alkenes and aromatics in the interior channel. UV-irradiation of the benzophenone macrocycle in oxygenated solvents resulted in the generation of singlet oxygen. Solid complexes of the host and 2-methyl-2-butene or cumene facilitated selective oxidation of the guest in good conversion when irradiated under an oxygen atmosphere.

In chapter three, we investigate the synthesis and assembly of macrocyclic systems that employ expanded aryl spacers. Incorporation of 2,7-dimethyl naphthalene resulted in a macrocycle that had a unique "bowl shaped monomer with an unusual parallel urea conformation that disrupted the typical urea self-assembly. The incorporation of 1,3-dimethyl and 4-bromo-1,3-dimethyl naphthalene spacers showed the formation of macrocycles that display favorable conformations for the assembly into columnar structures. The bromo analog shows a propensity for halogen bonding interactions.

Finally, in chapter four, we explore the co-crystallization of a pyridyl *bis*-urea macrocycle with halogenated compounds in order to examine the ability of this macrocycle to act as a Lewis base in the formation of halogen bonds. The macrocycle was co-crystallized with a series of halogen bond donors. X-ray quality crystals were obtained by slow evaporation of the host with iodopentafluoro benzene and diiodotetrafluoro ethane from methylene chloride solutions. The crystal structures of these complexes show very strong halogen bonds with R-X•••B distances from 2.179-2.745 Å that are of an average only 78 % of the sum of the Van der Waals radii for iodine and oxygen. These halogen bonds were also analyzed through DFT calculations, and we estimate the association energies to be 7.381 kcal mol^{-1} for iodopentafluoro benzene and 10.331 kcal mol^{-1} for diodotetrafluoro ethane. These results suggest that the pyridyl hosts will be a strong organizing motif for co-crystallizing electrophilic halides. In the future, we plan to explore the application of this motif for organizing molecules with important optical and electronic properties.

TABLE OF CONTENTS

LIST OF TABLES

LIST OF FIGURES

LIST OF SCHEMES

I. SUPRAMOLECULAR CHEMISTRY: ASSEMBLY AND SELF-ORGANIZATION.

1.1 Abstract

From the child making rock candy with his parents to the physicist studying the cosmic dust in deep space, the process of self-assembly organizes smaller building blocks into larger discrete structures without outside influence. In this chapter, we identify and examine some of the factors that guide, limit, and define these supramolecular structures from the atomic up to the centimeter scale with a focus on molecular building blocks. The concepts here-in provide the reader with an introduction to this fast developing field and highlight its important applications. This chapter was published as a chapter on Self-Assembly and Self-Organization in *Supramolecular Chemistry: from Molecules to Nanomaterials,* J. W. Steed and P. A. Gale (eds). John Wiley and Sons LTD, Chichester, UK, pp 167-180.

1.2 Introduction

Physicists, biologists, chemists, and material scientists have all observed the ability of small units to self-organize into larger defined entities long before this process was officially named. Self-assembly describes the formation of discrete architectures from building blocks that can range in size from atoms and molecules up to macroscopic units without help or guidance from an exterior source.[1] The formation of a more ordered ensemble from less ordered components seems counterintuitive from an entropy perspective. Yet atoms, molecules, and parts of macromolecules do self-assemble into discrete soluble architectures including folded structures, dimers, trimers, etc. These small assemblies may further associate into monolayers, films, and polymers up to macroscopic structures such as vesicles,[2] liquid crystals,[3] and crystals.[4] On the macroscale, spontaneous assembly has been humorously visualized on YouTube by a pile of Legos™ miraculously assembling into the Millennium Falcon through the magic of stop-action photography. In this case, we are fooled and the guiding source is an unseen person; however, even children can observe self-assembly in every day life as they grow rock candy crystals and watch the formation of soap bubbles.

Supramolecular structures have the potential to extend to very complex extended structures. Nature has provided inspirational examples of functional assemblies. In the tobacco mosaic virus 2130 identical protein units self-assemble around an RNA strand to form the ~ 300 nm x 18 nm rod structure (Figure 1).[5] Amazingly, this structure can be dismantled, isolated as its component parts, and reconstituted in vitro to afford the intact assembled virus.[6] Early work distinguished the terms self-assembly and self-organization by thermodynamics, with self-assembly implying a spontaneous, reversible process that

reaches equilibrium while self-organization required energy to afford a non-equilibrium state.[7,8] The tobacco mosaic virus is an example of a spontaneous self-assembling system. Most people now use these terms interchangeably, although Lehn[9] and others typically reserve self-organization for multi-stable dynamic systems and this term is most often encountered in the biological area.[10,11]

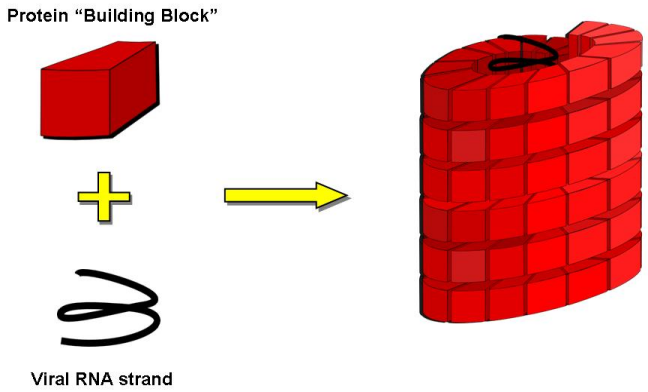

Figure 1.1. Cartoon representation of the assembly of the tobacco mosaic virus from its protein building blocks that self assemble around the strand of viral RNA.[5]

Since no outside force is required for this spontaneous assembly, the directions and driving force must be embedded in the building blocks themselves and influenced by the surrounding environment. We are still far from elucidating general rules that guide self-assembly at size scales that range eight orders of magnitude from angstroms to centimeters. The rules governing pattern formation over this huge range appear to be similar but not identical.[12,13,14] For example, the balance of the forces that guide molecules into three-dimensional crystals versus two-dimensional films may have different relative strengths and contributions at these different length scales.[15,16] Researchers often refer to three distinct size ranges that include the molecular, nanoscale,

and macroscopic. This chapter will focus primarily on identifying variables that are important to the assembly process in all ranges and will examine some simple molecular examples of self-assembly.

1.3 Key Players in Self-assembly

Our conceptualization of the self-assembly/self-organization process requires us to consider all the components of the system that could influence the formation of ordered ensembles. Here, we take a closer look at these components, which include: (1) the molecular structure and physical properties of the building blocks, (2) the strength, directionality, and reversibility of the intra and intermolecular forces or bonds, and (3) the solvent or solid interfaces in the surrounding environment.

1.3.1 Building Blocks.

The building blocks used by chemists, which are also referred to as construction units or tectons,[17] are typically molecules. The size, shape, functional groups, and physical properties (solubility, mp, etc) of these building blocks must be considered. Obviously the size and shape of these building blocks has a marked effect on how they may assemble into more ordered structures. Shape complementarity is an important design consideration in self-assembling systems. Figure 2 shows the schematic self-assembly of identical molecular building blocks that are wedges, L-shapes, or disks to give cyclic hexamers, blocks, or columnar structures. Although seemingly simple, there are many examples of these assembly patterns that give rise to functional systems for practical applications. In slightly more complex systems two different building blocks

could assemble. For example, melamine and barbituric acid derivatives form cyclic hexamers that are also called rosettes.[18]

Complexity builds quickly. A combination of organic and inorganic building blocks can be used to construct two and three dimensional networks that yield interpenetrated or porous coordination polymers or metal organic frameworks (MOFs).[19,20,] Small geometric changes in the relative size and shape of the building block are amplified in the assembly process and ultimately control the size and shape of the final complex pattern that emerges.[21,22,23,24] Block copolymers[25,26,27,28] and dendrimers[29,30] also self-assemble into micelles, lamellar sheets, and microtubules. Alternatively, these interactions may drive intramolecular associations and cause the macromolecule, polymer, or peptide to fold into a more ordered complex structure, which usually endows function.

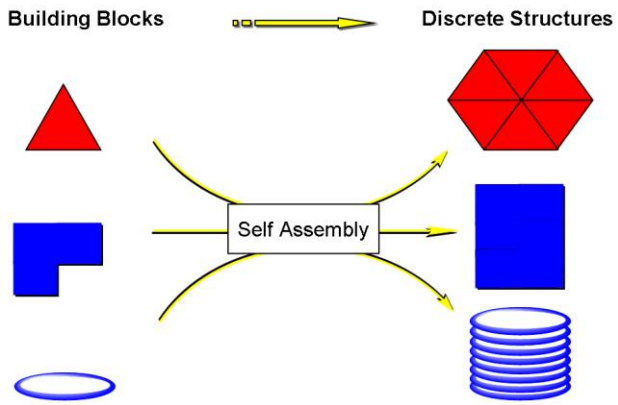

Figure 1.2. Schematic assembly of building blocks with various shapes to form discrete supramolecular structures.

Other molecular attributes also influence this organization including the type and position of functional groups within these molecular building blocks. These functional groups (carboxylates, carboxylic acids, amides, amines, ammonium salts, halogens, etc.)

may form strong directional interactions that are discussed in the next section. Thus, their location, geometry, and orientation within the assembly unit have a major impact on the inter- and intramolecular contacts that are both possible and accessible. The physical properties of these building blocks are also important as these molecules need to interact with themselves and with other building blocks during the assembly process. For example, melting points and solubility help govern their ability to mix freely in a melt or solution. Mobility is also a requirement for assembly. A physical chemist or material scientist might discuss this in terms of mass transport and mixing.[31]

1.3.2 Intra and Intermolecular Forces: Strength and Directionality

Inter- and intra-molecular interactions have been used to guide self-assembly. There are three key issues to consider in the use of a specific covalent or non-covalent interaction for supramolecular assembly: (1) strength; (2) reversibility; and (3) directionality. Non-covalent forces range in strength from weak interactions (0-40 kcal mol^{-1}) that include van der Waals,[32] hydrophobic interactions,[33] close packing,[34] hydrogen bonding,[35,36,37,38] halogen bonding,[39,40] aryl stacking,[41,42] dipole-dipole,[43] ion-dipole, and donor-acceptor interactions up to strong ion-ion interactions[44,45] and dative bonds that are similar in strength to covalent bonds (60-190 kcal mol^{-1}). The strengths of these interactions span a considerable range, and many can be context dependent. Individual hydrogen bonds, for example, are stronger in the gas phase or in non-polar solvents, ranging from 5-40 $kcal^{-1}$; however, in solvents that compete for hydrogen bonds such as water, they are very weak ~ 0 kcal mol^{-1}.[35] In systems with multiple hydrogen bond donors and acceptors, the number, positioning, and separation distance can

modulate the strengths of these interactions over several orders of magnitude.[46,47,48] A quadruple hydrogen bond array in 2-ureido-4-pyrimidone derivatives from Sijbesma et. al. displays association constants of K_{dim} – 6 x 10^7 L mol^{-1} in $CHCl_3$.[49] The energetics, geometric features, and relative contributions of some of these interactions is still under debate. For example the origins, strengths, and geometries of aryl stacking interactions are still a very active area of fundamental research.[50,51,52] For a complete discussion of these interactions see smc015 on supramolecular interactions.

The strength of these interactions covers a huge range from very weak, as compared to thermal energies, to intermediate strength but reversible dative interactions to a special set of strong covalent bonds. These interactions can be used alone or in concert to afford assemblies. In general, a stronger the association constant is usually indicative of a less reversible process. Like a contractor building a house, one would assume that the stronger mortar would afford a more stable assembled structure; however, since the molecular structure builds itself, it must be allowed to equilibrate and find the thermodynamic minimum. Figure 3 compares a reversible process with an irreversible one. In a reversible process, the molecules associate and dissociate in a dynamic equilibrium. This reversibility allows the individual building blocks to adjust their position and orientation and to eventually find the thermodynamic ordered structure. The dynamic nature of these systems allows for 'error checking', which is a controlled disassembly of thermodynamically unstable structures that endows the process with inherent self-correction. Potentially the assembly/disassembly equilibrium allows for these structures to respond to their environment.[53] For example, a dynamic and reversible metallosupramolecular assembly could be post-modified by addition of a new ligand or a

template.[54,55] In the case of an irreversible interaction, such as the formation of a C-C bond or an irreversible dative bond, the individual components cannot adjust or reorganize their structures to form the most stable lattices (Figure 3). Strong but poorly labile metal-ligand interactions, such as complexes of CrIII, RuII, OsII PdII, PtII often form local but not global order. The formation of these complexes is kinetically controlled and often results in non-crystalline solids and glasses. It is conceivable that an irreversible interaction can drive the kinetic self-assembly to afford discrete structures. Like a cascade reaction, all bonds must form correctly as there is no way to correct a mistake.

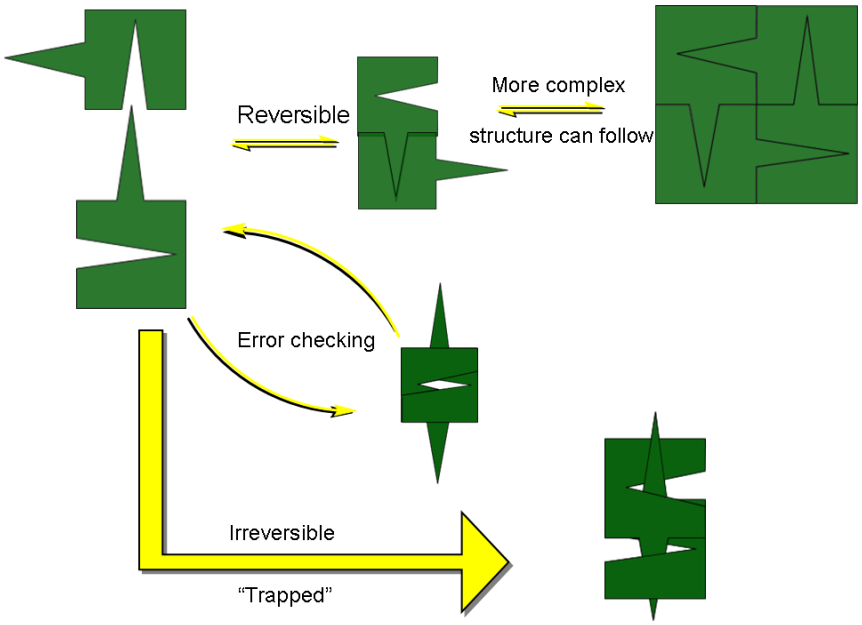

Figure 1.3. Comparison of reversible and irreversible steps and their effects on the supramolecular assembly.

In comparison to abundant examples of non-covalent supramolecular assemblies,[56,57,58,59] relatively few structures have been built with strong covalent bonds. This is due to the fact that normal covalent bonds are not easily broken and reformed.

One can manipulate the temperature and conditions so that the formation of stable imines,[60,61] esters,[62,63,64,65] disulfides,[66] hydrazones,[67] and boronate esters[68] is reversible. Some examples of these covalent self-assembled systems include disulfide hosts[69,70] and covalent organic frameworks.[71,72,73,74,75] Chapter smc011 delves deeper into the reversible covalent bond toolbox. The equilibration of these strong covalent bonds, often referred to as dynamic covalent chemistry,[76] is kinetically slower in comparison to weaker non-covalent interactions and often requires a catalyst. An extreme example might also include the formation of carbon nanotubes and fullerenes. While not spontaneous at room temperature, carbon vapor at high temperature does 'assemble' to form these intricate and beautiful structures.

In addition to the strength of these individual interactions, one must also consider their directionality. Like a covalent single bond, in which the shared electrons are localized between the two atoms, some of the non-covalent interactions are directional in nature including dative bonds, hydrogen bonding, halogen bonding, ion-dipole, donor-acceptor, and ion-ion interactions. In the design step, directional interactions are important for programming a building block to adopt a specific assembly. Section 3 will highlight a number of examples of designed building blocks that assemble into discrete structures using directional interactions. However, many individual forces and effects contribute to the stability of the final complex assembly. Challenges remain in identifying each of these forces and weighing their individual contributions for assembly at atomic to macroscale sizes.

1.3.3 Surrounding Environment

In solution, the process of spontaneous self-assembly is thought to follow a thermodynamic model where the building blocks form an aggregate in solution that gives rise to initial intermolecular interactions (nucleation) followed by growth.[77] The nucleation step is typically thermodynamically unfavorable and an entropy deficit must be overcome. In a cooperative process, the formation of many small favorable associations during the growth phase work to overcome this initial deficit. Molecular motion is a requirement for these nucleation and growth processes. With the advent of neutron scattering and X-ray crystallography, people can now actively study the nucleation process, work that will hopefully yield new insights.[78,79] Typically, the assembly is carried out in a solution or in a melt to aid molecular motion. Thus, we need at the very least to consider the solvent in this process and often a solid interface as well. The solvent can have interactions with the building blocks and can help or hinder the assembly process.

Solid interfaces can also aid or hinder assembly. Indeed, the very process of nucleation and growth on a surface may be different due to thermodynamics of adsorption, surface diffusion, and chemical binding that may occur before or at the same time as growth processes.[80,81,82] These environmental effects give rise to a range of new interactions to consider: solvent/solvent, solvent/solute, solid/solvent, and solid/solute. Perhaps these are the underlying cause for the subtle differences between assembly on the molecular, nanoscale, and macroscopic size scales.[15,16] A nice example of the solid interface influencing assembly is the differential growth of crystals in the presence of insoluble polymers.[83,84] It could be argued that this is no longer a case of spontaneous

self-assembly as Matzger et. al. propose that the solid polymer aids in nucleation and may selectively stabilize one polymorphic form of a pharmaceutical over another form. However, this intriguing method for discovering polymorphs highlights the difficulty in determining the role of the environment in guiding 'spontaneous' self-assembly. Such processes are often referred to as assisted or directed self-assembly. In biology, molecular chaperones can assist the folding of a protein. In chemistry, there are many examples of such template-assisted assembly[85,86,87,88,89] used to facilitate covalent bond formation. One such example is in the synthesis of threaded and interlocked linked compounds[90,91,92] such as the synthesis of a rotaxane (Figure 4) through the clipping method. Self-assembly brings the open ring around the 'bar', which can then be subsequently closed to complete the synthesis of the rotaxane.

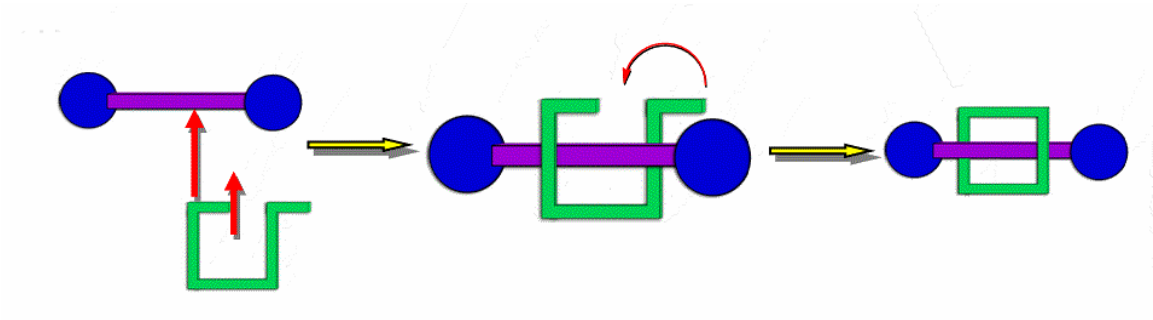

Figure 1.4. Schematic synthesis of rotaxanes through the clipping method.

The dynamic nature of these structures can complicate their characterization as the act of sample preparation for different analytical techniques can promote disassembly. For example, diluting a sample with a solvent might induce an equilibration of the material to afford an on average smaller assembly. In the case of supramolecular polymers, dilution would be expected to lower the degree of polymerization.[93] Section 2 in this volume will focus on the different techniques that have been used to probe these self-assembled structures.

1.4. Assembly in Solution to Yield Discrete Structures.

Self-assembly is used to organize molecules into amazing and complex structures. Small molecular weight molecules can be assembled into structures of varying degrees from dimers and trimers all the way up to and including supramolecular polymers.[1] Simple amphiphiles form micelles and vesicles.[94] Dendrimers, DNA based materials, peptides, and peptides amphiphiles have been assembled into nanostructured fibrals reminiscent of the extracellular matrix.[95,96,97,98] Obviously, we cannot cover here even a fraction of the creative and functional assembled systems reported. In this section, we will highlight selected symmetrical self-assembled systems to illustrate how different intermolecular interactions can be used cooperatively to afford discrete structures that are of interest for molecular recognition, as nanoreactors, for sensing, and in light harvesting applications. A minimalist would consider the association of two identical molecules together to form dimeric structures or capsules as a good model of self-assembly. While conceptually simple, a large number of aesthetically pleasing and functional structures have been synthesized that form dimers.

1.4.1 Dimeric Structures and Capsules.

An early example from the Cram group takes advantage of dipole-dipole, van der Waal's, and solvophobic interactions to drive assembly of two identical units into dimers.[99] These velcraplexes are cyclic aryl systems that incorporate quinoxoline "flaps" in an equatorial position to the aryl ring reminiscent of an octopus with four legs setting on the ocean floor (Figure 5a). The dimers are formed from the "stacking" of the faces (the bottom side of the analogous octopus) of two of the monomers so that the axial

facing methyl groups on the inner aryl cycle set toward the face of the opposing aryl rings that are equatorial directed of the second monomer. These dimers are held together by CH-pi stacking, and the quinoline groups are offset from one another in a typical aryl-aryl offset stack. The -ΔG values for the formation of these dimers was shown to vary greatly from <1 to >9 kcal mol^{-1}. Polar solvents also helped to facilitate the formation of these dimers.[100]

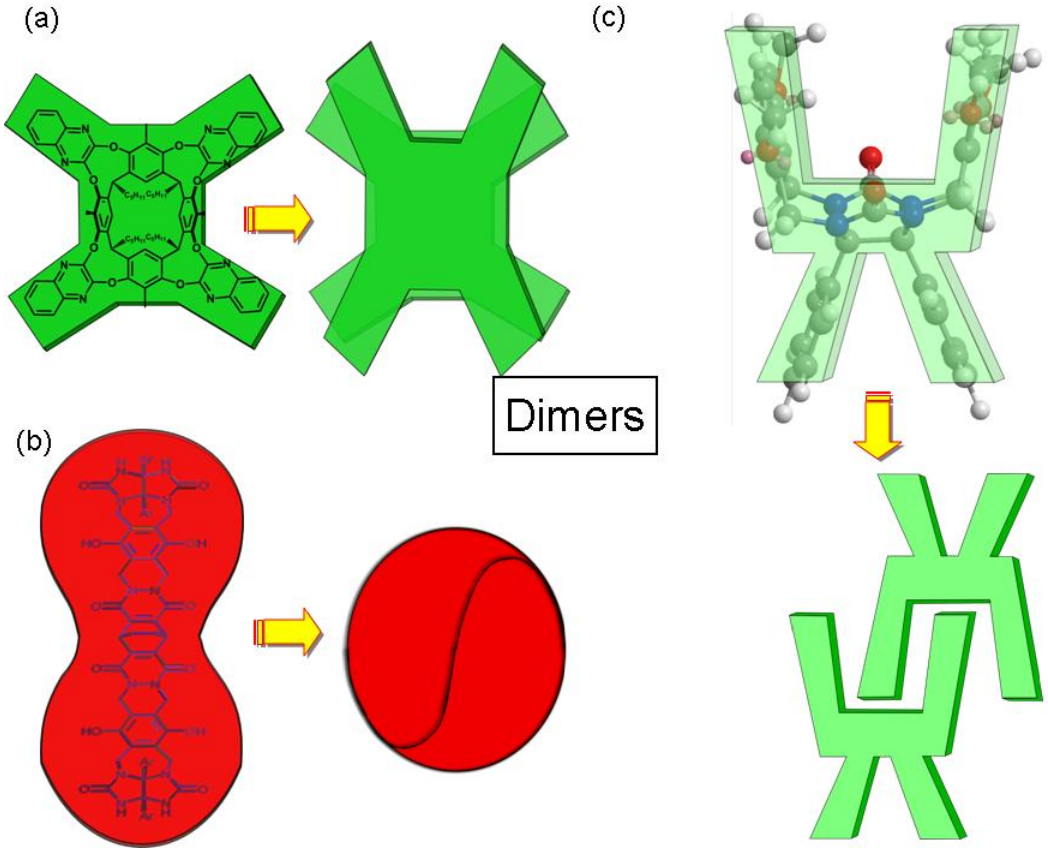

Figure 1.5. Examples of self-complementary molecules that yield dimeric assemblies: (a) Cartoon representation of velcrand dimers that assemble through CH-pi, aryl-aryl stacking, and entropic effects;[99-100](b) Rebek's "softball" dimers assembled through H-bonding;[103-6] (c) Nolte's molecular clips assemble into dimers through aryl-stacking and entropic effects[107].

Examples of self-assembled dimers stabilized by hydrogen bonds are the 'baseballs', 'tennis balls', and 'softballs' from the Rebek group. These are formed from

self-complementary curved pieces that are comprised of two glycouril units separated by different spacers such as durene,[101] quinone,[102] and triphenelene.[103,104,105,106] Figure 5b illustrates the assembly of two long curved polycyclic units into large "softballs", which are knit together with eight pairs of hydrogen bonds. These systems have a wide range of internal volumes, from 60 $Å^3$ to 300 $Å^3$,[103-6] and have been shown to exchange their guest molecules through an entropic process. The exchange of solvent guests for larger molecules like adamantanes and ferrocene displays stabilizing effects of approximately 1-3 kcal mol^{-1}.[104,105]

Symmetric molecular clips from the Nolte group rely on size and shape complementarity and aryl-aryl stacking interactions. These C-shaped clips are formed from a *bis*-imidazolidine core decorated with four aryl groups.[107] This molecule forms a C-shaped clip that dimerizes in solution by interlocking the aryl groups (Figure 5c) through aryl-aryl stacking, and what the Nolte group calls "cavity filling effects". Typically, these aryl-aryl interactions are considered to be less directional. Yet clips with long alkane tails form well ordered lamellar thin films and may have use in liquid crystalline applications.[108]

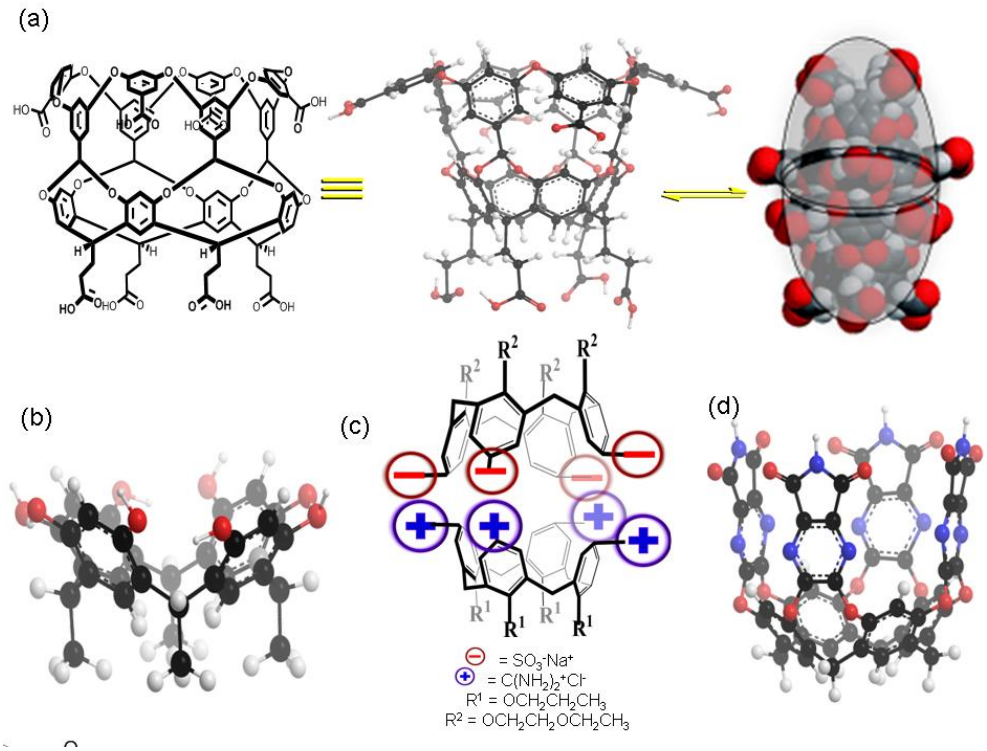

Figure 1.6. Examples of self-assembled capsules: (a) Gibbs water-soluble cavitands forms a capsule in the presence of hydrophobic molecules;[126-7] (b) Atwood cavitand that forms a hexameric cavitand with a volume of ~1400 Å^3;[133] (c) Cavitands from the Reinhoudt group employ ionic interactions. [136](d) Rebek's cavitands take advantage of H bonds for self assembly.[137-8]

Egg-shaped or spherical capsules can be formed by the assembly of two halves or hemispheres. Like their covalent carcerand and hemicarcerand counterparts,[109] self-assembled capsules are of interest for drug delivery and as containers for stabilizing reactive intermediates and for inducing selectivity in reactions. Capsules have been assembled from dynamic covalent bonds,[110,111,112,113,114] and non-covalent interactions that include hydrogen bonds,[115,116,117,118,119] coordination chemistry,[120,121,122,123] ionic interactions,[124,125] and solvophobic interactions. The Gibb group provides an example that relies on solvophobic interactions. They synthesized cavitands based on resorcinarenes that were composed of twelve aryl systems that are functionalized with eight carboxylic

acids. The octa-acid groups enhanced the solubility of these cavitand hosts in basic aqueous solution, where they were monomeric and unassembled (Figure 6a).[126-7] Upon addition of a guest that was small and non-polar, two of the octa-acid hemispheres dimerized forming a capsule. Using isothermal titration calorimetery Sun, Gibb, and Gibb found that the driving force for this complexation[127] was the expulsion of a hydrophobic guest molecule from aqueous solution (solvophobic) as it was taken up in the cavity of the capsule and shielded from water.[127] The guest therefore played an integral role in the assembly process, and perhaps these are better viewed as trimeric or larger assemblies depending on the number of guests. Most interesting was the ability of these capsules to open and close, thereby allowing exchange of guests or enabling the expulsion of products upon completion of a reaction. Gibbs and Ramamurthy demonstrated the utility of these assembled systems as reaction vessels for selective oxidation,[128] photochemistry,[129,130,131] and hydrocarbon separation.[132]

Other examples of capsules include the spherical molecular assemblies from Atwood's group.[133] The spontaneous self-assembly of 6 identical calix[4]resorcinarenes (Figure 6b) and eight water molecules gave a snub cube with an internal volume of ~1375 $Å^3$.[134,135] A complex from the Reinhoudt group was formed from the 1:1 assembly of oppositely charged calix[4]arene building blocks in a polar mixture of $MeOH/H_2O$ (Figure 6c).[136] This entropy driven assembly displayed association constants in the range of 10^6 M^{-1}. The elongated capsules from Rebek and co-workers were assembled from derivations of calix[4]resorcinarene (Figure 6d) and use H-bond donors and acceptors to form cylindrical capsules with cavities ~600 $Å^3$. These capsules could accommodate molecules of up to 22 Å in length.[137, 138] The study of the assembly of relatively small

organic capsules is advantageous as it allows one to follow the assembly/disassembly process and in the cases where guests are encapsulated, enables one to probe the effects of this confinement on the physical properties and chemical reactivity of the guests.

1.4.2 Trimers and Larger Functional Assemblies.

Because of their strength, directionality, and selectivity, metal-ligand interactions are valuable for assembling large functional structures.[139,140] One example is Wasielewski's trimers formed from three chlorophyll derivatives connected by a phenyl triethynelene in a trefoil-like structure (Figure 7a).[141] Two porphyrins from separate trefoils assemble through dative bonds from zinc within the chlorophyll pieces to diazo bicyclooctane ligands that connect to neighboring trimers. The dative bond directs the porphyrins to stack one on top of another creating a pseudo-hexagonal shaped center cavity. This assembly is being studied for light harvesting capabilities and exhibits interesting dual singlet-singlet annihilation energy transfer processes that suggest two separate time scale energy transfers within the molecule.[142]

Self-assembled coordination cages are a fascinating and active research area with much promise for delivering active and functional materials.[143,144] Stang's group has capitalized on the directionality and the selective interaction of carboxylates with platinum to assembled neutral complexes.[145] The size and shape of the resulting structures are dependent on the geometries and bend angle of the platinum pieces. For example 3,6-*bis*-platinum phenanthrene takes on a 90^{o} geometry that restricts the options for the diacid ligand and results in a tetragonal structure (Figure 7b). Alternately the 4,4'-*bis*-platinum benzophenone has a geometry of 120^{o} that opens the angles between the

diacids and results in a hexagonal structure (Figure 7c). Several excellent reviews highlight the utility of these materials.[146]

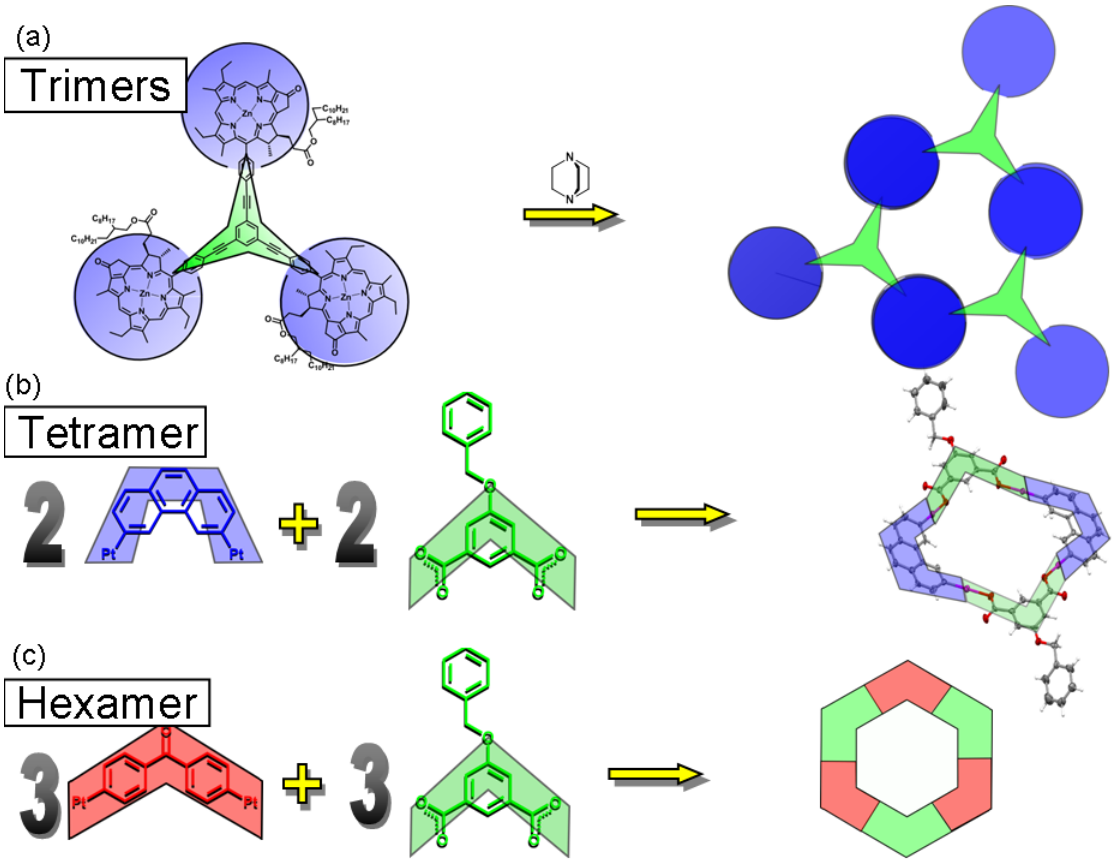

Figure 1.7. Examples of dative directed assemblies: (a) Wasielewski porphyrin trefoil that uses diazo-bicyclic octane to form a trimer with a hexagonal center cavity;[141] (b) Stang's tetrameric structures are formed by the assembly of two *bis*-platinum phenanthrenes and 2 disodium carboxylates;[145] (c) Three *bis*-platinum benzophenone units and three disodium carboxylates organize to form hexagonal structures.[146]

A water soluble coordination cage was assembled via a tridentate tripyridyl-triazine ligand, and Pd salts.[147] The Fujita group's octahedral tetramer was formed from four triazines and six palladium atoms to form an octahedral tetramer with triazine "panels", which occupied opposite faces of the octahedron and created a hydrophobic cavity (Figure 5a). This cage has been used to accelerate room temperature Diels-Alder reactions and the reactive substrates appeared to be preorganized within the pocket,

which resulted in high stereoselectivity.[148] More recently, Sun et. al. has demonstrated the self-assembly of 24 metals and 48 ligands into amazingly large $M_{24}L_{48}$ coordination spheres.[149]

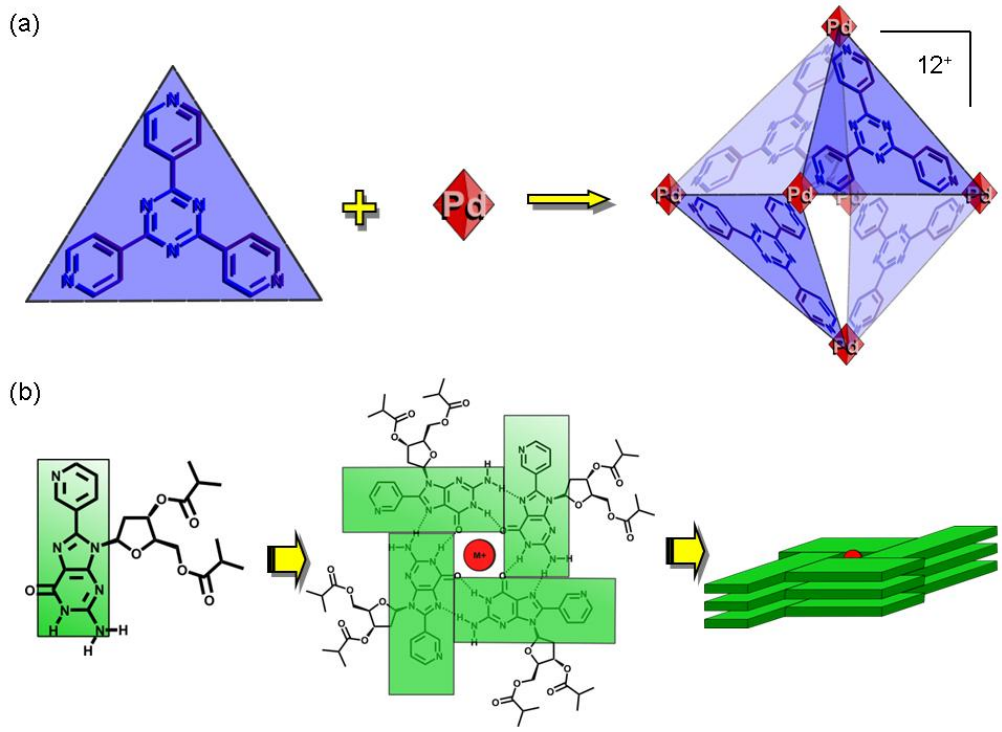

Figure 1.8. Coordination driven assembly to discrete structures: (a) Fujita group's assembly with four tridentate ligands and six palladium atoms forms a tetrameric cage[147]; (b) Guanine derivatives assemble into planar tetramers that can use a metal coordinate to stack into more complex structures.[156]

Hydrogen bonded guanosine tetramers (G-quartets) have a rich biological and materials chemistry.[150,151,152] Upon first inspection of guanosine derivatives, one notes the self-complementary hydrogen bond donors and acceptors and the aromatic surfaces. It is not surprising that these units self assemble into ribbons[153] and tetrameric macrocycles.[154] In the presence of metal cations two tetramers can assemble further into octomers, dodecamers, hexadecamers, and higher ordered structures known as G-quadruplexes.[155]

By tuning the exterior functional groups on the tetramer to control repulsive and attractive interactions discrete assembled systems can be stabilized. For example, the 8-aryl-2'deoxyguanosine derivative from Rivera in Figure 8b exhibits selective stabilization of a dodecamer (94%) upon titration with 0.7 equiv of KI in CD_3CN.[156] Assembled guanosine derivatives are of interest as anticancer agents,[157] gelators,[158,159] and for molecular electronics.[160]

1.4.3 Disk Shaped Building Blocks.

Natural tubular assemblies show remarkable biological functions. For example, tubular shaped channels aid the transport of materials in and out of cells. Given that simple self-assembling macrocycles and disks form assemblies reminiscent of these biological structures, it is not surprising that they have been a very active area of research.[161,162,163,164,165,166] The stacking of macrocycles ureas, such as the bis-urea in Figure 9a, quickly generates tubular shaped channels with homogeneous channels.[167] The macrocycles are relatively flat with the ureas preorganized perpendicular to the plane of the macrocycles, a conformation that aids columnar assembly. The size, shape, and interior functionality of the channels are controlled by the single macrocyclic unit used in their construction.[168] These straws shaped columns formed via the three-centered urea hydrogen bonding motif pack together to generate crystals with permanent porosity.[169] Such homogeneous porous solids can be used to facilitate selective photocycloadditions.[170, 171]

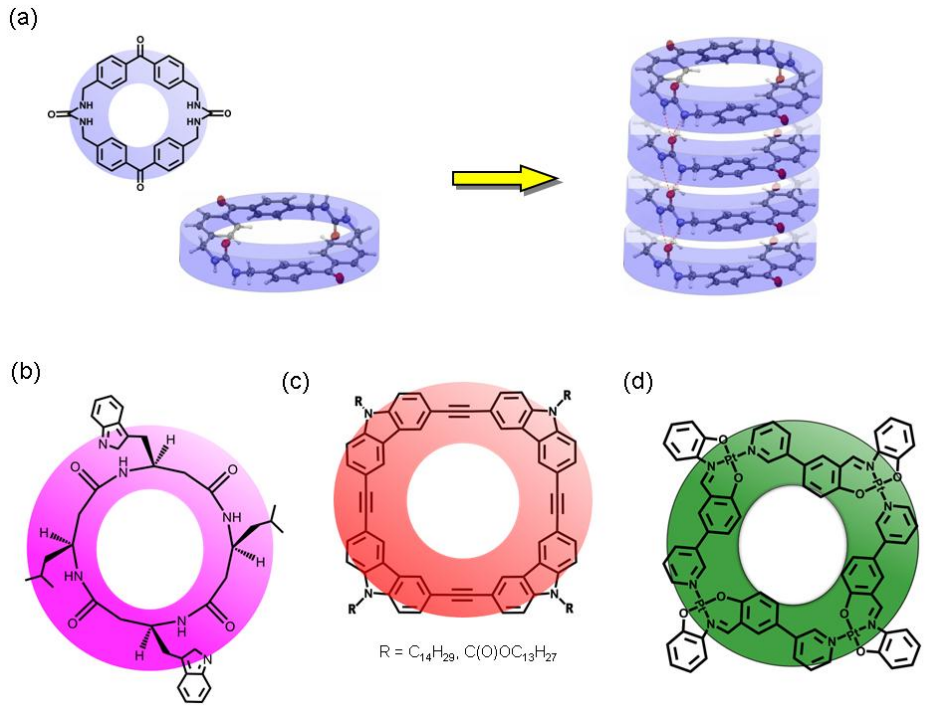

Figure 1.9. Examples of self-assembling stacking macrocycles: (a) *bis*-ureas from Shimizu et. al.;[167](b) cyclic peptides of Ghadiri et. al.;[173] (c) carbazole arylene ethynylene macrocycle (AEM) of Moore et. al.;[180] and (d) MacLachlan's Pt_4 rings.[182]

Cyclic peptides with alternating D- and L-amino acids,[172] such as the example from Ghadiri and co-workers (Figure 9b), assembled into robust columnar structures via amide hydrogen bonds.[173] The spontaneous assembly process could be triggered by controlled acidification of a basic solution of the peptides to afford needle like crystals.[174] Temperature studies in chloroform gave an estimated association constants of ~ 2500 M^{-1}.[175] Cyclic peptides have been made from a wide range of natural and unnatural amino acids. Like the bis-ureas macrocycles, cyclic peptides that can adopt flat structures with the amide oriented perpendicular to the macrocycles more readily assemble into tubular structures.[176,177] Columnar and nanotubular peptide structures show promise as functional bionanomaterials with potential applications as sensors, electronics, drug delivery, ion transport, and tissue engineering.[178, 179]

As the demand for smaller and smaller electronic devices grows, the need for one-dimensional electronically active materials also expands. The macrocyclic columnar structures such as arylene ethynylene macrocycles (AEMs) from Moore's group (Figure 9b) are potentially simple building blocks for controlled one-dimensional assembly. These systems can be cyclized in high yield through an alkyne metathesis process.[180] Casting of AEMs with linear alkyl side chains on carbon films afforded entangled nanofibrils via aryl stacking interactions and side chain interdigitation.[181] These fibrils showed polarized emission parallel to the aryl-stacking of the cycles, which indicated an intermolecular delocalization of the π clouds. The delocalization led to long range fluorescence quenching. This together with the electron donating capability of the AEM and the porous structure of the nanofibrils deposited on a surface enabled the detection of oxidative molecules (such as TNT) at the part-per-trillion scale.[186]

Frischmann et. al. synthesized a neutral macrocyclic complex (Figure 9d) with the goal of forming columnar structures through metal-metal interactions.[182] This platinum-Schiff base complex was synthesized in a one-pot reaction with salicylaldimine proligands in basic DMSO. The ligands assembled in a head-to-tail manner to yield cyclic structures. These macrocyclic systems displayed liquid crystalline phases in seven different solvents. They also showed birefringence and an uncommon aggregation in solution of concentrations even as low as 10^{-6} mol L^{-1}. Because of their aggregation properties and possible Pt-Pt interactions these structures are being probed in the possibilities of liquid crystal applications and conductive nanotubes.

1.4.4 Specificity in the Assembly Process

In nature, some assemblies form preferentially in the presence of mixtures of many other competitors. Consider for example a simple mixture with two assembly units (A and B). Each of these units has some preference to self-assemble and form homodimers (AA and BB) (Figure 10). They may also have some propensity to form heterodimers (AB) in a mixture. From a thermodynamic standpoint, selective self-assembly to afford exclusively homodimers is governed by the three equilibrium constants (K_{AA}, K_{BB} and K_{AB}), concentration, temperature, and the presence of competitors. This selectivity for a component is often referred to as self-sorting, which has been described by Lyle Isaacs as "the high-fidelity recognition of self from non-self."[183]

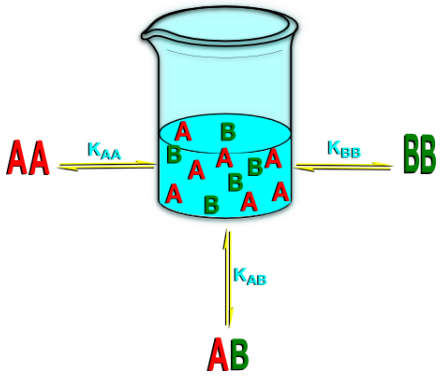

Figure 1.10. Comparison of an assembly process that could afford both heterodimers (AA and BB) and homodimers (AB).

One can imagine the homodimers continuing to grow selective and finally yield a crystal containing only As and a separate crystal containing only Bs. Perhaps an extreme example of such a self-assembly process is the formation of enantiopure crystals from a racemic solution. This spontaneous resolution of enantiomers was first observed in 1848 with Louis Pasteur's physical separation of hemihedral crystals of two types of enantiopure tartaric acid.[184] The reasons for this preference are still under debate and the

process is not yet predictable.[185] But spontaneous resolution can also afford chiral liquid crystals, monolayers and supramolecular polymers and is likely controlled by subtle non-covalent interactions including crystal packing forces and crystallization kinetics. Obviously, it would be both fascinating and extremely useful to be able to predict and control this process.

Biological systems offer a lot of inspiration for chemists and do not solely rely on high-fidelity spontaneous self-assembly. Depending on the situation, nature employs both covalent and non-covalent templates, helpers, or chaperones to mediate assembly. Cells can also physically separate the building blocks that are needed for the assembly from other competing functionality by sequestering the assembly units within organelles. For supramolecular chemists, the next challenge is to understand and rationally influence the selectivity of this process for practical applications. In some cases, high fidelity assembly of one unit in the presence of a complex mixture may be extremely important. For example, highly selective self-assembly can be of practical use in synthesis, self-replicating systems[186,187,188] and kinetic resolution.[189] Alternatively, a less selective and more promiscuous process can rapidly generate libraries of hetero and homodimers from a relatively small number of building blocks. The templated formation of a molecular host using dynamic covalent chemistry[79] relies on a sampling of many different possible self-assembled receptors before a single structure is selected by the template as an optimal thermodynamic sink.

1.5 Summary and conclusions.

Although this chapter has focused on molecular self-assembly, manipulation of

matter on the larger scale may be of greater practical and commercial importance.[190] We are challenged to combine dynamic covalent and non-covalent interactions in complex mixtures to yield functional self-assembled materials through both spontaneous and assisted assembly. Such controlled self-assembly will have practical applications over a larger range of fields from medicine to electronics. For example, organic based semiconductors have promising applications in electronic and optoelectronic devices but are not nearly as developed as their inorganic counterparts.[191] Basic issues of how structure, both molecular and supramolecular architectures, influence electronic and optical properties are still under exploration. The goal of fabricating useful commercial electronics, batteries, and light harvesting devices will require not only control of assembled structures but also regulation of their ordering and registration within heterogeneous solids and interfaces. This means that there is much work ahead for the supramolecular chemist.

In this thesis, we investigate the scope and applications of *bis*-urea macrocycle building blocks for self-assembly. Specifically, chapter 2 investigates the photophysical properties of the bis-urea macrocycle shown in figure 9a. This benzophenone containing macrocycle acts as a triplet sensitizer, efficiently generates singlet oxygen and shows an unusually stable radical at ambient conditions. We examine the absorption of guests within this host and its ability to facilitate the oxidation of guests under UV-irradition in the solid-state under an oxygen atmosphere as well as in oxygenated solutions. In Chapter 3, we explore the effect of modification of the "c"-shaped spacer on the ability for the *bis*-ureas to self-assemble. By synthesizing a series of naphthalene derivatives including 2,7-dimethyl naphthalene, 1,3-dimethyl naphthalene and 4-bromo-1,3-dimehtyl

naphthalene, we explore the outcome of an expanded aryl spacer on the self assembly and structure of the *bis*-urea macrocycles. These new expanded aryl spacers showed unique confomers as well as interesting assembly motifs. Finally, Chapter 4 explores the capacity of an included functional group in the urea macrocyclic system, pyridine, to bind guest molecules through halogen-bonding motifs.

1.6 References.

[1] G. Ercolani, *J. Phys. Chem. B* **1998**, *102*, 5699-5703.

[2] M. Antonietti, S. Forster, *Adv. Mater.* **2003**, *15*, 1323-1333.

[3] T. Kato, N. Mizoshita, K. Kishimoto, *Angew. Chem. Int. Ed.* **2006**, *45*, 38-68.

[4] B. Moulton, M. J. Zaworotko, *Chem. Rev.*, **2001**, *101*, 1629-1658.

[5] A. Klug, *Angew. Chem. Int. Ed.* **1983**, *22*, 565-582.

[6] H. Fraenkel-Conrat, R.C. Williams, *P. Natl. Acad. Sci. USA*, **1955**, *41*, 690-698.

[7] G. Nicolis, I. Prigogine, *Self-organization in nonequilibrium systems*; Wiley: New York, 1977.

[8] D. J. Kushner, *Bacteriol. Rev.* **1969**, *33*, 302-345.

[9] J.-M. Lehn, Supramolecular Chemistry; Weinheim: New York, 1995.

[10] S. Camazine, J.-L. Deneubourg, N. Franks, G. Theraulaz, E. Bonabeau, Self-Organization in Biological Systems; Princeton University Press: New Jersey 2001.

[11] J. D. Halley, D. A. Winkler, D. A. *Complexity* **2008**, *14*, 10-17.

[12] M. Surin, P. Samori, A. Jouaiti, N. Kyritsaka, M. W. Hosseini, *Angew. Chem. Int. Ed.* **2007**, *46*, 245-249.

[13] K. J. M. Bishop, C. E. Wilmer, S. Soh, B. A. Grzybowski, *Small* **2009,** *5* 1600-1630.

[14] Y. J. Min, M. Akbulut, K. Kristiansen, Y. Golan, J. Israelachvili, *Nat. Mater.* **2008,** *7* 527-538.

[15] S. Furukawa, S. De Feyter, *Top. Curr. Chem.* **2009**, *287*, 83-133.

[16] T. Kudernac, S. B. Lei, J. A. A. W. Elemans, S. De Feyter, *Chem. Soc. Rev.* **2009**, *38*, 402-421.

[17] M. Simard, D. Su, J. D. Wuest, *J. Am. Chem. Soc.* **1991**, *113*, 4696-4698.

[18] G. M. Whitesides, E. E. Simanek, J. P. Mathias, C. T. Seto, D. N. Chin, M. Mammen, D. M. Gordon, *Acc. Chem. Res.* **1995,** *28* 37-44.

[19] S. R. Batten, R. Robson, R. *Angew. Chem. Int. Ed.* **1998**, *37*, 1460-1494.

[20] N. W. Ockwig, O. Delgado-Friedrichs, M. O'Keeffe, O. M. Yaghi, *Accounts Chem. Res.* **2005**, *38*, 176-182.

[21] A. Muller, S. Roy, *Coordin. Chem. Rev.* **2003**, *245*, 153-166.

[22] B. Olenyuk, M. D. Levin, J. A. Whiteford, J. E. Shield, P. J. Stang, *J. Am. Chem. Soc.* **1999**, *121*, 10434-10435.

[23] D. L. Caulder, K. N. Raymond, *Accounts Chem. Res.* **1999**, *32*, 975-982.

[24] Saalfrank, R. W.; Stark, A.; Peters, K.; Vonschnering, H. G. *Angew. Chem. Int. Ed.* **1988**, *27*, 851-853.

[25] C. Park, J. Yoon, E. L. Thomas, *Polymer* **2003**, *44*, 6725-6760.

[26] G. Riess, *Prog. Polym. Sci.* **2003**, *28*, 1107-1170.

[27] S. Forster, T. Plantenberg, *Angew. Chem. Int. Edit.* **2002**, *41*, 689-714.

[28] A. Halperin, M. Tirrel, T. P. Lodge, *Adv. Polym. Sci.* **1992**, *100*, 31-71.

[29] B. M. Rosen, C. J. Wilson, D. A. Wilson, M. Peterca, M. R. Imam, V. Percec, *Chem. Rev.* **2009**, *109*, 6275-6540.

[30] R. W. Zeng, S. C. Zimmerman, *Chem. Rev.* **1997**, *97*, 1681-1712.

[31] A. Piruska, M. Gong, J. V. Sweedler, P. W. Bohn, *Chem. Soc. Rev.* **2010,** *39* 1060-1072.

[32] J. W. Steed, J. L. Atwood, J. L. *Supramolecular Chemistry;* John Wiley and sons Ltd: Chichester, 2000.

[33] N. T. Southall, K. A. Dill, A. D. J. Haymet, *J. Phys. Chem. B* **2002,** *106* 2812.

[34] P. Dauber, A.T. Hagler, *Accounts Chem. Res.*, **1980**, *13*, 105-112.

[35] G. R. Desiraju, *Accounts Chem. Res.* **2002**, *35*, 565-573.

[36] G. M. Whitesides, E. E. Simanek, J. P. Mathias, C. T. Seto, D. N. Chin, M. Mammen, D. M. Gordon, *Accounts Chem. Res.* **1995**, *28*, 37-44.

[37] M. Mammen, E. E. Simanek, G. M. Whitesides, *J. Am. Chem. Soc.* **1996**, *118*, 12614-12623.

[38] T. Steiner, *Angew. Chem. Int. Ed.* **2002**, *41*, 48-76.

[39] P. Metrangolo, H. Neukirch, T. Pilati, G. Resnati, G. *Accounts Chem. Res.* **2005**, *38*, 386-395.

[40] P. Metrangolo, F. Meyer, T. Pilati, G. Resnati, G. Terraneo, *Angew. Chem. Int. Edit.* **2008**, *47*, 6114-6127.

[41] Meyer, E. A.; Castellano, R. K.; Diederich, F. *Angew Chem Int Edit* **2003**, *42*, 1210-1250.

[42] C. A. Hunter, J. K. M. Sanders, *J. Am. Chem. Soc.* **1990**, *112*, 5525-5534.

[43] H. J. Schneider, *Angew. Chem. Int. Ed.* **2009**, *48*, 3924-3977.

[44] G. W. Gokel, L. J. Barbour, R. Ferdani, J. X. Hu, *Accounts Chem. Res.* **2002**, *35*, 878-886.

[45] J. C. Ma, D. A. Dougherty, D. A. *Chem. Rev.* **1997**, *97*, 1303-1324.

[46] W. L. Jorgensen, J. Pranata, *J. Am. Chem. Soc.* **1990**, *112*, 2008-2010.

[47] J. Pranata, S. G. Wierschke, W. L. Jorgensen, *J. Am. Chem. Soc.* **1991**, *113*, 2810-2819.

[48] T. J.; Murray, S. C. Zimmerman, *J. Am. Chem. Soc.* **1992**, *114*, 4010-4011.

[49] R. P. Sijbesma, F. H. Beijer, L. Brunsveld, B. J. B. Folmer, J. H. K. K. Hirschberg, R. F. M. Lange, J. K. L. Lowe, E. W. Meijer, *Science* **1997**, *278*, 1601-1604.

[50] S. Grimme, *Angew Chem Int Edit* **2008**, *47*, 3430-3434.

[51] E. Kim, S. Paliwal, C. S. Wilcox, *J Am Chem Soc* **1998**, *120*, 11192-11193.

[52] Y. S. Chong, W. R. Carroll, W. G. Burns, M. D. Smith, K. D. Shimizu, *Chem.-Eur. J.* **2009**, *15*, 9117-9126.

[53] J. M. Lehn, *Science* **2002**, *295*, 2400-2403.

[54] M. Chas, D. Abella, V. Blanco, E. Pia, G. Blanco, A. Fernandez, C. Platas-Iglesias, C. Peinador, J.M. Quintela, *Chem. Eur. J.* **2007**, *13*, 8572-8582.

[55] E. Stulz, S. M. Scott, A. D. Bond, S. J. Teat, J. K. M. Sanders, *Chem. Eur. J.* **2003**, *9*, 6039-6048.

[56] D. S. Lawrence, T. Jiang, M. Levett, *Chem. Rev.***1995**, *95*, 2229-2260. B) M. M. Conn, J. Rebek, *Chem. Rev.* **1997,** *97* 1647-1668.

[57] B. A. Grzybowski, C. E. Wilmer, J. Kim, K. P. Browne, K. J. M. Bishop, *Soft Matter* **2009,** *5* 1110-1128.

[58] S. Y. Kim, I. S. Jung, E. Lee, J. Kim, S. Sakamoto, K. Yamaguchi, K. Kim, *Angew. Chem. Int. Edit.* **2001,** *40* 2119-2121.

[59] M. Yoshizawa, J. K. Klosterman, M. Fujita, *Angew. Chem. Int. Edit.* **2009,** *48* 3418-3438.

[60] I. Huc, J. M. Lehn, *P. Natl. Acad. Sci. USA* **1997**, *94*, 2106-2110.

[61] S. Klekota, B. L. Miller, *Tetrahedron* **1999**, *55*, 11687-11697.

[62] P. G. Swann, R. A. Casanova, A. Desai, M. M. Frauenhoff, M. Urbancic, U. Slomczynska, A. J. Hopfinger, G. C. LeBreton, D. L. Venton, *Biopolymers*, **1996**, *40,* 617-625.

[63] P. A. Brady, J. K. M. Sanders, *J. Chem. Soc. Perk. Trans. 1* **1997**, 3237-3253.

[64] S. J. Rowan, J. K. M. Sanders, *Chem. Commun.* **1997**, 1407-1408.

[65] S. J. Rowan, P. S. Lukeman, D. J. Reynolds, J. K. M. Sanders, *New J. Chem.* **1998**, *22*, 1015-1018.

[66] R. J. Sarma, S. Otto, J. R. Nitschke, *Chem.-Eur. J.* **2007**, *13*, 9542-9546.

[67] P. Kuhn, M. Antonietti, A. Thomas, *Angew. Chem. Int. Ed.* **2008**, *47*, 3450-3453.

[68] K. Severin, *Dalton T* **2009**, 5254-5264.

[69] S. Otto, R. L. E. Furlan, J. K. M. Sanders, *Science*, **2002**, *297*, 590-593.

[70] S. Otto, R. L. E. Furlan, J. K. M. Sanders, *J. Am. Chem. Soc.* **2000**, *122*, 12063-12064.

[71] A. P. Cote, A. I. Benin, N. W. Ockwig, M. O'Keeffe, A. J. Matzger, O. M. Yaghi, *Science*, **2005**, *310*, 1166-1170.

[72] P. Kuhn, M. Antonietti, A. Thomas, *Angew Chem Int Edit*, **2008**, *47*, 3450-3453.

[73] R. W. Tilford, W. R. Gemmill, H.-C. zur Loye, J. J. Lavigne, *Chem Mater*, **2006**, *18*, 5296-5301.

[74] R. W. Tilford, S. J. Mugavero, P. J. Pellechia, J. J. Lavigne, *Adv Mater*, **2008**, *20*, 2741-2746.

[75] E. L. Spitler, W. R. Dichtel, *Nature Chem.* **2010**, DOI: 10.1038/NCHEM.695.

[76] S. J. Rowan, S. J. Cantrill, G. R. L. Cousins, J. K. M. Sanders, J. F. Stoddart, *Angew Chem Int Edit*, **2002**, *41*, 898-952.

[77] J. S. Lindsey, *New J. Chem.* **1991**, *15,* 153-180.

[78] R. J. Davey, J. Garside, *From molecules to crystallizers-an introduction to crystallization*; Oxford University Press: Oxford, 2000.

[79] R. C. Burton, E. S. Ferrari, R. J. Davey, J. L. Finney, D. T. Bowron, *J Phys Chem B*, **2010**, *114*, 8807-8816.

[80] J. D. Epping, B. F. Chmelka, *Curr. Opin. Colloid In.* **2006,** *11* 81-117.

[81] J. A. Venables, G. D. T. Spiller, M. Hanbucken, *Rep Prog Phys*, **1984**, *47*, 399-459.

[82] A. L. Grzesiak, A. J. Matzger, *Inorg Chem*, **2007**, *46*, 453-457.

[83] C. P. Price, A. L. Grzesiak, A. J. Matzger, *J. Am. Chem. Soc.*, **2005**, *127*, 5512-5517.

[84] A. L. Grzesiak, F. J. Uribe, N. W. Ockwig, O. M. Yaghi, A. J. Matzger, *Angew Chem Int Edit*, **2006**, *45*, 2553-2556.

[85] H. A. Becerril, A. T. Woolley, *Chem. Soc. Rev.* **2009**, *38*, 329-337.

[86] D. K. Bucar, G. S. Papaefstathiou, T. D. Hamilton, Q. L. L. Chu, I. G. Georgiev, L. R. MacGillivray, *Eur. J. Inorg. Chem.*, **2007**, 4559-4568.

[87] C. D. Meyer, C. S. Joiner, J. F. Stoddart, *Chem. Soc. Rev.*, **2007**, *36*, 1705-1723.

[88] D. Y. Wang, H. Mohwald, *J. Mater. Chem.*, **2004**, *14*, 459-468.

[89] Y. Yin, Y. Lu, B. Gates, Y. Xia, *J. Am. Chem. Soc.* **2001**, *123*, 8718-8729.

[90] A. Harada, A. Hashidzume, H. Yamaguchi, Y. Takashima, *Chem Rev*, **2009**, *109*, 5974-6023.

[91] L. Fang, M.A. Olson, D. Benitez, E. Tkatchouk, W.A. Goddard, J.F. Stoddart, *Chem Soc Rev*, **2010**, *39*, 17-29.

[92] Arico, F.; Chang, T.; Cantrill, S. J.; Khan, S. I.; Stoddart, J. F. *Chem.-eur. J.* **2005**, *11*, 4655-4666.

[93] J. Xu, E.A. Fogleman, S.L. Craig, *Macromolecules*, **2004**, *37*, 1863-1870.

[94] J. Israelachvili, *Intermolecular & Surfaces Forces*, 2nd edn., Academic Press, London, 1992, part III.

[95] H. G. Cui, M. J. Webber, S. I. Stupp, *Biopolymers* **2010,** *94* 1-18.

[96] L. C. Palmer, S. I. Stupp, *Accounts Chem. Res.* **2008,** *41* 1674-1684.

[97] S. Cavalli, F. Albericio, A. Kros, *Chem. Soc. Rev.* **2010,** *39* 241-263.

[98] A. Carlsen, S. Lecommandoux, *Curr. Opin. Colloid Int.* **2009,** *14* 329-339.

[99] Cram, D. J.; Choi, H. J.; Bryant, J. A.; Knobler, C. B. *J. Am. Chem. Soc.* **1992**, *114*, 7748-7765.

[100] J. R. Moran, J. L. Ericson, E. Dalcanale, J. A. Bryant, C. B. Knobler, D. J. Cram, *J. Am. Chem. Soc.* **1991,** *113* 5707-5714.

[101] R. Wyler, J. de Mendoza, J. Rebek, *Angew. Chem. Int. Edit.*, **1993**, *32*, 1699-1701.

[102] X. Garcias, J. Rebek, *Angew. Chem. Int. Edit.*, **1996**, *35*, 1225-1228.

[103] R. S. Meissner, J. Rebek, J. De Mendoza, *Science* **1995,** *270* 1485-1488.

[104] R. S. Meissner, X. Garcias, S. Mecozzi, J. Rebek, *J. Am. Chem. Soc.* **1997,** *119* 77-85.

[105] T. Szabo, G. Hilmersson, J. Rebek, *J. Am. Chem. Soc.* **1998,** *120* 6193-6194.

[106] J. Rebek, *Accounts Chem. Res.* **1999,** *32* 278-286.

[107] J. N. H. Reek, J. A. A. W. Elemans, R. de Gelder, P. T. Beurskens, A. E. Rowan, R. J. M. Nolte, *Tetrahedron* **2003,** *59* 175-185.

[108] S. J. Holder, J. A. A. W. Elemans, J. J. J. M. Donners, M. J. Boerakker, R. de Gelder, J. Barbera, A. E. Rowan, R. J. M. Nolte, *J. Org. Chem.* **2001,** *66*, 391-399.

[109] D. J. Cram, J. M. Cram, *Container Molecules and Their Guests*; Royal Society of Chemistry: Cambridge, 1994.

[110] J. Y. Sun, B. O. Patrick, J. C. Sherman, *Tetrahedron*, **2009**, *65*, 7296-7302.

[111] Y. Liu, X. Liu, R. Warmuth, *Chem.-eur. J.*, **2007**, *13*, 8953-8959.

[112] S. Ro, S. J. Rowan, A. R. Pease, D. J. Cram, J. F. Stoddart, *Org. Lett.*, **2000**, *2*, 2411-2414.

[113] P. Skowronek, J. Gawronski, *Org. Lett.*, **2008**, *10*, 4755-4758.

[114] N. Nishimura, K. Yoza, K. Kobayashi, *J. Am. Chem. Soc.*, **2010**, *132*, 777-790.

[115] A. Shivanyuk, E. F. Paulus, V. Bohmer, *Angew. Chem. Int. Edit.*, **1999**, *38*, 2906-2909.

[116] R. G. Chapman, J. C. Sherman, *J. Am. Chem. Soc.*, **1995**, *117*, 9081-9082.

[117] F. Sansone, L. Baldini, A. Casnati, E. Chierici, G. Faimani, F. Ugozzoli, R. Ungaro, *J. Am. Chem. Soc.*, **2004**, *126*, 6204-5.

[118] M. H. K. Ebbing, M. J. Villa, J. M. Valpuesta, P. Prados, J de Mendoza, *P. Natl. Acad. Sci. USA*, **2002**, *99*, 4962-4966.

[119] K. Kobayashi, K. Ishii, S. Sakamoto, T. Shirasaka, K. Yamaguchi, *J. Am. Chem. Soc.*, **2003**, *125*, 10615-10624.

[120] P. Jacopozzi, E. Dalcanale, *Angew. Chem. Int. Edit.*, **1997**, *36*, 613-615.

[121] A. Ikeda, S. Shinkai, *Chem. Rev.*, **1997**, *97*, 1713-1734.

[122] O. D. Fox, M. G. B. Drew, P. D. Beer, *Angew. Chem. Int. Edit.*, **2000**, *39*, 136-140.

[123] S. J. Park, D. M. Shin, S. Sakamoto, K. Yamaguchi, Y. K. Chung, M. S. Lah, J. I. Hong, *Chem.-eur. J.*, **2005**, *11*, 235-241.

[124] G. V. Oshovsky, D. N. Reinhoudt, W. Verboom, *J Am Chem Soc*, **2006**, *128*, 5270-5278.

[125] B. Hamelin, L. Jullien, C. Derouet, C. H. du Penhoat, P. Berthault, *J. Am. Chem. Soc.* **1998**, *120*, 8438-8447.

[126] S. Liu, B. C. Gibb, *Chem. Commun.* **2008,** 3709-3716.

[127] H. Sun, C. L. D. Gibb, B. C. Gibb, *Supramol. Chem.* **2008,** *20* 141-147.

[128] A. Natarajan, L. S. Kaanumalle, S. Jockusch, C. L. D. Gibb, B. C. Gibb, N. J. Turro, V. Ramamurthy, *J. Am. Chem. Soc.* **2007,** *129* 4132-4133.

[129] A. K. Sundaresan, L. S. Kaanumalle, C. L. D. Gibb, B. C. Gibbb, V. Ramamurthy, *Dalton T.* **2009,** 4003-4011.

[130] C. L. D. Gibb, A. K. Sundaresan, V. Ramamurthy, B. C. Gibb, *J. Am. Chem. Soc.* **2008,** *130* 4069-4080.

[131] L. S. Kaanumalle, C. L. D. Gibb, B. C. Gibb, V. Ramamurthy, *J. Am. Chem. Soc.* **2004,** *126* 14366-14367.

[132] S. Liu, B. C. Gibb, *Chem. Commun.* **2008,** 3709-3716.

[133] S. J. Dalgarno, N. P. Power, J. L. Atwood, *Coordin. Chem. Rev.*, **2008**, *252*, 825-841.

[134] S. J. Dalgarno, P. K. Thallapally, L. J. Barbour, J. L. Atwood, *Chem. Soc. Rev.*, **2007**, *36*, 236-245.

[135] L. R. MacGillivray, J. L. Atwood, *Nature*, **1997**, *389*, 469-472.

[136] F. Corbellini, R. Fiammengo, P. Timmerman, M. Crego-Calama, K. Versluis, A.J.R. Heck, I. Luyten, D.N. Reinhoudt, *J. Am. Chem. Soc.*, **2002**, *124*, 6569-6575.

[137] D. Ajami, J. Rebek, *J.Org. Chem.* **2009,** *74* 6584-6591.

[138] J. Rebek, *Accounts Chem. Res.* **2009,** *42* 1660-1668.

[139] J. J. Perry, J. A. Perman, M. J. Zaworotko, *Chem. Soc. Rev.*, **2009**, *38*, 1400-1417.

[140] S. De, K. Mahata, M. Schmittel, *Chem. Soc. Rev.*, **2010**, *39*, 1555-1575.

[141] V. L. Gunderson, S. M. M. Conron, M. R. Wasielewski, *Chem.Commun.***2010,** *46* 401-403.

[142] M. R. Wasielewski, *Accounts Chem. Res.* **2009**, *42*, 1910-1921.

[143] B. Olenyuk, M. D. Levin, J. A. Whiteford, J. E. Shield, P. J. Stang, *J. Am. Chem. Soc.*, **1999**, *121*, 10434-10435.

[144] B. H. Northrop, Y. R. Zheng, K. W. Chi, P. J. Stang, *Accounts Chem. Res.*, **2009**, *42*, 1554-1563.

[145] G. V. Oshovsky, D. N. Reinhoudt, W. Verboom, *J Org Chem*, **2006**, *71*, 7441-7448.

[146] R. W. Saalfrank, H. Maid, A. Scheurer, *Angew. Chem. Int. Edit.*, **2008**, *47*, 8794-8824.

[147] M. Fujita, D. Oguro, M. Miyazawa, H. Oka, K. Yamaguchi, K. Ogura, *Nature* **1995,** *378* 469-471.

[148] T. Kusukawa, T. Nakai, T. Okano, M. Fujita, *Chem. Lett.* **2003,** *32* 284-285.

[149] Q.-F. Sun, J. Iwas, D. Ogawa, Y. Ishido, S. Sato, T. Ozeki, Y. Sei, K. Yamaguchi, M. Fujita, *Science*, **2010**, *328*, 1144-1147.

[150] M. Gellert, M.N. Lipsett, D.R. Davies, *P. Natl. Acad. Sci. USA*, **1962**, *48*, 2013-2018.

[151] A. T. Phan, *Febs. J.*, **2010**, *277*, 1107-1117.

[152] L. Oganesian, T. M. Bryan, *Bioessays*, **2007**, *29*, 155-165.

[153] S. Lena, G. Brancolini, G. Gottarelli, P. Mariani, S. Masiero, A. Venturini, V. Palermo, O. Pandoli, S. Pieraccini, P. Samori, G. P. Spada, *Chem.-eur J.*, **2007**, *13*, 3757.

[154] J. T. Davis, *Angew. Chem. Int. Edit.*, **2004**, *43*, 668-698.

[155] J. T. Davis, G. P. Spada, *Chem. Soc. Rev.*, **2007**, *36*, 296-313.

[156] M. D. Rivera-Sanchez, I. Andujar-de-Sanctis, M. Garcia-Arriaga, V. Gubala, G. Hobley, J. M. Rivera, *J. Am. Chem. Soc.*, **2009**, *131*, 10403-10404.

[157] P. J. Bates, D. A. Laber, D. M. Miller, S. D. Thomas, J. O. Trent, *Exp. Mol. Pathol.*, **2009**, *86*, 151-164.

[158] M. O. M. Piepenbrock, G. O. Lloyd, N. Clarke, J. W. Steed, *Chem. Rev.*, **2010**, *110*, 1960-2004.

[159] K. Araki, I. Yoshikawa, *Top. Curr. Chem.*, **2005**, *256*, 133-165.

[160] S. D'Amico, G. Maruccio, P. Visconti, E. D'Amone, R. Cingolani, R. Rinaldi, S. Masiero, G. P. Spada, G. Gottarelli, *Microelectr. J.*, **2003**, *34*, 961-963.

[161] D. T. Bong, T. D. Clark, J. R. Granja, M. R. Ghadiri, *Angew. Chem. Int. Edit.*, **2001**, 40, 988-1011.

[162] A. T. ten Cate, R. P. Sijbesma, *Macromol. Rapid Comm.*, **2002**, 23, 1094-1112.

[163] M. A. B. Block, C. Kaiser, A. Khan, S. Hecht, *Top. Curr. Chem.*, **2005**, *245*, 89-150.

[164] D. Pasini, M. Ricci, *Curr Org Synth*, **2007**, *4*, 59-80.

[165] V. Semetey, C. Didierjean, J. P. Briand, A. Aubry, G. Guichard, *Angew. Chem. Int. Edit.*, **2002**, *41*, 1895-1898.

[166] D. Ranganathan, C. Lakshmi, I. L. Karle, *J. Am. Chem. Soc.*, **1999**, *121*, 6103-6107.

[167] L. S. Shimizu, A. D. Hughes, M. D. Smith, M. J. Davis, B. P. Zhang, H.-C. zur Loye, K. D. Shimizu, *J. Am. Chem. Soc.*, **2003**, *125*, 14972-14973.

[168] M. B. Dewal, Y. W. Xu, J. Yang, F. Mohammed, M. D. Smith, L.S. Shimizu, *Chem. Commun.*, **2008**, 3909-3911.

[169]M. B. Dewal, M. W. Lufaso, A. D. Hughes, S. A. Samuel, P. Pellechia, L. S. Shimizu, *Chem. Mater.*, **2006**, *18*, 4855-4864.

[170] J. Yang, M. B. Dewal, L. S. Shimizu, *J. Am. Chem. Soc.*, **2006**, *128*, 8122-3.

[171] J. Yang, M. B. Dewal, S. Profeta, M. D. Smith, Y. Y. Li, L. S. Shimizu, *J. Am. Chem. Soc.*, **2008**, *130*, 612-621.

[172] P. De Santis, S. Morosetti, R. Rizzo, *Macromolecules*, **1974**, 7, 52-58.

[173] T. D. Clark, L. K. Buehler, M. R. Ghadiri, *J. Am. Chem. Soc.* **1998,** *120* 651-656.

[174] M. R. Ghadiri, J. R. Granja, R. A. Milligan, D. E. Mcree, N. Khazanovich, *Nature*, **1993**, *366*, 324-7.

[175] T. D. Clark, J. M. Buriak, K. Kobayashi, M. P. Isler, D. E. McRee, M. R. Ghadiri, *J. Am. Chem. Soc.*, **1998**, *120*, 8949-8962.

[176] D. Seebach, J. L. Matthews, A. Meden, T. Wessels, C. Baerlocher, L. B. McCusker, *Helv. Chim. Acta.*, **1997**, *80*, 173-182.

[177] R. J. Brea, J. R. Granja, *"Self-assembly of cyclic peptides in hydrogen-bonded nanotubes",* in *Dekker Encyclopedia of Nanoscience and Nanotechnology*, ed. J. A. Schwarz, C. I. Contescu, K. Putyera, Marcel Dekker Inc., New York, 2004, pp. 3439-3457.

[178] R. J. Brea, C. Reiriz, J. R. Granja, *Chem. Soc. Rev.*, **2010**, *39*, 1448-1456.

[179] X. Y. Gao, H. Matsui, *Adv. Mater.*, **2005**, *17*, 2037-2050.

[180] K. Balakrishnan, A. Datar, W. Zhang, X. M. Yang, T. Naddo, J. L. Huang, J. M. Zuo, M. Yen, J. S. Moore, L. Zang, *J. Am. Chem. Soc.* **2006**, *128* 6576-6577.

[181] L. Zang, Y. K. Che, J. S. Moore, *Accounts Chem. Res.*, **2008**, *41*, 1596-1608.

[182] P. D. Frischmann, S. Guieu, R. Tabeshi, M. J. MacLachlan, *J. Am. Chem. Soc.* **2010,** *132* 7668-7675.

[183] A. Wu, L. Isaacs, *J. Am. Chem. Soc.*, **2003**, *125*, 4831-4835.

[184] L. Pasteur, *Ann. Chim. Phys.,* **1848**, *24*, 442.

[185] J. Jacques, A. Collet, S. H. Wilen, *Enantiomers, Racemates and Resolutions,* Krieger Publishing Company, Malabar, Fl, 1994.

[186] L. E. Orgel, *Nature*, **1992**, *358*, 203-209.

[187] A. Vidonne, D. Philp, *Eur. J. Org. Chem.*, **2009**, 593-610.

[188] E. A. Wintner, M. M. Conn, J. Rebek, *Accounts Chem. Res.*, **1994**, *27*, 198-203.

[189] J. M. Keith, J. F. Larrow, E. N. Jacobsen, *Adv. Synth. Catal.*, **2001**, *343*, 5-26.

[190] M. Law, J. Goldberger, P. Yang, *Annu. Rev. Mater. Res.*, **2004**, *34*, 83-122.

[191] J. R. Long, B. Dunn, D. R. Rolison, H. S. White, *Chem. Rev.*, **2004**, *104*, 4463-4492.

II. SELF-ASSEMBLED BENZOPHENONE BIS-UREA MACROCYCLES FACILITATE SELECTIVE OXYDATIONS BY SINGLET OXYGEN.

2.1 Abstract.

Benzophenone is a well-known triplet sensitizer. This chapter investigates how incorporation of benzophenone within a self-assembled *bis*-urea macrocycle influences its photo-physical properties and discusses the subsequent generation of a remarkably stable organic radical at ambient conditions. As expected, UV-irradiation of the host **2.1** suspended in oxygenated solvents efficiently generates singlet oxygen similar to the parent benzophenone. However, the self-assembled benzophenone *bis*-urea host can bind guests such as 2-methyl-2-butene and cumene (isopropyl benzene) and form stable solid host-guest complexes. Subsequent UV-irradiation of these complexes facilitated the selective oxidation of 2-methyl-2-butene into the allylic alcohol, 3-methyl-2-buten-1-ol, at 90% selectivity as well as the selective reaction of cumene to the tertiary alcohol, 2-phenyl-isopropanol, at 63% selectivity. These products usually arise through radical pathways and are not observed in the presence of benzophenone. More typically, reactions with benzophenone result in the formation of the reactive oxygen species, singlet oxygen. Then, sequentially, the oxygen reacts with double bonds to form endoperoxides, diooxetanes, or hydroperoxides. The resulting oxidized small molecules are important in industrial and pharmaceutical applications. A greater understanding of

the underlying process that enables the selective oxidation of these molecules in the presence of our host could lead to development of greener oxidants.

2.2 Background.

Oxidations of small molecule alkenes are of importance in the synthesis of pharmaceuticals[1], as feedstock for industrial chemicals,[2] and have important repercussions in biological systems.[3] Typical oxidants include potassium permanganate, selenium dioxide, and strong acids such as chromic and nitric acid, which are highly reactive, toxic, and generate stoichiometric amounts of waste. An alternative and more environmentally friendly oxidation method would incorporate molecular oxygen, the smallest conceivable oxidant. The first excited electronic state of molecular oxygen, also known as singlet oxygen, is produced by UV-irradiation of oxygen (g) in the presence of a triplet sensitizer such as rose bengal, TPP (5,10,15,20-tetraphenyl porphyrin), or benzophenone.[4]

A triplet sensitizer is a chromophore that absorbs radiation (typically in the UV or visible range) and is excited to the first electronic excited state. Through intersystem crossing the electron becomes spin un-paired resulting in a slightly less energetic, more stable, and usually longer lived excited triplet state.[5] The energy from this excited state is then transferred to an accepting molecule (such as molecular oxygen) resulting in the sensitized excited state of the acceptor and the reciprocal ground state of the sensitizer. Figure 2.1 illustrates the typical pathway for the triples sensitization of molecular oxygen by benzophenone. The initial excitation of benzophenone to the first excited singlet state (S_1) then and conversion to the triplet state (T_1) through inter system crossing (ISC). The

transfer of energy to molecular oxygen can happen three ways. First is through the triplet-triplet annihilation in which the energy is transferred through the weak orbital overlap and collisional energy transfer. The second is through the electron transfer from the sensitizer to the oxygen and third is through bond formation resulting in a diradical. The commonly accepted mechanism of the sensitization of singlet oxygen by benzophenone is through the triplet-triplet annihilation pathway.

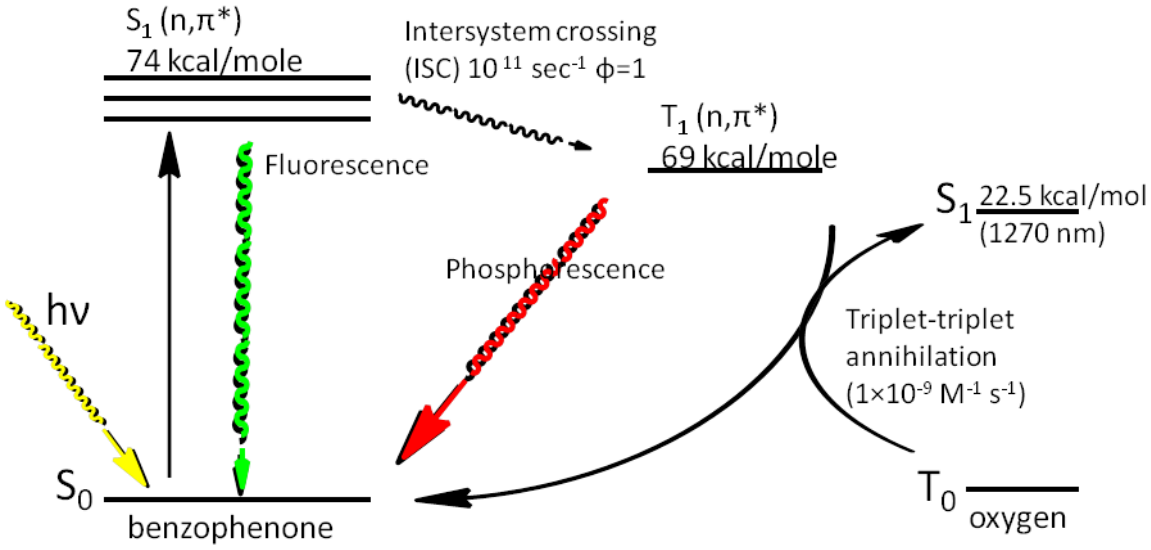

Figure 2.1. Jablonski diagram illustrating the benzophenone triplet sensitization and production of singlet oxygen.

Our group has developed *bis*-urea macrocycles (**2.1** and **2.2**) that assembled into columnar nanotubes, which have accessible intrinsic channels for binding guests.[6] A phenylether *bis*-urea macrocycle (host **2.2**) was used to facilitate the selective reaction of enones such as cyclohexenone and methyl cyclopentenone to afford their [2+2] cycloadducts in the solid state.[7] Herein, we investigate the photophysical properties of a bis-urea macrocycle **2.1** that has two benzophenone units in its framework and show that this self-assembled material generates an unusually stable radical under ambient light and atmospheric conditions. When UV-irradiated in oxygenated solutions or under an

oxygen atmosphere, this self-assembled macrocycle also acts as a sensitizer to generate single oxygen. In this chapter we examine the use of the self-assembled *bis*-urea macrocycle **2.1** as a porous material to absorb small molecule guests and to facilitate the selective oxidation of the encapsulated guest upon UV-irradiation in an oxygen atmosphere (Figure 2.2).

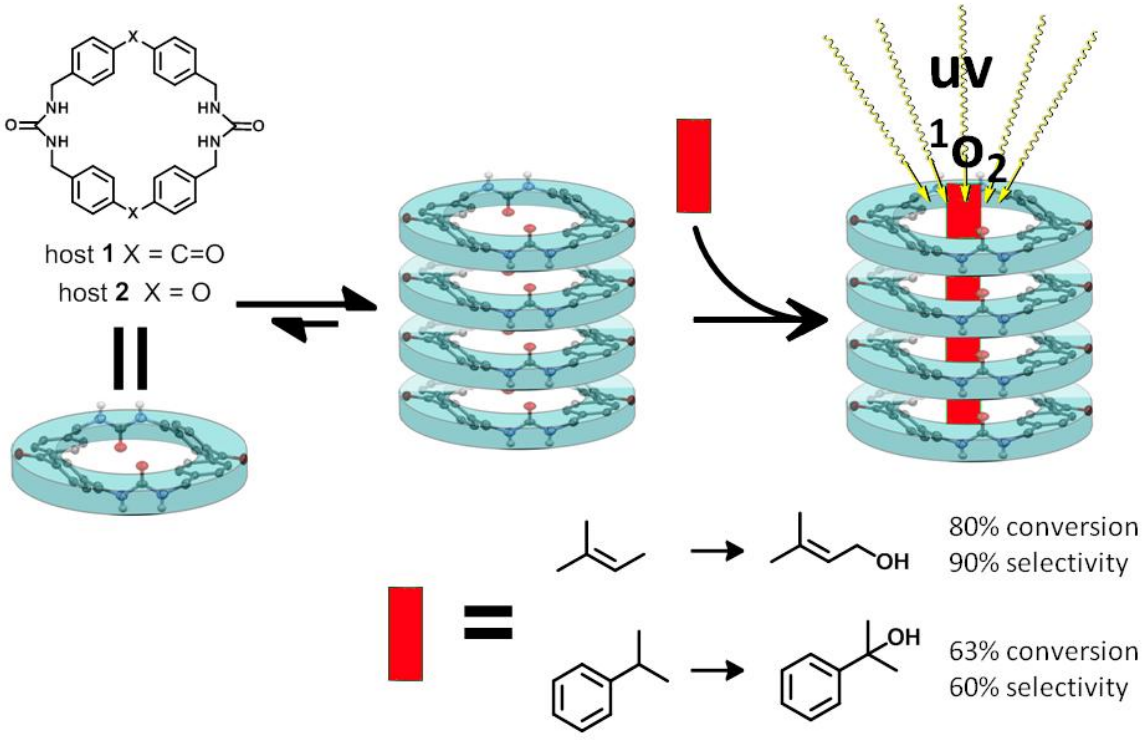

Figure 2.2. Host **2.1**, a benzophenone containing *bis*-urea macrocycle, self-assembles into crystalline columnar structures that can absorb small guests.[8] UV-irradiation of these solid complexes under an oxygen atmosphere affords selective oxidations.

The small size and high reactivity of singlet oxygen often leads to unselective oxidation reactions. In order to tune the selectivity and region-chemistry of the oxidation, researchers have investigated the use of molecular containers such as porous polymers,[9] zeolites,[10] and micro emulsions.[11] For example, Arumugam reported the use

of sodium infused Nafion beads as a micro-environment for the oxidation of 1,2-dimethyl cyclohexene with singlet oxygen at high yields (85 %) and high conversion (90%) to selectively afford the endocyclic allylic peroxide, 1,2-dimethyl cyclohex-2-ene peroxide (89:11, endo:exo).[9b] Ramamurthy *et al.* facilitated the selective oxidation and '*cis*'-hydrogen abstraction of alkenes in a Na-Y dye-supported zeolite.[10a, 10e] Whereas, Tung *et al.* observed hydrogen abstraction from the largest branch of the alkene during oxidation in the presence of a ZSM-5 zeolite.[10c] Work by Griesbeck demonstrated the use of SDS microemulsions to convert a tertiary peroxide into an epoxy enone.[11] These examples showed that confinement was an effective way to control the reactivity and selectivity of molecular oxygen and inspired us to design a system that incorporated a sensitizer, such as benzophenone, into the spacer group of our *bis*-urea macrocycles.

Benzophenone is an efficient triplet sensitizer, with an intersystem crossover quantum yield from the singlet excited state to the triplet state that is unity and a cross-over rate of 10^{11} sec^{-1}.[5] Benzophenone has been used for systems such as photoinitiators in polymerizations,[12] as substrates for the oxidation of environmental pollutants[13], and as anti-microbial coatings.[14] Macrocycle **2.1** (Figure 2.2) preorganizes two benzophenone groups close in space within a small macrocycle.[8] These sensitizers are separated by urea and two methylene units and the X-ray structure shows that the two benzophenone carbonyl carbons within a single macrocycle are separated by ~ 7 Å accounting for van der Waals. Macrocycle **2.1** self-assembles through typical three centered urea hydrogen bonding assisted by aryl stacking interactions to give host **2.1**. This porous host has been used to absorb *trans*-beta methyl styrene and facilitated the *cis-trans* isomerization under UV-irradiation, a process that requires a triplet sensitizer.[8]

This chapter investigates the effect of the proximity of benzophenone units in host **2.1** on their photo-physical properties including on their absorption and emission spectra, phosphorescence quantum yield and radical generation. The solid-state emission quantum yield and lifetimes of host **2.1** were observed to be considerably less/shorter than that of benzophenone itself. Under ambient conditions, we observed a remarkably stable organic radical with host **2.1** in contrast to the radical of benzophenone, which can only be observed through radical trapping or at low temperatures.[15] UV-irradiation of **2.1** suspended in oxygenated $CDCl_3$ gave singlet oxygen, which was identified by its emission in the near IR.[1, 4b] We then studied the uptake of a series of small molecules by host **2.1** to form stable solid inclusion complexes. Finally, we investigate the oxidation of the guest in these crystalline complexes and observed that cumene and 2-methyl-2-butene afforded selective oxidation reactions, while other guests were unreactive. Our hypothesis is that oxidation of these two guests proceeds through a radical mediated oxidation mechanism (auto-oxidation) in the presence of host **2.1**.

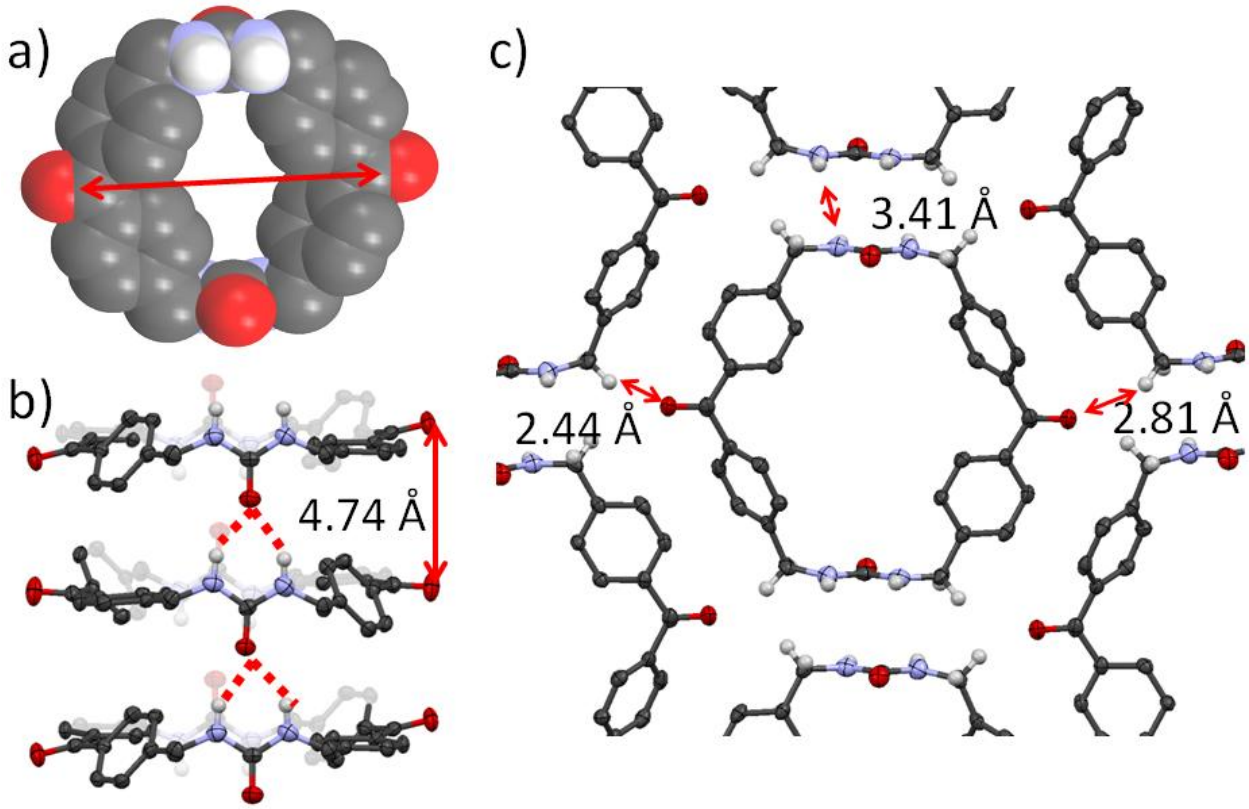

Figure 2.3. Views from the crystal structure of host **2.1**.[8] a) Space filling model of a single macrocycle highlighting the cavity. The distance between the carbonyl carbons of benzophenone is 6.84 Å accounting for van der Waals. b) View along a single column illustrates the three-centered urea hydrogen bonding motif, which controls the average distance between neighboring benzophenone carbonyls (C•••C) to 4.74 Å.. c) Crystal packing showing select close contacts between one macrocycle and its nearest neighbors. (ellipsoids shown at 60 % probability level and some hydrogens have been omitted for clarity)

2.3. Structural analysis of host 2.1.

The *bis*-urea benzophenone macrocycle (host **2.1**) was synthesized as previously reported.[8] The 4,4'-dibromomethyl benzophenone was cyclized with triazinanone in basic conditions. The triazinanone protecting groups were removed by heating in an acidic aqueous/methanol (1:1 v/v) solution of diethanol amine to afford the *bis*-urea macrocycle **2.1**. Upon crystallization from DMSO, compound **2.1** self-assembled into columnar structures through strong directional urea-urea hydrogen bonding assisted by

edge-to-face aryl-aryl stacking to give host **2.1**.[8] Inspection of the crystal structure of host **2.1** shows the resulting columnar structure with an internal cavity having 6.84 Å (urea carbonyl C••• urea carbonyl C minus van der Waals) × 4.68 Å (aryl•••aryl minus van der Waals) dimensions (Figure 2.3a). In the assembled structure, the benzophenone groups on neighboring macrocycles (above and below) are close in space with an average distance of 4.74 Å (Figure 2b). Individual columns pack together into a hexagonal array. Figure 2.3c illustrates the close contacts between the neighboring tubes with respect to the benzophenone carbonyl and the urea groups. The benzophenone carbonyl oxygen forms a close interaction with the acidic methylene CH's on the adjacent column with O•••H(C) distances of 2.44 and 2.81 Å. The urea groups of the neighboring columns are also close packed with a N•••N distance of 3.41 Å. In solution, the parent benzophenone is a monomer and an efficient triplet sensitizer. Our first question was how the incorporation of two benzophenone monomers into a cyclic small molecule would affect its photophysical properties?

2.4. Photophysical characterization of host 2.1.

To probe the photophysical properties of host **2.1**, we examined its absorption and emission (phosphorescence) spectra, along with its phosphorescent quantum yield in solution where it is not assembled. Next, we address the effects of assembly and crystal packing on the photophysical properties by characterizing its phosphorescent quantum yield and its excited state lifetime in the solid-state, where the assembly is expected to further impact the photo-physical properties.

The absorption and emission of monomer **2.1** (unassembled) and benzophenone was compared. UV-vis and fluorescence studies were conducted on a 0.025 mM solution of benzophenone and the macrocycle **2.1** in DMSO. The host was only soluble in DMSO, an aggressive solvent that precludes self-assembly. Figure 2.4a shows the adsorption and phosphorescence of macrocycle **2.1** (red) and benzophenone (black). Comparing the two spectra, we see that macrocycle **2.1** retains the major spectroscopic properties that are observed with benzophenone. The absorption spectra both show the typical bands for π-π^* excitation at λ_{max} ~ 270 nm, and the n-π^* excitation at λ_{max} ~345 nm. No additional bands are apparent, suggesting that the proximity of the two benzophenones within a macrocycle has little effect on the absorption. Figure 2.5 shows the calculated molar absorptivity of benzophenone and macrocycle **2.1** over the wavelength range of 300 – 400 nm for the concentration range 0.024 mM -0.1 mM. These show that the molar absorptivity for macrocycle **2.1** does not vary within the concentration range tested. Calculation of the molar absorptivity of over a range of concentrations (0.012 – 0.111 mM) shows that macrocycle **2.1** has a molar absorptivity coefficient at 355nm of ε =620 +/-20 $M^{-1}cm^{-1}$ in DMSO (Figure 2.5a), approximately twice that of benzophenone (ε = 340 +/-60 $M^{-1}cm^{-1}$, Figure 2.5b).

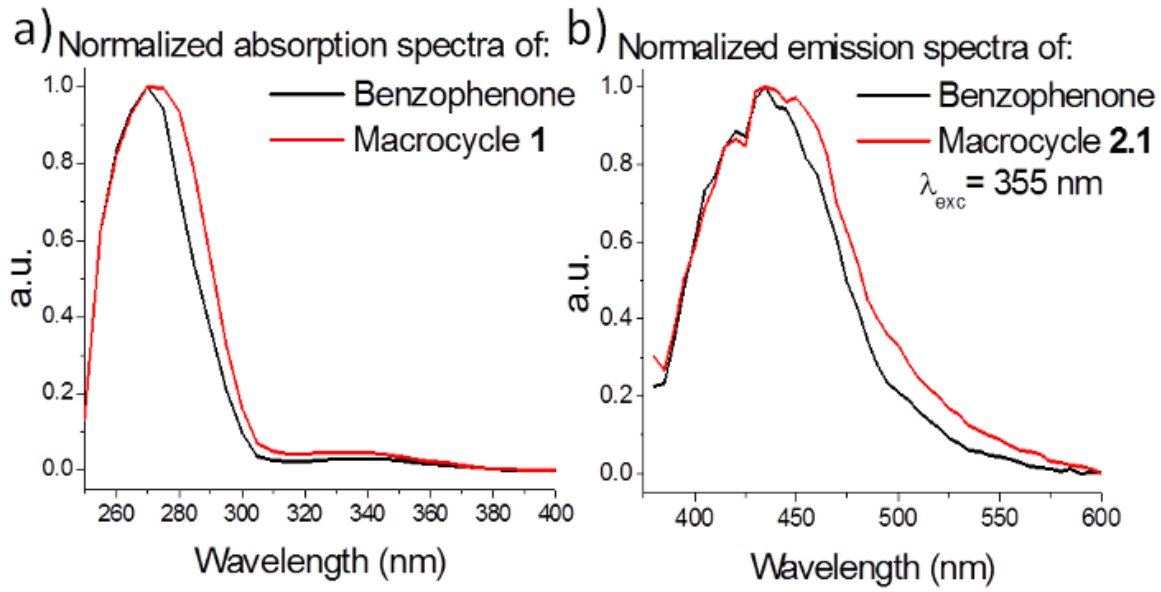

Figure 2.4. Normalized absorption and emission spectra of host **2.1** (red) versus benzophenone (black) in DMSO. (a) UV-Vis absorption of 2.5×10^{-5} M solution of benzophenone (black) and macrocycle **2.1** (red) in DMSO (b) normalized emission spectra of the same solutions excited at 355 nm.

Next, both benzophenone and macrocycle **2.1** DMSO solutions were excited at 355 nm. The emission of **2.1** and benzophenone are similar both with a λ_{max} at 435 nm. The broadening of the peaks is due to the polarization effect of DMSO. These studies suggest that the cyclization did not influence the photophysical character of the benzophenone and allows us to compare the emission quantum yields of the two compounds.

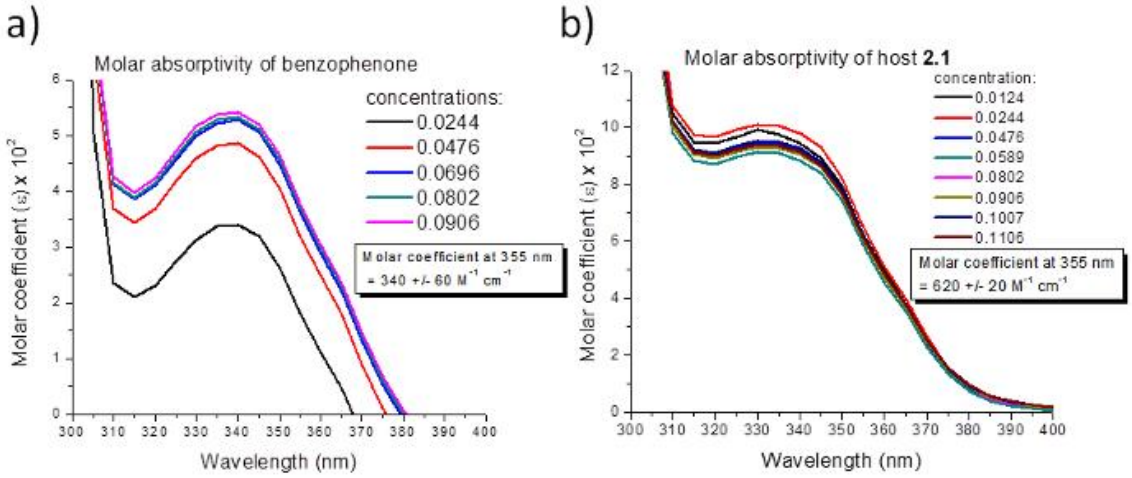

Figure 2.5. Graphs of molar absorptivity (300-400 nm) of a) macrocycle **2.1** and b) benzophenone in select concentration of DMSO.

To study the phosphorescence quantum yields, a series of five solutions of benzophenone (concentrations = 0.012 – 0.070 mM) and eight solutions of macrocycle **2.1** (benzophenone concentrations (two per cycle) = 0.012 – 0.091 mM) were prepared in argon-degassed DMSO. The absorption and the emission spectra for each solution were recorded on a Molecular Devices Spectra Max M2 fluorimeter. Figure 2.6 shows the absorption and emission spectra over selected range to excite the triplet state of benzophenone and macrocycle **2.1**. These graphs display the dependence of the absorption and the phosphorescence on the concentration range tested that allows us to calculate the quantum yields. The absorption and integrated emission were plotted and fitted using a linear relation method (Figure 2.7). Analysis of Figure 2.7 demonstrated that in the concentration range of 0.012 – 0.070 mM the cyclization of two benzophenones within host **2.1** resulted in a 50% increase of the quantum yield relatively to the free benzophenone in DMSO.

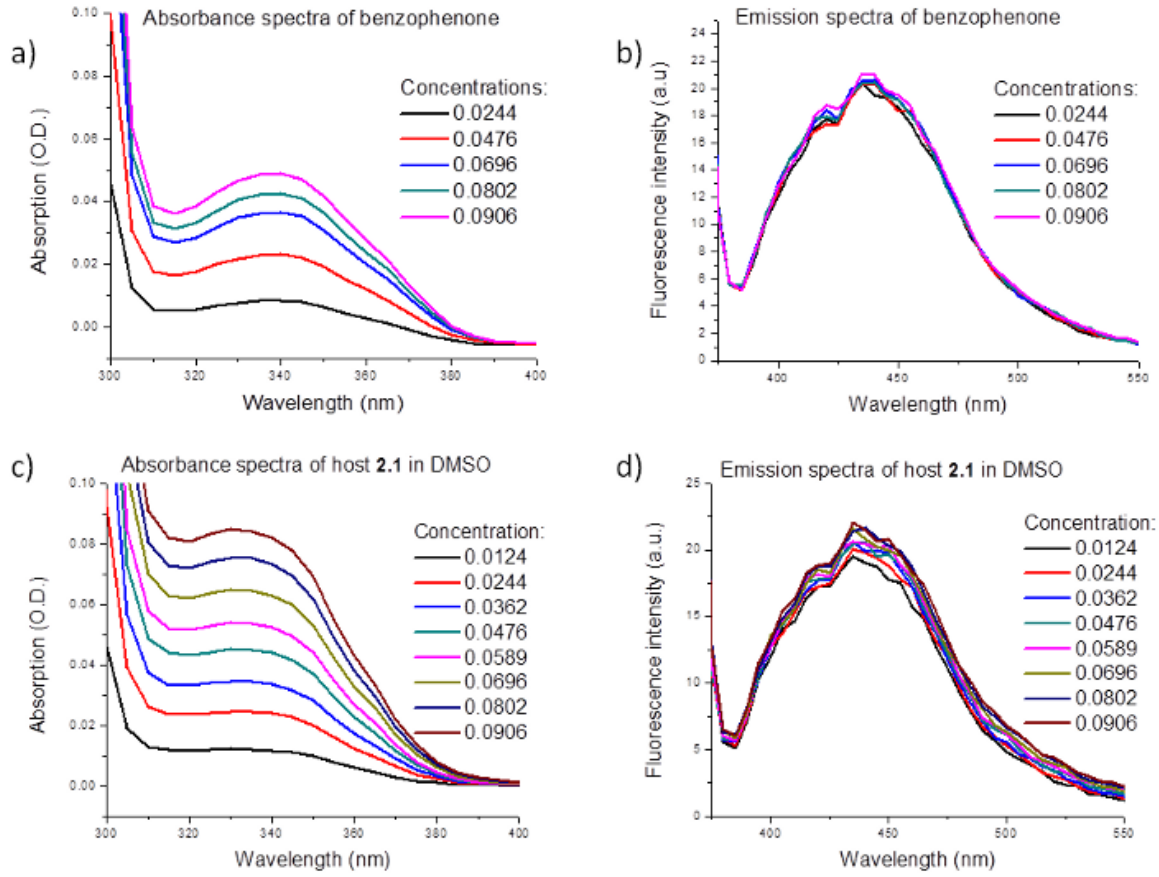

Figure 2.6. Absorbance and emission spectra of benzophenone (a,b) and macrocycle **2.1** (c,d) over select concentrations in DMSO.

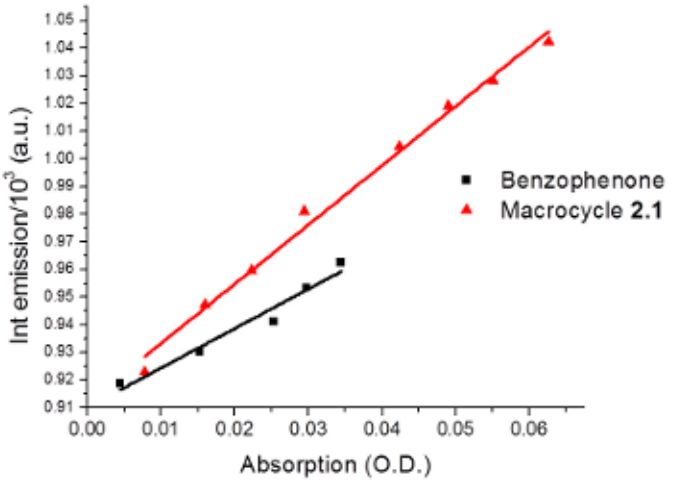

Figure 2.7. The plot of the absorption vs. integrated emission of macrocycle **2.1** (red) vs benzophenone (black). The ratio of the linear plots slopes was 1.5.

Emission quantum yields are effected by solvent polarity,[16] proximity or availability of quencher,[17] and assembly or aggregation.[5] Thus, we were interested if the increase in quantum yield observed in solution is retained in the solid-state. Host **2.1** was prepared by crystallization from a slow cooled solution in DMSO. A 10 mg powder sample of benzophenone and 10 mg of freshly evacuated crystals of host **2.1** were used to measure the quantum yield. The quantum yield was measured on a Horiba Fluorolog 3 with the fiber optic and Quanta-φ accessories. Figure 2.8 shows the resulting spectra with the expected phosphorescent peaks for benzophenone (black) with a quantum yield of 0.5% at ambient conditions. Surprisingly, the luminescence of the host **2.1** crystals (Figure 2.7 red) was not detected by the instrument, which indicates a quantum yield of < 0.1 %. Such difference between the liquid and the solid-state emission behaviors of benzophenone and the host **2.1** suggests the close proximity of benzophenone moieties within the assembled host **2.1** system significantly increases the quenching of the excited states. In light of these results, we next evaluated the lifetimes of the two samples.

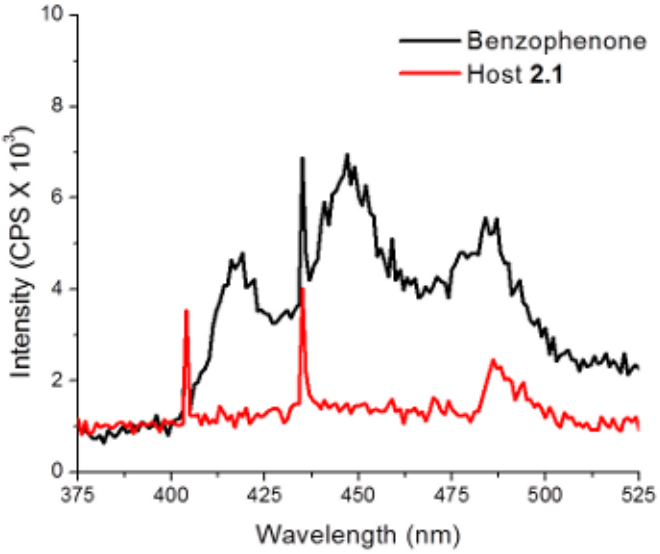

Figure 2.8. Emission spectra of solid host **2.1** and benzophenone showing the phosphorescent peaks between 375 and 525 nm (λ_{ex}= 355 nm). (The measurements were taken in a Horiba Quanta-φ integrating sphere at ambient conditions).

Crystalline powder samples of the benzophenone and host **2.1** system were sandwiched between two quartz slides, and the samples were excited at 372 nm with a picoseconds pulsed diode laser (LDH-P-C-375) with a repetition rate of 1 KHz for the benzophenone sample and 2.5 MHz for the host **2.1** sample (Figure 6). The solid state room temperature phosphorescent lifetimes of benzophenone shows a single exponential decay with the expected lifetime of 22.6 ± 0.3 μs. This value compares well to literature values.[18] The solid-state emission of the host **2.1** crystals had similar steady-state spectra to benzophenone, but the lifetime decay was markedly shorter. The phosphorescence decay showed a multi-exponential character independent of the observation wavelength (430-640 nm). Table 2.1 shows that the decays ranged from 36 ps (τ_1) to 4.3 ns (τ_4) with the average lifetime of 320 ps (weighted average). The decrease in the solid-state quantum yield and lifetime of host **2.1** suggests that the assembly and/or packing of

benzophenone within the host **2.1** solid-state structure makes the benzophenone more accessible to quenching or non-radiative relaxation than that of the compact structure of benzophenone in the solid-state.

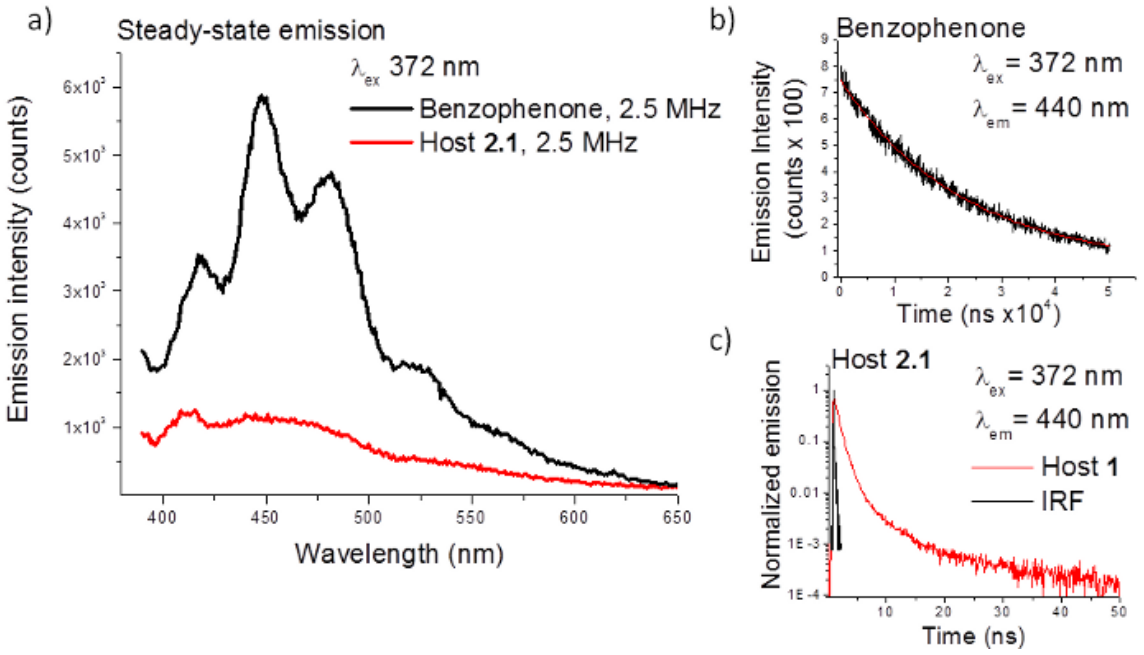

Figure 2.9. Steady state and lifetime emission of host **2.1** vs benzophenone. a) Steady state emission spectra (λ_{ex}= 372 nm) of benzophenone and host **2.1** taken on TCSPC (time-correlated single photon counting) system. b) Lifetime decay of benzophenone powder showing single exponential decay fit (red) with lifetime of 22.6 μs. c) lifetime decay of host **2.1** (blue) with multi-exponential fit average life time of 0.32 ns.

Table 2.1. Values of the time constants (τ_i) and normalized (to 1) pre-exponential factors (A_i) of the multi-exponential function fitting the emission transients of solid-state host **2.1** at room temperature. The excitation wavelength was 372 nm.

Lifetime (τ, ns)[1]	Pre-exponential factor (A)[2]
0.036	0.64
0.33	0.14
1.0	0.21
4.3	0.01

[1]The fit quality was inspected using the weighted residuals, and the values of χ^2 which in all cases was <1.1.
[2]All amplitudes are normalized in the following way: $\sum_{i=1}^{n} \mathrm{A}i = 1$

2.5. Production of singlet oxygen.

Our absorption/emission studies suggested that in solution, host **2.1** has similar photo-physical properties to benzophenone and may have an increased phosphorescent quantum yield. In contrast, in the solid-state, the lifetime of host **2.1** appears to be significantly shortened. Our primary interest in these self-assembled macrocycles is to produce functional materials for controlling reactivity. Thus, we proceeded to test if host **2.1** could facilitate the production of singlet oxygen in spite of its diminished emission lifetime and quantum yield. Therefore, freshly prepared crystals of host **2.1** were suspended in oxygenated $CDCl_3$ and irradiated at 345 nm (λ_{max} absorption of host **2.1**) and the emission in the near IR was monitored. A strong emission at 1270 nm was observed corresponding to the phosphorescence of the $^1O_2$ species (Figure 2.10).[5] The fact that the strong emission for singlet oxygen is present, suggests that one mode of

quenching of the lifetime of host **2.1** system may be due in part to the presence of atmospheric oxygen.

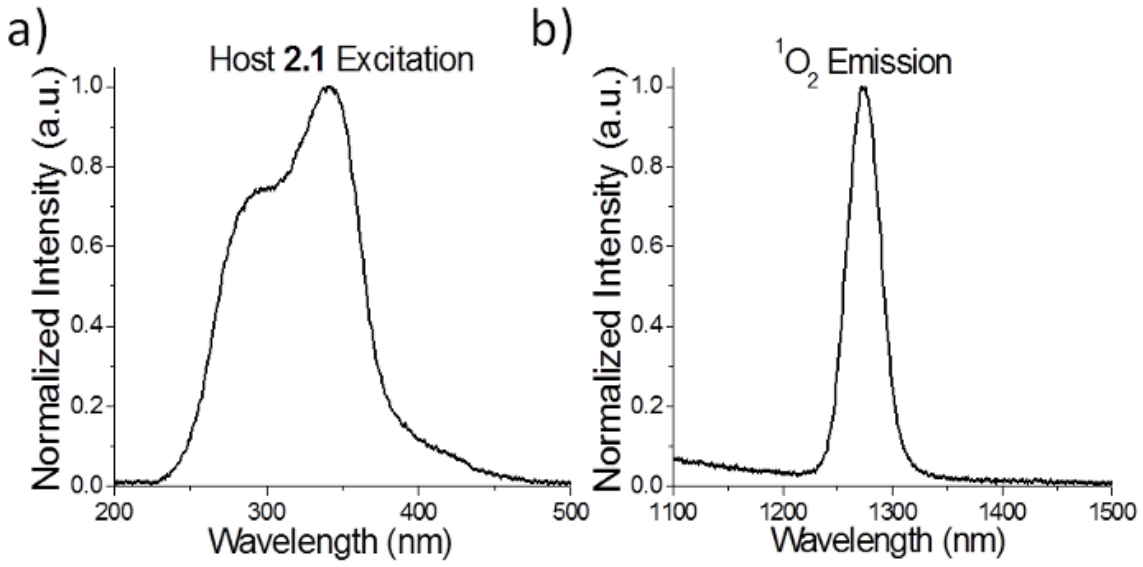

Figure 2.10. The absorption spectra of host **2.1** suspended in oxygenated $CDCl_3$: a) The absorption spectra of host **1** crystal suspension showing a λ_{max} of 345 nm. b) The near IR emission spectra of singlet oxygen produced from the excitation of the host **2.1** crystals at λ_{max}.

2.6. Absorption of small molecules by host 2.1 crystals.

Work done by Adams, Clennen, and others,[1, 4b, 19] suggested simple alkenes react with singlet oxygen to form peroxides and are then subsequently reduced to the corresponding alcohols. Would host **2.1** also mediate the oxidation of small molecules with singlet oxygen? We selected alkenes based on their size and shape, mindful of the size of our hosts' cavity, which forms a linear channel that runs the length of the crystals and has a dimension of ~7 × 4 Å. We then examined the loading of these alkenes into the host **2.1** crystals. First, crystals of **2.1** were soaked in a neat liquid of the alkene for 18 h. The crystals were vacuum filtered and rinsed with hexanes to remove any surface

absorbed alkene and allowed to set on the filter apparatus for 10 min to remove excess hexanes. The loading of guests was monitored by TGA analysis and ^{1}H-NMR. The loading of 2-methyl-2-butene was monitored by TGA and showed a single step desorption curve at 75 ℃ which corresponded to a 3.5 % weight loss (Figure 8). Assuming this weight loss is due to lose of 2-methyl-2-butene, we calculated the host:guest ratio as 3:1 (Table 2.2). An independent assessment of the host:guest ratio was also done by dissolving a sample of the complex (2 mg) in DMSO-δ_6. Figure 2.11a shows the ^{1}H-NMR spectra when integrated gives a host:guest ratio of 3.2:1, similar to the TGA experiment. Also, figure 2.11b shows the ^{1}H-NMR spectra of the host **2.1**•cumene complex, when integrated gives a host guest ratio of 5.6:1. This is the same as what was found by TGA desorption experiments.

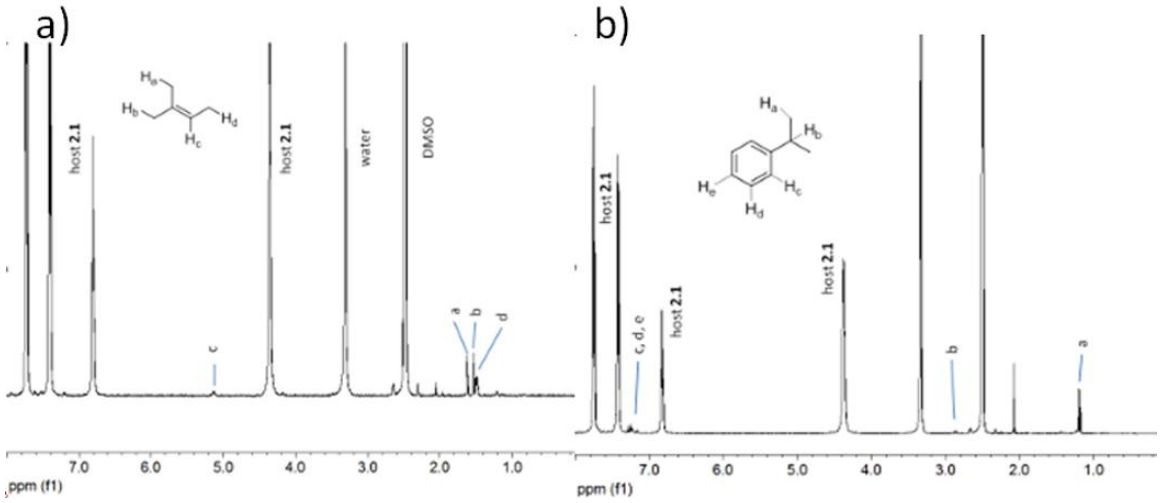

Figure 2.11. NMR spectra of host **2.1**•guest complexes: a) ^{1}H-NMR (400 MHz, δ_6-DMSO) of host **2.1**•2-2methyl-2-butene complex. b) ^{1}H-NMR (400 MHz, δ_6-DMSO) of host **2.1**•cumene complex.

Table 2 summarizes the host:guest loading for a series of guests as determined by TGA. The reported values are an average of at least three binding experiments. In general, the smaller more compact alkenes were loaded in higher ratio with

cyclohexadiene affording a 2:1 host:guest complex, while the styrenes, trans-2-pentene and 2-methyl-2-butene formed ~ 3:1 complexes. The 2,3-dimethy-butene and 3-methyl-2-buten-1-ol displayed ~4:1 host:guest ratios. Cumene and 2-methyl-2-pentene loaded at the lowest ratios, having a 6:1 and 5:1 host:guest ratios respectively. No loading was observed for methyl cyclopentene and methylcyclohexene and 1,2-dimethylcyclohexene.

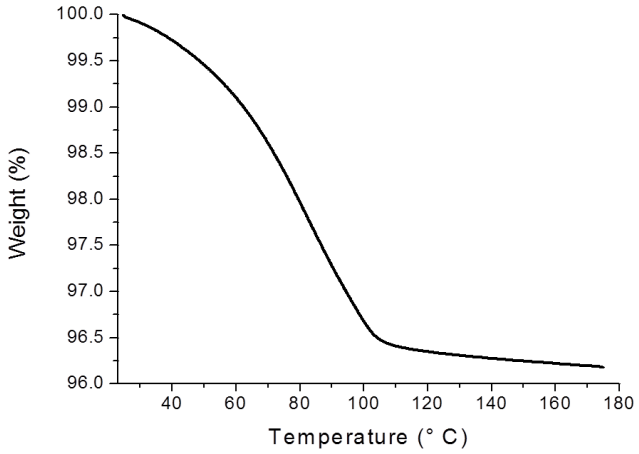

Figure 2.12. TGA graph with a single step desorption of 2-methyl-2-butene from the host:guest complex showing to 3.5% weight loss which corresponds to a 3:1 binding of 2-methyl-2-butene with host **2.1**.

Table 2.2. Absorption of guests by host **2.1** as determined by TGA experiments.

Alkene	Loading (host:guest)[a]	Guest	Loading (host:guest)[a]
2-methyl-2-butene 	3.0:1	cumene (isopropyl benzene) 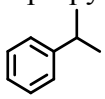	5.6:1
2,3-dimethyl-2-butene 	4.0:1	hex-5-enenitrile 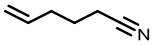	5:1
3-methyl-2-buten-1-ol 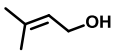	4.0:1	cyclohexadiene 	2:1
2-methyl-2-pentene 	5.0:1	Divinyl benzene 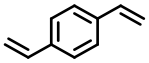	3.5:1
trans-2-pentene 	2.7:1	α-methyl styrene 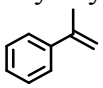	3:1
4-methyl-2-pentene 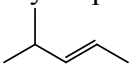	6.5:1	β-methyl styrene 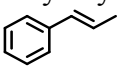	2.5:1

[a] all host:guest ratios are an average of at least 3 separate loading experiments.

Preorganization of guests inside the cavity of our system appears to be a key feature for inducing selectivity inside *bis*-urea host systems,[6c, 7a, 20] although selectivity can also be enhanced by the fit of the products as seen with coumarins in the phenylethynylene host.[6d] We tested the effect of guest encapsulation on the crystallinity of host **2.1**. Host **2.1** crystals freshly recrystallized from DMSO, which typically gave microcrystals of ~ 150 μm x 10 μm as assessed by SEM, which were too small for single crystal analysis, although larger crystals were occasionally observed. Both sizes of crystals were subjected to TGA or heated to 180 °C for 2 h to remove the DMSO solvent and afford the 'empty host'. Unfortunately upon removal of solvent, the large single crystals were not of quality for single crystal analysis. Host **2.1**•DMSO crystals were ground to a powder and examined by powder X-ray diffraction (PXRD) experiments to monitor structural changes upon absorption/desorption of guests. As observed in figure

2.13, the PXRD pattern of the ground crystals was similar to the theoretical pattern, generated from the single crystal structure, suggesting that the ground powder was of single phase with a similar structure.

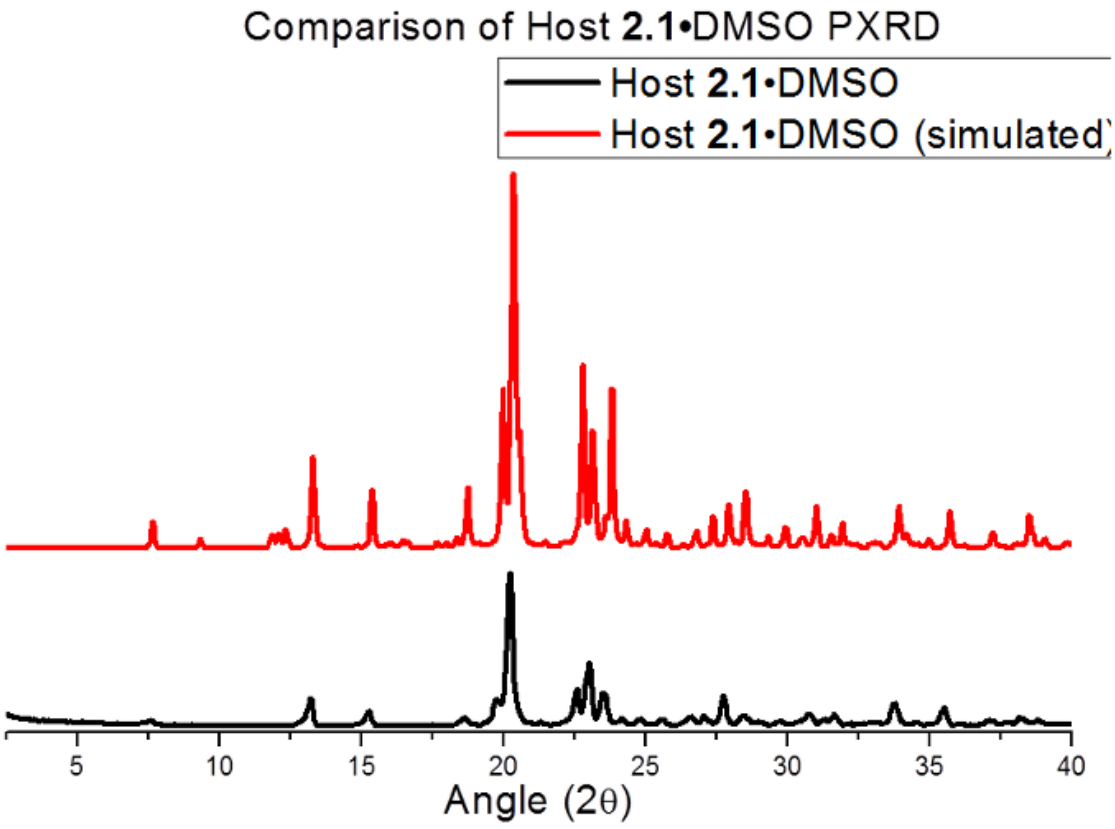

Figure 2.13. Comparison of simulated (top) and experimental (bottom) host **2.1**•DMSO PXRD patterns.

The DMSO was removed by heating, and the powder submitted for PXRD. The 'empty' host **2.1** crystals show a distinct and well-defined pattern that suggests a highly crystalline and ordered system (Figure 2.14, bottom). The host **2.1** powder was treated with 2-methyl-2-butene as described to give the 3:1 host:guest complex, which gave the middle pattern (Figure 2.14). While qualitatively the two patterns appear similar, we

observed differences which include but are not limited to shifts in low angle peaks (7.75 to 7.65 in the complex), a sharpening of the broad band at 13.4, and disappearance or shifting of the 16.10 to a new band at 15.50. The 2-methyl-2-butene guest was removed by TGA (25-180 °C, heating rate 10 °C/min), which gave a pattern nearly identical to the empty host, suggesting that absorption and desorption of guest does not irrevocably change the host structure. Treatment of host **2.1** with 3-methyl-2-buten-1-ol afforded the 4:1 host:guest complex, and treatment of host **2.1** with cumene afforded a 5.6:1 host guest complex. Both of these complexes were also highly crystalline (Figure 2.14, top). Comparison of the three patterns in Figure 2.14 suggest that there are some changes in the structure of the host but that each complex is well-ordered and highly crystalline.

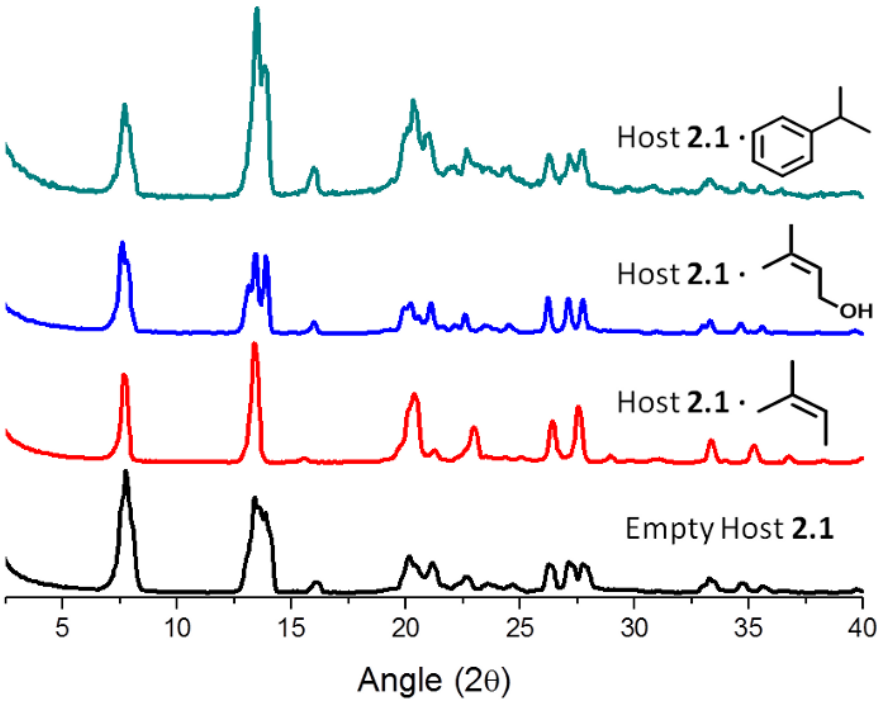

Figure 2.14. Comparison of PXRD patterns of host **2.1** empty, host **2.1**•2-methyl-2-butene complex, host **2.1**•3-methyl-2-butene-1-ol complex and host **2.1**•cumene.

2.7. Oxidation of host 2.1:guest complexes.

Next, we tested if host **2.1** could facilitate the oxidation of these guests within each of these complexes. Host **2.1**•guest complex crystals (10 mg) were loaded into a quartz test tube and purged with dry oxygen for 5 min. The crystals were then irradiated in a Rayonet RPR-200 UV reactor equipped with RPR-3500 lamps for 0-18h. Samples (2 mg) of the host•guest complexes were removed at intervals, dissolved in δ_6-DMSO and analyzed by NMR spectroscopy. Integration of the ^{1}H NMR spectra gave estimates of conversion. Complexes that showed reaction were further analyzed by extracting the guest from the complex with deuterated solvents (sonication 2 x 10 min in CD_2Cl_2 or CD_3CN) and subsequent analysis by GC/MS, ^{1}H-NMR and GC/FID to monitor conversion and product distribution. Interestingly, no quench or neutralization workup was required, yet no peroxides were detected. In most cases, UV-irradiation of the complexes did not facilitate any reaction, and the starting material (2,3-dimethyl-2-butene, the pentenes, α-methyl styrene, divinyl benzene, and hex-5-enenitrile) were simply re-isolated from each complex. UV-irradiation of host **2.1**•β-methyl styrene afforded benzaldehyde, which is the typical product observed with singlet oxygen.[4a, 21]

UV-irradiation of the host **2.1**•2-methyl-2-butene complex facilitates a selective oxidation and gave a product distribution that differs from what is typically observed with oxygen/triplet sensitizer conditions.[4a, 22] After thirty minutes of UV-irradiation in an oxygen rich atmosphere, we observed 50% conversion of 2-methyl-2-butene as estimated by integration of the 1H-NMR spectra in δ_6-DMSO. Monitoring of the ^{1}H-NMR spectra saw the emergence of four new peaks, 1.58 (s), 1.66 (s), 3.90 (t) and 5.25(t) ppm consistent with the formation of an allylic alcohol. Upon increase of the irradiation time,

we observed increased conversion (60% at 1h and 80% at 2h). Longer irradiation times gave no further conversion.

Figure 2.15 shows the GC/MS trace of the extracted products from the oxidation of host **2.1**•2-methyl-2-butene complex, which were identified by co-injection with commercial standards. The 2-methyl-2-butene is not shown due to the high vapor pressure (low boiling point) of the starting material. Integration of the GC/FID also suggested an 80% conversion at 2 h. The first product was the allylic alcohol, 3-methyl-2-butene-1-ol, which was formed in 90% selectivity. The second product corresponded to 3-methyl-2-buten-1-al (10%), which represents the further oxidation of the initial alcohol to the corresponding aldehyde. In comparison, reaction of 2-methyl-2-butene in oxygenated benzene/CH_3CN with benzophenone as a sensitizer give 68% conversion at 3.5 h to afford the oxirane as the major product (65% selectivity) from the [2+2]-cycloaddition as well as two oxygen-ene products in ~ 2:1 ratio (Scheme 2.1 entry 3).[4a, 22] We repeated our experiments at 0 ºC to examine the effect of temperature and observed similar selectivity and conversion. The product of the oxidation of the guest in the host **1**•2-methyl-2-butene complex is one that could arise through a radical mechanism also referred to as an auto-oxidation.[5] This product is also observed upon oxidation of 2-methyl-2-butene using selenium dioxide, where the selenium dioxide coordinates with the alkene and then through a [1,3] sigmatropic rearrangement forms the allylic selenium ester. Subsequent hydroxylation of the ester then results in the allylic alchohol with efficient selectivity of the *E* isomer.[23]

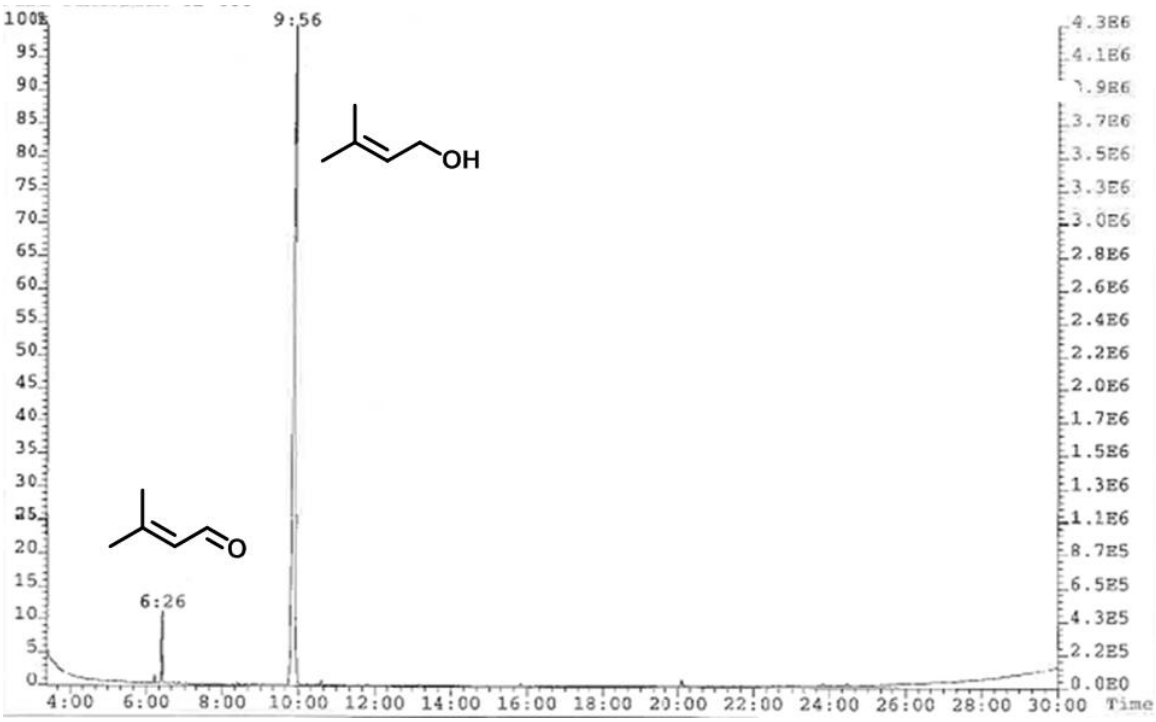

Figure 2.15. GC trace from the UV-irradiation (2 h) of host **2.1**•2-methyl-2-butene under oxygen atmosphere shows two oxidation products.

Scheme 2.1. Oxidation of 2-methyl-2-betutene under selected reaction conditions.

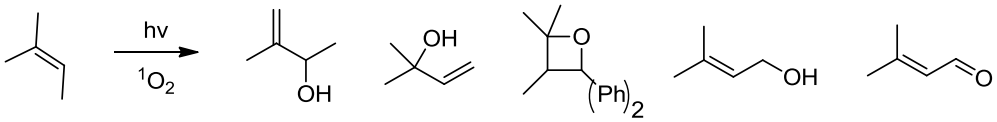

Conditions	% conversion			Selectivity		
Host **2.1**	80	--	--	--	90	10
Host **2.2**	--	--	--	--	--	--
Benzophenone/ benzene CH_3CN[a]	68	12	23	65	--	--
Zeolite/thionin[b]	75	72	28	--	--	--

[a]Conversion after 3.5 h = 68%: Bartlett, P. D., *J. Am. Chem. Soc.*, **1976,** 98, 4193-4200.
[b] isolated yields 65-75% no time reported: Robbins, R., Ramamurthy, V., *Chem. Commun*. **1997**, 1071.

Given the unusual product observed in the oxidation of 2-methyl-2-butene in the complex, we next tested if the host **2.1** could be used as a catalyst to mediate the

oxidation of the alkene in solution. We looked at water, acetonitrile, and water/acetonitrile mixtures due to the relatively short lifetime of singlet oxygen in these solvents (τ^1O_2 ~ 3.5 μs in H_20 versus 54 μs in CH_3CN). In addition, water and water/acetonitrile mixtures should favor absorption of the alkene by the host.[24] The host (1 mg, 5 mole %) was suspended in oxygenated alkene solutions (10 mM, 5 mL). The suspensions were then irradiated under UV light in a Rayonette reactor for 2 h. A sample of the products was extracted and neutralized with excess triphenyl phosphine to reduce the peroxide, and the products were monitored by GC/FID with phenol as an internal standard. The retention times were compared with known standards of the products. We observed no selectivity for 3-methyl-2-butene-1-ol, suggesting that only a low percentage of the reaction occurred in confinement. We observed 25% conversion upon 2 h of UV-irradiation in water and acetonitrile/water mixtures to give only two products: 2-methyl-3-buten-2-ol (47%), 3-methyl-3-buten-2-ol (53%), which are the typical products when benzophenone is used as a sensitizer. None of the 1° allylic alcohol was observed. In acetonitrile after 2h of UV-irradiation, the reaction reached 50% conversion affording 2-methyl-3-buten-2-ol (44%), 3-methyl-3-buten-2-ol (47%), and the 1° allylic alcohol, 3-methyl-2-butene-1-ol (9%). Our hypothesis is that 3-methyl-2-butene-1-ol, a 1° allylic alcohol, is produced when the reaction occurs in confinement. Studies are being conducted to optimize the reaction conditions with other solvent systems such as acetone and acetone/acetonitrile mixtures to promote the catalytic activity. If this process can be further developed and optimized, it might yield a greener catalyst for the formation of pharmaceutical and industrial feedstock.

In order to examine the reaction pathway further, we explored the other substrates that undergo auto-oxidations. Thus, we turned to guests known to oxidize through the radical pathway such as 1,2-dimethyl cyclohexene and cumene.[25] The auto-oxidation of cumene to the benzyl alcohol has been well developed and is known to proceed through a radical mechanism with an initiator to afford α,α'-dimethyl benzyl alcohol, an important industrial product (Scheme 2.2). Our host does not absorb 1,2-dimethyl cyclohexene even upon prolonged (24 h) soaking in the liquid; however, cumene is absorbed to form a 5.6:1 host:guest complex as seen by TGA and ^{1}H-NMR. The host **2.1**•cumene complex was similarly irradiated (0-18 h), samples were removed at intervals, extraction in CD_2Cl_2, and monitored by ^{1}H-NMR and GC/MS. Analysis of figure 2.16 shows that by GC/MS cumene was converted (69%) to three products: α,α'-dimethyl benzylalcohol (71%), acetophenone (25%) and α-methyl styrene (4%). The product formation from the oxidation of cumene inside the host **2.1** system suggests that the oxidation is proceeding through a radical mechanism.[25] In the oxidation of cumene, the work done by Mayer *et al.* showed that the mechanism occurs through an initial hydrogen atom transfer to the ruthenium oxo group that is then trapped by the ruthenium complex. Solvolysis of the ruthenium cumyl complex then gives the α,α'-dimethyl benzylalcohol at 67 % conversion.[25a] Also, the work of Zeng *et al.* showed that the use of copper oxide nanoparticles can be used as a catalyst to produce α,α'-dimethyl benzylalcohol in 7 h at 93 % selectivity. They also displayed that the nanoparticles are active at lower temperatures (318-358 °C) and retain their activity after prolonged use (6 cycles).[25b]

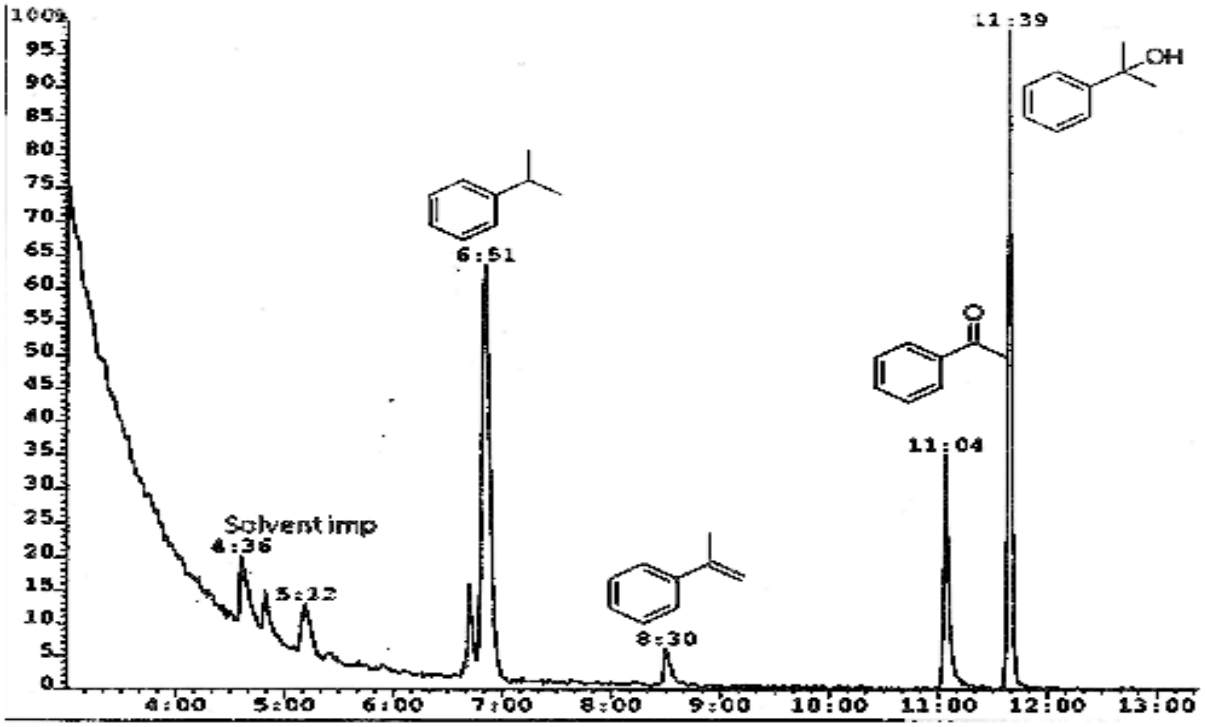

Figure 2.16. GC trace of oxidation products isolated after UV-irradition (18 h) of host **2.1**•cumene under an oxygen atmosphere.

Scheme 2.2. Oxidation of cumene under selected reaction conditions.

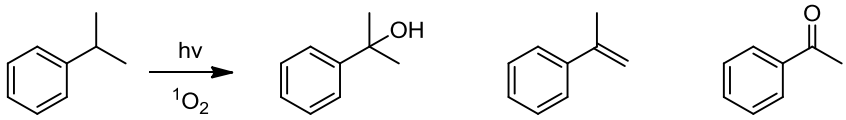

Conditions	% conversion	Selectivity		
Host 2.1	69	71	4	25
Ru $^{IV}O^{+2}$ /CH_3CN[a]	67	69	13	18
CuO nanoparticle[b]	44.2	93	2.5	4.5

[a] Along with trace amounts of 2-phenylpropanal and 2-phenylpropenal; Bryant, J. R.; Matsuo, T.; Mayer, J. M. *Inorg. Chem.* **2004**, *43*, 1587.
[b] Zhang, M.; Wang, L.; Ji, H.; Wu, B.; Zeng, X. *J. Nat. Gas Chem.***2007**, *16*, 393

2.8. EPR experiments.

Given that host **2.1** facilitates the production of singlet oxygen, binds guests, and affords oxidation products that are usually observed through radical mediated mechanisms, we next investigated if the host itself might give radicals. The formation of a stable host radical during the UV-irradiated might also explain our observations of the curiously shortened phosphorescence lifetime in solid host **2.1**. The literature provides examples where the parent benzophenone radical is observed; however, it is certainly not long-lived and has not been observed at room temperature. The benzophenone radical has been detected through radical trapping with nitroxides,[15b, 26] through H-abstraction,[27] at low temperatures (2 or 77 K)[15a, 15c, 28] or through time-resolved ESR measurements in the nanosecond timescale.[15d, 29] In the case of host **2.1**, our experiments suggest that such a radical formed after UV-irradiation might be significantly stabilized and detected at room temperature by electron paramagnetic resonance (EPR). Freshly evacuated crystals of host **2.1** (10 mg) were loaded into an EPR tube and kept in the dark for a week. The sample was purged with argon gas for 30 min in the dark and the EPR spectra recorded (Figure 2.17, black line), which shows no signal. The sample was then left on the bench top for 30 minutes under typical room lights (fluorescent). Surprisingly, the EPR spectra (Figure 2.17, red line) shows a peak, indicative of a radical with a g-factor of 2.0049, which is in the range for a lone unpaired electron in an organic substrate.[30] Next, the sample was exposed to UV radiation in a Rayonet reactor equipped with 16 x 120 W lamps (350 nm) for 30 min. The EPR spectra shows a single peak with g= 2.0051. Benzophenone was also similarly treated, and as expected, no radical was observed at room temperature.

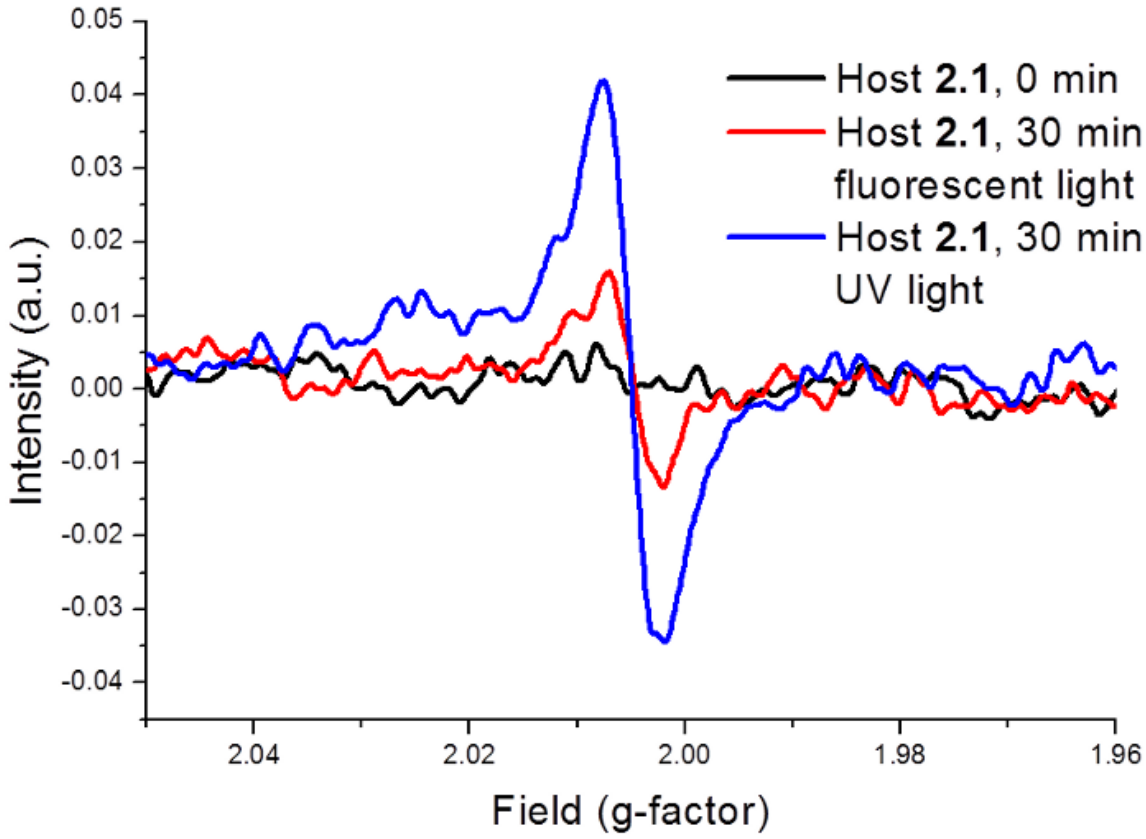

Figure 2.17. Generation of radicals from host **2.1** crystals as monitored by EPR. Host **2.1** was kept in the dark for 1 week (black line), then exposure to fluorescent lighting (30 min, red line), and finally UV-irradiated (30 min, blue line).

We next tested if the host **2.1** radical can be generated under ambient air. Host **2.1** was irradiated (1 h) in Rayonet reactor, figure 2.18 shows that a similar EPR spectra is observed before and after UV irradiation. Analysis of the EPR spectra results in the host **2.1** sample having an identical g-factor to that of the host **2.1** irradiated under argon.

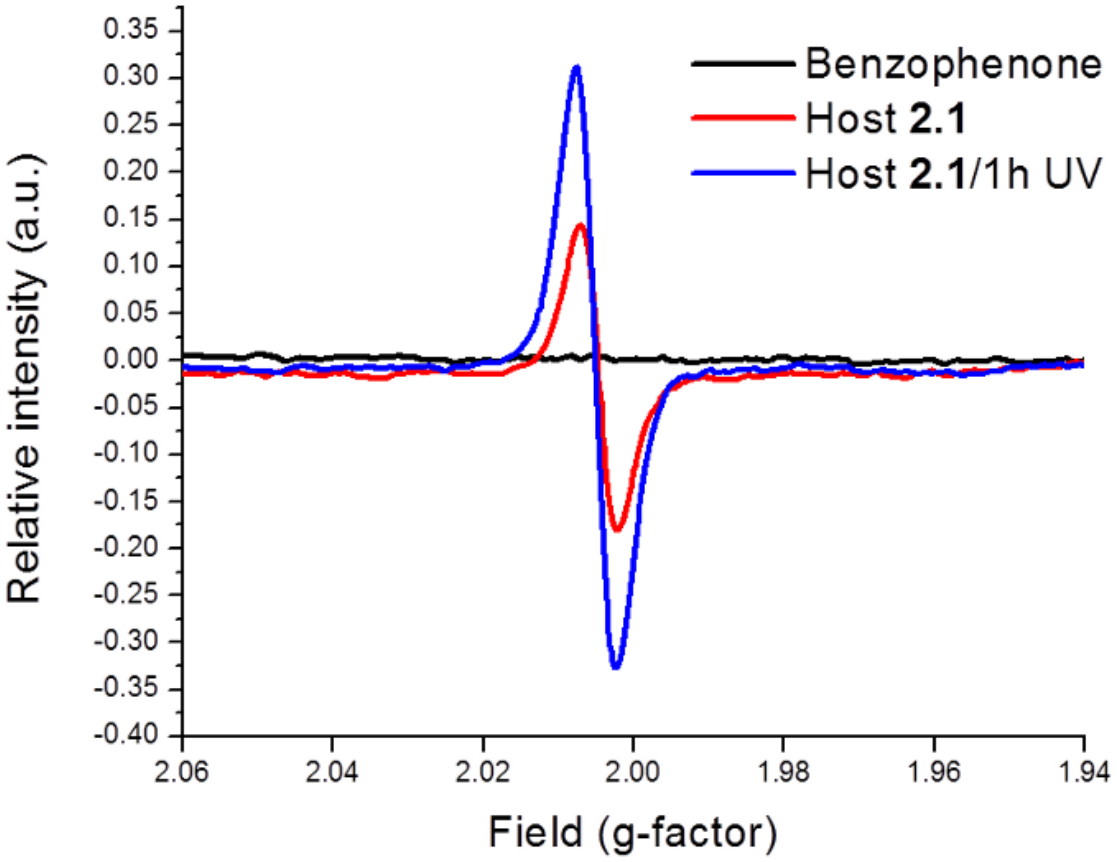

Figure 2.18. Comparison of EPR spectra of benzophenone, host **2.1** (ambient conditions), and host **2.1** (1 h UV exposure).

Next, we kept the sample in the dark and monitored the EPR over the following week to estimate the time needed for the radical to be completely quenched. The EPR signal persisted for days, suggesting that host **1** generates an unusually stable radical that is not quenched by oxygen, nitroxide, or hydroxide radicals from the atmosphere. Stable radicals are of interest for their material properties, in catalysis and for living polymerizations. Stable or persistent families of organic radicals include nitroxide and nitronyl nitroxide radicals,[31] heterocyclic thiazyls,[32] triphenylmethyl,[33] and verdazyl radicals.[34]

Our hypothesis is that selective oxidation of cumene and 2-methyl-2-butene facilitated by our host may proceed via a radical process. Could the radical be similarly observed in the corresponding solid host•guest complexes? Figure 2.19 compares the EPR spectra obtained for the host **2.1**•cumene complex and host **2.1** after each of these solids were UV-irradiated for 1 h at r.t. under oxygen.

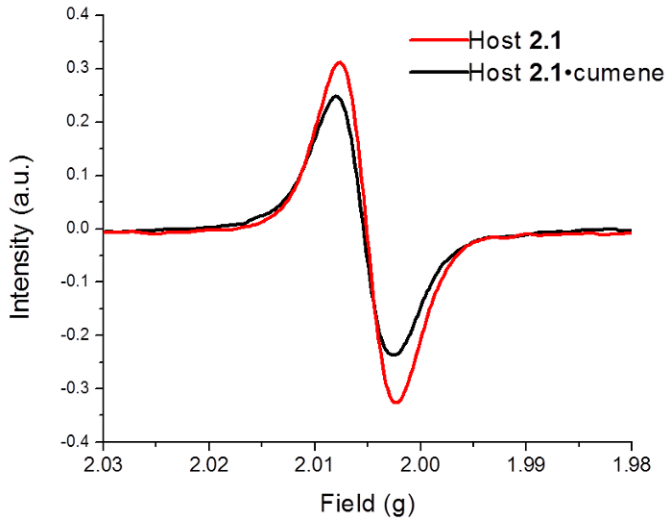

Figure 2.19. EPR spectra of host **2.1** and host **2.1**•cumene complex after 1 h UV radiation.

In each case, a strong signal was observed at g = 2.0051. In order to probe the effect of different guest inside the host**2.1** system the EPR of each of the reactive guests were examined. Figures 2.20 and 2.21 show the EPR spectra of the host **2.1**•cumene and host **2.1**•2-methyl-2-butene complexes before and after UV irradiation, which resulted in an EPR signal similar to that of the host **2.1** without guest. Therefore, this suggests that the radical is not influenced to a great degree by the guest encapsulated. In light of this evidence, it may be possible to include a guest that can utilize the radical in selective reactions.

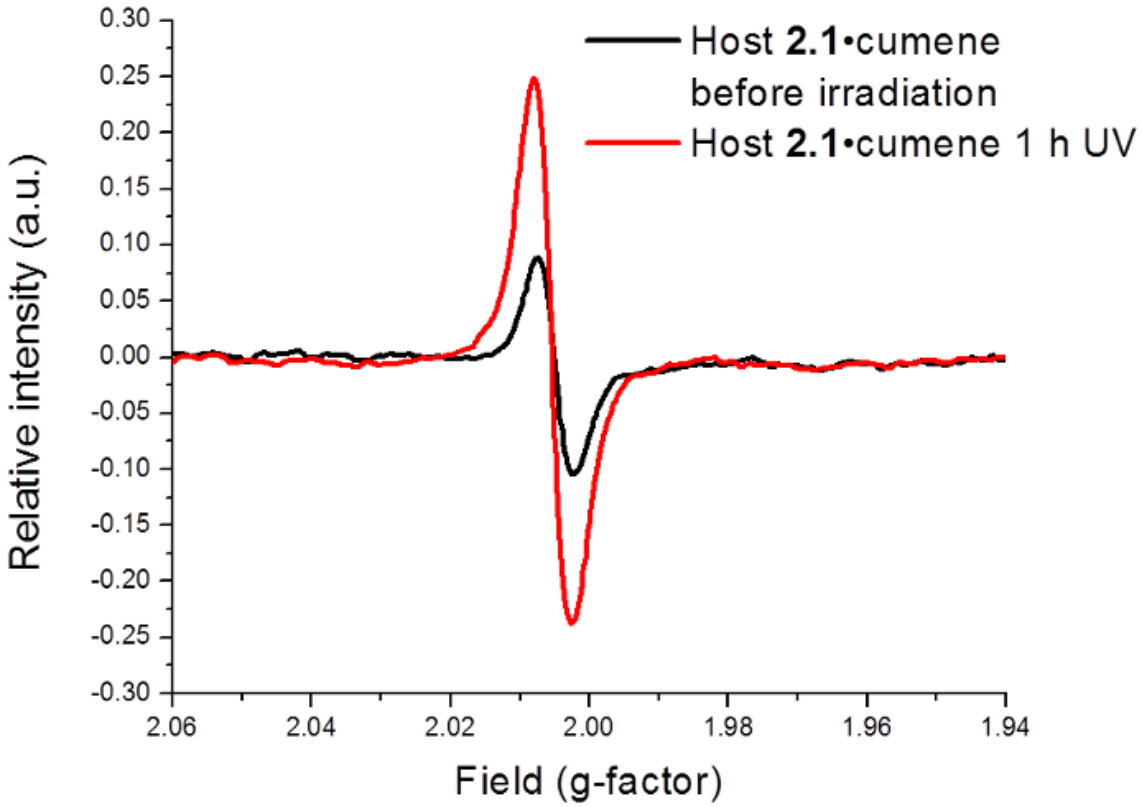

Figure 2.20. EPR spectra of host 2.1•cumene complex before (black) and after (red) UV irradiation.

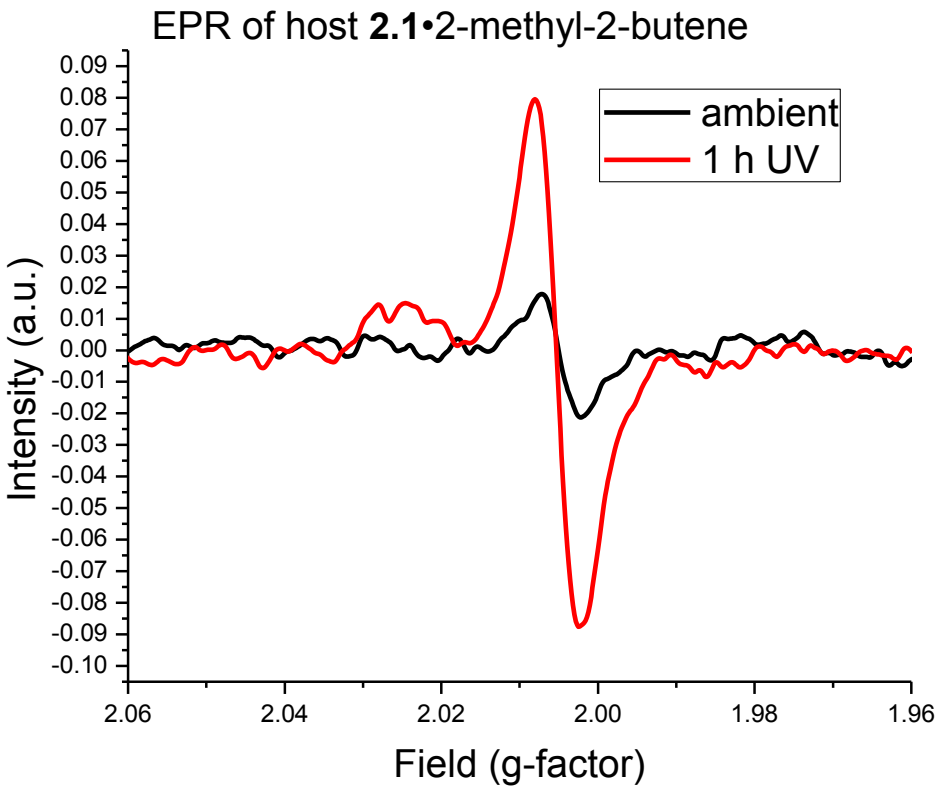

Figure 2.21. EPR spectra of host **2.1**•2-methyl-2-butene before and after UV irradiation.

Taken together, the data from the EPR experiments suggests that the incorporation of benzophenone into a cyclic *bis*-urea appears to have a stabilization effect on the ketyl-radical that is typically formed in the excitation of benzophenone producing a stable radical at room temperature. The lack of splitting of the peaks suggests that there is no strong coupling with neighboring radicals or nuclei and that the radical is stabilized either through resonance or fast exchange H abstraction or a combination of the two.[29a, 35] A collaborative effort is underway to investigate the nature of this radical computationally to understand its origin and explain its stability. We surmise that the assembled system results in conditions that stabilize the radical, either through a distorted

geometry or through a quick hydrogen abstraction with neighboring columns that might account for both the surprisingly stable radical and the lack of coupling.

2.9 Future Work.

Further testing is in progress to determine whether it is the production of singlet oxygen or the formation of the radical that is responsible for the selectivity observed in this host or if it is some combination of the two pathways. Currently, we are collaborating with Prof. Rassolov to investigate the structure of radicals within the columnar assembly. DFT calculations will be used to investigate the structure of the radical in the monomeric host and in assembled columns of three to five macrocycles. We will compare the minimized conformations of these systems to the conformation observed in the crystal structure. This, along with a prediction of the local spin densities by DFT calculations, should provide insights about the structure of the radical as well as provide some explanation for its unusual stability. Alternatively, the radical stability could also be due to close packing of the columns, which might not be observed in the analysis of a single column.

Another method to examine the type of radical is to use a higher frequency EPR such as Q- (35 GHz) or W-band (95 GHz) EPR to provide higher resolution spectra and to see the possible coupling that may not be visible with X-band (9 GHz) spectrometer that was used for our experiments in section 2.8.[36] A higher frequency EPR instrument could provide higher resolution spectra and detect coupling bands that are too weak for X-band frequency. A better understanding of the nature of the radical could give us insight for optimizing the conditions (solvent, temperature, etc.) of oxidation reactions in

solution. For example, solution conditions can be tuned to further stabilize the radical or conditions can be selected to inhibit the reaction outside the channel. These efforts to engineer the system to afford a more effective oxidation catalyst for small alkenes in solution.

We also plan to explore this system to sensitize the oxidation of other small molecules as well as to mediate radical polymerizations of encapsulated monomers. For example, lactones and lactams are currently being investigated by the Wiskur group for preparing enantioenriched compounds through silylation-based kinetic resolutions reactions. Small unsubstituted lactones, such as tetrahydro pyranone, are difficult to oxidize at the alpha site and show poor selectivity and low conversion.[37] Scheme 2.4 shows the typical method for direct oxidation of lactone through the lithiation to form the enolate and subsequent substitution. This method tends to be low yielding and unselective and affords both enantiomers as well as ring opened products.

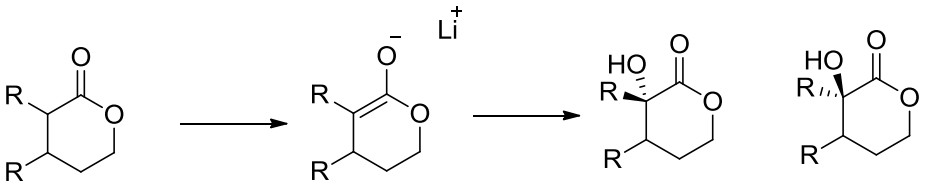

Scheme 2.3. Typical method for oxidation of lactone shows the lithiation and subsequent substitution of the enolate to give both the R and S isomers of the hydroxy lactone among other byproducts.

One method Renaud *et al.* are using to avoid the selectivity and reactivity problem of lactones is through iodine substitution and subsequent radical reaction to substitute the iodine with hydroxide.[38] Another approach is a selective Bayer-Villiger oxidation using organic seleninic acids as demonstrated by Sheldon et al.[39] In their work, they show that the four or five member ketone selectively produces the corresponding lactone by a

Bayer-Villiger oxidation with seleninic acid formed from organic selenium oxide and peroxides. While promising, this route still involves toxic selenium and high amounts of waste and leave room for improvement.

Another application of the host **2.1** system would be to induce the isotactic radical polymerization of encapsulated monomers. It is challenging to synthesize isotactic polymers. Isotactic versus atactic polymer show differences in their glass transition temperatures and in their mechanical behaviors.[40] The encapsulated polymers may show greater stability controlled morphology and enhanced optical properties and conductivity.[41] Indeed encapsulated dyes, such as the squaraine rotaxanes from Bradley Smith's group, show decreased susceptibility to chemical and photodegradation.[42] Conjugated polymers encapsulated in nanotubes would also be expected to show increased stability and could be of use in nanoscale fabrication of conductors and capacitors. Some common polymers for conductive applications include polythiophene and polypyrole. Ikeda and Higuhci have shown that the polyrotaxane of polythiophene shows faster chromic response to electrical stimulation than polythiophene.[43] We expect that encapsulation of the polymers in the host **2.1** system would show similar responses. Preliminary work with the host **2.1** system shows that both these monomers can be loaded at 2:1 host:guest ratio by TGA and ^{1}H-NMR to give host **2.1**•thiophene and host **2.1**•pyrole complexes. Encapsulation of these monomers within the channel of host **2.1** should limit their orientation and may be beneficial for radical polymerization. Figure 2.22 shows the general outline of the loading of pyrole and the polymerization that is expected. Indeed, the crystals of the host **2.1**•pyrole when exposed to a ferrous chloride solution did turn black in color. Further characterization of these crystals is in progress.

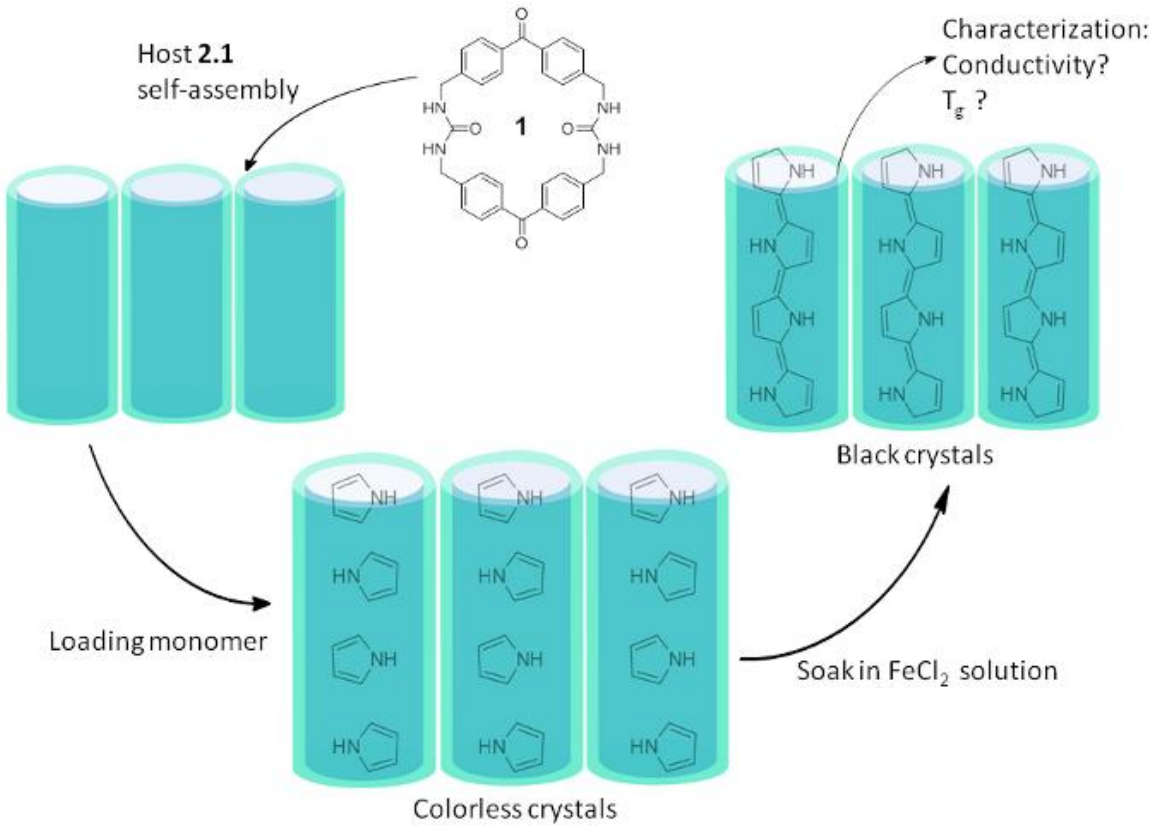

Figure 2.23. Self-assembly of host **2.1** into columnar porous assemblies allows for the absorption of pyrole and thiophene monomers both at 2:1 host:guest ratios. The arrangement of the monomers may allow for the polymerization through radical pathway resulting in structurally characteristic polymers.

Finally, another possible application for the host **2.1** system is in the production of a singlet oxygen bubbler similar to that of Greer *et al.*[44] Figure 2.23a shows the setup of the oxygen bubbler with the incorporation of phthalocyanine crystals into a membrane, irradiation of the phthalocyanate infused membrane with a flow of oxygen produces singlet oxygen bubbles that are size dependant on the porosity of the membrane. This singlet oxygen then diffuses into the aqueous media that the oxygen is bubbled into resulting in toxicity toward *E. coli* in the aqueous medium. We have demonstrated the ability of the host **2.1** system to produce singlet oxygen and selectively oxidize guests inside. Figure 2.23b shows the proposed setup of host **2.1** system to produce a singlet

oxygen bubbler. We hypothesize that crystallization of the host **2.1** system inside a capillary could forgo the need of a membrane. The porosity of the crystals themselves with average pore size of ~ 4 × 7 Å would regulate the size of the singlet oxygen bubbles and eliminate the need for a membrane. To investigate the feasibility of this singlet oxygen bubbler, the host must first be crystallized inside a capillary. Next, we would need to demonstrate that UV-irradiation of the capilliary produces singlet oxygen under a steady flow of oxygen (g). Such a system might have applications in chemical lithography and in bacterial sterilization?

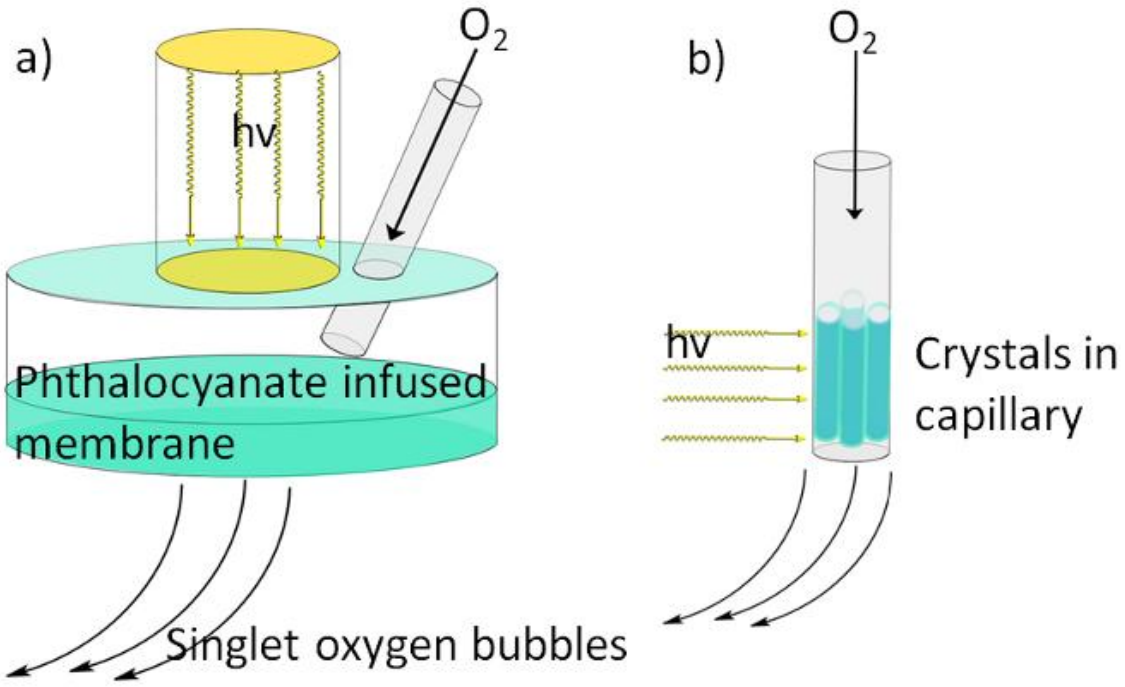

Figure 2.24. Schematic representations of singlet oxygen bubblers: a) Singlet oxygen bubbler by Greer *et al.* with the phthalocyanate crystal infused membrane sensitizing the production of singlet oxygen as oxygen gas is flowed through the apparatus. b) Graphic representation of setup of crystals of host **2.1** inside a capillary that can produce singlet oxygen upon irradiation of oxygen gas flow through the capillary.

2.10 Conclusion.

Incorporation of benzophenone into a cyclic *bis*-urea system resulted in a macrocycle that forms crystalline columnar assemblies through the self-assembly of the ureas. The resulting macrocycle monomer showed an increase in its phosphorescent quantum yield in solutions and dramatic quenching upon assembly into the columnar structures in the solid-state. Studies of the solid-state lifetime of our host displayed a sub-ns decay time suggesting the solid-state structure is more prone to quenchers such as molecular oxygen and atmospheric water or to non-radiative pathways such as formation of a stabilized radical. Indeed, EPR studies demonstrate that host **2.1** does give a stable radical when UV-irradiated under Argon or at atmospheric conditions. Even ambient fluorescent light was enough to generate the radical, which was stable for days. In contrast, the parent benzophenone does not form a stable radical under ambient conditions. Our hypothesis is that it is the supramolecular assembly that gives rise to this stabilized radical. Other supramolecular assemblies, such as thin films of 1,4,5,8-naphthalene diimides and zirconium also show persistent radicals.[45]

Despite its low quantum yield and short lifetime, we found that host **2.1** could be used to readily generate singlet oxygen both in solution and also when the solid host was irradiated under oxygen atmosphere. Although host **2.1** crystals readily absorbed of small molecule guests to form complexes, only some of these complexes were reactive. The complexes were UV-irradiated under an oxygen atmosphere at room temperature and then extracted into deuterated solvent without any additive to neutralize peroxides normally observed in singlet oxygen-ene reactions. In most cases, UV-irradiation of the complexes did not facilitate any reaction, and the starting materials were re-isolated.

However, three complexes facilitated the oxidation of guests in the solid state. Host **2.1**•β-methyl styrene afforded benzaldehyde, which is the typical product under singlet oxygen. Host **2.1**•2-methyl-2-butene complex facilitated a selective oxidation in 80% conversion to afford the 1° allylic alcohol, 3-methyl-2-butene-1-ol in 90% selectivity. This product is not typically observed using organic sensitizers. Furthermore, host **2.1**•cumene complex was oxidized in 69% conversion under similar conditions to α,α'-dimethyl benzylalcohol at 71% selectivity. Cumene is known to undergo auto-oxidation via a radical process. Thus, our hypothesis is that host **2.1** acts through a dual role of singlet oxygen sensitization and radical formation the benzophenone *bis*-urea macrocycle to selectively oxidize 2-methyl-2-butene and cumene within host:guest complexes.

2.11. Experimental.

2.11.1. Materials and instruments.

Triazinanone was synthesized as previously described.[46] All chemicals were purchased from Aldrich or TCI Inc. and used without further purification. ^{1}H-NMR and ^{13}C-NMR spectra were recorded on Varian Mercury/VX 300 and 400 NMR spectrometers. The thermometer for melting point was not calibrated. Photoreactions were carried out in a Rayonet RPR-200 UV reactor equipped with RPR-3500 lamps. The temperature of the set up was kept below 25 ºC unless otherwise stated. The Scanning Electron Microscopy image was recorded on a Quanta 200 ESEM with accelerating voltage of 30 kV. The X-ray powder diffraction data were collected on Rigaku Dmax- 2100 & 2200 powder X-ray diffractometers using Bragg-Brentano geometry with CuKα radiation with step scans of 0.05 º over 2-40 º 2θ. Thermogravimetric analysis (TGA) was carried out on TA

instruments SDT-Q600 simultaneous DTA/TGA at a rate of 10 º min^{-1} from 25 – 180 º C under ultrapure helium. Absorption and fluorescence data for the solution was recorded on Molecular Devices Spectramax M2. Solid state absorption and emission spectra were recorded on a Horiba Flourolog 3 equipped with an F-3000 fiber optic platform and a Quanta-φ integrating sphere. Lifetime studies were conducted with an Edinburgh Instruments time correlated single photon counting (TCSPC) system with a 372 nm picoseconds pulsed diode laser (LDH-P-375) with laser pulse of 110 ps (FWHM and a high speed Microchannel Plate Photomultiplier Tube (MCP-PMT. Hamamatsu R3809U-50) as the detector. The steady state phosphorescence emission and excitation spectra of $^1O_2$ (generated by a suspension of host **2.1** in deuterated $CDCl_3$) were recorded by using a HORIBA Jobin-Yvon IBH FL-322 Fluorolog 3 spectrometer equipped with excitation and emission double-grating monochromators (1.8 nm/mm dispersion, 1800 grooves/mm blazed at 500 nm in the visible spectral range; 3.9 nm/mm dispersion, 830 grooves/mm blazed at 1200 nm in the NIR spectral range) equipped with an air-cooled Hamamatsu H10330-75 (InP/InGaAs) PMT detector. Emission spectra were corrected for detector sensitivity and emission monochromator blaze angle by the software provided with the equipment; a baseline correction was also performed. Excitation spectra were corrected for source profile (450W xenon lamp) and emission monochromator blaze angle, by collecting the reference signal with a built-in calibrated photodiode. Electon paramagnetic resonance (EPR) spectra were recorded on a Bruker EMX plus equipped with a Bruker premium X X-band microwave bridgehead and Xenon software (v 1.1b.66).

2.11.2. Synthesis of benzophenone *bis*-urea macrocycle (host 2.1).

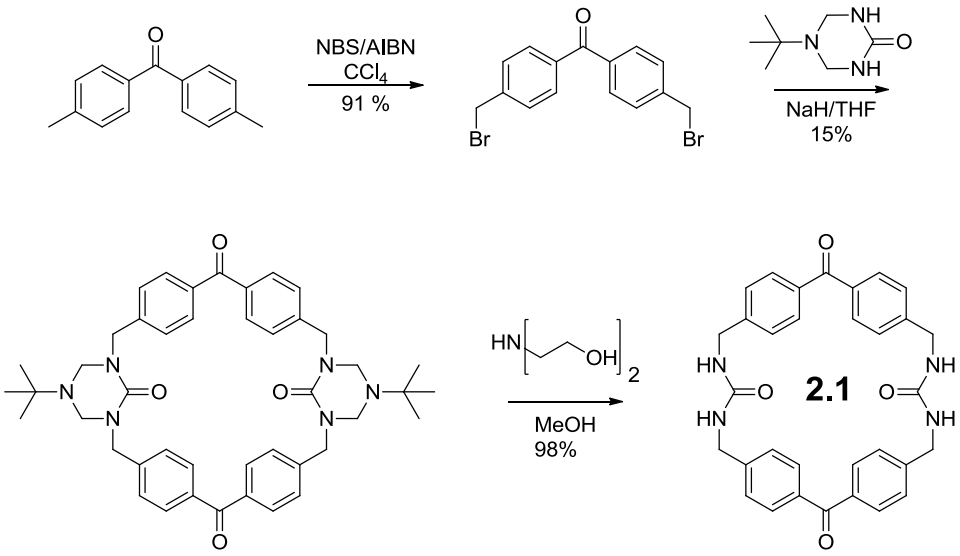

Scheme 2.4. Synthesis of the *bis*-urea benzophenone macrocycle (host **2.1**). Reagents and Conditions: 4,4-dimethylbenzophenone was reacted with N-bromosuccinimide **(**NBS) and 2,2'-azo*bis*(isobutyronitrile) (AIBN) in CCl_4 to produce 4,4'-*bis*(bromomethyl) benzophenone. This was then reacted with triazinanone and NaH in refluxing THF to give the cyclized product. The protected macrocycle was deprotected in an acidic diethanol amine aqueous/methanol mixture to yield the desired *bis*-urea benzophenone macrocycle (**2.1**).

2.11.3. Synthesis of 4,4'-*bis* (bromomethyl) benzophenone.

Commercially available 4,4'-benzophenone (10.27 g, 49 mmol) was reacted with N-bromo succinimide (NBS) (18.26 g, 103 mmol) and 2,2'-azo*bis*(isobutyronitrile) (AIBN) (0.080 g, 0.488 mmol) in refluxing carbon tetrachloride (130 mL) for 18 h. The reaction mixture was cooled to rt then cooled in an ice bath and the precipitate was filtered off and washed with cold methylene chloride (3 x 10 mL). The product was purified by flash chromatography (1:9 ethyl acetate: hexanes) to afford a pale yellow solid (16.41 g, 91%) ^{1}H-NMR: (300 MHz; $CDCl_3$) δ= 7.78 (4H, d, *J*=8.1), 7.51(4H, d, *J*=8.4), 4.54 (4H, s); ^{13}C-NMR: (75 MHz, $CDCl_3$) δ= 195.46, 142.52, 137.45, 130.75,

129.25, 32.43. HRMS (EI): [M^+] Calculated for formula $C_{15}H_{12}Br_2O$: 365.9255, Found: 365.9244.

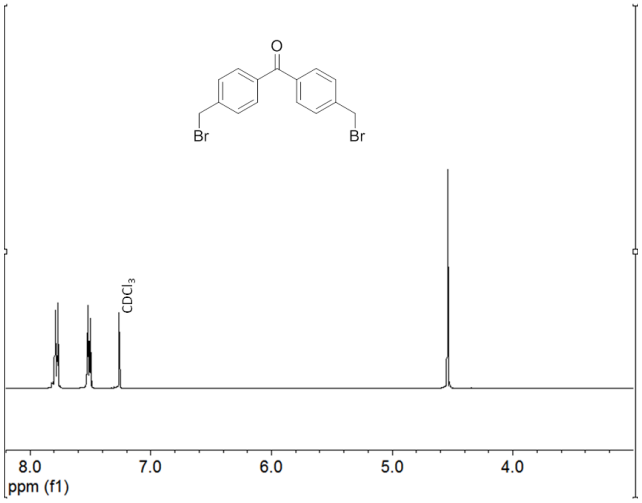

Figure 2.25. ^{1}H NMR (300 MHz, $CDCl_3$) of 4,4'-*bis*(bromomethyl) benzophenone.

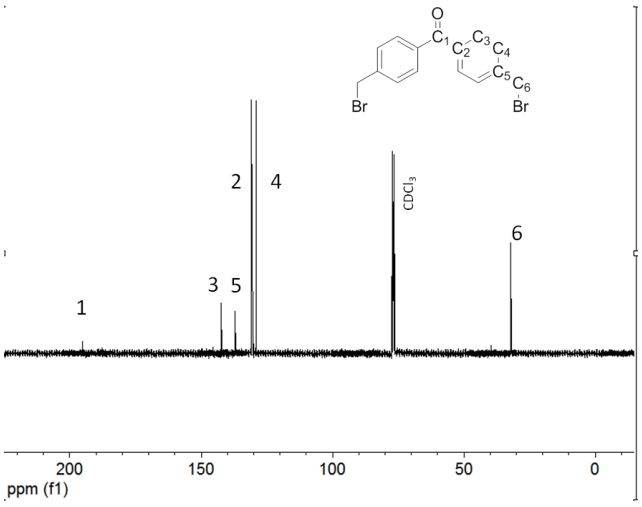

Figure 2.26. ^{13}C NMR (75 MHz, $CDCl_3$) of 4,4'-*bis*(bromomethyl) benzophenone.

2.11.4. Synthesis of triazinanone protected *bis*-urea benzophenone macrocycle.

All glassware was dried by heating under vacuum. Triazinanone (1.00 g, 6.36 mmol) and NaH (60 % suspension in mineral oil, 0.916 g, 38.16 mmol) were heated to

reflux in freshly distilled dry THF (300 mL) under nitrogen atmosphere for 1.5 h. Then the suspension was cooled to room temperature and a solution of 4,4'-*bis*(bromomethyl)benzophenone (2.34 g, 6.36 mmol) in dry THF (200 mL) was added drop-wise over 1 h. The reaction mixture was heated to reflux for 48 h. Upon completion, the reaction mixture was cooled to room temperature and excess NaH was neutralized with 1N HCl (10 mL) and distilled water (100 mL). The reaction mixture was reduced to ~100 mL *in vacuo* and the crude product was extracted with methylene chloride (3 × 100 mL). Combined organic layers were washed with brine and dried over anhydrous Mg_2SO_4. The product was purified by flash chromatography with methanol:ethyl acetate (1:9) eluent as a white solid (0.694 g, 15%). mp= 230-233 °C; ^{1}H-NMR: (300MHz, $CDCl_3$) δ= 7.81 (8H, d, *J*=8.4), 7.45 (8H, d, *J*=8.1), 4.36 (8H, s), 1.10 (18H, s); ^{13}C-NMR (75 MHz, $CDCl_3$) δ= 196.02, 155.69, 143.52, 136.62, 131.00, 127.35, 62.99, 54.35, 49.24, 28.45. HRMS (EI): [M^+] calculated for formula $C_{44}H_{51}N_6O_4$: 727.3972, Found: 727.3981.

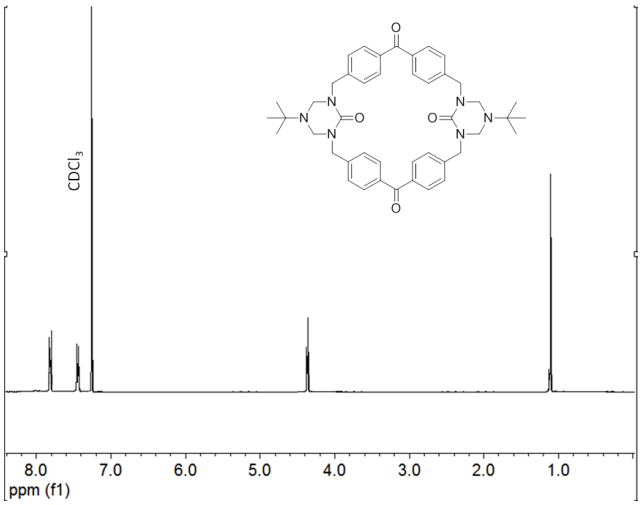

Figure 2.27. ^{1}H NMR (300 MHz, $CDCl_3$) of protected *bis*-urea macrocycle.

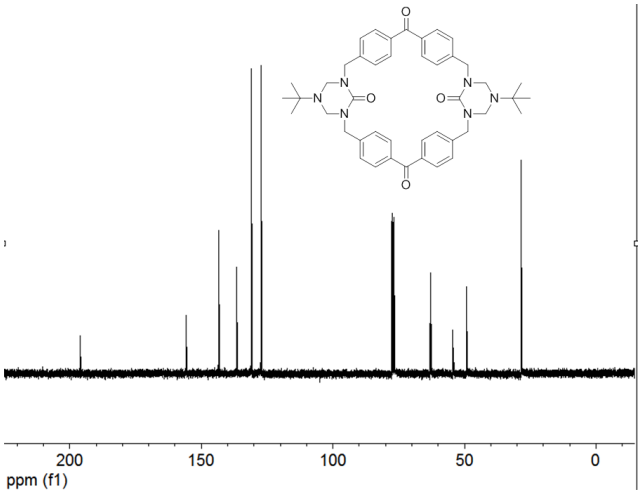

Figure 2.27. ^{13}C NMR (75 MHz, $CDCl_3$) of protected *bis*-urea macrocycle**.**

2.11.5. Deprotection of *bis*-urea benzophenone macrocycle to give macrocycle 2.1.

Triazinanone protected *bis*-urea macrocycle (0.200 g, 0.275 mmol) was heated to reflux in 1:1 20% diethanol amine (pH~2 with conc. HCl)/water:methanol solution (100 mL) for 48 h. The product **2.1** precipitated out of solution as a white powder. The powder was vacuum filtered and washed with 1N HCl (20 mL) and distilled water (3 × 100 mL) then dried *in vacuo* (0.144 g, 98 %). Decomposes at 340 °C; ^{1}H-NMR (300MHz, δ_6-DMSO) δ= 7.73 (8H, d, *J*=8.1), 7.41 (8H, d, *J*=8.1), 6.81 (4H, t), 4.36 (8H, d, *J*=5.4); ^{13}C-NMR: (75 MHz, δ_6-DMSO) δ= 196.02, 155.69, 143.52, 136.62, 131.00, 127.35, 62.99, 54.35, 49.24, 28.45. HRMS (EI): [M^+] Calculated for formula $C_{32}H_{28}N_4O_4$: 532.2111, Found: 532.2096.

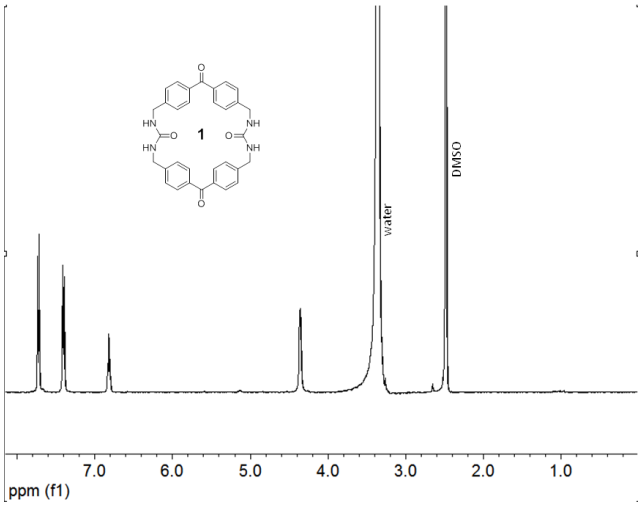

Figure 2.29. ^{1}H NMR (300 MHz, δ_6-DMSO) of benzophenone *bis*-urea macrocycle (host **2.1**).

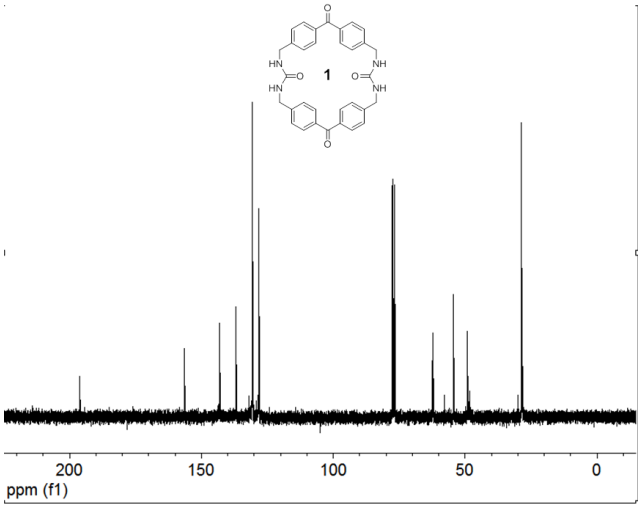

Figure 2.30. ^{13}C-NMR (75 MHz**,** δ_6-DMSO) of benzophenone *bis*-urea macrocycle (host **2.1**).

2.11.6. Recrystallization and preparation of host 2.1 crystals.

Host **2.1** (50 mg) was stirred in hot DMSO (20 mL) in a pressure tube. The mixture was heated to 130 ℃ untill all was dissolved. The solution was then allowed to

slow cool at a rate of 1 °C h^{-1} to room temperature. The colorless needle crystals were vacuum filtered and heated to 180 °C for 1-2 h to remove any residual DMSO solvent. The crystals were then stored in a desiccator until used.

2.11.7. Fluorescence and Quantum yield measurements.

Fluorescence and absorbance for solutions were measured on a Molecular Devices Spectramax M2. The concentrations of all solutions during quantum yield measurements were such that the absorbance of the band at 310-380 nm was never above 0.1 Abs. Solutions were made by addition of sequential 20 µL aliquots of a 0.10 mM benzophenone or host **2.1** solution to 1.50 mL of DMSO. The absorbance and emission were recorded after each addition.

The solid state luminescence was measured on a Horiba Fluorolog 3 equipped with an F-3000 fiber optic platform and Quanta-φ integrating sphere. The powder samples (10 mg) of benzophenone and host **2.1** were loaded into the Spectralon™ coated sample cup and loaded into the integrating sphere. The corrected emission spectra were recorded for the benzophenone, host **2.1**, and the empty integrating sphere.

2.11.8. Lifetime studies.

The lifetime measurements were conducted with the help of Kyril Solntsev from Georgia Tech. The solid samples of benzophenone and host **2.1** (~2 mg) were sandwiched between two quartz slides. The Phosphorescence lifetimes were measured using an Edinburgh Instruments time-correlated single photon counting (TCSPC) system. The system used a 372 nm picosecond pulsed diode laser (LDH-P-C-375) with laser pulse of 110 ps (FWHM). The detection system consisted of a high speed MicroChannel

Plate PhotoMultiplier Tube (MCP-PMT, Hamamatsu R3809U-50) and TCSPC electronics. The repetition rate varied from 1 KHz for benzophenone to 2.5 MHz for host **2.1**.

2.11.9. Singlet oxygen phtotoluminescence studies.

The production of singlet oxygen by host **2.1** was monitored in a suspension of empty crystals of host **2.1** in oxygenated $CDCl_3$. These studies were carried out by Prof. Cristian Strassert at the Physikalisches Institut and Center for Nanotechnology (CeNTech) at the Universitat Münster in Germany. The suspension was irradiated at λ_{max}= 345 nm and the phosphorescent signature of singlet oxygen recorded recorded by using a HORIBA Jobin-Yvon IBH FL-322 Fluorolog 3 spectrometer equipped with excitation and emission double-grating monochromators (1.8 nm/mm dispersion, 1800 grooves/mm blazed at 500 nm in the visible spectral range; 3.9 nm/mm dispersion, 830 grooves/mm blazed at 1200 nm in the NIR spectral range) equipped with an air-cooled Hamamatsu H10330-75 (InP/InGaAs) PMT detector at 1270 nm.

2.11.10. General loading procedure.

Host **2.1** crystals (20 mg) were loaded into a 3-mL scintillation vial and then soaked in 0.50 mL of neat alkene for 2-18 h. The crystals were vacuum filtered and rinsed with 1.5 mL of hexanes (0.5 mL × 3). The crystals were then allowed to set on the filtering apparatus for 10 min to allow any excess solvent to evaporate. The guest binding was monitored by TGA and ^{1}H-NMR.

2.11.11. TGA desorption studies.

Guest desorption studies were carried out on 10-20 mg of guest absorbed sample using a TA instruments SDT-Q600. The TGA analysis was done under high purity helium at a heating rate of 10 °C min^{-1} from 25-180 °C with an isotherm at 180 °C for 5 min. Samples were recollected after analysis for further characterization. The host **2.1**:guest ratios were calculated using the following formula:

$$\boldsymbol{Molar\ ratio\ host\ 1: guest} = \frac{\boldsymbol{moles\ guest}}{\boldsymbol{moles\ host\ 1}}$$

$$\boldsymbol{Moles\ host\ 1} = \frac{\boldsymbol{final\ weight}}{\boldsymbol{molecular\ weight\ of\ host\ 1}}$$

$$\boldsymbol{Moles\ guest} = \frac{\boldsymbol{\Delta\ weight}}{\boldsymbol{Moelcular\ weight\ guest}}$$

2.11.12. ^{1}H-NMR loading analysis.

All ^{1}H- and ^{13}C- NMR analysis were conducted on a Varian Mercury 300 and 400 MHz NMR spectrometer. Host **2.1**•guest complexes (~2 mg) were dissolved in δ_6-DMSO (0.500 mL) and the ratios were determined by integration of the resultant peaks. The host **2.1**:guest ratios were calculated using the following formulas:

$$\boldsymbol{Integration\ per\ H} = \frac{\boldsymbol{peak\ intergal}}{\boldsymbol{number\ of\ H}}$$

$$\boldsymbol{molar\ ration\ host\ 1: guest} = \frac{\boldsymbol{ave\ integral\ per\ H\ guest}}{\boldsymbol{average\ integral\ per\ H\ host 1}}$$

2.11.13. Powder X-ray diffraction studies.

Empty host **2.1** crystals as well as freshly loaded crystals of host **2.1**•guest (~30 mg) were ground to a powder and examined by PXRD. Diffraction data was collected on a Rigaku DMAX-2100 and DMAX-2200 powder X-ray diffractometers using CuKα radiation. The step-scans were collected at +0.05 ° steps at angular range 2-40 °2θ at ambient conditions.

2.11.14. General Oxidation procedures.

Solid crystal inclusion complexes: Host **2.1**•alkene complex crystals (10 mg) were loaded into a quartz test tube and purged with dry oxygen for 5 min. The crystals were then irradiated in a Rayonet RPR-200 UV reactor equipped with RPR-3500 lamps for 2h. A 1-2 mg sample of the host•guest complex was separated from the sample and dissolved in δ_6-DMSO to examine the product ^{1}H-NMR peaks with respect to the host peaks. The remaining sample products were extracted from the host **2.1** complex with deuterated methylene chloride or deuterated acetonitrile and analyzed by GC/mass, ^{1}H-NMR and GC/FID.

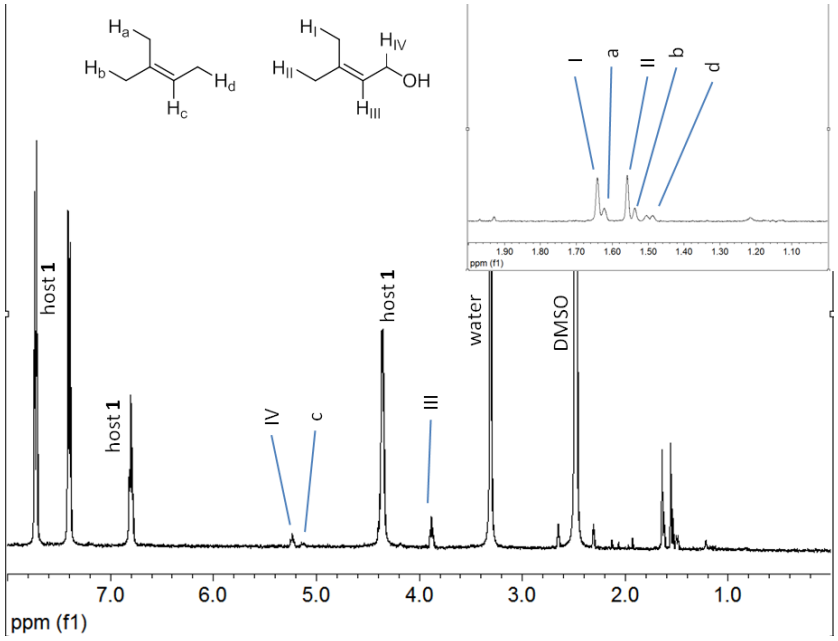

Figure 2.31. ^{1}H-NMR (400 MHz, δ_6-DMSO) of host **2.1**•oxidation products from 2-methyl-2-butene.

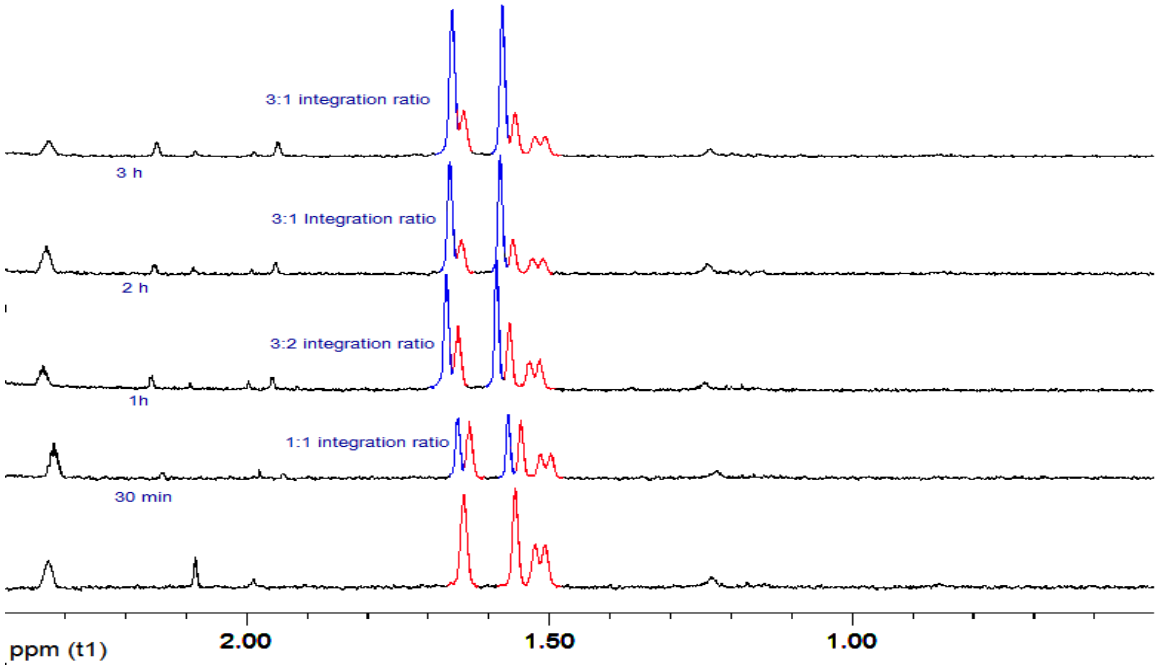

Figure 2.32. Comparison of ^{1}H-NMR (300 MHz, δ_3-AcCN) of oxidation products of 2-methy-2-butene at 0, 30, 60, 120, and 180 min.

Solutions: All solvents were aerated with dry oxygen prior to use by bubbling oxygen through the solvent during sonication (30 min). Host **2.1** crystals (5 mg) were suspended in the aerated solvent in a quartz test tube. Then 10 molar equivalents of the alkene were added. The suspension was then irradiated in a Rayonet RPR-200 UV reactor equipped with RPR-3500 lamps for 2h. The suspension was neutralized with excess triphenyl phosphine and filtered. The filtrate was analyzed by GC/mass, GC/FID, and ^{1}H-NMR. The crystals were dissolved in δ_6-DMSO and analyzed by ^{1}H-NMR to check for bound products.

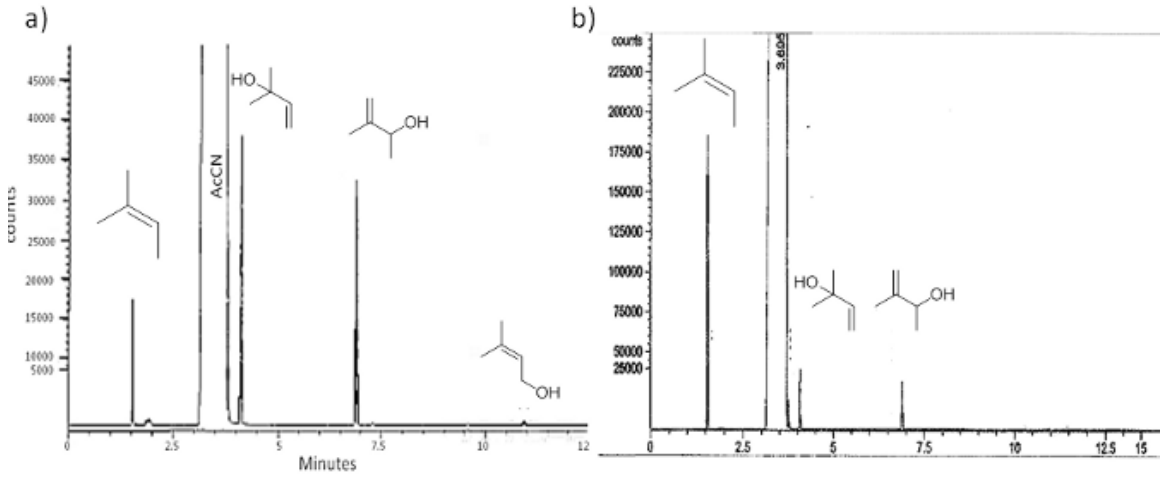

Figure 2.33. GC traces of products from solution: a) Comparison of GC of oxidation products from suspension of host **1** in acetonitrile. b) Comparison of GC of oxidation products from suspension of host **1** in acetonitrile/water mixtures.

Argon: The host **2.1**•guest complexes (10 mg) were loaded as previously described. The smaple was placed into quartz test tubes fitted with septum and two needles, inlet and outlet. The sample was purged with argon for 10 min and the needles were removed. The

sample was then irradiated in a Rayonet UV reactor equipped with 350 nm UV bulbs for 18 h. The products were extracted with methylene chloride and GC/Mass was used to monitor the product formation.

2.11.15. EPR studies.

EPR experiments were conducted on 10-30 mg of empty or guest absorbed sample. EPR spectra were recorded on a Bruker EMX plus equipped with a Bruker premium X X-band microwave bridgehead and Xenon software version 1.1b.66.

Dark experiment: Freshly evacuated host **2.1** crystals (10 mg) were loaded into an EPR tube that was wrapped in aluminum foil and stored in the dark until no EPR signal was observed (~ 5 days). The sample was then purged with argon gas (99.99% purity) in the dark and the EPR was recorded. Then the sample was allowed to set on the benchtop under fluorescent lighting (GE Ecolux) for 30 min and the EPR recorded. Then the sample was irradiated in a Rayonet UV reactor equipped with 3500 Å bulbs for 30 min and the EPR was recorded.

Empty experiments: Benzophenone (20 mg) and host **2.1** crystals (freshly evacuated, 20 mg) were loaded into separate EPR tubes and the individual spectra were recorded. The host **2.1** sample was then transferred to the Rayonet UV reactor and irradiated for 1 h and the spectra recorded.

Loaded experiments: Crystals of host **2.1** (20 -30 mg) were loaded as previously reported and the EPR recorded. After initial spectra were recorded, the sample was transferred in the sealed EPR tube to the Rayonet UV reactor and irradiated for 1 h. After irradiation, the sample was transferred back to the EPR to record the spectra.

2.12. References.

1. Hoffmann, N., Photochemical reactions as key steps in organic synthesis. *Chemical Reviews* **2008,** *108* (3), 1052-1103.
2. Kessel, D.; Reiners, J., Light-Activated Pharmaceuticals: Mechanisms and Detection. *Israel Journal of Chemistry* **2012,** *52* (8-9), 674-680.
3. (a) Ogilby, P. R., Singlet oxygen: there is indeed something new under the sun. *Chemical Society Reviews* **2010,** *39* (8), 3181-3209; (b) Ogilby, P. R., Singlet oxygen: there is still something new under the sun, and it is better than ever. *Photochemical & Photobiological Sciences* **2010,** *9* (12), 1543-1560.
4. (a) Foote, C. S., Photosensitized Oxygenations and Role of Singlet Oxygen. *Accounts of Chemical Research* **1968,** *1* (4), 104-&; (b) Clennan, E. L.; Pace, A., Advances in singlet oxygen chemistry. *Tetrahedron* **2005,** *61* (28), 6665-6691.
5. Turro, N. J., *Modern Molecular Photochemistry*. 1 ed.; University Science Books: CA, 1991; p 628.
6. (a) Shimizu, L. S.; Smith, M. D.; Hughes, A. D.; Shimizu, K. D., Self-assembly of a bis-urea macrocycle into a columnar nanotube. *Chem Commun* **2001,** (17), 1592-1593; (b) Shimizu, L. S.; Hughes, A. D.; Smith, M. D.; Davis, M. J.; Zhang, B. P.; zur Loye, H. C.; Shimizu, K. D., Self-assembled nanotubes that reversibly bind acetic acid guests. *J. Am. Chem. Soc.* **2003,** *125* (49), 14972-14973; (c) Dewal, M. B.; Lufaso, M. W.; Hughes, A. D.; Samuel, S. A.; Pellechia, P.; Shimizu, L. S., Absorption properties of a porous organic crystalline apohost formed by a self-assembled bis-urea macrocycle. *Chemistry of Materials* **2006,** *18*

(20), 4855-4864; (d) Dawn, S.; Dewal, M. B.; Sobransingh, D.; Paderes, M. C.; Wibowo, A. C.; Smith, M. D.; Krause, J. A.; Pellechia, P. J.; Shimize, L. S., Self-Assembled Phenylethynylene Bis-urea Macrocycles Facilitate the Selective Photodimerization of Coumarin. *J. Am. Chem. Soc.* **2011,** *133* (18), 7025-7032.

7. (a) Yang, J.; Dewal, M. B.; Shimizu, L. S., Self-assembling bisurea macrocycles used as an organic zeolite for a highly stereoselective photodimerization of 2-cyclohexenone. *J. Am. Chem. Soc.* **2006,** *128* (25), 8122-8123; (b) Yang, J.; Dewal, M. B.; Profeta, S.; Smith, M. D.; Li, Y. Y.; Shimizu, L. S., Origins of selectivity for the 2+2 cycloaddition of alpha,beta-unsaturated ketones within a porous self-assembled organic framework. *J. Am. Chem. Soc.* **2008,** *130* (2), 612-621.

8. Dewal, M. B.; Xu, Y. W.; Yang, J.; Mohammed, F.; Smith, M. D.; Shimizu, L. S., Manipulating the cavity of a porous material changes the photoreactivity of included guests. *Chem Commun* **2008,** (33), 3909-3911.

9. (a) Weiss, R. G.; Ramamurthy, V.; Hammond, G. S., Photochemistry in organized and confining media: a model. *Accounts of Chemical Research* **1993,** *26* (10), 530-536; (b) Arumugam, S., Alkali metal cation exchanged Nafion as an efficient micro-environment for oxidation of olefins by singlet oxygen. *Journal of Photochemistry and Photobiology A: Chemistry* **2008,** *199* (2–3), 242-249.

10. (a) Shailaja, J.; Sivaguru, J.; Robbins, R. J.; Ramamurthy, V.; Sunoj, R. B.; Chandrasekhar, J., Singlet Oxygen Mediated Oxidation of Olefins within Zeolites: Selectivity and Complexities. *Tetrahedron* **2000,** *56* (36), 6927-6943; (b) Pace, A.; Clennan, E. L., A New Experimental Protocol for Intrazeolite

Photooxidations. The First Product-Based Estimate of an Upper Limit for the Intrazeolite Singlet Oxygen Lifetime. *J. Am. Chem. Soc.* **2002,** *124* (38), 11236-11237; (c) Chen, Y.-Z.; Wu, L.-Z.; Zhang, L.-P.; Tung, C.-H., Confined Space-Controlled Hydroperoxidation of Trisubstituted Alkenes Adsorbed on Pentasil Zeolites. *The Journal of Organic Chemistry* **2005,** *70* (12), 4676-4681; (d) Clennan, E. L., Mechanisms of oxygenations in zeolites. In *Advances in Physical Organic Chemistry*, Richard, J. P., Ed. 2008; Vol. 42, pp 225-269; (e) Li, X.; Ramamurthy, V., Selective Oxidation of Olefins within Organic Dye Cation-Exchanged Zeolites. *J. Am. Chem. Soc.* **1996,** *118* (43), 10666-10667.

11. Griesbeck, A. G.; Cho, M., Singlet oxygen addition to homoallylic substrates in solution and microemulsion: novel secondary reactions. *Tetrahedron Lett* **2009,** *50* (1), 121-123.

12. (a) Griesser, M.; Rosspeintner, A.; Dworak, C.; Höfer, M.; Grabner, G.; Liska, R.; Gescheidt, G., Initiators Based on Benzaldoximes: Bimolecular and Covalently Bound Systems. *Macromolecules* **2012,** *45* (21), 8648-8657; (b) Tehfe, M.-A.; Dumur, F.; Graff, B.; Morlet-Savary, F.; Fouassier, J.-P.; Gigmes, D.; Lalevée, J., Trifunctional Photoinitiators Based on a Triazine Skeleton for Visible Light Source and UV LED Induced Polymerizations. *Macromolecules* **2012,** *45* (21), 8639-8647.

13. Marin, M. L.; Santos-Juanes, L.; Arques, A.; Amat, A. M.; Miranda, M. A., Organic Photocatalysts for the Oxidation of Pollutants and Model Compounds. *Chemical Reviews* **2011,** *112* (3), 1710-1750.

14. (a) Lim, K. S.; Oh, K. W.; Kim, S. H., Antimicrobial activity of organic photosensitizers embedded in electrospun nylon 6 nanofibers. *Polym. Int.* **2012,** *61* (Copyright (C) 2013 American Chemical Society (ACS). All Rights Reserved.), 1519-1524; (b) Dhende, V. P.; Samanta, S.; Jones, D. M.; Hardin, I. R.; Locklin, J., One-Step Photochemical Synthesis of Permanent, Nonleaching, Ultrathin Antimicrobial Coatings for Textiles and Plastics. *ACS Applied Materials & Interfaces* **2011,** *3* (8), 2830-2837.

15. (a) Barash, L.; Wasserman, E.; Yager, W. A., Generation of methylenes from germinal diazides via excited nitrenes. *J. Am. Chem. Soc.* **1967,** *89* (15), 3931-3932; (b) Lin, T.-S., EPR study of diphenylnitroxide in benzophenone. *J. Chem. Phys.* **1972,** *57* (Copyright (C) 2013 American Chemical Society (ACS). All Rights Reserved.), 2260-4; (c) Murai, H.; Imamura, T.; Obi, K., Time-resolved ESR detection of benzophenone nπ* triplet state in glassy matrixes at 77 K. *Chem. Phys. Lett.* **1982,** *87* (Copyright (C) 2013 American Chemical Society (ACS). All Rights Reserved.), 295-8; (d) Qu, B.; Hawthorn, G.; Mau, A. W. H.; Dai, L., Photochemical Generation of Polymeric Alkyl-C60 Radicals: ESR Detection and Identification. *The Journal of Physical Chemistry B* **2001,** *105* (11), 2129-2134.

16. (a) Simon, J. D.; Peters, K. S., Solvent effects on the picosecond dynamics of the photoreduction of benzophenone by aromatic amines. *J. Am. Chem. Soc.* **1981,** *103* (21), 6403-6406; (b) Sakamoto, M.; Cai, X.; Fujitsuka, M.; Majima, T., Solvent Effect on the Deactivation Processes of Benzophenone Ketyl Radicals in

the Excited State. *The Journal of Physical Chemistry A* **2006,** *110* (42), 11800-11808.

17. (a) Hoshino, M.; Shizuka, H., Photochemistry of benzophenone in aliphatic amines studied by laser photolysis in the temperature range 300-77 K. *The Journal of Physical Chemistry* **1987,** *91* (3), 714-718; (b) Lewandowska-Andralojc, A.; Kazmierczak, F.; Hug, G. L.; Horner, G.; Marciniak, B., Photoinduced CC-coupling reactions of rigid diastereomeric benzophenone-methionine dyads. *Photochem. Photobiol.* **2013,** *89* (Copyright (C) 2013 American Chemical Society (ACS). All Rights Reserved.), 14-23.

18. Kuzmanich, G.; Simoncelli, S.; Gard, M. N.; Spanig, F.; Henderson, B. L.; Gudi, D. M.; Garcia-Garibay, M. A., Excited State Kinetics in Crystalline Solids: Self-Quenching in Nanocrystals of 4,4 '-Disubstituted Benzophenone Triplets Occurs by a Reductive Quenching Mechanism. *J. Am. Chem. Soc.* **2011,** *133* (43), 17296-17306.

19. (a) Adam, W.; Prein, M., π-Facial Diastereoselectivity in the [4+2] Cycloaddition of Singlet Oxygen as a Mechanistic Probe. *Accounts of Chemical Research* **1996,** *29* (6), 275-283; (b) Ogilby, P. R.; Foote, C. S., Chemistry of singlet oxygen. 36. Singlet molecular oxygen (1.DELTA.g) luminescence in solution following pulsed laser excitation. Solvent deuterium isotope effects on the lifetime of singlet oxygen. *J. Am. Chem. Soc.* **1982,** *104* (7), 2069-2070; (c) Sivaguru, J.; Poon, T.; Franz, R.; Jockusch, S.; Adam, W.; Turro, N. J., Stereocontrol within Confined Spaces: Enantioselective Photooxidation of Enecarbamates Inside Zeolite Supercages. *J. Am. Chem. Soc.* **2004,** *126* (35), 10816-10817; (d) Griesbeck, A.

G.; Adam, W.; Bartoschek, A.; El-Idreesy, T. T., Photooxygenation of allylic alcohols: kinetic comparison of unfunctionalized alkenes with prenol-type allylic alcohols, ethers and acetates. *Photochemical & Photobiological Sciences* **2003,** *2* (8), 877-881.

20. Shimizu, L. S.; Hughes, A. D.; Smith, M. D.; Samuel, S. A.; Ciurtin-Smith, D., Assembled columnar structures from bis-urea macrocycles. *Supramol Chem* **2005,** *17* (1-2), 27-30.

21. (a) Sharma, S.; Sinha, S.; Chand, S., Polymer Anchored Catalysts for Oxidation of Styrene Using TBHP and Molecular Oxygen. *Ind Eng Chem Res* **2012,** *51* (26), 8806-8814; (b) Zhan, W.; Guo, Y.; Wang, Y.; Liu, X.; Guo, Y.; Wang, Y.; Zhang, Z.; Lu, G., Synthesis of Lanthanum-Doped MCM-48 Molecular Sieves and Its Catalytic Performance for the Oxidation of Styrene. *The Journal of Physical Chemistry B* **2007,** *111* (42), 12103-12110.

22. Foote, C. S.; Wexler, S.; Ando, W.; Higgins, R., Chemistry of Singlet Oxygen .4. Oxygenations with Hypochlorite-Hydrogen Peroxide. *J. Am. Chem. Soc.* **1968,** *90* (4), 975-&.

23. (a) Trachtenberg, E. N.; Carver, J. R., Stereochemistry of selenium dioxide oxidation of cyclohexenyl systems. *The Journal of Organic Chemistry* **1970,** *35* (5), 1646-1653; (b) Trachtenberg, E. N.; Nelson, C. H.; Carver, J. R., Mechanism of selenium dioxide oxidation of olefins. *The Journal of Organic Chemistry* **1970,** *35* (5), 1653-1658; (c) Stephenson, L. M.; Speth, D. R., Mechanism of allylic hydroxylation by selenium dioxide. *The Journal of Organic Chemistry* **1979,** *44* (25), 4683-4689; (d) Sharpless, K. B.; Lauer, R. F., Selenium dioxide oxidation of

olefins. Evidence for the intermediacy of allylseleninic acids. *J. Am. Chem. Soc.* **1972,** *94* (20), 7154-7155.

24. (a) Lissi, E. A.; Encinas, M. V.; Lemp, E.; Rubio, M. A., Singlet oxygen O2(1.DELTA.g) bimolecular processes. Solvent and compartmentalization effects. *Chemical Reviews* **1993,** *93* (2), 699-723; (b) Long, C. A.; Kearns, D. R., Radiationless decay of singlet molecular oxygen in solution. II. Temperature dependence and solvent effects. *J. Am. Chem. Soc.* **1975,** *97* (8), 2018-2020.

25. (a) Bryant, J. R.; Matsuo, T.; Mayer, J. M., Cumene Oxidation by cis-[RuIV(bpy)2(py)(O)]2+, Revisited. *Inorg Chem* **2004,** *43* (4), 1587-1592; (b) Zhang, M.; Wang, L.; Ji, H.; Wu, B.; Zeng, X., Cumene Liquid Oxidation to Cumene Hydroperoxide over CuO Nanoparticle with Molecular Oxygen under Mild Condition. *Journal of Natural Gas Chemistry* **2007,** *16* (4), 393-398.

26. Qu, B.; Xu, Y.; Shi, W.; Raanby, B., Photoinitiated crosslinking of low-density polyethylene. 7. Initial radical reactions with model compounds studied by spin-trapping ESR spectroscopy. *Macromolecules* **1992,** *25* (20), 5220-5224.

27. Tsierkezos, N. G.; Ritter, U., Application of electrochemical impedance spectroscopy for characterisation of the reduction of benzophenone in acetonitrile solutions. *Physics and Chemistry of Liquids* **2011,** *49* (6), 729-742.

28. Lin, A. A.; Sastri, V. R.; Tesoro, G.; Reiser, A.; Eachus, R., On the crosslinking mechanism of benzophenone-containing polyimides. *Macromolecules* **1988,** *21* (4), 1165-1169.

29. (a) Woodward, J. R.; Lin, T.-S.; Sakaguchi, Y.; Hayashi, H., Biphotonic photochemistry of benzophenones in dimethylsulphoxide: a flash photolysis EPR

study. *Mol Phys* **2002,** *100* (8), 1235-1244; (b) Kawai, A.; Hirakawa, M.; Abe, T.; Obi, K.; Shibuya, K., Specific Solvent Effects on the Structure and Reaction Dynamics of Benzophenone Ketyl Radical. *The Journal of Physical Chemistry A* **2001,** *105* (42), 9628-9636.

30. Lucarini, M.; Mezzina, E., EPR investigations of organic non-covalent assemblies with spin labels and spin probes. *Electron Paramagn. Reson.* **2011,** *22* (Copyright (C) 2013 American Chemical Society (ACS). All Rights Reserved.), 41-70.
31. Nakatsuji, S.; Anzai, H., *J. Mater. Chem.* **1997,** *7*, 2161-2174.
32. Rawson, J. M.; Alberola, A.; Whalley, A. E., *J. Mater. Chem.* **2006,** *16*, 2560-2575.
33. Rajca, A., *Chem. Rev.* **1994,** *94*, 871-893.
34. Hikcks, R. G., *Org. Biomol. Chem.* **2007,** *5*, 1321-1338.
35. (a) Polyakov, N. E.; Okazaki, M.; Toriyama, K.; Leshina, T. V.; Fujiwara, Y.; Tanimoto, Y., Product Yield Detected ESR Study on the Dynamic Behavior of Radical Pairs Generated in Photoreduction of Acetylenic Ketones in SDS Micellar Solution. *The Journal of Physical Chemistry* **1994,** *98* (41), 10563-10567; (b) Akiyama, K.; Sekiguchi, S.; Tero-Kubota, S., Origin of an Absorptive Electron Spin Polarization Observed in Photochemical Hydrogen Abstraction Reaction by Benzophenone Derivatives. CW and Pulsed EPR Studies. *The Journal of Physical Chemistry* **1996,** *100* (1), 180-183.
36. Reijerse, E., High-Frequency EPR Instrumentation. *Appl Magn Reson* **2010,** *37* (1-4), 795-818.

37. Wasserman, H. H.; Lipshutz, B. H., REACTIONS OF LITHIUM ENOLATES WITH MOLECULAR-OXYGEN ALPHA-HYDROXYLATION OF AMIDES AND OTHER CARBOXYLATE DERIVATIVES. *Tetrahedron Lett* **1975,** (21), 1731-1734.

38. Kihara, N.; Ollivier, C.; Renaud, P., Efficient Radical Oxygenation of α-Iodocarboxylic Acid Derivatives. *Organic Letters* **1999,** *1* (9), 1419-1422.

39. ten Brink, G.-J.; Vis, J. M.; Arends, I. W. C. E.; Sheldon, R. A., Selenium catalysed oxidations with aqueous hydrogen peroxide. Part 3: Oxidation of carbonyl compounds under mono/bi/triphasic conditions. *Tetrahedron* **2002,** *58* (20), 3977-3983.

40. Cowie, J. M. G.; Arrighi, V., *Polymers: Chemistry and Physics of Modern Materials*. 3rd ed.; CRC Press Taylor and Francis Group: Boca Raton, 2008.

41. (a) Heinze, J.; Frontana-Uribe, B. A.; Ludwigs, S., Electrochemistry of Conducting Polymers—Persistent Models and New Concepts†. *Chemical Reviews* **2010,** *110* (8), 4724-4771; (b) Uemura, T.; Horike, S.; Kitagawa, K.; Mizuno, M.; Endo, K.; Bracco, S.; Comotti, A.; Sozzani, P.; Nagaoka, M.; Kitagawa, S., Conformation and Molecular Dynamics of Single Polystyrene Chain Confined in Coordination Nanospace. *J. Am. Chem. Soc.* **2008,** *130* (21), 6781-6788.

42. (a) Gassensmith, J. J.; Barr, L.; Baumes, J. M.; Paek, A.; Nguyen, A.; Smith, B. D., Synthesis and Photophysical Investigation of Squaraine Rotaxanes by "Clicked Capping". *Organic Letters* **2008,** *10* (15), 3343-3346; (b) Arunkumar, E.; Fu, N.; Smith, B. D., Squaraine-Derived Rotaxanes: Highly Stable,

Fluorescent Near-IR Dyes. *Chemistry – A European Journal* **2006,** *12* (17), 4684-4690.

43. Ikeda, T.; Higuchi, M., Electrochromic Properties of Polythiophene Polyrotaxane Film. *Langmuir* **2011,** *27* (7), 4184-4189.

44. Bartusik, D.; Aebisher, D.; Lyons, A. M.; Greer, A., Bacterial Inactivation by a Singlet Oxygen Bubbler: Identifying Factors Controlling the Toxicity of 1O2 Bubbles. *Environ Sci Technol* **2012,** *46* (21), 12098-12104.

45. (a) Bhosale, S. V.; Jani, C. H.; Langford, S. J., *Chem. Soc. Rev.* **2008,** *37*, 331-342; (b) Katz, H. E.; Lovinger, A. J.; Kloc, C.; Siegrist, T.; Li, W.; Lin, Y.-Y.; Dodabalapur, A., *Nature* **2000,** *404* (478-481).

46. Mitchell, A. R.; Pagoria, P. F.; Coon, C. L.; Jessop, E. S.; Poco, J. F.; Tarver, C. M.; Breithaupt, R. D.; Moody, G. L., Nitroureas .1. Synthesis, Scale-up and Characterization of K-6. *Propell Explos Pyrot* **1994,** *19* (5), 232-239.

III. SYNTHESIS, CHARACTERIZATION AND CRYSTAL ENGINEERING OF NAPHTHALENE *BIS*-UREA MACROCYCLES.

3.1 Abstract

This chapter investigates the synthesis of *bis*-urea macrocycles with expanded aryl-spacers, examines the conformations of the macrocycles by computational methods, probes their assembly into crystals under a range of conditions, and characterizes their solid-state structure by X-ray crystallography. We focused on naphthalene spacer groups due to the ready bromination of the commercially available precursors, which affords the intermediates necessary for cyclization. These studies allow us to probe the effects of the enlargement of the aryl shelves on the low energy conformations of the macrocycle, on its subsequent self-assembly, and on the overall crystal packing. Incorporation of 2,7-dimethyl naphthalene into the spacer group of the macrocycle afforded a structure that showed parallel ureas and a "bowl"-shaped macrocycle. Incorporation of 1,3 naphthalene species resulted in a protected macrocycle that shows favorable conformation for the self-assembly into columnar structure. Finally, incorporation of the bromonaphthalene resulted in macrocycle with similar conformation and showed the propensity for halogen bonding. This chapter is published in part in *Cryst. Eng. Commun*. 2011.[1]

3.2 Background

The understanding of the bulk morphology of materials is important in the pharmaceutical industry and has an impact on the material's solubility, stability, and therapeutic properties.[2] One example, reported by Kato *et al.*, showed that the three forms of phenobarbital, a widely used anti-convulsant, had differing dissolution rates with the metastable form, form II-Ba, having the highest.[3] In this aspect, it is important to understand the correlation between the bulk properties and the crystal packing of compounds, such as in the work of Corvis *et al.*[4] The two polymorphic forms of glutaric acid, a common co-crystallizing agent for pharmaceuticals, were studied. They examined the bulk properties of the α-form including its thermal properties and high resolution PXRD. Through study of these bulk properties, they were able to propose a crystal structure for this elusive polymorph at higher temperatures.[4] They also studied the thermal properties to gain a better understanding of the high temperature solid-to-solid phase transition between the two forms.

Previous work by our group demonstrated the synthesis of cyclic structures containing two urea groups separated by two rigid aryl spacers that formed robust columnar structures through the self-assembly of urea three atom centered hydrogen bonding.[5] The lowest energy conformations of the macrocycle as predicted by gas phase calculations indicated that the urea groups preferred an anti-parallel arrangement that oriented them approximately perpendicular to the plain of the macrocycle. The propensity for columnar self-assembly of these macrocycles appears to be governed by the urea self-assembly and by favorable aryl-aryl stacking and was observed regardless of crystallization conditions. Previously reported macrocycles were designed with spacer

groups that incorporated functionality and expanded the size of the macrocyclic building blocks. Figure 3.1 shows the bis-urea macrocycles with these spacers that include *m*-xylene (**3.1**), *p*-xylene (**3.2**), benzophenone (**3.4**), phenyl ether (**3.3**), and phenyl ethynylene (**3.5**) groups.[5a, b, 6] With the incorporation of these substituents into the spacer groups, benzophenone and phenyl ether were shown to form porous structures that have been useful in the incorporation of guest molecules into the interior of the cavity.[5b, c, 7]

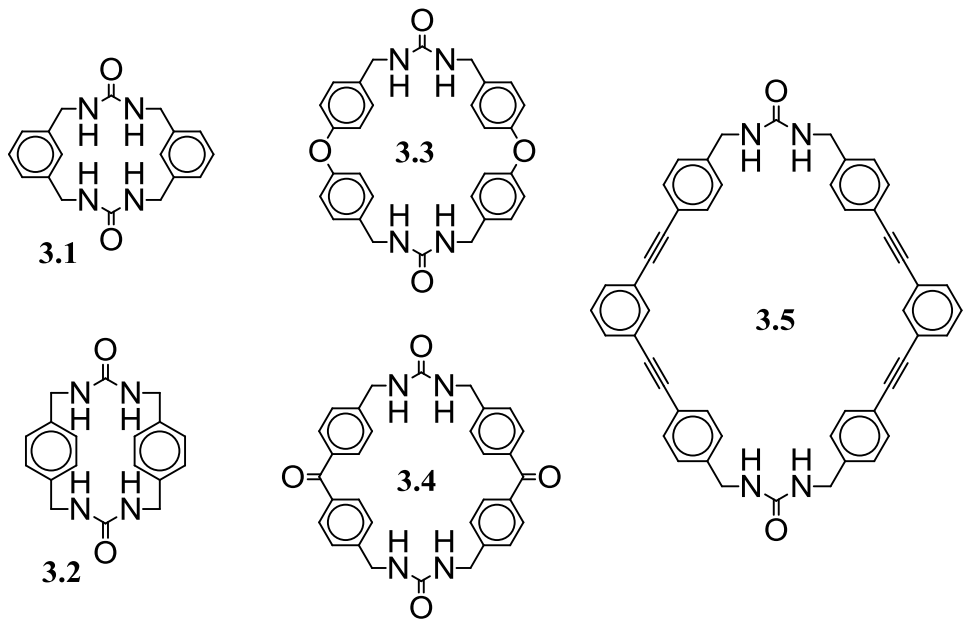

Figure 3.1. *Bis*-urea macrocycle with spacers that include: **3.1** *m*-xylene, **3.2** *p*-xylene, **3.3** phenyl ether, **3.4** benzophenone, and **3.5** phenyl ethynylene.

Rigid spacer groups appear to be a key design element that preorganize the urea motif approximately perpendicular to the plain of the macrocycle and prevent collapse of the cavity. In addition, the spacer should not introduce strain into the system. These design elements were tested using a series of macrocycles to identify systems that gave columnar assembly with high fidelity. For example, the bent *m*-xylene spacer gave a urea that assembled into columns from a number of different solvents (Figure 3.2a). In

contrast, the linear *p*-xylene spacer, disrupted the planarity of the urea groups and twists them from the optimal perpendicular geometry with respect to the plane of the macrocycle. Indeed, while the macrocycle gave a columnar type structure, it was through an amide type assembly (Figure 3.2b).

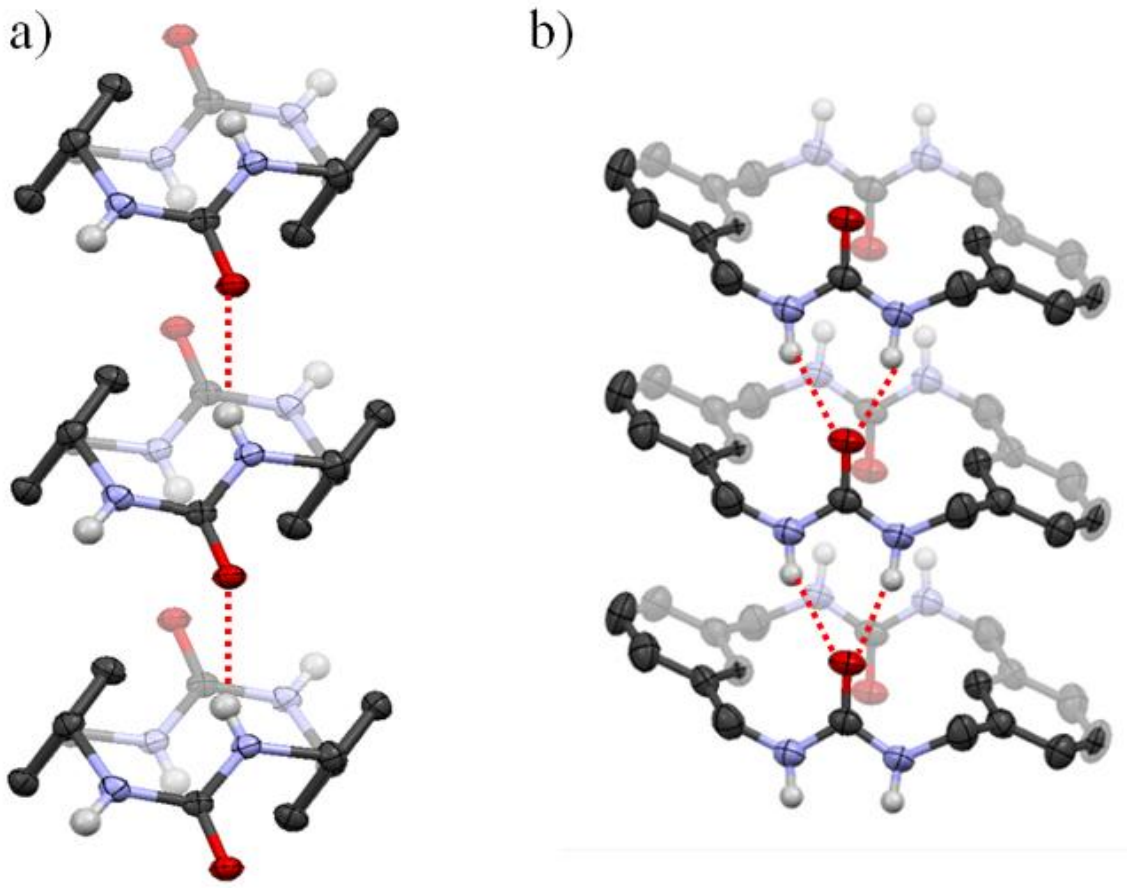

Figure 3.2. Crystals structures of two columnar assembled *bis*-urea macrocycles. a) The *p*-xylene macrocycle showing the amide type bonding that assists the columnar assembly. b) The *m*-xylene macrocycle showing the three centered urea hydrogen bonding that assits the columnar assembly.

The urea NH that was out of the plane participated in hydrogen bonding with intervening water molecules.[5c] Jun Yang further tested the design elements by synthesizing and crystallizing a series of macrocycles that contained one rigid C-shaped spacer, two urea groups, and one more flexible spacer.[8] These flexible linkers included crown ether type

links that had two (**3.7**, **3.10**, and **3.11**) or three (**3.6**, **3.8**a & b, and **3.9**) ether units and either a two or three carbon chain separating the two ureas (Figure 3.3). These unsymmetrical macrocycles showed low association constants between 5 and 600 M^{-1}. While some of these macrocycles assembled into columnar structures, such as macrocycle **3.7**, it was a much lower fidelity building block.

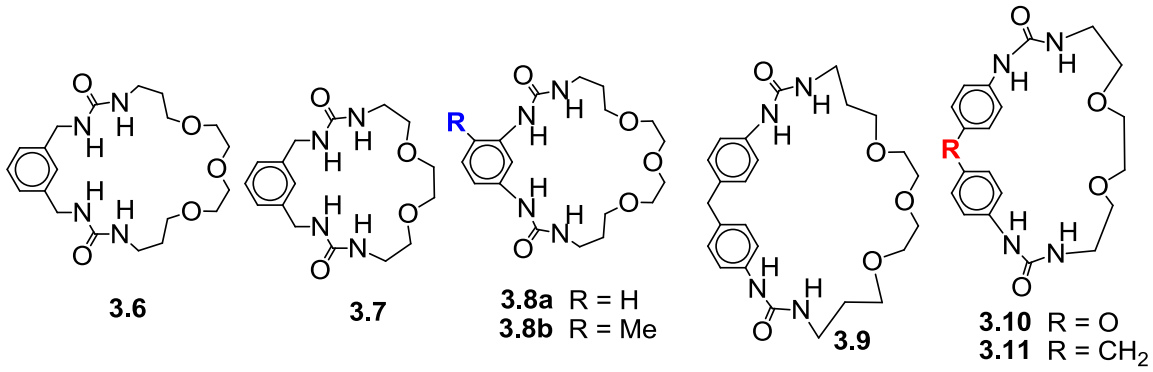

Figure 3.3. The macrocycles designed by Jun Yang that incorporate flexible spacer groups.

Extension of the flexible spacer from a macrocycle **3.7** to macrocycle **3.8a** resulted in the change of the assembled structure from columns to ribbons (Figure 3.4).[8] This suggested that some of the information to control and direct assembly was lost upon incorporation of a more flexible spacing element. In summary, for high fidelity columnar assembly, new *bis*-urea macrocycles should use 'C'-shaped spacers that provide rigidity and optimal angles for perpendicular preorganization of the ureas without introducing unnecessary strain into the structure.

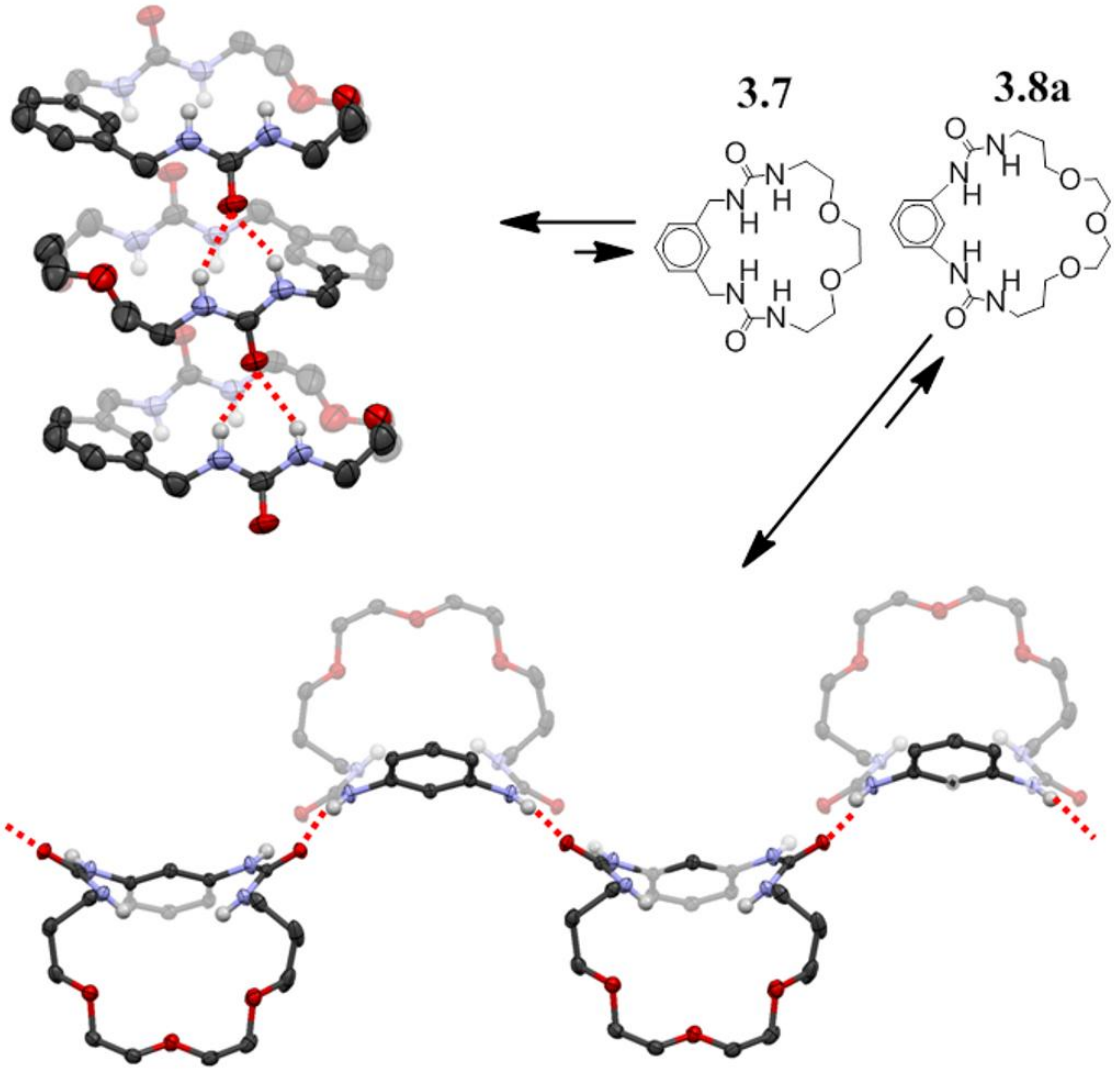

Figure 3.4. Comparison of macrocycle **3.7** and **3.8.** Simple extension of the flexible spacer resulted in the change from columnar stack to ribbon arrangement through amide bonding.

To evaluate the efficiency of the 'C'-shaped spacer to orient the urea groups in a specific macrocycle, we use X-ray crystal structures and molecular models. For example, Figure 3.5 shows the conformation of a single meta-xylene bis-urea macrocycle from its reported X-ray structure.[5c] We can draw a plane through the six carbons that make up the main ring structure of the macrocycle and compare the orientation of the spacer groups and the urea groups to get a basis to compare the overall geometries of the ring (Figure 3.4). Our working hypothesis is that the orientation of the ureas with respect to this plane of the macrocycle facilitates columnar assembly in high fidelity. Figure 3.4 shows that the ureas in the *meta*-xylene macrocycle are tilted slightly from perpendicular to the plane of the ring at 88.0° and the *m*-xylene spacer groups are tilted 26° from the plane of the macrocycle. The same plane created for the benzophenone derivative and phenyl ether macrocycle shows that the spacer groups lie in the plane of the macrocycle and that

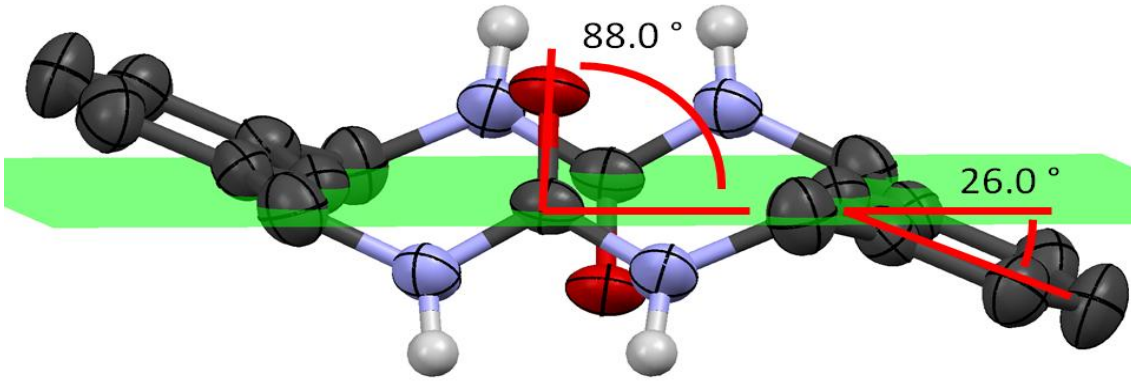

Figure 3.5. The crystal structure of the *m*-xylene macrocycle showing the plane of the macrocycle (green) and the orientation of the spacer group tilted 26.0 ° from the plane and the urea tilted at 88.0 ° from the plane.

the ureas are tilted slightly from perpendicular to the plane of the macrocycle at about 86° (Figure 3.4). All three of these macrocycles reported previously have an orientation that places the urea group perpendicular to the plane of the macrocycle and the spacers close to or within the plane of the macrocycle to relieve any sterics around the urea groups and

allow for their self-assembly. In contrast to these macrocycles that form columnar assemblies through the three atom centered urea hydrogen bonding, when the spacer group is replaced with a *p*-xylene group the ureas are then tilted from the plane of the macrocycle to 59.5°. The ureas are still prone to self-assemble, but the three atom centered assembly is not observed. Instead, only one hydrogen bond is formed between the two urea groups and the second hydrogen bonding site of the carbonyl oxygen is bonded to a water molecule.

In this chapter, we will investigate the synthesis and characterization of new *bis*-urea macrocycles that contain extended aryl spacer units including 2,7-dimethyl naphthalene, 1,3-dimethyl naphthalene and 4-bromo-1,3-dimethylnaphthalene. We will investigate the effect these spacer groups have on the flexibility of the macrocyclic ring as well as the effect on the orientation of the ureas. We will also look into the effect of a halide substituent on the ring of the spacer group and the effect that halide has on the self-assembly of the macrocycles.

3.3 Analysis of the bis-urea building block and design of new macrocycles.

The strengths and geometries of aryl-aryl interactions is still an active area of fundamental research, and the origins of this interaction are still under debate.[9] What is agreed upon are the typical interactions seen by aryl groups. The quadrapole electrostatics exhibited by aryl groups, such as benzene, are such that along the equator of the ring there is partial positive character. Partial negative character is observed above and below the ring. This electrostatic potential allows for these groups to orient themselves in three distinct orientations that can afford stabilizing attractions that assist in

the assembly of larger molecules. Figure 3.5 shows three typical interactions.[10] The edge to face interaction in which the partial positive character along the equator of the molecule is directed toward the partial negative character above or below the ring resulting in a "T" shape association between the two rings (Figure 3.5a). The face-to-face orientation is usually seen when two aromatic rings have different electronic substituents attached allowing for one ring to be less negative and the other to be slightly more negative in the electron cloud above and below the ring.[10c] This results in an orientation of the rings laying directly over one another (Figure 3.5b). Finally, the offset aryl stacking is the association of the partial positive and partial negative characteristic in such a way that the rings adopt a slipped disk type of orientation, or that they are offset from face-to-face to maximize the attractive interactions (Figure 3.5c).[10a]

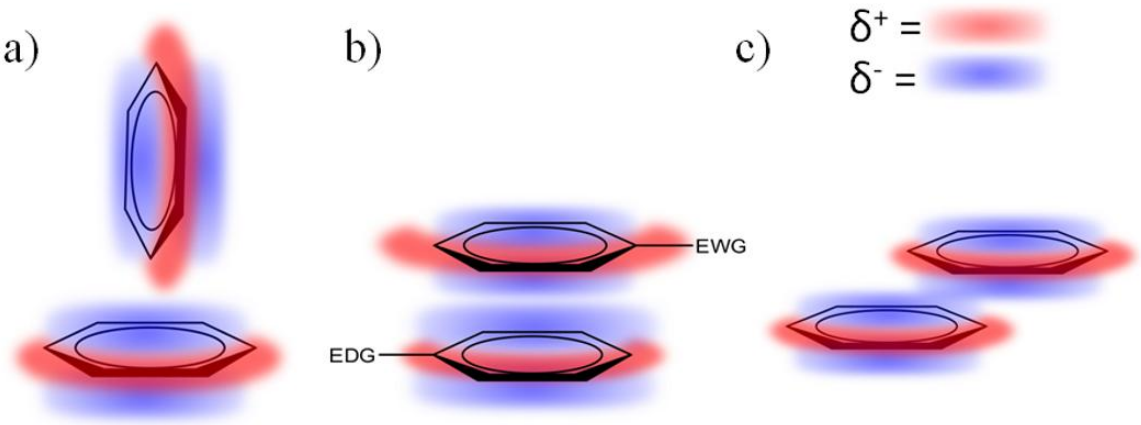

Figure 3.6. Pi-pi stacking motif: a) edge to face aryl-aryl stacking b) face-to-face aryl stacking c) offset aryl stacking.

Previously studied macrocycles from our group, such as the benzophenone and phenyl-ether cycles, show geometries and distances that suggest edge-to-face aryl stacking interactions provide additional stabilizing forces. Figure 3.6 (left) illustrates the

edge-to-face aryl stacking that assists with the self-assembly of the benzophenone *bis*-urea macrocycle (**3.4**) into columnar structures. Additionally, Figure 3.6 (right) highlights the offset aryl stacking of *meta* xylene macrocycles (**3.1**) and shows a center to center distance of (insert) 3.68 Å.

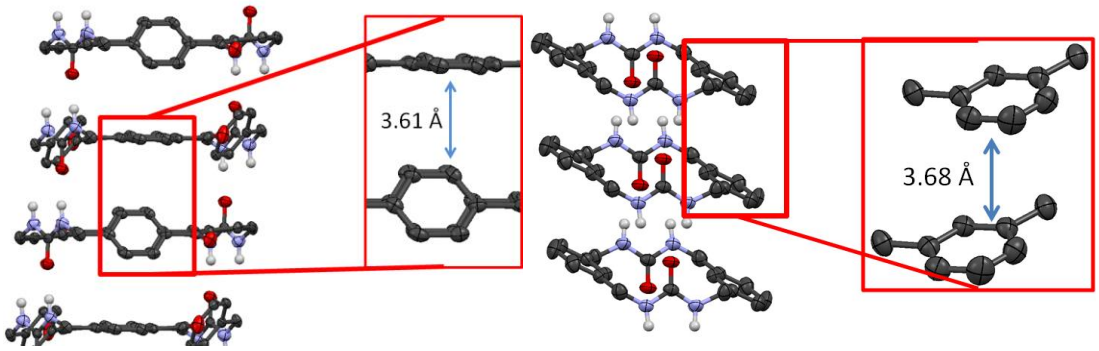

Figure 3.7. Crystal structures of stacked macrocycles: (left) The crystal structure of the benzophenone *bis*-urea macrocycle showing the edge-to-face aryl stacking that assists with the self-assembly of the macrocycle into columnar structures. (insert) View of an individual aryl stacking motif with a distance of 3.61 Å. (right) The crystal structure of the meta xylene macrocycle with offset aryl stacking with a distance of (insert) 3.68 Å.

To probe the contribution of the aryl stacking interaction and understand the limits of *bis*-urea assembly motif, a series of macrocycles with expanded aryl spacer groups were synthesized to compare with the original meta-xylene derivative. Figure 3.7 compares the new expanded systems with the meta-xylene bis-urea macrocycle. The first is the 2,7-dimethyl naphthalenyl *bis*-urea macrocycle **3.12**, in which the expansion of the aryl shelf occurs in the circumference of the cyclic ring. The next was 1,3-dimethyl naphthalenyl *bis*-urea macrocycle **3.13** that extends the aryl shelf of the spacer group out from the macrocycle. We expect this extension to mimic the *m*-xylene cycle in that the geometry of the main cyclic structure is maintained. With the extension of the aryl shelf we can explore the possibility of an increase in aryl interactions on the self-assembly of the macrocycle. Lastly, with the incorporation of a halide on the naphthalene ring, as with

macrocycle **3.14**, we can study the possibility of introducing a secondary effect, such as halogen bonding, that promotes the further association of columns with each other.

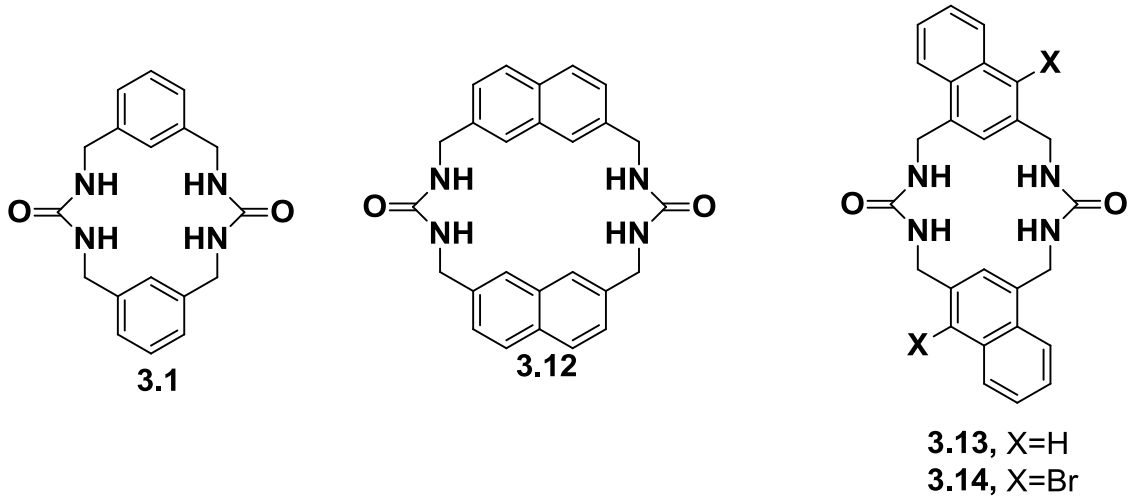

Figure 3.7. Comparison of *bis*-ureas with expanded aryl shelves.

3.4 Synthesis of 2,7-Dimethyl Naphthalene *Bis*-Urea Macrocycle (3.12)

To probe the effect of the expanded aryl-shelf the 2,7-dimethyl naphthalenyl *bis*-urea macrocycle (**3.12**) was synthesized in three steps. Commercially available 2,7-dimethyl naphthalene was brominated under radical conditions using NBS and AIBN in carbon tetrachloride to give dibromomethyl naphthalene. The dibromide was then cyclized with *tert*-butyl triazinanone to yield the protected macrocycle. Treatment with 20% acidic diethanol amine in a mixture of water and methanol gave the bis-urea **3.12** (scheme 1).

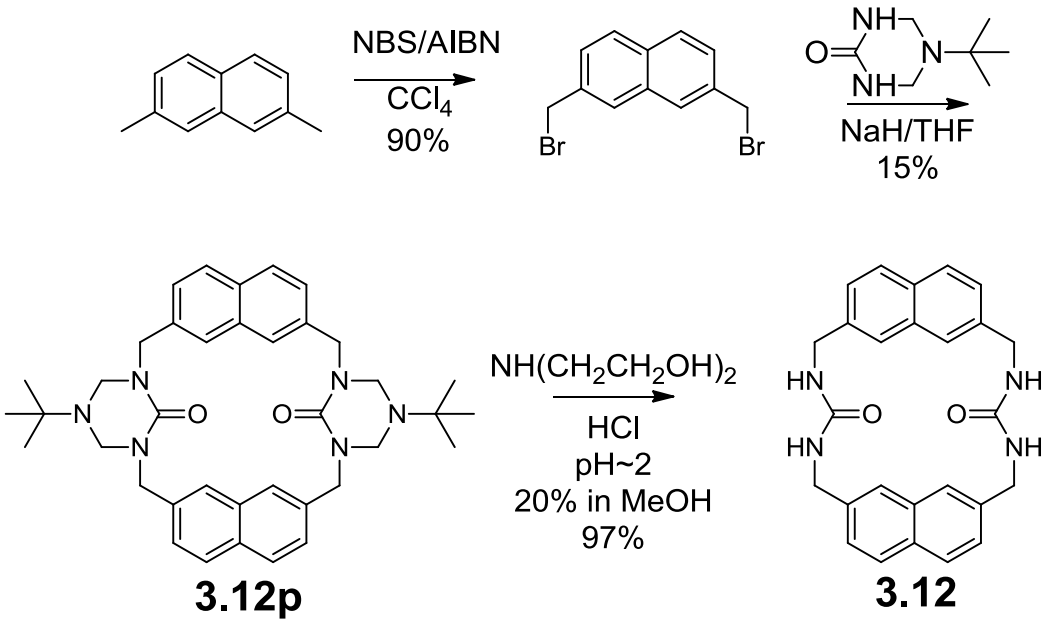

Scheme 3.1. Synthetic scheme of 2,7 dimethylnaphthalene macrocycle (**3.12**).

3.5 Crystal Structure Characterization of 2,7-Dimethyl Naphthalene *Bis*-Urea Macrocycle

The protected 2,7-dimethyl naphthalene macrocycle was crystallized from an ethyl acetate : methanol solution (9:1 by volume) to give colorless needle crystals that were suitable for single crystal X-ray diffraction. The crystal structure revealed the solvent-free protected macrocycle (**3.12p**) ($C_{38}H_{46}N_6O_2$) with the centrosymmetric macrocycle monomers aligned in a herringbone arrangement (Fig. 3.3).

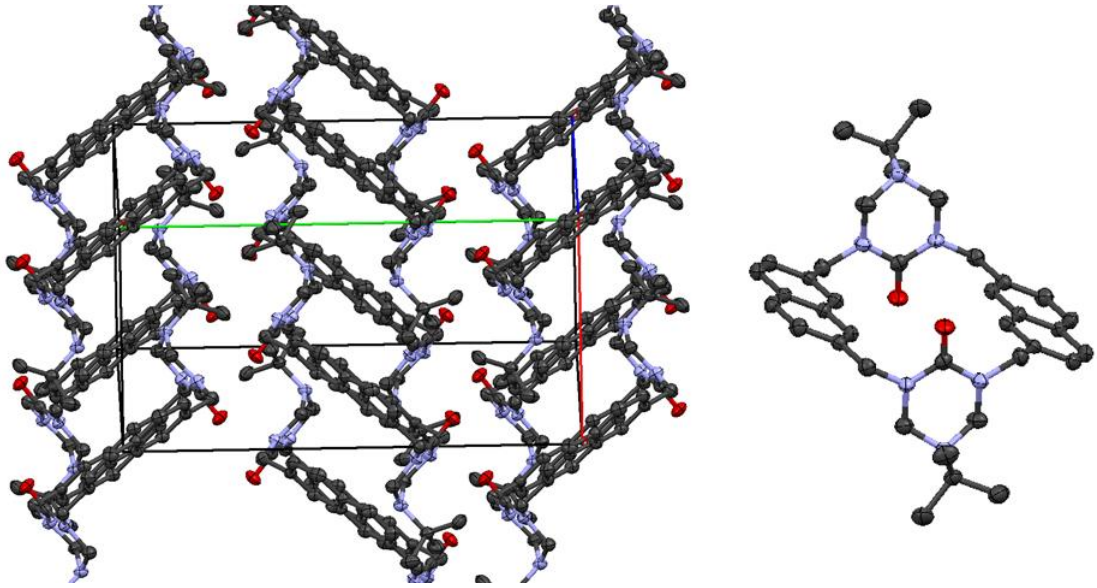

Figure 3.9. Protected *bis*-urea 2,7-dimethyl naphthalene macrocycle **3.12**. (left) Crystal packing of the macrocycle shows the herringbone arrangement of the naphthalenes. (right) The macrocycle shows the anti-parallel and perpendicular orientation of the protected ureas and the planar orientation of the naphthalene spacer groups expected to be beneficial to the self-assembly of the ureas into columnar structures

Examination of the monomeric macrocycle shows that the naphthalene spacers adopt the flat parallel planar arrangement with the naphthalene spacer group tilted slightly out of the plane of the macrocycle at 25.3°. The ureas are oriented in an anti-parallel fashion perpendicular to the plane of the macrocycle at 89.5°. This orientation is typically observed for *bis*-urea macrocycles, as seen in the *m*-xylene macrocycle (Fig. 3.6) and is assumed to be ideal for the self-assembly of the free ureas and the formation of the columnar assemblies seen with other systems. Upon deprotection of the ureas, the crystal structure shows the expected *bis*-urea macrocycle but in an unexpected orientation. The macrocycle crystallized from a DMSO/water solution to form colorless block crystals that upon structural examination formed a columnar structure interpenetrated by two water molecules that occupy the urea hydrogen bonding sites. The water molecule to the left hand side of the columnar structure is bonded to both nitrogens of the macrocycle

above (N···O distance =20934(3) Å and 3.000(3) Å) and the oxygen below (O···O distance = 2.756(3) Å). This water molecule is also bonded to the centrally located DMSO molecule (O···O distance = 2.756(3) Å). The opposite water molecule is hydrogen bonded to one nitrogen of the macrocycle above (N···O distance = 3.025(3) Å) and to the oxygen of the macrocycle below (O···O distance =2.777(3) Å), and to the carbonyl oxygen of a macrocycle from an adjacent column (O···O distance = 3.053(3) Å). Figure 3.9 shows this expanded column that results in an average distance between macrocycles within a column of 5.3 Å resulting in an extended columnar structure.

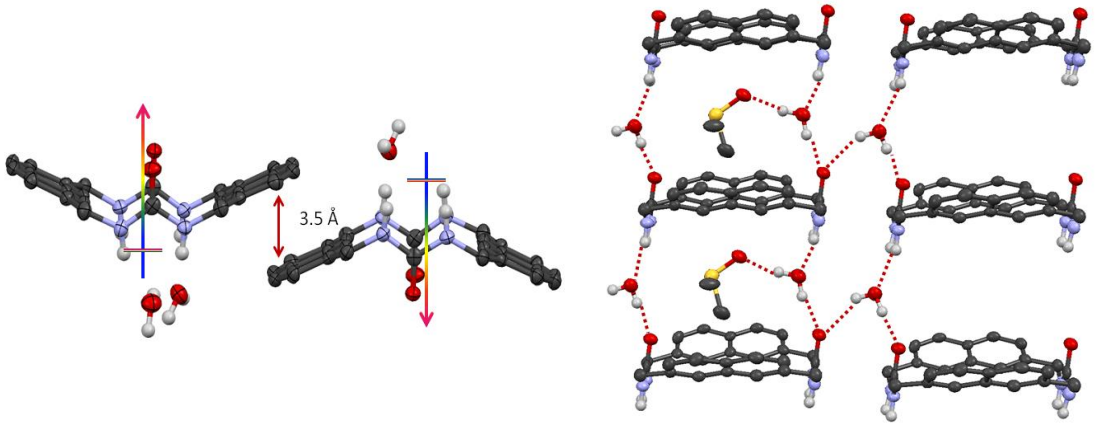

Figure 3.10. Crystal packing of 2,7 Naphthalene macrocycle **3.12**. (left) View along the b-axis of the extended column shows the opposite dipole moments and the aryl-aryl spacing of the adjacent columns. (right) The extended columnar structure formed from the slow evaporation of DMSO/Water solution showing the hydrogen bonding scheme (some hydrogens and DMSO and water molecules were deleted for clarity).

The individual macrocycle also showed an unusual orientation with the ureas adopting a parallel conformation that resulted in the macrocycle having a dipole moment. Along with this, the naphthalene spacers are arranged into a bowl-shape oriented toward the electron rich carbonyls instead of the planar conformation that is seen with the *meta*-xylene macrocycle.[6a] In addition to this unusual conformation, the crystal structure suggests some ring strain is present as indicated by the increase in the sp^3 bond angle

from the methylene carbon that connects the naphthalene to the urea moieties. This bond angle increases from 109° to 115°. There is also a 6° tilt of the ureas from perpendicular to the naphthalene spacers. (Figure 3.10)

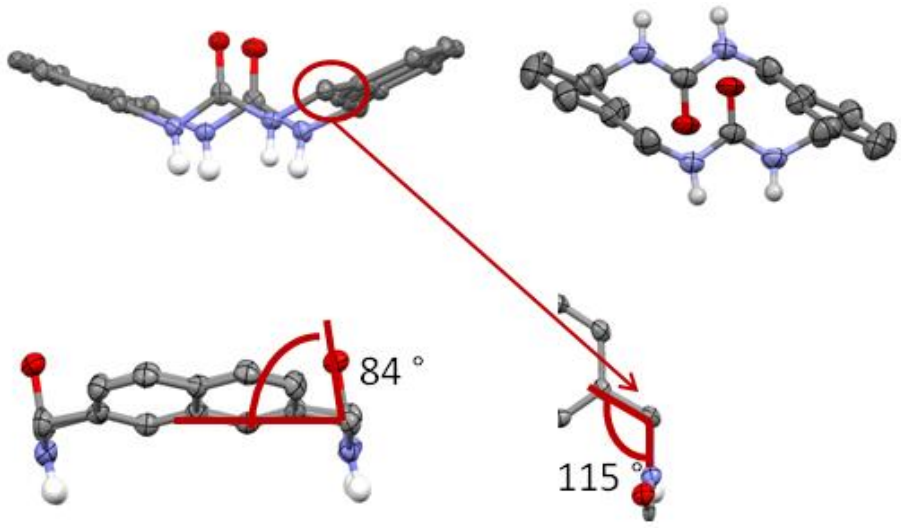

Figure 3.11. Crystal structure of 2,7-dimethyl naphthalene macrocycle (**3.12**) and *m*-xylene macrocycle(**3.1**): (top) comparison of the naphthalene macrocycle with *m*-xylene macrocycle shows the flipped orientation of the urea to parallel and bowl-shaped conformation of the naphthalene spacer units. (Bottom left) The ureas are tilted 6° from perpendicular to the plane of the naphthalenes to alleviate strain of the methylene group (bottom right) that is extended to 115°. Some hydrogens have been omitted for clarity.

The parallel orientation of the ureas and the bowl-shape of the spacer group in the napthalene macrocycle were not observed in the protected precursor. To examine if this was an effect of the solvent, the macrocycle was crystallized from other solvents including benzene, acetonitrile, DMSO, and methanol. Microcrystals were observed from these solvents that were not suitable for single crystal X-ray analysis. X-Ray quality crystals were observed from the vapor diffusion of methanol into a 1 mg mL^{-1} DMSO solution of *bis*-urea 2,7-dimethyl naphthalene macrocycle. The macrocycle crystallized along with two disordered methanol molecules [$C_{26}H_{24}N_4O_2 \cdot 2(CH_3OH)$]. No DMSO molecules were present. The macrocycle retains the bowl shape arrangement of the

naphthalenes and the parallel orientation of the ureas similar to the DMSO/water crystal. The packing of the macrocycle is observed to be a lamellar structure consisting of chains of macrocycles directly hydrogen-bonded to one another in an offset, tilted fashion. (Fig. 3.11) The carbonyl of one urea forms hydrogen bonds with the two NH groups of the neighboring macrocycle urea (N···O = 2.826(2) Å). The hydrogen bonded chains of macrocycle were separated by disordered methanol molecules with an average distance between macrocycles of adjacent chains of 5.4 Å. The methanol molecules are hydrogen bonded to the unoccupied carbonyls below with O···O distances ranging from 2.692(3) – 2.809(4) Å and to the urea nitrogens above (N···O distance = 3.053(3)). Once these hourglass shaped twin crystals are removed from the mother liquor they desolvate beyond X-ray quality.

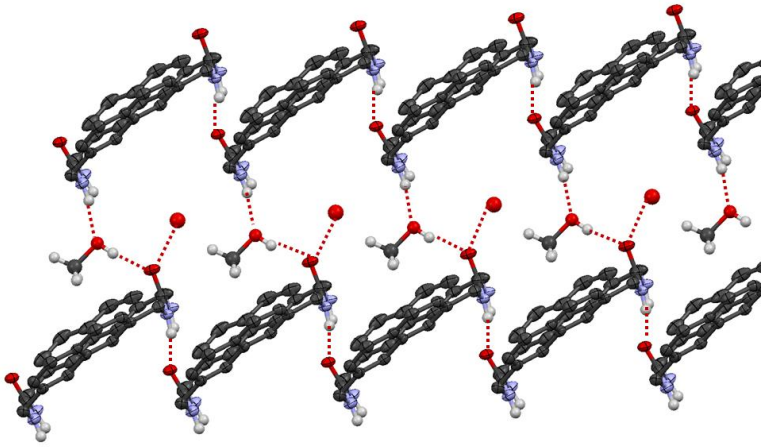

Figure 3.12. Crystal packing of the 2,7-naphthalene macrocycle resulting from the vapor diffusion of methanol into DMSO solution showing the lamellar arrangement of the macrocycles and the hydrogen bonding motif with themselves and the disordered methanol (some hydrogens and methanol molecules have been omitted for clarity).

3.6 Synthesis of 1,3-Dimethyl Naphthalene *Bis*-Urea Macrocycle

To further examine into the effect of the aryl group, we used 1,3-dimethylnaphthalene spacers to construct a bis-urea macrocycle **3.14.** The 1,3 dimethyl naphthalene better mimics the *m*-xylene spacer that has been shown to self-assemble into columnar structures. Unlike the 2,7-dimethyl naphthalene macrocycle that disrupts the three centered self-assembly of the ureas, the 1,3-naphthalene spacer should adopt a conformation that orients the ureas in the preferred anti-parallel conformation. It was shown previously that the assembled columnar crystal structure of the meta-xylene macrocycle that there was a secondary offset aryl-aryl interaction that assisted in the assembly of the macrocycles. With the extension of that aryl shelf we will examine the effect on the stacking of the naphthalene macrocycle to see if the assembly is enhanced by the increase in aryl interactions.

The 1,3-dimethyl naphthalenyl *bis*-urea macrocycle was synthesized from commercially available 1,3-dimethyl naphthalene. The benzyl positions were brominated under radical conditions with NBS (86% yield). Next, the dibromide was cyclized with triazinanone under basic conditions to afford **3.13p**. The triazinanone groups were subsequently deprotected in acidic diethanol amine/water (1:1) solution to give the 1,3-naphthenyl *bis*-urea product **3.13**.

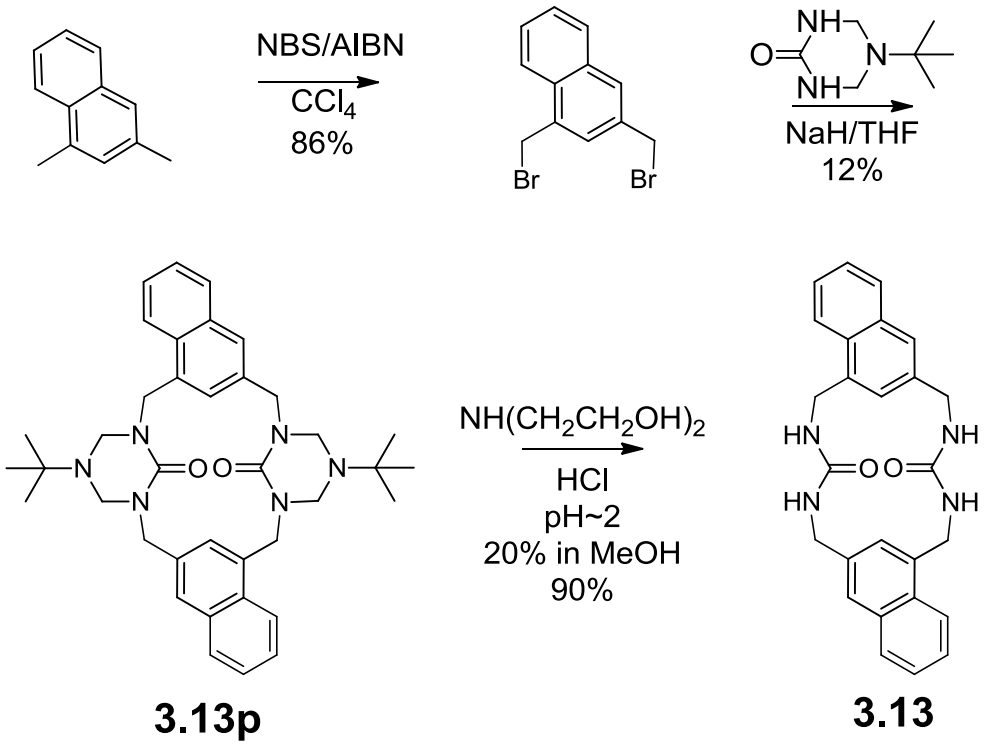

Scheme 3.2. Synthetic scheme of 1,3dimethyl naphthalene macrocycle (**3.13**).

3.7 Crystal Structure Characterization of 1,3-Dimethyl Naphthalene *Bis*-Urea Macrocycle [$C_{38}H_{46}N_6O_2$].

Large crystals of the protected *bis*-urea 1,3-dimethyl naphthalene macrocycle **3.13p** were formed from the slow evaporation of a dichloromethane solution (~1 mg mL^{-1}). Two different colorless crystals formed, long needles and short blocks that were of high enough quality for single crystal X-ray diffraction. The two crystals proved to be separate polymorphs. The needle shape crystals crystallized in the triclinic space group $P\bar{1}$. The unit cell consist of one half of each of two independent macrocycles located on the crystallographic inversion center. The packing of these crystals incorporated no solvent

molecules and showed no close interaction between the aryl spacer groups with an average distance between macrocycles of ~3.5 Å. Figure 3.12 shows the orientation of the naphthalene spacers arranged in a perpendicular geometry from the macrocycle above to the macrocycle below. The only short contacts appear between the methylene group and the naphthalene ring of an adjacent macrocycle below (C-H···aryl distance = 3.280 Å) and between the methylene group with the carbonyl oxygen (C-H···O distance = 3.827 Å). The orientation of the systems with respect to others suggests the packing to be governed by close packing and Van der Waal's forces (Fig. 3.12).

Examination of the monomer shows that the macrocycle adopts a conformation similar to that of the *meta*-xylene macrocycle. The urea groups are oriented perpendicular to the plane of the macrocycle (angle = 89.1º). The spacer groups adopt a planer orientation with the naphthalenes tilted only slightly out of that plane (angle = 26.6º). These, along with the anti-parallel orientation of the ureas, suggest that upon deprotection of the macrocycle we should expect the formation of columnar structures.

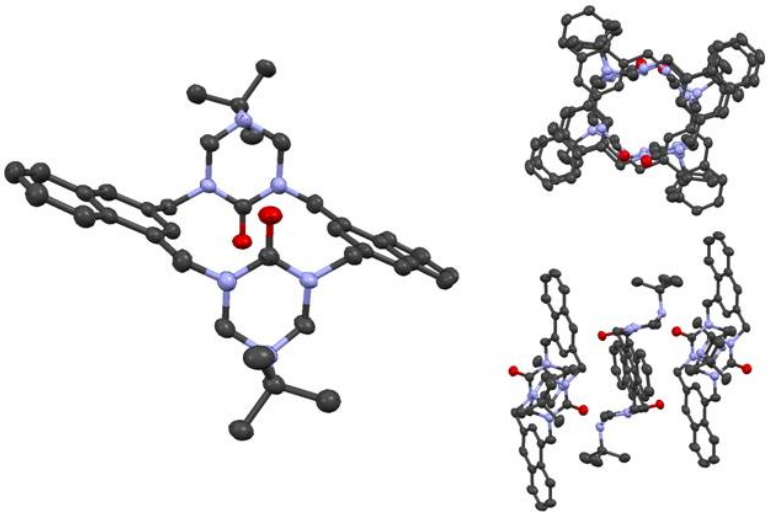

Figure 3.13. The crystal structure of the protected *bis*-urea 1,3 dimethylnaphthalene macrocycle **3.13p** and crystal packing of the triclinic crystal. (left) The crystal structure of the 1,3 naphthalene macrocycle that shows the planar orientation of the naphthalene spacers with the perpendicular and anti-parallel ureas. (right) The crystal packing of the monoclinic crystals shows the orientation of the naphthalenes that are perpendicular to each other resulting in no interactions between the groups (hydrogens omitted for clarity).

The second colorless blocky crystals crystallized in the monoclinic space group *P*21/n also without solvent molecules. The unit cell has similar dimensions to that of the triclinic form and consists of one half of one macrocycle located on the crystallographic inversion center. In this structure, the macrocycles pack together in lamellar sheets when viewed perpendicular to the b-axis. The neighboring macrocycles show an offset aryl-aryl stacking between the naphthalene spacer groups with a center-to-center distance of 3.324 Å. (Fig. 3.13)

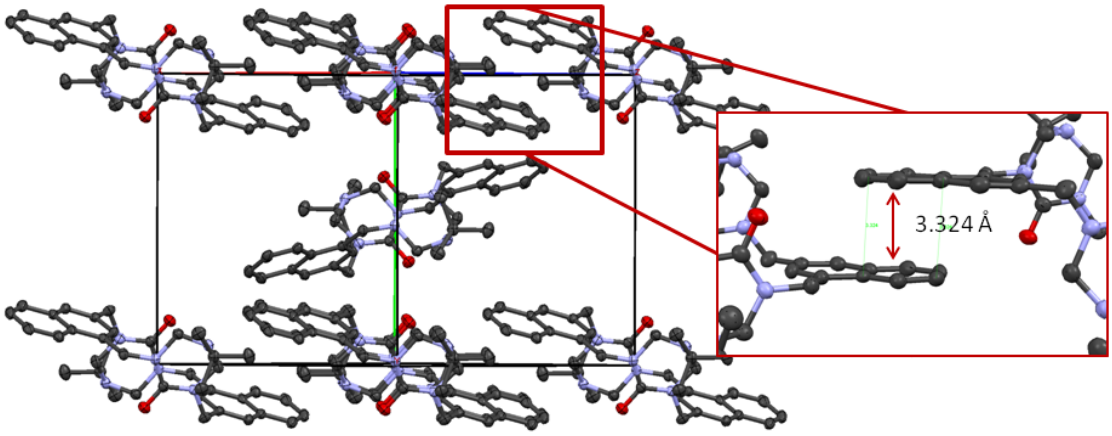

Figure 3.14. Crystal packing of the 1,3-naphthlene macrocycle **3.13p** monoclinic crystal viewed along the c*-axis. (inset) the aryl-aryl distance of 3.324 Å between the macrocycles suggests aryl interaction that assists in the packing of the monoclinic crystals (hydrogens omitted for clarity).

Comparison of the monomer to that of the triclinic system sees that the orientation and geometries are similar with ureas adopting an anti-parallel arrangement and perpendicular to the plane of the macrocycle (angle =89.5º). The naphthalenes are also tilted slightly from the plane of the macrocycle at an angle of 23º. These are similar to that of the m-xylene macrocycle **3.1**. Therefore, we expect that upon deprotection that it will adopt a conformation that is beneficial for columnar assembly. Currently, we are investigating crystallization conditions for the formation of the columnar assemblies. To date a series of crystallization conditions have been tried, such as slow cooling, vapor diffusion, and solvothermal. These have resulted in the formation of a precipitate or microcrystals too small for single crystal X-ray analysis.

3.8 Synthesis of 4-Bromo-1,3-Dimethyl Naphthalene *Bis*-Urea Macrocycle (3.14)

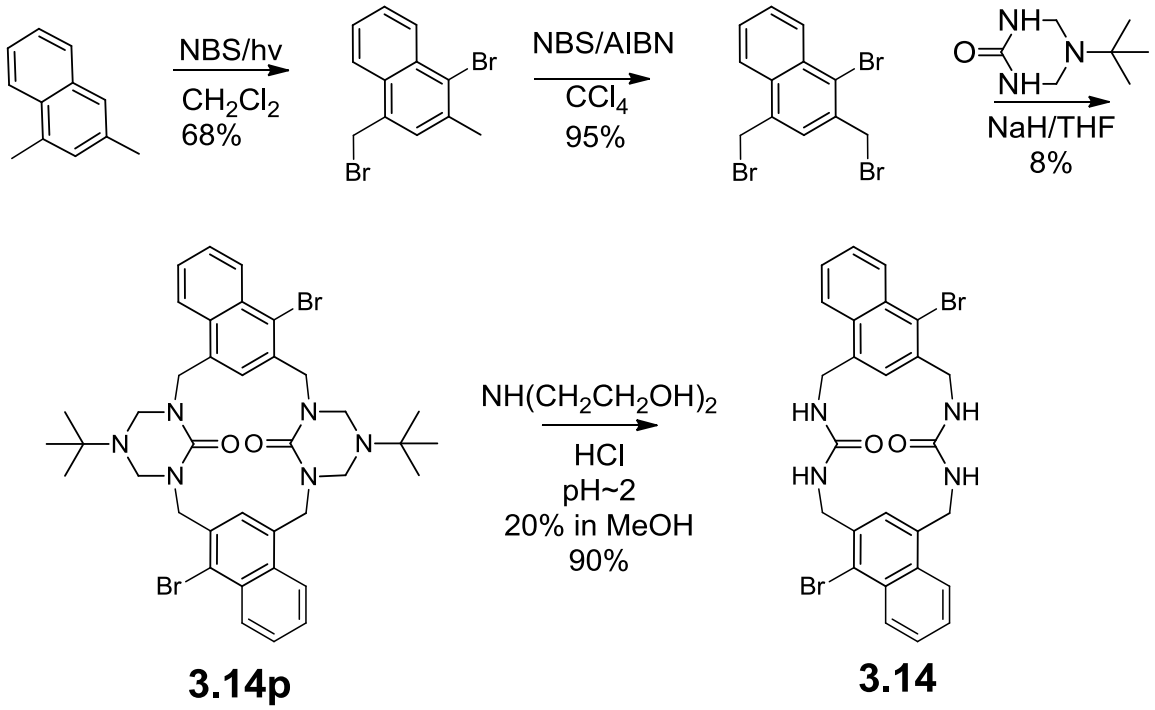

Scheme 3.3. Synthetic scheme of 4-bromo-1,3-dimethylnapthalene macrocycle (**3.14**).

The 4-bromo-1,3-naphthlene *bis*-urea macrocycle was synthesized in 4 steps. First, commercially available 1,3-dimethyl naphthalene was irradiated under UV light source to brominate one methyl group and the 4-position on the naphthalene ring. This step resulted in the formation of two products, 4-bromo-3-bromomethyl-1-methyl naphthalene and 1,3-dibromonaphthalene. These were separated and purified through column chromatography (6:1 hexanes:methylene chloride). Then the dibromide product was brominated further through radical bromination with NBS in the presence of AIBN. The resulting tribromide was then cyclized under basic condition with the protected urea

group. Finally, the protecting group was removed by refluxing in an acidic 20% diethanol amine aqueous/methanol (1:1 v/v) solution to afford macrocycle **3.14** (5% overall).

3.9 Crystal Structure Characterization of 4-Bromo-1,3-Dimethyl Naphthalene *Bis*-Urea Macrocycle (3.14).

The slow evaporation of the tri-bromo naphthalene (~1 mg mL^{-1}) from a methylene chloride/hexanes solution afforded colorless plate-like crystals large enough for single crystal X-ray analysis. The crystals ($C_{12}H_9Br_3$) were colorless plate-like crystals that crystallized in the monoclinic $P2_1/c$ space group. The unit cell consists of one tribromide molecule. The resulting structure shows the expected dimethyl naphthalene with three bromide substitutions, one each on the methyl groups in the 1 and 3 position of the naphthalene ring, the third in the 4 position directly attached to the ring. It is unusual for radical conditions to favor the bromination of the benzyl site over the aryl substitutions.[11] The naphthalenes pack in dimers with the dimers forming a herringbone arrangement. Figure 3.14b shows the dimers in close contact with each other (center to center distance of 3.856 Å) in an offset structure manner. The bromines attached to the methyl groups both point toward the same side of the naphthalene ring (figure 3.14a). These bromines assist in the packing through short contacts with the aryl hydrogens of the adjacent ring (aryl-C···Br distance =3.861 and 3.687 Å) well within the sum of van der Waal's radii (4.55 Å). Also of note, figure 3.14c shows the formation of a halogen Br•••Br bond that is 3.404 Å long (92 % of Van der Waals' radii-3.70 Å) at a 156.28 º angle. This is a Type I halogen bond that will be discussed in detail in chapter 4. The existence of the halogen bond between the two aryl bromides suggests that the bromine substituent can assist in the columnar packing as well

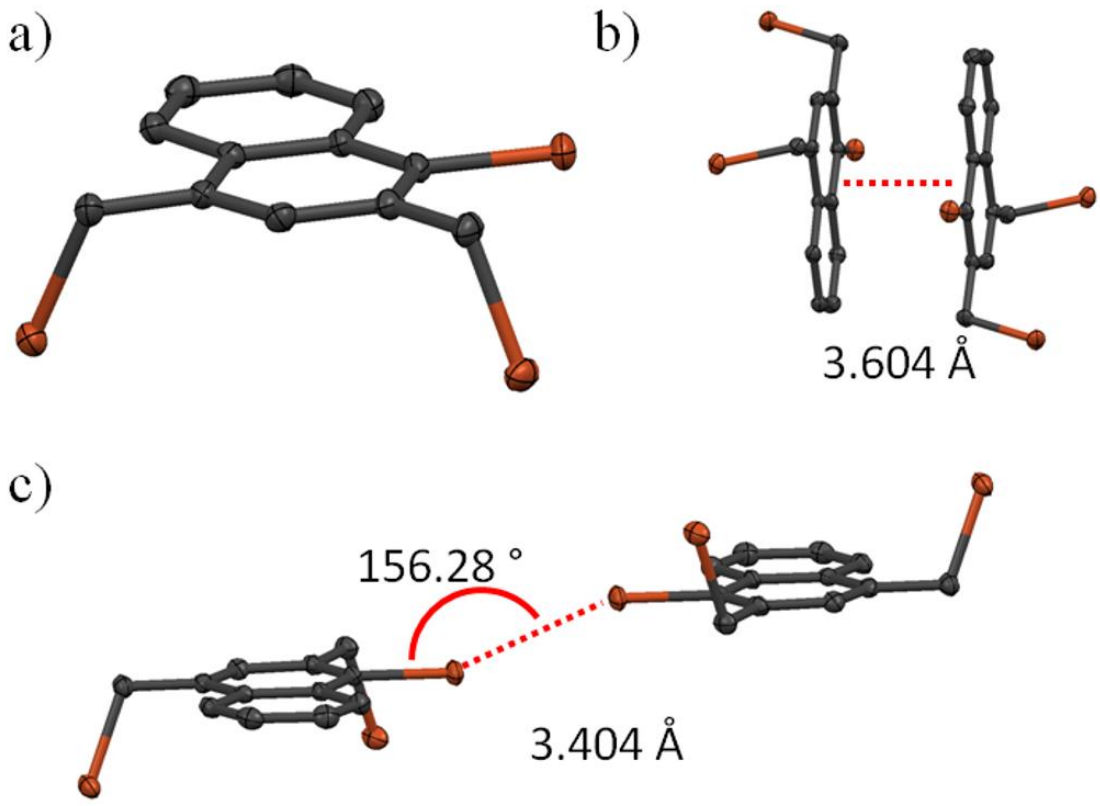

Figure 3.15. Crystal structure of 4-bromo-1,3-dibromomethyl naphthalene. a) Depiction of the orientation of the bromide substituents with the third bromine attached directly to the ring and the two bromines at the benzyl sites directed toward the same side of the ring. b) The tribromide dimers with an offset packing with a distance of 3.604 Å. c) The Type I halogen bond formed between the two aryl bromides with halogen bond distance of 3.404 Å which is 8% shorter than the sum of Van der Waal's radii for bromine (3.70 Å).

Upon cyclization the macrocycle **3.14p** crystallized from the slow evaporation of the solution in chloroform (~1 mg mL^{-1}) to form colorless needle crystals. The compound $[C_{38}H_{44}Br_2N_6O_2 \cdot 2(CDCl_3)]$ crystallized in the triclinic space group $P^{-}1_2$ and the unit cell consists of one half of one macrocycle 3.14p on the crystallographic center along with a chloroform molecule disordered over two positions. One of the macrocycle's *tert*-butyl groups is also disordered over two positions. Figure 3.15 shows the crystal packing that consists of a layered orientation of the macrocycle 3.14 separated by the disordered chloroform molecules. The macrocycles in each layer are in close contact with one

another through offset aryl stacking with a center-to-center distance of 3.456 Å. The macrocycle itself has a similar conformation to that of macrocycle **3.1** and **3.13p.** The ureas are oriented in an anti-parallel conformation (angle = 88.54º) with the naphthalenes tilted slightly out of the plane of the plane of the macrocycle (angle = 27.88 º). The aryl bromides are not involved in any short contacts in this crystal structure, which suggests the weak interaction that the bromide display in halogen bonds and are easily disrupted.

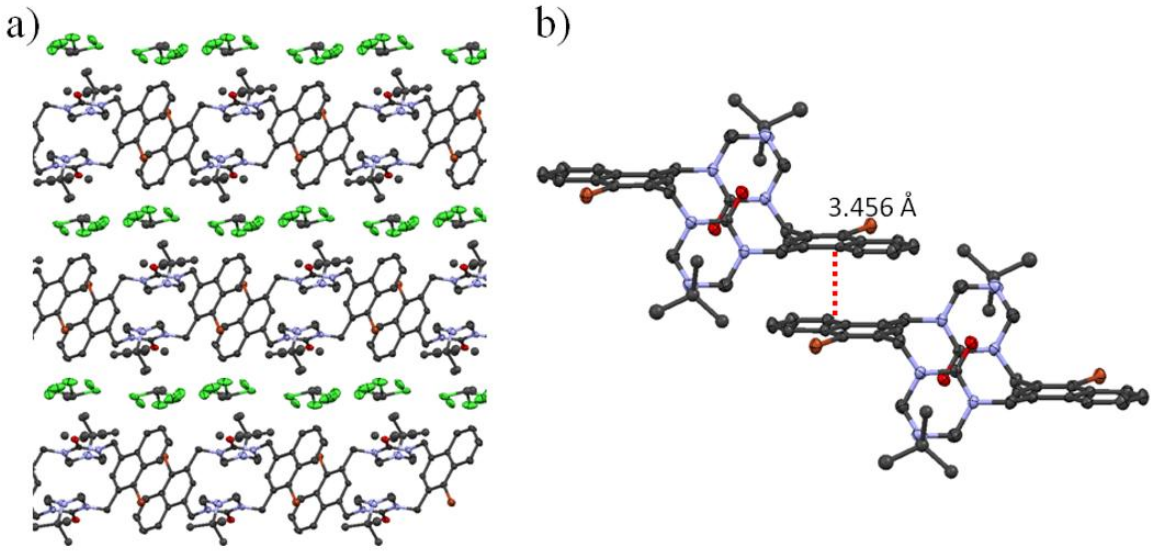

Figure 3.16. Crystal structure of macrocycle **3.14p** from the slow evaporation of chloroform. a) The layered packing of the crystal shows layers of macrocycle **3.14p** separated by disordered chloroform molecules. b) The offset aryl stacking that is seen between the macrocycles that assists in the crystallization of the macrocycle layer.

3.10. Conclusions.

In summary, we synthesized three macrocycles with extended aryl spacers, 2,7 dimethyl naphthalene macrocycle **3.12**, 1,3 dimethyl naphthalene macrocycle **3.13**, and 4-bromo-1,3-dimethyl naphthalene macrocycle **3.14**. The incorporation of the 2,7-dimethyl naphthalene spacer resulted in a unique urea conformation that prevented the self-assembly of the ureas through the typical three centered hydrogen bond. The

naphthalenes formed two crystal structures that both had similar macrocycle conformation that oriented the naphthalene spacers in a bowl shape despite the conformation of the protected macrocycle showing the desired conformation where the ureas are perpendicular to the plane of the macrocycle.

The incorporation of the 1,3 dimethyl and 4-bromo-1,3dimethyl spacer groups have resulted in protected macrocycles with the conformation that is seen with the *m*-xylene macrocycle **3.1** that promote the self-assembly of the ureas to form columnar structures. The free ureas have not yet afforded crystals suitable for single X-ray quality from DMSO slow cooling or through vapor diffusion into DMSO solvents. We are currently working on more crystallization conditions to elucidate the structure and assembly motif of these deprotected macrocycles. The addition of the aryl bromide in the 4-bromo-1,3-naphthalene spacer has also shown a potential to form halogen bonds between the macrocycles that may also promote the assembly of the columnar structures with each other.

3.11. Summary and Future Work

The effect of naphthalene spacer on the self assembly of the *bis*-urea macrocyclic system is still underway and the crystallization of the macrocycles in this chapter will help elucidate some of those effects. Other spacer moieties can also be explored to further this study such as those listed in Table 3.1. For example, what effect would the expansion in two directions have on the assembly? With the incorporation of spacer groups such as anthracene **3.16**, phenanthrene **3.17,** or phenalene **3.16** we can explore the further expansion of the aryl shelf and what the effect would be on the self-assembly of the

ureas. Also, the extension of the spacer group using a ethynyl extender, such as with the phenylethynylene macrocycle, did not disrupt the self assembly and resulted in columnar structures with larger pore sizes.[6b] We can modify the naphthalene spacer moieties (Table 3.1, **3.18** and **3.19**) and study the effect of the extension on the self-assembly of the macrocycles. Do we see the same disruption or would the extension allow for the ureas to assemble.

Table 3.1. Proposed spacers for the study of the assembly motif of the *bis*-urea macrocycles.

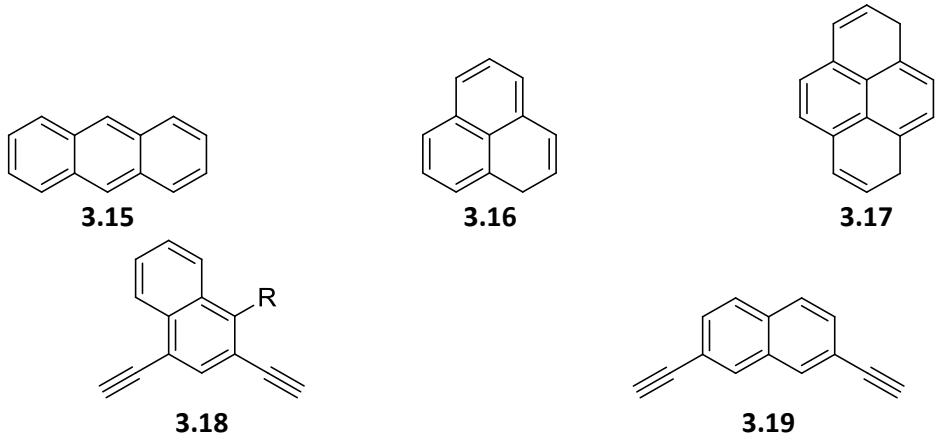

3.15 **3.16** **3.17** **3.18** **3.19**

Due to the roles anions play in environment and biological systems selective detection of these anions has become important.[12] Ureas have been shown to be efficient anion receptors.[13] When incorporated into metal organic frameworks, such as those studied by Custelcean and Remy,[14] the incorporation of urea moieties in the ligands are then coordinated with Mg^{+} and Li^{+} salts and show a high affinity for SO_3^{2-} and CO_3^{2-} while excluding SeO_4^{2-}.[14] With the incorporation of the ureas into a cyclic structure and the inclusion of fluorescent molecules into the spacer group, the naphthyl macrocycles could have a propensity for selective anion binding. Preliminary work in this chapter shows that the macrocycles, at least the 2,7dimethyl naphthalene macrocycle **3.12**, does

not assemble into columnar assemblies but can assemble with assistance from hydrogen bond donors (water and methanol). Will anions assist with assembly, and will the binding be selective for anions of complementary size to that of the macrocycles? The study of the assembly process of the *bis*-urea macrocycles is still in its infancy and a closer look at the spacers and the assembly process will allow us to better understand and design macrocycles with utility in this area.

3.12. Experimental

3.12.1. Materials and Instrumentation

All chemicals were used as purchased without further purification. ^{1}H-NMR and ^{13}C-NMR spectra were recorded on Varian Mercury/VX 300 and VX 400.

3.12.2. Synthesis

2,7-*bis*(bromomethyl) naphthalene

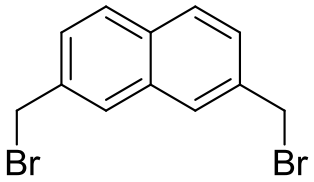

N-bromosuccinimide (32 mmol, 5.7g) and 2,7-dimethylnaphthalene (16 mmol, 2.5 g) were dissolved into carbon tetrachloride (40 mL). Azobisisobutyronitrile (AIBN) (5%, 0.80 mmol, 0.131 g) was added, and the reaction mixture was heated to 80 ° C for 18 h. Upon completion, the reaction mixture was cooled to room temperature and the precipitate was filtered off and rinsed with dichloromethane. The filtrate was reduced in *vacuo* and the product was purified *via* column chromatography (8:2 hexanes:dichloromethane) to afford a pale yellow powder (4.65 g, 90%), mp 150-152 °C.

^{1}H-NMR (300MHz, $CDCl_3$): δ 7.82 (d, J=8.8 Hz, 4H), 7.52 (d, J=8.5 Hz, 2H), 4.65 (s, 4H). ^{13}C-NMR (100 MHz, $CDCl_3$): δ 135.8, 128.6, 127.9, 127.5, 33.7. Direct probe EIMS (*m/z*): 314 (calculated for $C_{12}H_{10}Br_2$: 314.02).

Triazinanone protected *bis*-(urea 2,7-dimethyl naphthalene) macrocycle 3.12p.

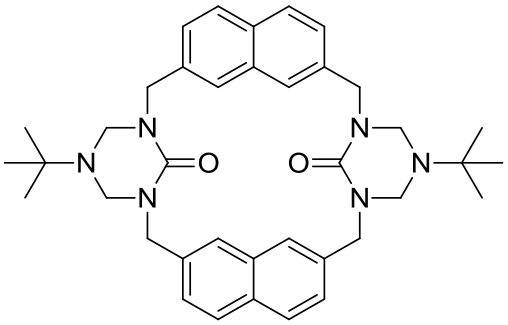

A 60% suspension of sodium hydride in mineral oil (7.5 mmol NaH, 0.300g) and 5-*tert*-butyltetrahydro-1,3,5-triazin-2(1H)-one (2.5 mmol, 0.39g) were added to freshly distilled THF and heated to reflux for 1 h. The reaction mixture was cooled to room temperature and a solution of 2,7-*bis*(bromomethyl) naphthalene (2.5mmol, 0.79 g) in 100 mL THF was added dropwise over 1 h. The reaction mixture was heated to reflux for 48 h and then cooled to room temperature and neutralized with 20 mL 1 N HCl and 80 mL distilled water. The mixture was reduced in *vacuo* to ~ 100 mL and extracted with methylene chloride (3 x 100 mL). The organic layer was rinsed with brine and dried over anhydrous magnesium sulfate. The product was isolated by column chromatography (95:5 EtOAc:MeOH) to yield a white crystalline powder (118.4 mg, 15 %). ^{1}H-NMR (400 MHz, $CDCl_3$): δ 7.87 (s, 4H), 7.79 (d, J=8.2 Hz, 4H), 7.27 (d, J=8.6 Hz, 4H), 5.88 (d, J= 16.2 Hz, 4H), 4.47 (d, J= 11.5 Hz, 4H), 4.22 (d, J= 11.7 Hz, 4H), 3.84 (d, J= 16.4 Hz, 4H), 1.20 (s, 18 H). ^{13}C-NMR (100MHz, $CDCl_3$): δ 155.9, 136.1, 134.0, 132.0, 128.0, 125.4, 124.4, 63.1, 54.1, 49.4, 28.6. TOF ESI-MS: *m/z* 619 (100%) $[M + H]^+$ (calculated for $C_{38}H_{46}N_6O_2$: 618.81).

1,1'-*bis*(2,7-dimethyl naphthalenyl)-*bis*-urea macrocycle 3.12.

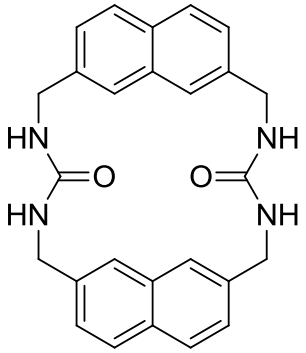

The protected macrocycle (100 mg) was added to an aqueous solution of 20 % diethanol amine (pH ≈ 2) and methanol (1:1 by volume) and heated to reflux overnight. After cooling, the reaction mixture was neutralized with 10 mL 1 N HCl and 10 mL distilled water. The resulting precipitate was filtered off and rinsed with 1 N HCl (3 x 10 mL) and distilled water (3 x 10 mL) yielding a white crystalline powder (68 mg, 97 %). Decomposes at 330 ºC. ^{1}H-NMR (300 MHz, δ_6-DMSO): δ 7.83 (d, J=8.5 Hz, 4H), 7.74 (s, 4H), 7.32 (d, J= 8.2 Hz, 4H), 6.84 (s, 4H). ^{13}C-NMR (100 MHz, δ_6-DMSO): δ 158.14, 139.7, 139.6, 133.2, 130.9, 127.5, 124.8, 42.4.

3-methyl-1-bromomethyl-4-bromo naphthalene

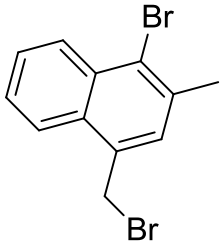

To freshly distilled dichloromethane (30 mL), 1,3-dimethyl naphthalene (6.401 mmol, 1.00 g) was added. To this solution, N-bromosuccinimide (13.44 mmol, 2.393 g) was added and the solution was irradiated under a medium pressure mercury lamp for 18 h. The solution was then cooled in an ice bath and the precipitate collected through

vacuum filtration and rinsed with dichloromethane (2 x 5 mL). The filtrate was evaporated and the product isolated by column chromatography (9:1 Hexanes: CH_2Cl_2) to yield an off-white powder (1.139 g, 58 %), and 1,3-dibromomethyl naphthalene (0.8042 g, 40%). ^{1}H-NMR (300 MHz, $CDCl_3$): δ 8.38 (m, 1H), 8.10 (m, 1H), 7.61(m, 2H), 7.44 (s, 1H), 4.90 (s, 2H), 2.61(s, 3H). ^{13}C-NMR (75 MHz, $CDCl_3$): δ 134.7, 131.7, 130.4, 130.4, 129.5, 127.0, 126.5, 125.8, 125.2, 124.7, 26.6, 31.9.

1,3-dibromomethyl-4-bromo naphthalene

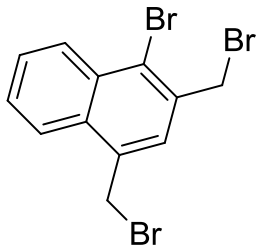

The 3-bromomethyl-1-methyl-4-bromo naphthalene (3.19 mmol, 1.00 g) was stirred in carbon tetrachloride (20 mL) and N-bromo succinimide (3.19 mmol, 0567 g) and AIBN (5%, 1.59 mmol) were added. The reaction mixture was heated to reflux for 18 h. The reaction mixture was cooled to room temperature and then further cooled in an ice bath forming a white precipitate. The precipitate was collected by vacuum filtration and rinsed with dichloromethane (3x 5 mL). The tribromonaphthalene was purified by column chromatography (1:9 CH_2Cl_2:hexanes) and isolated as a white crystalline powder (87%, 1.086g). ^{1}HNMR (300 MHz, $CDCl_3$): δ 8.41 (m, 1H), 8.13 (m, 1H), 7.67 (m, 2H), 7.60 (s, 1H), 4.89 (s, 2H), 4.82 (s, 2H). ^{13}C-NMR (75 MHZ,$CDCl_3$): δ133.7, 131.7, 130.6,130.4, 129.7, 129.5, 126.9, 127.0, 125.5, 124.4, 32.5, 30.5.

Protected 4-bromo-1,3-dimethyl napthalnenyl *bis*-urea macrocycle 3.14p

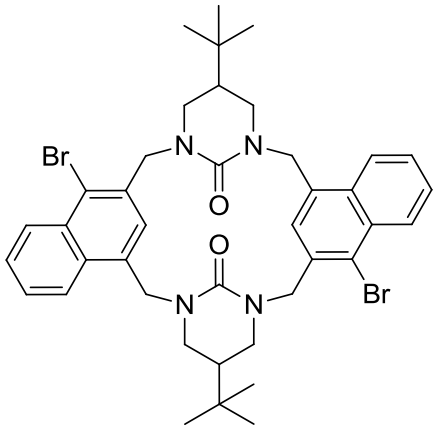

To freshly distilled THF (300 mL), 5-tert-butyltetrahydro-1,3,5-triazin-2(1H)-one (0.202 g, 1.29 mmol) and sodium hydride (0.206g, 5.16 mmol) were added and the suspension was heated to reflux for 2 h. The suspension was allowed to cool to room temperature, and then a solution of 4-bromo-1,3-dibromomethylnaphthalene (1.00 g, 1.29 mmol) in THF (200 mL) was added. The reaction mixture was then heated to reflux for 48 h. After completion (give TLC conditions), the reaction mixture was cooled to room temperature and quenched with 10 mL 1 N HCl and distilled water (90 mL). The solution was then reduced in *vacuo* to ~ 100 mL volume and extracted with methylene chloride. The organic layer was washed with brine and dried over magnesium sulfate (anhydrous) and then the solvent was removed in *vacuo*. The product was purified by column chromatography (eluent) as an of white powder (8%). ^{1}HNMR (300 MHz, $CDCl_3$): δ 8.38 (m, 1 H), 8.10 (m, 1H), 7.61(m, 2H), 7.36 (s, 1H), 4.84 (s, 2H), 2.59 (s, 3H), ^{13}CNMR(75 MHz, $CDCl_3$) δ 135.7, 133.0, 132.5, 130.4, 130.3, 128.3, 127.9, 127.6, 126.4, 124.0, 35.1, 31.2, 24.1, 19.3.

1,1'-*bis*(4-bromo-1,3-dimethylnaphthalenyl)-*bis*-urea macrocycle

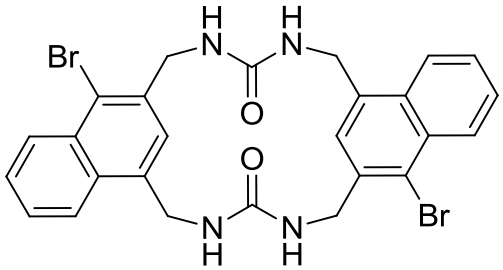

The protected macrocycle **3.14p** (100 mg, 0.129 mmol) was added to an aqueous solution of 20 % diethanol amine (pH ≈ 2) and methanol (1:1 by volume) and heated to reflux overnight. After cooling, the reaction mixture was neutralized with 10 mL 1 N HCl and 10 mL distilled water. The resulting precipitate was filtered off and rinsed with 1 N HCl (3 x 10 mL) and distilled water (3 x 10 mL) yielding a white crystalline powder (67 mg, 90%). Decomposes at 375 ºC. ^{1}H-NMR (300 MHz, δ_6-DMSO): δ 8.64 (d, J=8.5 Hz, 4H), 7.70(s, 4H), 7.48 (d, J= 8.2 Hz, 4H), 6.34(s, 4H). ^{13}C-NMR (75 MHz, δ_6-DMSO): δ 162.1, 139.7, 139.6, 133.2, 130.7, 127.5, 124.8, 42.3.

1,3-dibromomethyl naphthalene

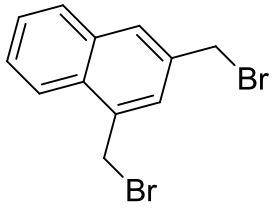

To a stirred solution of dimethyl naphthalene (1.00 g, 6.40 mmol) in carbon tetrachloride (40 mL), N-bromo succinimide (2.39 g, 13.4 mmol), and AIBN (5 %, 0.32 mmol) were added. The reaction mixture was heated to 80 ºC for 18 h and monitored by TLC (5:1; hexanes:dichlormethane). The reaction mixture was then cooled in an ice bath and the precipitate was filtered off by vacuum filtration and rinsed with dichloromethane

(3 x 10 mL). The filtrate was reduced in *vacuo* to a brown oil. The product was purified by column chromatography (5:1; hexanes:dichlormethane) to afford a white powder (1.93 g, 96 %). ^{1}H-NMR (300 MHz, $CDCl_3$): δ 8.14 (d, J=8.2, 1H), 7.85 (m, 2H), 7.59 (m, 3H), 4.94 (s, 2H), 4.63 (s,2H).^{13}C-NMR (75MHz, $CDCl_3$) δ 134.7, 134.3, 133.9, 129.5, 128.9, 128.5, 128.3, 127.3, 126.9, 123.7, 33.3, 31.1.

Protected 1,3-dimethylnaphthylenyl *bis*-urea macrocycle (3.13p).

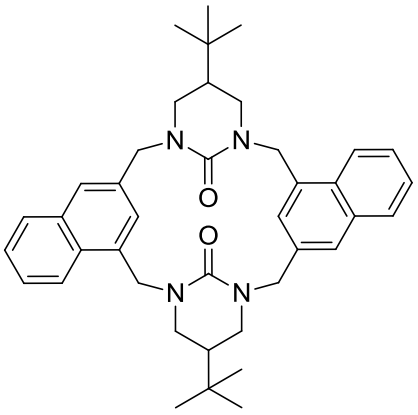

To freshly distilled THF (300 mL), 5-tert-butyltetrahydro-1,3,5-triazin-2(1H)-one (0.501 g, 3.18 mmol) and sodium hydride (0.510 g, 12.72 mmol) were added and the suspension was heated to reflux for 2 h. The suspension was allowed to cool to room temperature, and then a solution of 4-bromo-1,3-dibromomethylnaphthalene (1.00 g, 3.18 mmol) in THF (200 mL) was added. The reaction mixture was then heated to reflux for 48 h. After completion (give TLC conditions), the reaction mixture was cooled to room temperature and quenched with 10 mL 1 N HCl and distilled water (90 mL). The solution was then reduced in *vacuo* to ~ 100 mL volume and extracted with methylene chloride. The organic layer was washed with brine and dried over magnesium sulfate (anhydrous) and then the solvent was removed in *vacuo*. The product was purified by column chromatography (eluent) as an of white powder (197 mg, 10%). ^{1}H NMR (300

MHz, $CDCl_3$): δ 8.38 (m, 1 H), 8.10 (m, 1H), 7.61(m, 2H), 7.50 (s, 1H), 4.84 (s, 2H), 2.59 (s, 3H), ^{13}C NMR(75 MHz, $CDCl_3$) δ 135.7, 133.0, 132.5, 130.4, 130.3, 128.3, 127.9, 127.6, 126.4, 124.0, 35.1, 31.2, 24.1, 19.3.

1,1'-*bis*(1,3-dimethylnaphthalenyl urea) macrocycle (3.13).

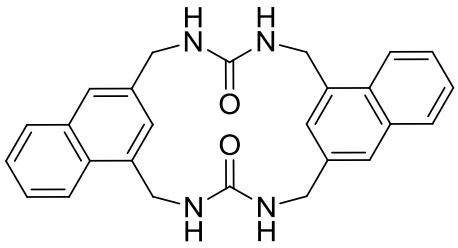

The protected macrocycle **3.13p** (100 mg, 0.129 mmol) was added to an aqueous solution of 20 % diethanol amine (pH ≈ 2) and methanol (1:1 by volume) and heated to reflux overnight. After cooling, the reaction mixture was neutralized with 10 mL 1 N HCl and 10 mL distilled water. The resulting precipitate was filtered off and rinsed with 1 N HCl (3 x 10 mL) and distilled water (3 x 10 mL) yielding a white crystalline powder (67 mg, 90%). Decomposes at 375 ºC. ^1H-NMR (300 MHz, δ_6-DMSO): δ 8.64 (d, J=8.5 Hz, 4H), 7.70(s, 4H), 7.48 (d, J= 8.2 Hz, 4H), 6.34(s, 4H). ^{13}C-NMR (75 MHz, δ_6-DMSO): δ 162.1, 139.7, 139.6, 133.2, 130.7, 127.5, 124.8, 42.3.

3.12.3 X-ray crystal structure determination of protected 2,7-dimethyl naphthalenyl *bis*-urea macrocycle (3.12p) [$C_{38}H_{46}N_6O_2$]:

X-ray intensity data from a colorless needle crystal were measured at 150(1) K on a Bruker SMART APEX diffractometer (Mo Kα radiation, λ = 0.71073 Å).[15] Raw area detector data frame processing was performed with the SAINT+ program.[15] Although

the selected crystal was among the largest available, the dataset was truncated at 2θ = 46.5° because of the small size and weak diffracting power of the crystal. Final unit cell parameters were determined by least-squares refinement of 939 reflections from the data set. Direct methods structure solution, difference Fourier calculations and full-matrix least-squares refinement against F^2 were performed with SHELXTL.[16]

The compound crystallizes in the space group $P2_1/n$ as determined uniquely by the pattern of systematic absences in the intensity data. The asymmetric unit consists of half of one molecule, which is located on a crystallographic inversion center. All non-hydrogen atoms were refined with anisotropic displacement parameters. Hydrogen atoms were located in difference maps before being placed in geometrically idealized positions and included as riding atoms.

Table 3.2 Crystal data and structure refinement [$C_{38}H_{46}N_6O_2$].

Empirical formula	C38 H46 N6 O2	
Formula weight	618.81	
Temperature	150(2) K	
Wavelength	0.71073 Å	
Crystal system	Monoclinic	
Space group	$P2_1/n$	
Unit cell dimensions	a = 8.8432(11) Å	α= 90°.
	b = 18.133(2) Å	β= 111.470(3)°.
	c = 10.7628(13) Å	γ = 90°.
Volume	1606.1(3) $Å^3$	
Z	2	
Density (calculated)	1.280 Mg/m^3	
Absorption coefficient	0.081 mm^{-1}	

F(000)	664
Crystal size	0.22 x 0.04 x 0.04 mm^3
Theta range for data collection	2.25 to 23.26°.
Index ranges	-9<=h<=9, -20<=k<=20, -11<=l<=11
Reflections collected	12794
Independent reflections	2304 [R(int) = 0.0976]
Completeness to theta = 23.26°	100.0 %
Absorption correction	None
Refinement method	Full-matrix least-squares on F^2
Data / restraints / parameters	2304 / 0 / 211
Goodness-of-fit on F^2	0.806
Final R indices [I>2sigma(I)]	R1 = 0.0413, wR2 = 0.0588
R indices (all data)	R1 = 0.0867, wR2 = 0.0696
Largest diff. peak and hole	0.139 and -0.143 e.$Å^{-3}$

3.12.4 X-ray crystal structure determination of 2,7-dimethyl naphthalenyl *bis*-urea macrocycle (3.12).

[$(C_{26}H_{24}N_4O_2)$•$((CH_3)_2SO)(H_2O)_2$].

X-ray intensity data from a colorless block-like crystal were measured at 100(2) K using a Bruker SMART APEX diffractometer (Mo Kα radiation, λ = 0.71073 Å).[15] Raw area detector data frames were reduced with the SAINT+ program.[15] Final unit cell parameters were determined by least-squares refinement of 2100 reflections from the data set. Direct methods structure solution, difference Fourier calculations and full-matrix least-squares refinement against F^2 were performed with SHELXTL.[16]

The compound crystallizes in the space group $P2_1/c$ as determined by the pattern of systematic absences in the intensity data. The asymmetric unit consists of one $C_{26}H_{24}N_4O_2$ molecule, one DMSO molecule and two water molecules. All non-hydrogen atoms were refined with anisotropic displacement parameters. Hydrogen atoms bonded to carbon were placed in geometrically idealized positions and included as riding atoms. Hydrogen atoms bonded to nitrogen and oxygen atoms were located in difference maps and refined isotropically, with N-H and O-H distances restrained to be similar to those of the same type.

Table 3.3 Crystal data and structure refinement [$(C_{26}H_{24}N_4O_2)$•$((CH_3)_2SO)(H_2O)_2$].

Identification code	mg2045m	
Empirical formula	C28 H34 N4 O5 S	
Formula weight	538.65	
Temperature	100(2) K	
Wavelength	0.71073 Å	
Crystal system	Monoclinic	
Space group	P 21/c	
Unit cell dimensions	a = 7.1366(4) Å	α= 90°.
	b = 10.9517(6) Å	β= 94.2780(10)°.
	c = 33.5506(18) Å	γ = 90°.
Volume	2614.9(2) $Å^3$	
Z	4	
Density (calculated)	1.368 Mg/m^3	
Absorption coefficient	0.171 mm^{-1}	
F(000)	1144	

Crystal size	0.16 x 0.10 x 0.08 mm^3
Theta range for data collection	1.96 to 24.36°.
Index ranges	-8<=h<=8, -12<=k<=12, -38<=l<=38
Reflections collected	26330
Independent reflections	4293 [R(int) = 0.1011]
Completeness to theta = 24.36°	100.0 %
Absorption correction	None
Refinement method	Full-matrix least-squares on F^2
Data / restraints / parameters	4293 / 12 / 375
Goodness-of-fit on F^2	0.826
Final R indices [I>2sigma(I)]	R1 = 0.0418, wR2 = 0.0655
R indices (all data)	R1 = 0.0823, wR2 = 0.0748
Largest diff. peak and hole	0.331 and -0.318 e.$Å^{-3}$

[$C_{26}H_{24}N_4O_2$•2(CH_3OH)].

X-ray intensity data from a colorless plate crystal were measured at 100(2) K using a Bruker SMART APEX diffractometer (Mo Kα radiation, λ = 0.71073 Å).[15] The crystals desolvate within minutes in air and were transferred quickly to the diffractometer cold stream to avoid decomposition. Raw area detector data frame processing was performed with the SAINT+ program.[15] Final unit cell parameters were determined by least-squares refinement of 3418 reflections from the data set. Direct methods structure solution, difference Fourier calculations and full-matrix least-squares refinement against F^2 were performed with SHELXTL.[16]

The compound crystallizes in the triclinic system. The space group P-1 (No. 2) was confirmed by the successful solution and refinement of the structure. The asymmetric unit consists of one cycle and two independent methanol molecules of crystallization. Both methanol molecules are disordered over two roughly equally populated positions, and were refined isotropically with C-O distances restrained to 1.45(2) Å. All other non-hydrogen atoms were refined with anisotropic displacement parameters. Hydrogen atoms bonded to carbon were placed in geometrically idealized positions and included as riding atoms. The urea hydrogens were located in difference maps and refined isotropically with their N-H distances restrained to be approximately equal. Reasonable positions for the four methanolic protons were located in difference maps. Their coordinates were adjusted to O-H = 0.85 Å and they were included as riding atoms with $U_{iso,H} = 1.5U_{iso,O}$. Their positions should be regarded as approximate.

Table 3.4 Crystal data and structure refinement [$C_{26}H_{24}N_4O_2$•2(CH_3OH)].

Identification code	mg2048m	
Empirical formula	C28 H32 N4 O4	
Formula weight	488.58	
Temperature	100(2) K	
Wavelength	0.71073 Å	
Crystal system	Triclinic	
Space group	P -1	
Unit cell dimensions	a = 6.9772(4) Å	α= 93.9040(10)°.
	b = 10.5977(6) Å	β= 90.3930(10)°.
	c = 17.1780(9) Å	γ = 104.4030(10)°.
Volume	1227.03(12) $Å^3$	

Z	2
Density (calculated)	1.322 Mg/m^3
Absorption coefficient	0.090 mm^{-1}
F(000)	520
Crystal size	0.22 x 0.12 x 0.06 mm^3
Theta range for data collection	1.99 to 24.26°.
Index ranges	-8<=h<=8, -12<=k<=12, -19<=l<=19
Reflections collected	12870
Independent reflections	3966 [R(int) = 0.0532]
Completeness to theta = 24.26°	99.9 %
Absorption correction	None
Refinement method	Full-matrix least-squares on F^2
Data / restraints / parameters	3966 / 10 / 343
Goodness-of-fit on F^2	0.911
Final R indices [I>2sigma(I)]	R1 = 0.0397, wR2 = 0.0926
R indices (all data)	R1 = 0.0626, wR2 = 0.1005
Largest diff. peak and hole	0.179 and -0.196 $e.Å^{-3}$

3.12.4 X-ray crystal structure determination of protected 1,3-dimethyl naphthalenyl *bis*-urea macrocycle (3.13p) [$C_{38}H_{46}N_6O_2$].

Monoclinic:

X-ray intensity data from a colorless block-like crystal were collected at 100(2) K using a Bruker SMART APEX diffractometer (Mo Kα radiation, λ = 0.71073 Å).[15] The raw area detector data frames were reduced with the SAINT+ program.[15] Final unit cell

parameters were determined by least-squares refinement of 4615 reflections from the data set. Direct methods structure solution, difference Fourier calculations and full-matrix least-squares refinement against F^2 were performed with SHELXS/L[16] as implemented in OLEX2.[17]

The compound crystallizes in the monoclinic space group $P2_1/n$ as determined by the pattern of systematic absences in the intensity data. The asymmetric unit consists of half of one molecule, which is located on a crystallographic inversion center. Non-hydrogen atoms were refined with anisotropic displacement parameters. Hydrogen atoms were placed in geometrically idealized positions and included as riding atoms.

Table 3.5 Crystal data and structure refinement [$C_{38}H_{46}N_6O_2$] (monoclinic).

Empirical formula	$C_{38}H_{46}N_6O_2$
Formula weight	618.81
Temperature/K	100(2)
Crystal system	monoclinic
Space group	$P2_1/n$
a/Å	11.816(2)
b/Å	12.480(2)
c/Å	12.371(2)
α/°	90.00
β/°	116.623(3)
γ/°	90.00
Volume/Å^3	1630.9(5)
Z	2
ρ_{calc}mg/mm^3	1.260
m/mm^{-1}	0.080
F(000)	664.0
Crystal size/mm^3	0.4 × 0.35 × 0.3

2Θ range for data collection	3.96 to 52.74°
Index ranges	$-14 \leq h \leq 14, -15 \leq k \leq 15, -15 \leq l \leq 15$
Reflections collected	21188
Independent reflections	3334[R(int) = 0.0541]
Data/restraints/parameters	3334/0/211
Goodness-of-fit on F^2	1.060
Final R indexes [I>=2σ (I)]	$R_1 = 0.0506$, $wR_2 = 0.1369$
Final R indexes [all data]	$R_1 = 0.0700$, $wR_2 = 0.1457$
Largest diff. peak/hole / e $Å^{-3}$	0.34/-0.17

Triclinic (3.13p) [$C_{38}H_{46}N_6O_2$].

X-ray intensity data from a colorless flat needle crystal were collected at 100(2) K using a Bruker SMART APEX diffractometer (Mo Kα radiation, λ = 0.71073 Å).[15] The raw area detector data frames were reduced with the SAINT+ program.[15] Final unit cell parameters were determined by least-squares refinement of 3756 reflections from the data set. Direct methods structure solution, difference Fourier calculations and full-matrix least-squares refinement against F^2 were performed with SHELXS/L[16] as implemented in OLEX2.[17]

The compound crystallizes in the triclinic system. The space group P-1 (No. 2) was confirmed by the successful solution and refinement of the structure. The asymmetric unit consists of half each of two crystallographically independent but chemically similar molecules. Both are located on inversion centers. Non-hydrogen atoms were refined with anisotropic displacement parameters. Hydrogen atoms were placed in geometrically idealized positions and included as riding atoms.

Table 3.6 Crystal data and structure refinement [$C_{38}H_{46}N_6O_2$] (triclinic).

Identification code	MG063Cam
Empirical formula	$C_{38}H_{46}N_6O_2$
Formula weight	618.81
Temperature/K	100(2)
Crystal system	triclinic
Space group	P-1
a/Å	10.929(4)
b/Å	12.020(4)
c/Å	13.293(4)
α/°	72.974(7)
β/°	84.932(7)
γ/°	83.728(7)
Volume/Å^3	1656.9(9)
Z	2
ρ_{calc}mg/mm^3	1.240
m/mm^{-1}	0.078
F(000)	664.0
Crystal size/mm^3	0.32 × 0.1 × 0.04
2Θ range for data collection	3.2 to 50.06°
Index ranges	$-12 \leq h \leq 12$, $-14 \leq k \leq 14$, $-15 \leq l \leq 15$
Reflections collected	21296
Independent reflections	5849[R(int) = 0.0575]
Data/restraints/parameters	5849/0/421
Goodness-of-fit on F^2	0.937
Final R indexes [I>=2σ (I)]	R_1 = 0.0447, wR_2 = 0.0949
Final R indexes [all data]	R_1 = 0.0713, wR_2 = 0.1036
Largest diff. peak/hole / e Å^{-3}	0.29/-0.28

3.12.6 X-ray crystal structure determination of 4-bromo-1,3-dibromomethylnaphthalene [$C_{12}H_9Br_3$].

X-ray intensity data from a colorless plate were collected at 100(2) K using a Bruker SMART APEX diffractometer (Mo Kα radiation, λ = 0.71073 Å).[15] The raw area detector data frames were reduced and corrected for absorption effects with the SAINT+ and SADABS programs.[15] Final unit cell parameters were determined by least-squares refinement of 6881 reflections from the data set. Direct methods structure solution, difference Fourier calculations and full-matrix least-squares refinement against F^2 were performed with SHELXS/L[16] as implemented in OLEX2.[17]

The compound crystallizes in the monoclinic space group $P2_1/c$ as determined by the pattern of systematic absences in the intensity data. The asymmetric unit consists of one molecule. Non-hydrogen atoms were refined with anisotropic displacement parameters. Hydrogen atoms were placed in geometrically idealized positions and included as riding atoms. The largest residual electron density peak in the final difference map is located 0.76 Å from Br2.

Table 3.7 Crystal data and structure refinement [$C_{12}H_9Br_3$].

Identification code	mgiii27s
Empirical formula	$C_{12}H_9Br_3$
Formula weight	392.92
Temperature/K	100(2)
Crystal system	monoclinic
Space group	$P2_1/c$
a/Å	9.0261(6)
b/Å	12.6861(8)

c/Å	10.4051(7)
α/°	90.00
β/°	99.3180(10)
γ/°	90.00
Volume/Å^3	1175.73(13)
Z	4
ρ_{calc}mg/mm^3	2.220
m/mm^{-1}	10.255
F(000)	744.0
Crystal size/mm^3	0.26 × 0.22 × 0.18
2Θ range for data collection	4.58 to 60.18°
Index ranges	$-12 \leq h \leq 12$, $-17 \leq k \leq 17$, $-14 \leq l \leq 14$
Reflections collected	21495
Independent reflections	3446[R(int) = 0.0388]
Data/restraints/parameters	3446/0/136
Goodness-of-fit on F^2	1.038
Final R indexes [I>=2σ (I)]	R_1 = 0.0301, wR_2 = 0.0721
Final R indexes [all data]	R_1 = 0.0388, wR_2 = 0.0754
Largest diff. peak/hole / e Å^{-3}	1.17/-0.51

3.12.7. X-ray crystal structure determination of protected 4-bromo-1,3-dimethyl bis-urea naphthalene macrocycle (3.14p) [$C_{38}H_{44}Br_2N_6O_2 \cdot 2(CDCl_3)$].

X-ray intensity data from a colorless needle crystal were collected at 100(2) K using a Bruker SMART APEX diffractometer (Mo Ka radiation, l = 0.71073 Å).[1] The raw area detector data frames were reduced and corrected for absorption effects with the

SAINT+ and SADABS programs.[1] Final unit cell parameters were determined by least-squares refinement of 3554 reflections from the data set. Direct methods structure solution, difference Fourier calculations and full-matrix least-squares refinement against F^2 were performed with SHELXS/L[2] as implemented in OLEX2.[3]

The compound crystallizes in the space group P-1 (No. 2) of the triclinic system, as determined by the successful solution and refinement of the structure. The asymmetric unit consists of half of one $C_{38}H_{44}Br_2N_6O_2$, which is located on a crystallographic inversion center, and one $CDCl_3$ molecule disordered over two positions. The *tert*-butyl group C16-C19 is disordered over two orientations with populations A/B = 0.369(7) / 0.631(7) (constrained to unity). Components of the disordered chloroform-*d* molecule have refined populations 0.519(3) / 0.481(3). All non-hydrogen atoms were refined with anisotropic displacement parameters except for disordered carbon atoms (isotropic). A total of 37 distance restraints were used to assist in modeling the *tert*-butyl and chloroform-*d* disorder. Hydrogen and deuterium atoms bonded to carbon were placed in geometrically idealized positions and included as riding atoms.

Table 3.8 Crystal data and structure refinement [$C_{38}H_{44}Br_2N_6O_2 \cdot 2(CDCl_3)$].

Identification code	MG2432s
Empirical formula	$C_{40}H_{44}D_2Br_2Cl_6N_6O_2$
Formula weight	1017.36
Temperature/K	100(2)
Crystal system	triclinic
Space group	P-1

a/Å	9.033(2)
b/Å	10.464(3)
c/Å	12.796(3)
α/°	112.529(4)
β/°	99.161(5)
γ/°	98.575(5)
Volume/$Å^3$	1073.2(5)
Z	1
$\rho_{calc}mg/mm^3$	1.574
m/mm^{-1}	2.305
F(000)	516.0
Crystal size/mm^3	0.48 × 0.08 × 0.06
2Θ range for data collection	4.3 to 52.84°
Index ranges	$-11 \leq h \leq 11$, $-13 \leq k \leq 13$, $-15 \leq l \leq 15$
Reflections collected	14582
Independent reflections	4389[R(int) = 0.0497]
Data/restraints/parameters	4389/37/283
Goodness-of-fit on F^2	1.046
Final R indexes [I>=2σ (I)]	R_1 = 0.0487, wR_2 = 0.1193
Final R indexes [all data]	R_1 = 0.0629, wR_2 = 0.1266
Largest diff. peak/hole / e $Å^{-3}$	0.75/-0.35

3.13. References.

1. Geer, M. F.; Smith, M. D.; Shimizu, L. S., A bis-urea naphthalene macrocycle displaying two crystal structures with parallel ureas. *Crystengcomm* **2011,** *13* (11), 3665-3669.
2. (a) Blagden, N.; de Matas, M.; Gavan, P. T.; York, P., Crystal engineering of active pharmaceutical ingredients to improve solubility and dissolution rates. *Adv Drug Deliver Rev* **2007,** *59* (7), 617-630; (b) Davey, R. J., Pizzas, polymorphs and pills. *Chem Commun* **2003,** (13), 1463-1467; (c) Cheney, M. L.; Shan, N.; Healey, E. R.; Hanna, M.; Wojtas, L.; Zaworotko, M. J.; Sava, V.; Song, S. J.; Sanchez-Ramos, J. R., Effects of Crystal Form on Solubility and Pharmacokinetics: A Crystal Engineering Case Study of Lamotrigine. *Cryst Growth Des* **2010,** *10* (1), 394-405.
3. Kato, Y.; Okamoto, Y.; Nagasawa, S.; Ishihara, I., Relationship between polymorphism and bioavailability of drugs. IV. New polymorphic forms of phenobarbital. *Chem. Pharm. Bull.* **1984,** *32* (Copyright (C) 2013 American Chemical Society (ACS). All Rights Reserved.), 4170-4.
4. Espeau, P.; Négrier, P.; Corvis, Y., A Crystallographic and Pressure-Temperature State Diagram Approach for the Phase Behavior and Polymorphism Study of Glutaric Acid. *Cryst Growth Des* **2013**.
5. (a) Dewal, M. B.; Xu, Y. W.; Yang, J.; Mohammed, F.; Smith, M. D.; Shimizu, L. S., Manipulating the cavity of a porous material changes the photoreactivity of included guests. *Chem Commun* **2008,** (33), 3909-3911; (b) Shimizu, L. S.; Hughes, A. D.; Smith, M. D.; Davis, M. J.; Zhang, B. P.; zur Loye, H. C.;

Shimizu, K. D., Self-assembled nanotubes that reversibly bind acetic acid guests. *J. Am. Chem. Soc.* **2003,** *125* (49), 14972-14973; (c) Shimizu, L. S.; Hughes, A. D.; Smith, M. D.; Samuel, S. A.; Ciurtin-Smith, D., Assembled columnar structures from bis-urea macrocycles. *Supramol Chem* **2005,** *17* (1-2), 27-30.

6. (a) Shimizu, L. S.; Smith, M. D.; Hughes, A. D.; Shimizu, K. D., Self-assembly of a bis-urea macrocycle into a columnar nanotube. *Chem Commun* **2001,** (17), 1592-1593; (b) Dawn, S.; Dewal, M. B.; Sobransingh, D.; Paderes, M. C.; Wibowo, A. C.; Smith, M. D.; Krause, J. A.; Pellechia, P. J.; Shimize, L. S., Self-Assembled Phenylethynylene Bis-urea Macrocycles Facilitate the Selective Photodimerization of Coumarin. *J. Am. Chem. Soc.* **2011,** *133* (18), 7025-7032.

7. (a) Dewal, M. B.; Lufaso, M. W.; Hughes, A. D.; Samuel, S. A.; Pellechia, P.; Shimizu, L. S., Absorption properties of a porous organic crystalline apohost formed by a self-assembled bis-urea macrocycle. *Chemistry of Materials* **2006,** *18* (20), 4855-4864; (b) Roy, K.; Smith, M. D.; Shimizu, L. S., 1D coordination network formed by a cadmium based pyridyl urea helical monomer. *Inorganica Chimica Acta* **2011,** *376* (1), 598-604.

8. Yang, J.; Dewal, M. B.; Sobransingh, D.; Smith, M. D.; Xu, Y. W.; Shimizu, L. S., Examination of the Structural Features That Favor the Columnar Self-Assembly of Bis-urea Macrocycles. *Journal of Organic Chemistry* **2009,** *74* (1), 102-110.

9. (a) Chong, Y. S.; Carroll, W. R.; Burns, W. G.; Smith, M. D.; Shimizu, K. D., A High-Barrier Molecular Balance for Studying Face-to-Face Arene-Arene Interactions in the Solid State and in Solution. *Chemistry-a European Journal*

2009, *15* (36), 9117-9126; (b) Grimme, S., Do special noncovalent pi-pi stacking interactions really exist? *Angew Chem Int Edit* **2008,** *47* (18), 3430-3434; (c) Kim, E.; Paliwal, S.; Wilcox, C. S., Measurements of molecular electrostatic field effects in edge-to-face aromatic interactions and CH-pi interactions with implications for protein folding and molecular recognition. *J. Am. Chem. Soc.* **1998,** *120* (43), 11192-11193.

10. (a) Schneider, H.-J., Binding Mechanisms in Supramolecular Complexes. *Angewandte Chemie International Edition* **2009,** *48* (22), 3924-3977; (b) Riley, K. E.; Hobza, P., On the Importance and Origin of Aromatic Interactions in Chemistry and Biodisciplines. *Accounts of Chemical Research* **2012,** *46* (4), 927-936; (c) Sherrill, C. D., Energy Component Analysis of π Interactions. *Accounts of Chemical Research* **2012,** *46* (4), 1020-1028.
11. Fisher, T. H.; Meierhoefer, A. W., A kinetic study of the N-bromosuccinimide bromination of some 4-substituted 3-cyanotoluenes. *The Journal of Organic Chemistry* **1978,** *43* (2), 220-224.
12. (a) Gale, P. A., Anion and ion-pair receptor chemistry: highlights from 2000 and 2001. *Coordination Chemistry Reviews* **2003,** *240* (1–2), 191-221; (b) Gunnlaugsson, T.; Davis, A. P.; O'Brien, J. E.; Glynn, M., Fluorescent Sensing of Pyrophosphate and Bis-carboxylates with Charge Neutral PET Chemosensors†. *Organic Letters* **2002,** *4* (15), 2449-2452.
13. Jeong, H. A.; Cho, E. J.; Yeo, H. M.; Ryu, B. J.; Nam, K. C., Naphthalene urea derivatives for anion receptor: effects of substituents on benzoate binding. *Bull.*

Korean Chem. Soc. **2007,** *28* (Copyright (C) 2013 American Chemical Society (ACS). All Rights Reserved.), 851-854.

14. Custelcean, R.; Remy, P., Selective Crystallization of Urea-Functionalized Capsules with Tunable Anion-Binding Cavities. *Cryst Growth Des* **2009,** *9* (4), 1985-1989.

15. (a) *SMART* 5.630; Bruker Analytical X-ray Systems Inc.: Madison Wisconsin USA, 2003; (b) *SAINT+*, 6.45; Bruker Analytical X-ray Systems Inc.: Madison, Wisconsin, USA, 2003; (c) *SADABS*, 2.10; Bruker Analytical X-ray Systems: Madison, Wisconsin, USA, 2003.

16. Sheldrick, G. M., A short history of SHELX. *Acta Crystallogr A* **2008,** *64*, 112-122.

17. Dolomanov, O. V.; Bourhis, L. J.; Gildea, R. J.; Howard, J. A. K.; Puschmann, H., OLEX2: a complete structure solution, refinement and analysis program. *J Appl Crystallogr* **2009,** *42*, 339-341.

IV. CO-CRYSTALLIZATION THROUGH HALOGEN BONDING WITH PYRIDYL *BIS*-UREA MACROCYCLE.

4.1 Abstract.

A scan of recent literature shows a surge in manuscripts that report or utilize halogen bonding.[1] This interaction pairs halogenated compounds with electronegative atoms with lone pair of electrons such as oxygen, sulphur, and nitrogen. Halogen bonding has applications for cocrystallization and contributes to the activity of pharmaceutical agents. In this chapter, we investigate the propensity of the pyridyl *bis*-urea macrocycle to act as a Lewis base (R-B:) and form halogen bonds with a series of halogen bond donors (R-X) from moderate (diiodobenzene and iodobenzene) to strong (diiodotetrafluorobenzene, diiodotetrafluoroethane, and iodopentafluorobenzene). Crystallization of the pyridyl macrocycle with iodopentafluoro benzene or diiodotetrafluoro ethane by slow evaporation from methylene chloride solutions affords X-ray quality crystals that show short, strong halogen bonds with these halogen bond donors. The R-X···B distances range from 2.719 – 2.745 Å and average 78 % of the sum of the van der Wall's radii for O•••I. Through the systematic DFT calculations using PBE exchange-correlation, we estimate association energies of 7.381 kcal mol^{-1} for iodopentafluoro benzene and 10.331 kcal mol^{-1} for diodo tetrafluoro ethane.

4.2 Background.

The supramolecular interactions of halogen bonding are based on the close contact between a halide attached to a strongly electron withdrawing substituent and Lewis basic lone pair of electrons or π-electrons, such as those in aryl systems and unsaturated alkyl groups. These interactions are characterized by a contact distance that is shorter than the sum of the van der Waal's radii and an association geometry that aligns the electrostatic potential in a favorable manner. [2] The ability for halides to be attracted to the lone pair of electrons of a Lewis base can be seen in the electrostatic potential of simple representative molecules; CF_4, CF_3Cl, CF_3Br and CF_3I (Figure 4.1).[3] When a halogen is attached to a strongly electron withdrawing group, such as a trifluoromethyl group, the distribution of the electron density around the halogen is perturbed and causes an unsymmetrical distribution of the electron density about the halide. [3] Figure 4.1 shows the electronegative potential resulting in an electropositive region about the end of the atom in red. As the halides get larger, their electron clouds are more polarizable. This is illustrated in our series that show little to no electropositive region for CF_4 at the crown of the fluorine atoms. However, as we move down the column to chlorine, then bromine and finally to iodine there is increased positive character along the covalent bond axis. This generated positive character has been termed as the σ-hole.[4] The negative character lies along the equatorial position of the halogens and is represented in figure 4.1 in blue.

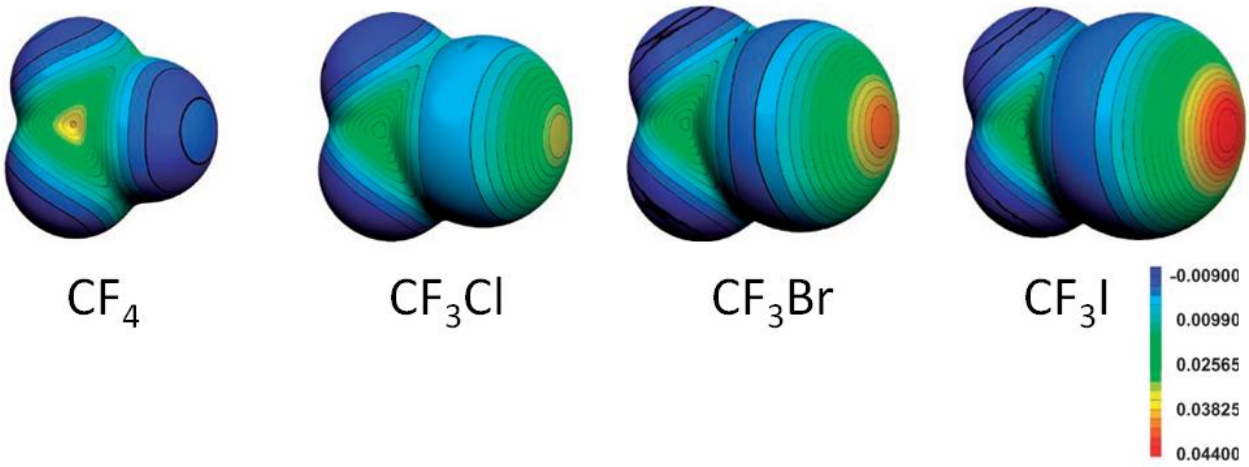

Figure 4.1. Electrostatic potential maps of CF_4 CF_3Cl CF_3Br and CF_3I showing the emergence of a positive potential about the crown of the halogens as the halogen species grows more polarizable. (reproduced with permission from reference 2. Copyright (2008) Wiley-VCH Verlag GmbH & Co.)

The uneven distribution also provides these molecules the ability to associate with Lewis bases along with the ability to associate with electrophiles. This ambiphilic nature of the halogen allows for the association through two types of interactions, incidentally coined Type I and Type II.[3] These interactions are described by the geometry of the association of the halide (R-X) and the Lewis base (R-B). In the Type I interaction, the association is in a direct overlap of the two halogens in a face to face offset manner. This overlap is such that the angle of the R-X···B (θ_1) is the same as the angle of the R-B···X angle (θ_2). This type of association allows the partial negative character of the lone pair to associate with the partial positive character of the sigma hole. A second type of halogen bond occurs as the lone pair of electrons directly associates with the sigma hole resulting in a 180° angle of the R-X···B bond and a 90° angle of the R-B···X association. Type II halogen bonds are the more commonly observed in crystal structures. In the example of the perfluoro iodomethane, the iodine has positive character along the C-I axis but also displays electronegative character perpendicular to this axis. Figure 4.2

illustrates the ability of the iodine to accept a halogen bond along the 180° axis as well as its preference to donate at an angle between 90-120°. Because of the character of the sigma hole and the size difference between halides and hydrogen, halogen bonds tend to be more directional and are affected by sterics more readily than similar hydrogen bonds.[3]

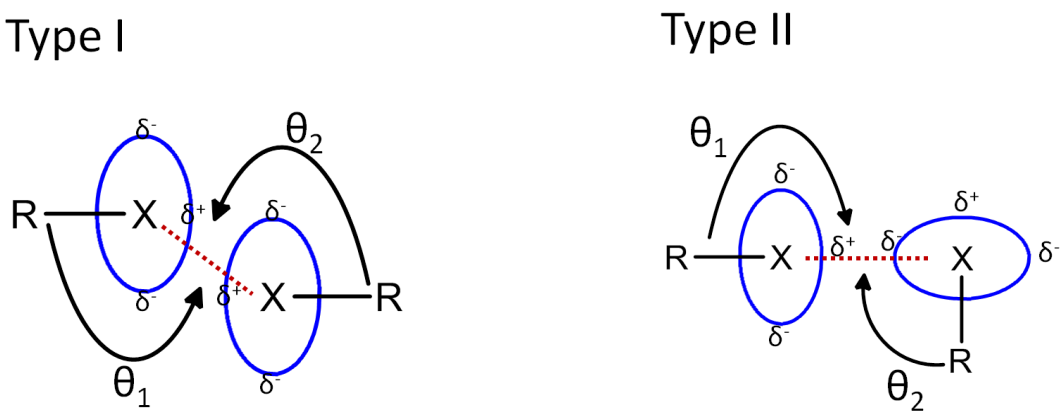

Figure 4.2. Typical halogen bond scheme a) Type I where both angles are the same ($\theta_1 \approx \theta_2$) b) Type II more traditional halogen bonding scheme with lone pair of electrons of the lewis base are directed toward the σ-hole of the halogen (θ_1= 180 °, θ_2= 90°).

The strength of halogen bonds spans a wide range that parallels hydrogen bonding, from the weak chlorocarbon Cl•••Cl interaction to the strong I^-•••I_2. These non-covalent interactions have strengths that range from 5 – 180 kJ/mol.[4] In most cases, the interactions are reactive intermediate complexes like those seen in the halogenations of alkenes and alkynes. The intermediate formed, such as the brominium ion, occurs as the result of the halogen bond formed between the bromine and the alkene or alkyne.[5] Many methods have been tested as ways of exploring the strengths and properties of these interactions.[2, 6] The results show that the strength of the donor follows a general paradigm of the halide's polarizability with I>Br>Cl>F, with fluorine only showing donor capability in fluorinated aromatics with triethylamine.[7] Also, the moiety that the

halogen is attached to contributes to the strength of the donor. Hydrocarbon substituents show a general pattern of alkyne (sp C-X) >aryl ~ alkene(sp^2C-X) >alkane (sp^3C-X), with an iodoalkyne showing the greatest affinity toward nucleophiles. Sterics appear to play a large role in the geometry of halogen bonding and also favor the 180 geometry. For example, Metrangolo's survey of crystal structures from the CCD the geometry of halogen bonds deviates only slightly from the ideal of 180 ° with respect to the halogen bond length.[4] Using computational and statistical analysis of the Cambridge Structural Database Frank Allan *et al*. analyzed the effect of the electronegative atom, the Lewis base, with respect to the strengths of halogen bonds.[8] They found that the more electronegative atom has a higher propensity for the formation of halogen bonds. As well, they observed greater instances of oxygen donors versus nitrogen or sulfur. They also examined the hybridization and found that the higher the order of hybridization the shorter the contacts, i.e. $sp^1<sp^2<sp^3$ in lengths ranging from ~2.7-3.2 Å. This was attributed to the idea that resonance along with sterics both played an integral part in the strengths of the halogen bond.

Halogen bonding is an important strategy for organization in materials such as liquid crystalline materials[9], organic semiconductors[9e, 10], and in the assembly of proteins and nucleic acids.[11] Although halogen bonding schemes are prevalent in nature,[12] the study of these interactions has just been recently brought to the forefront in chemical society. In the study of liquid crystals, the first example of thermotropic LC's from self-assembled complexes through halogen bonding was reported in the formation of iodopentafluorobenzene and 4-alkoxystilbazoles. Despite the starting materials being nonmesomorphic, the introduction of halogenated compounds resulted in nematic and

smectic properties.[9a] These complexes also showed evidence of a charge transfer from the nitrogen to the iodine.[9a, b] Halogen bonding has also been utilized in the pre-organization of tetrathiafulvalene to enhance the charge carrier property of these systems. The work by Imakubo *et al.* showed that the introduction of iodine to the tetrathiofulvalate molecule did not change the reduction potential of the molecule (Figure 4.3).[9c, 13] When crystallized in the presence of silver cyanate or bromine the molecule crystallized with short halogen-halogen and halogen-nitrogen distances significantly shorter than the sum of their van der Waal's radii. The resulting crystals were shown to have semiconducting properties at room temperature of 1 S cm^{-1}. [13] Halogen bonding is even utilized in the realm of biochemistry. Ho *et. al.* used a bromine substituted uracil to assist in the crystallization of the Holliday junction of DNA (Figure 4.4).[11a, 11c] The Holliday junction presumed to be the mechanism of homologous recombination that repairs DNA of harmful breaks. By replacing a cytosine at the N_7 nucleotide position with a brominated uracil, they were able to show a conformational preference for the halogen bond directed X- isomer versus the hydrogen bond H- isomer. They calculated a stabilization of 2-5 kcal mol^{-1} in favor of the halogen bond in an analogous biological condition.[11a, 11d]

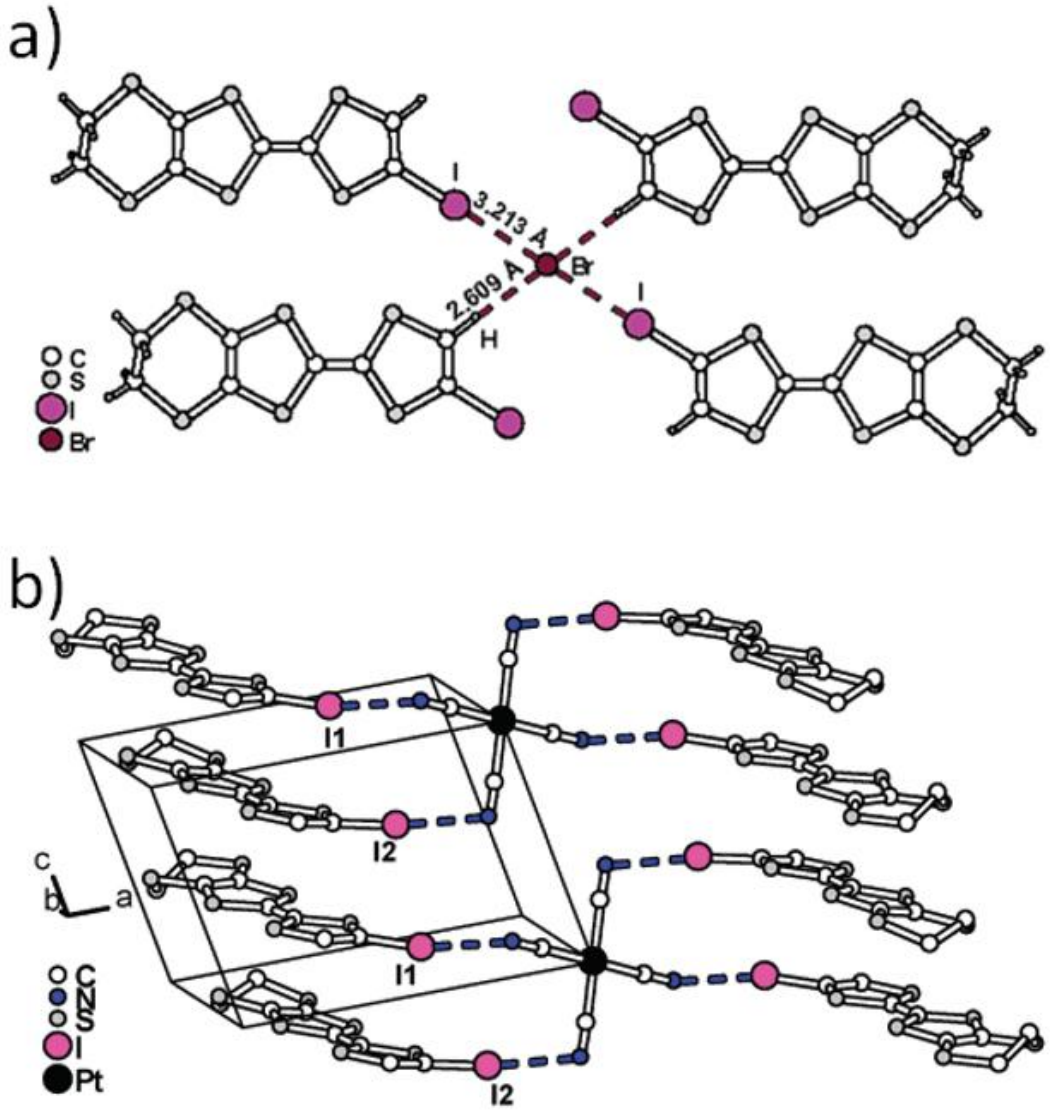

Figure 4.3. The short halogen-halogen and halogen-nitrogen distances exhibited by Imakubo et al in the crystal engineering of semiconductor materials from EDT-TTF complexes.[13] (reproduced with permission from reference 12. Copyright (1995) Elsevier Sciences)

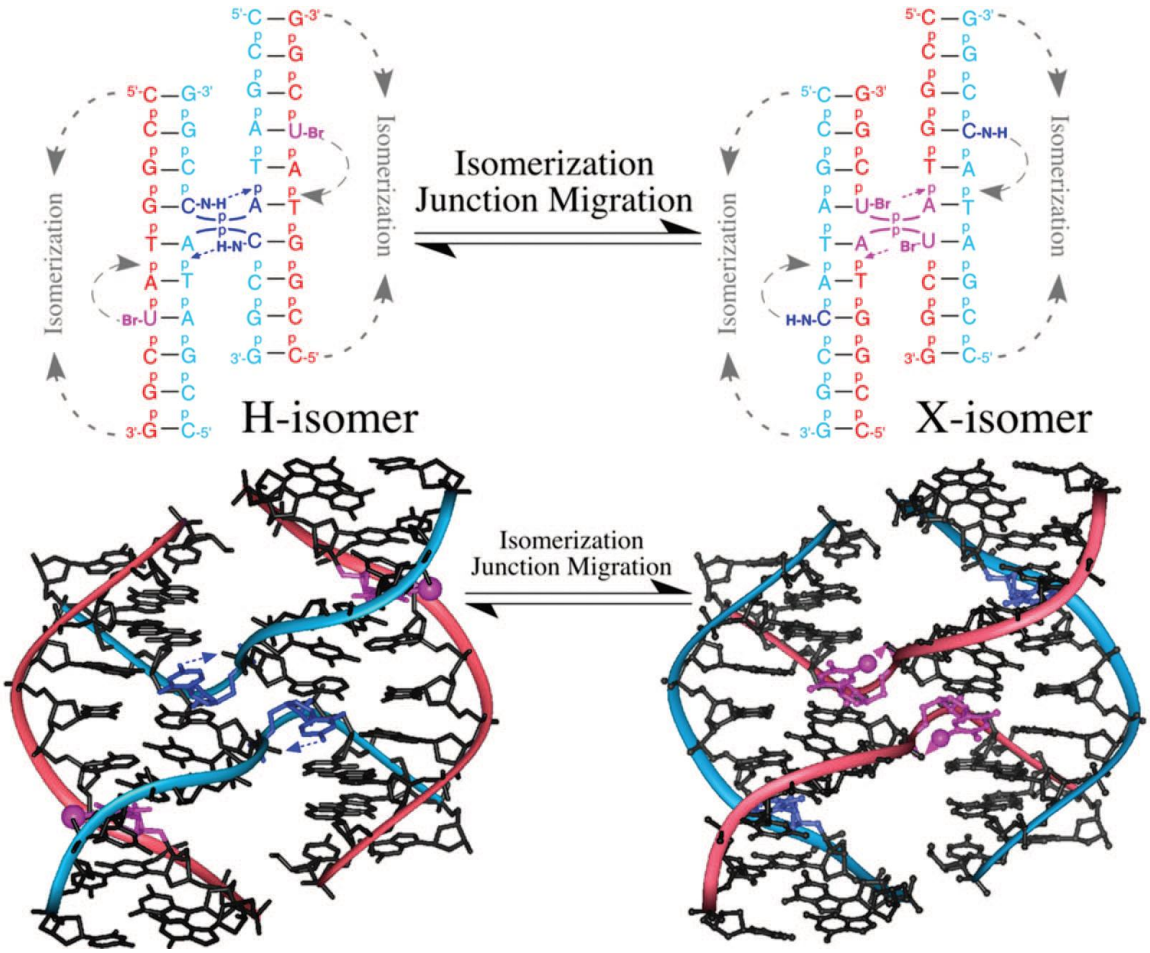

Figure 4.4. X- and H-isomer of Holliday complex shows conformational preference for halogen bond.[11a] (reproduced with permission from reference 10a. Copyright (2003) American Chemical Society)

Our group utilizes bis-urea macrocycles that typically assemble through the three centered urea hydrogen bonding into columnar structures and can incorporate guests within these inherently porous channels. In contrast, the pyridyl spacer group forms crystals through two separate hydrogen bonding interactions. Figure 4.5a shows the assembly of the pyridyl macrocycle into a close-packed structure, which has no apparent pores. But upon the exposure to hydrogen bond donors, the crystals expand and absorbed guest molecules. Figure 4.5b shows the crystal structure of macrocycle **4.2** before and

after the absorption of trifluoroethanol.[14] The guest molecules form hydrogen bonds with the unoccupied lone pair of the carbonyl oxygen.[14-15] In this chapter, we explore the ability of the pyridyl host to act as a halogen bond acceptor and test whether the halogen bond donors prefer to interact with the host via its carbonyl oxygen or through the pyridyl nitrogen.

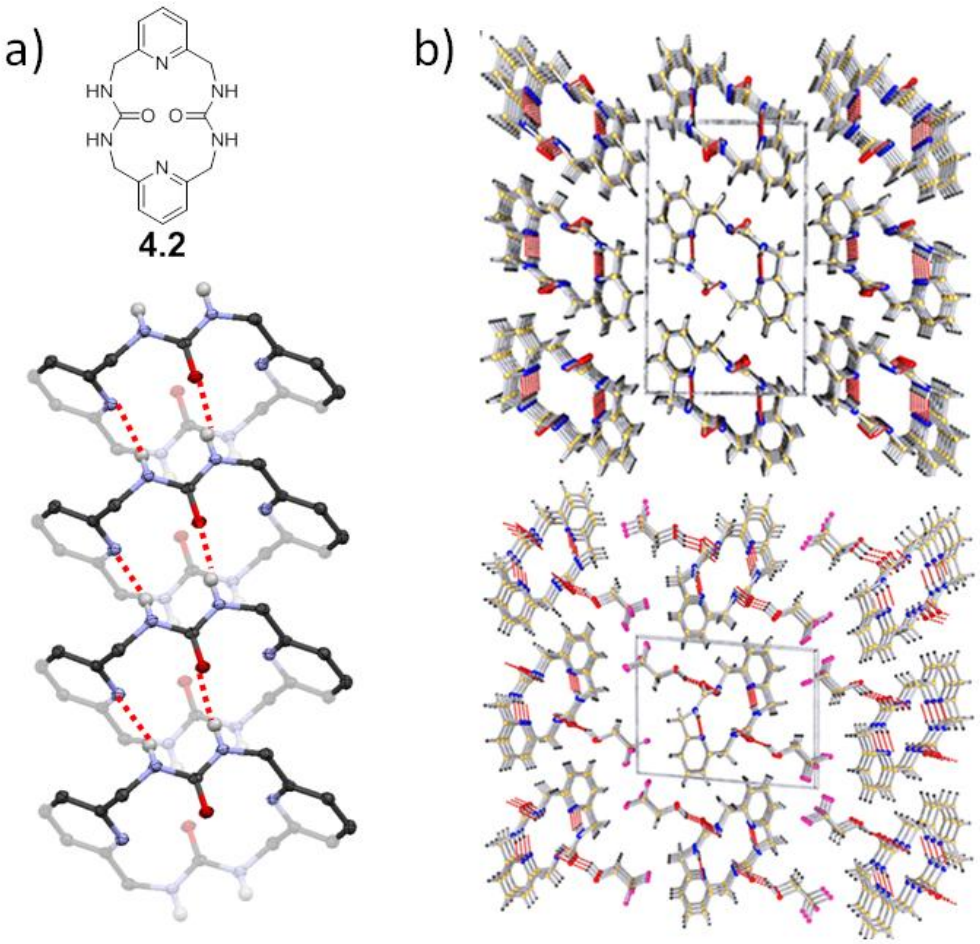

Figure 4.5. Crystal structure of macrocycle **4.2** before and after absorption of trifluoro ethanol. a) columnar structure of Macrocycle **4.2** showing the hydrogen bonding motif. b) the two crystal packing of macrocycle **4.2** (top) without guest (bottom) with trifluoroethanol guest showing the expansion of the crystal structure and hydrogen bonding with the available lone pair of electrons of the urea carbonyl.[14] (reproduced with permission from reference 13. Copyright (2012) American Chemical Society)

4.3 Design of Experiments.

This chapter examines the propensity of pyridyl bis-ureas **4.1** and **4.2** to co-crystallized with halogen bond donors. Specifically, we are testing the strength of the interactions that can be formed through the urea oxygen's lone pair and halogens. First we looked at systems in which the host only has Lewis basic sites and can only act as an acceptor in supramolecular interactions such as halogen or hydrogen bonding. Dr. Roy's initial synthesis (Scheme 4.1) of the pyridyl bis-ureas proceeds through a triazinanone intermediate that does not have hydrogen bond donors. In this case, the protected urea host **4.1** has basic carbonyl oxygens and pyridyl nitrogens. Thus, it readily provides us with the compound that can act only as a halogen bond acceptor. Next, we tested this interaction in systems that may also assemble through urea hydrogen bonds to test the synergistic effects of the two interactions or alternatively the competition between the two types of interactions. The synthesis of the host (Scheme 4.1) starts with the cyclization of 2,6-dibromomethylpyridine under basic conditions with triazinanone to afford macrocycle **4.1** in which the urea groups are protected with the triazinanones. After isolation and purification, the triazinanone protecting groups were removed by heating in an acidic aqueous/methanol (1:1 v/v) solution of diethanol amine to afford macrocycle **4.2**.

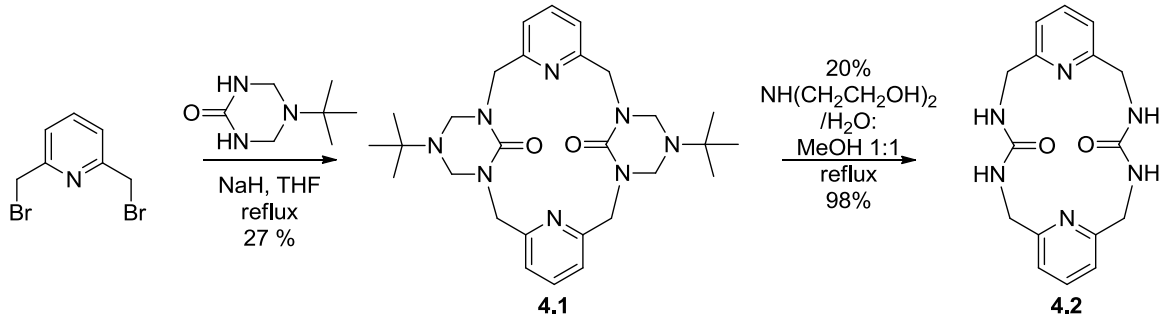

Scheme 4.1. The synthesis of the pyridyl *bis*-urea macrocycle (**4.2**). Conditions: *bis*(bromomethyl)pyridine was reacted with triazinanone and NaH in refluxing THF to form the protected pyridyl macrocycle (**4.1**) that was then deprotected in a 1:1 acidic methanol:aqueous diethanolamine (20%) solution to produce the pyridyl *bis*-urea macrocycle (**4.2**).[15]

Ureas have a high propensity for self-assembly and accordingly tend to have lower solubility. Macrocycle **4.2** has low or no solubility in many organic solvents. Protection of NH's with the triazinanone removes the hydrogen bond donors and prevents the self-association of these monomers through hydrogen bonding interactions. This increases the solubility of the macrocycle allowing for the examination of the binding and co-crystallization of these compounds from a myriad of solvents. We sought to utilize hosts **4.1** and **4.2** to compare halogen/hydrogen bond acceptors in the urea carbonyl vs the pyridyl nitrogen. In this small macrocycle, the pyridine nitrogens are pointing inward and may not be as accessible for supramolecular interactions. Thus, we have also begun to examine the larger more flexible tri and tetraurea pyridyl bis-urea macrocycles;[16] however, to date we have not yet obtained crystals suitable for X-ray diffraction studies on these larger pyridyl hosts.

4.4 Examining the pyridyl *bis*-urea macrocycle by computational methods.

In order to examine the pyridyl *bis*-urea macrocycles further, the crystal structures of both the macrocycle **4.1** and **4.2**, obtained by Roy and Smith were loaded into Spartan

10™. We truncated the structure to a single macrocycle and deleted the solvent molecules. The structures were then evaluated through DFT calculations at the 6-31+G* level of theory, and the electrostatic potential was examined. Figure 4.6 compares the resulting potential maps of the two structures. As expected, both show strong electronegative potential at the carbonyl oxygens with the deprotected macrocycle **4.1** displaying a greater electronegative potential. With this evidence we expect that 1) both macrocycles contain basic oxygen sites which could act as halogen bond acceptors, 2) the pyridine nitrogens are sterically crowded in the interior and are unlikely to interact and 3) macrocycle **4.2** displays a higher electronegative potential at the carbonyl oxygen versus macrocycle **4.1** as seen by the more intense red color. Therefore, we expect that **4.2** will act as a slightly stronger acceptor with the free ureas versus macrocycle **4.1.**

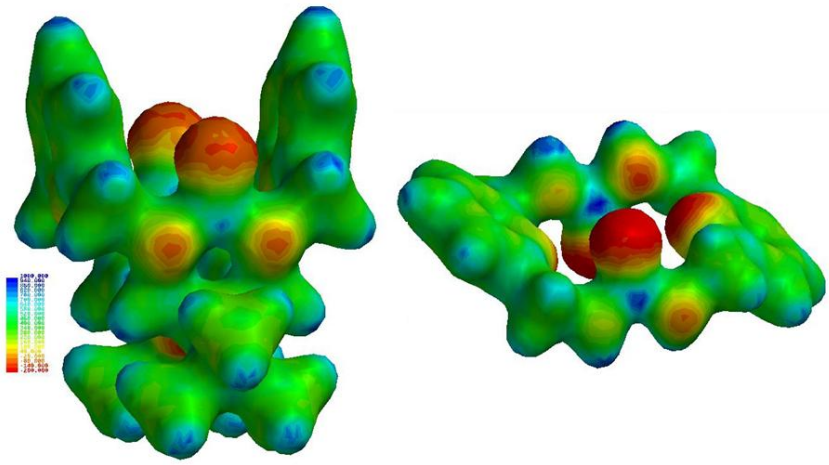

Figure 4.6. Comparison of the electrostatic potential distributions of the protected (**4.1**) and deprotected (**4.2**) pyridyl *bis*-urea macrocyclic monomers based on the DFT B3LYP calculation at the 6-31+G* level (Legend: -200 – 1000 kJ mol^{-1})

We next selected a series of five halogen bond donors to co-crystallize with these two pyridyl macrocycles. Table 4.1 lists the five donor compounds. Diiodo tetrafluoro

ethane (**4.3**), diiodo perfluorobenzene (**4.4**), and perfluoro iodo benzene (**4.5**) are strong halogen bond donors. In comparison, diiodobenzene (**4.6**) and iodobenzene (**4.7**) and are considered medium halogen bond donors. A weak halogen bond donor would include compounds such as bromo and chloro compounds.

Table 4.1. List of halogen bond donor molecules and their relative strengths.

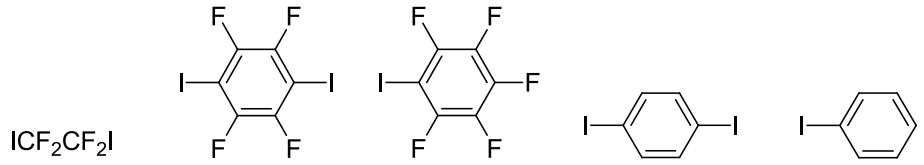

Compound:	4.3	4.4	4.5	4.6	4.7
		Strong donors		**Medium donors**	

4.5. Evaluation of the oxygen lone pair in pyridyl macrocycle 4.2 as a halogen bond acceptor.

We next investigated the formation of halogen bonds of the five compounds with macrocycle **4.1**. Solutions of macrocycle **4.1** were prepared in methylene chloride, chloroform and THF (40 mM) in separate scintillation vials. Then, to each solution the halogenated compounds **4.3**-**4.7** were added in either a 1:1 and 2:1 molar ratio. The solutions were then capped loosely and allowed to slow evaporate. The THF solutions yielded no crystals and instead resulted in precipitates. Dichloromethane appeared to be the best crystallization solvent and showed the highest propensity for crystal formation. The solutions of macrocycle **4.1** with *p*-diiodobenzene and iodobenzene gave none of the desired co-crystals and instead afforded solvates of macrocycle **4.1** and dichloromethane

solvent. This suggests that the halogen bond donor capabilities of the iodo compounds were not sufficient to overcome the solvent interactions with the macrocycle. X-ray quality crystals were obtained from solutions of macrocycle **4.1** with pentafluoro iodobenzene in dichloromethane, diiodotetrafluorethane in dichloromethane (two structures) and chloroform, and perfluoro diiodobenzene in chloroform.

Macrocycle 4.1 • pentafluoroiodobenzene [$(C_{28}H_{40}N_8O_2)$•$(C_6F_5I)_3$].

Slow evaporation of a 2:1 mixture of **4.1** and pentafluoro iodobenzene (40 mM) afforded a colorless mass of block crystals with the formula $(C_{28}H_{40}N_8O_2)(C_6F_5I)_3$. The macrocycle crystallized in the triclinic system in the *P*-1 space group, consisting of one macrocycle **4.1** and three independent pentafluoro iodobenzene molecules **4.5**. Figure 4.8 shows that the macrocycle itself adopts a conformation where the pyridyl nitrogens are both pointed down toward the triazinanone protecting groups and adopt a bowl shape. Two macrocycles form a "dimer" assisted by offset aryl-aryl stacking (center-center distance of 3.335 Å) (Figure 4.7 inset). Figure 4.7 also shows the formation of three separate halogen bonds between the three pentafluoro iodobenzenes and macrocycle **4.1**. Two of the pentafluoro iodobenzene form short, strong interactions with the carbonyl oxygen. The first, to the left of the structure, forms a halogen bond with the urea carbonyl with a I•••O distance of 2.719 Å and a C-I••O angle of 173.7 º. The second, to the right of macrocycle **4.1,** also forms a halogen bond with the second urea carbonyl oxygen with a I•••O distance of 2.745 Å and a C-I•••O angle of 177.1 º. The third halogen bond is formed with one of the triazinanone nitrogens with a I•••N distance of 3.001 Å and a C-I•••N angle of 169.32 º.

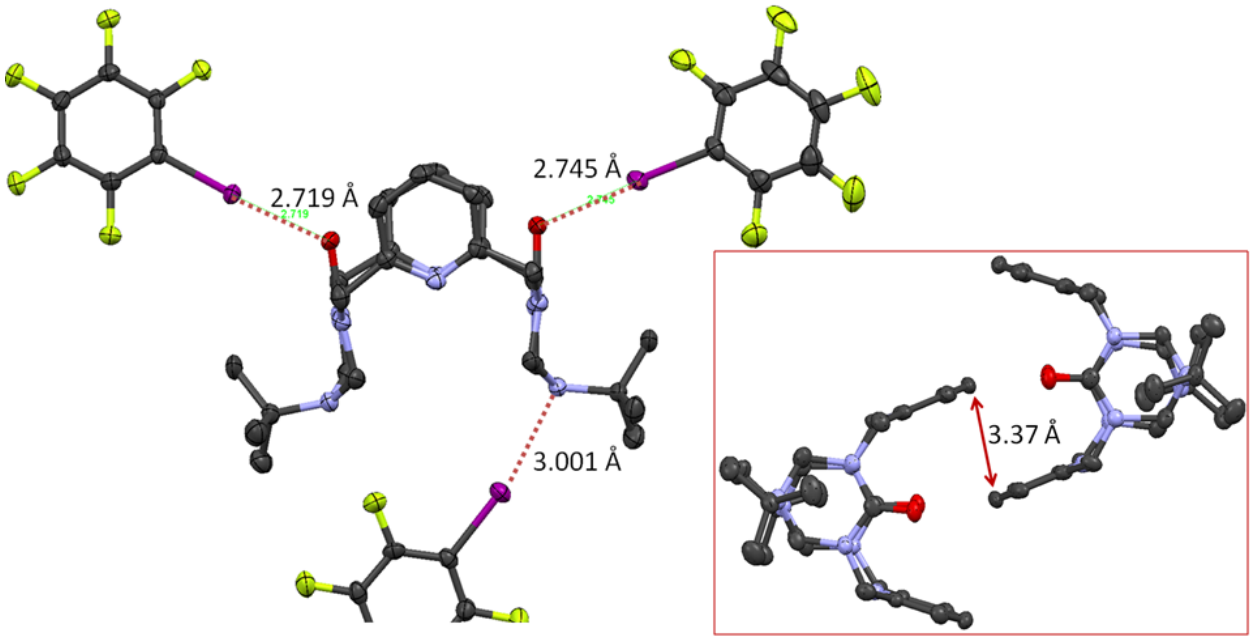

Figure 4.8. Crystal structure of protected pyridyl *bis*-urea macrocycle with pentafluoro iodobenzene: The structure shows the extremely short I···O halogen bonds and the I···N halogen bond. (inset) structure showing the offset aryl-aryl stacking that assists in the crystal packing. (Elipses drawn at the 50% probability level, C-black, O-red, N-blue, I-purple, F- yellow, Hydrogens have been removed for clarity.)

Interestingly, the two halogen bonds formed with the carbonyl oxygens are only 77.7 and 78.4% of the sum of the Van der Waal's radii for iodine and oxygen (3.50 Å) suggesting a very strong halogen bond. Indeed, these bonds are shorter than those reported by Resnati *et al*. that formed O•••I halogen bond between a nitro oxide and iodo compound with an O•••I distance of 2.745 Å.[17] The third halogen bond is also a very short contact being only 85.0 % of the Van der Waal's radii for nitrogen and iodine (3.53Å). No halogen bonds were formed with the pyridyl nitrogens as they point inwards in a conformation that sterically disfavors further interactions. The crystal packing shown in figure 4.8 adopts a layered conformation with dimers of macrocycle **4.1** separated by the iodo compounds **4.5**. The pentafluoro iodobenzene molecules are

associated through offset aryl-aryl stacking with an average center-center distance of 3.56 Å.

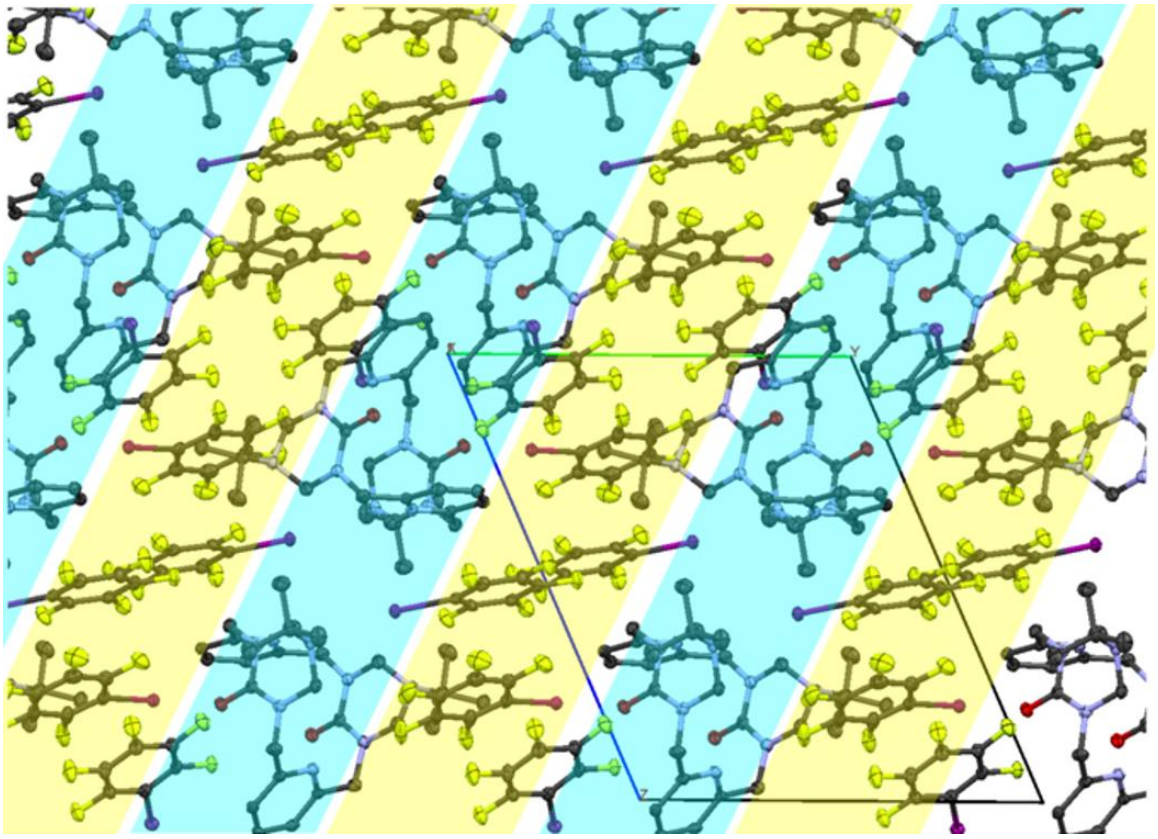

Figure 4.8. The crystal packing of the halogen bonded macrocycle **4.1**•pentafluoro iodobenzene complex showing the layers of iodo molecules (yellow highlight) and macrocycle **4.1** (blue highlight).

Macrocycle 4.1•tetrafluoro diiodoethane [($C_{28}H_{40}N_8O_2$)•($C_2F_4I_2$)].

Macrocycle **4.1** was crystallized from the slow evaporation of a 1:1 mixture with tetrafluoro diiodoethane from methylene chloride. In order to avoid light induced elimination of the tetrafluoro diiodoethane, the crystallization was conducted in the dark. The resulting crystals were a colorless block crystal with the formula

($C_{28}H_{40}N_8O_2$)($C_2F_4I_2$). The macrocycle crystallized in triclinic system (*P*-1 space group) consisting one half of a macrocycle **4.1** and one half of a diiodotetrafluoroethane molecule located on the crystallographic inversion centers. The macrocycle adopts the typical planar and anti-parallel urea orientation seen with other *bis*-urea macrocycle such as the *m*-xylene.[18] Figure 4.9 shows that each of the two carbonyl oxygens are involved in halogen bonds with separate diiodotetrafluoro ethane molecules with a I•••O distance of 2.737 and a C-I•••O angle of 175.93º.

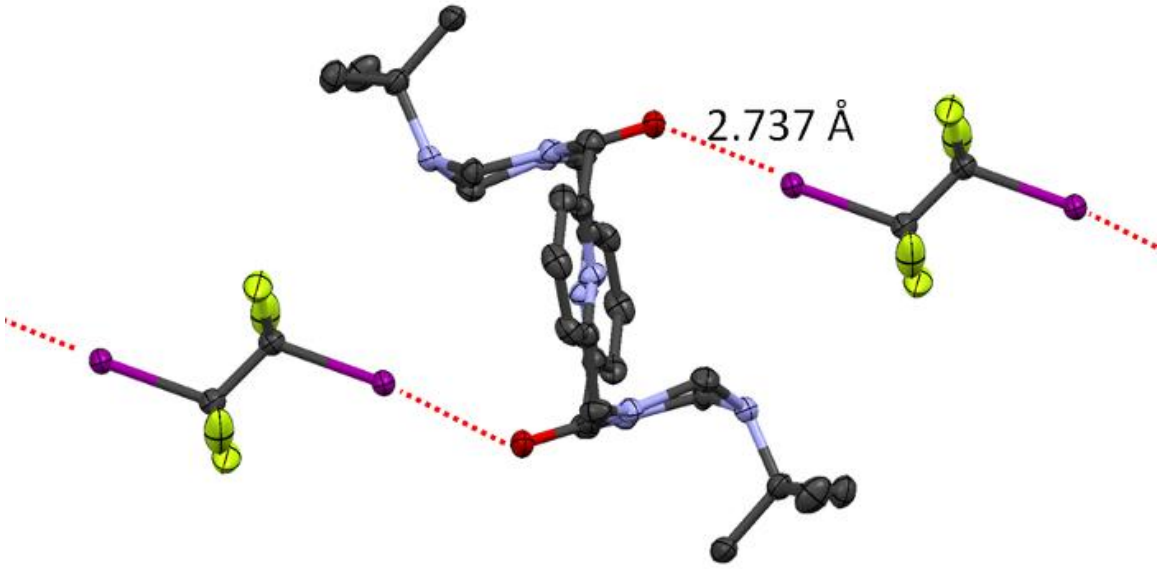

Figure 4.9. The pyridyl macrocycle with halogen bonding to diiodo tetrafluoro ethane showing very short halogen bonding distances of 2.737 Å (O•••I) (VDW = 3.50 Å) this is 22% shorter than the sum of the Van der Waal;s radii (3.50 Å). (Ellipses drawn at the 50% probability level, C-black, O-red, N-blue, I-purple, F- yellow, Hydrogens have been removed for clarity.)

The I•••O distance is 78.2 % of the Van der Waal's radii, which suggests a very strong halogen bond. Figure 4.10a shows the space filling model of the linear chain that is formed by the halogen bonded complex [($C_{28}H_{40}N_8O_2$)($C_2F_4I_2$)] and the overall crystal packing of the complex (Figure 4.10b) that shows linear chains forming ribbons packed

together. Between the ribbons there is offset aryl-aryl staking between two adjacent pyridyl macrocycles with a center to center distance of 3.786 Å that aids in the packing.

This crystal structure and the iodoperfluorobenzene structure together support our hypothesis that the carbonyl oxygen is very electronegative and a good halogen bond acceptor. With the open orientation of the nitrogens in the triazinanone group of the diodotetrafluoroethane, we observed no association with the nitrogen lone pairs suggesting the carbonyl oxygens are better halogen bond acceptors. This evidence along with the calculation done on macrocycle **4.1** suggests that macrocycle **4.2** will be a stronger Lewis acid and a better halogen bond accepting species.

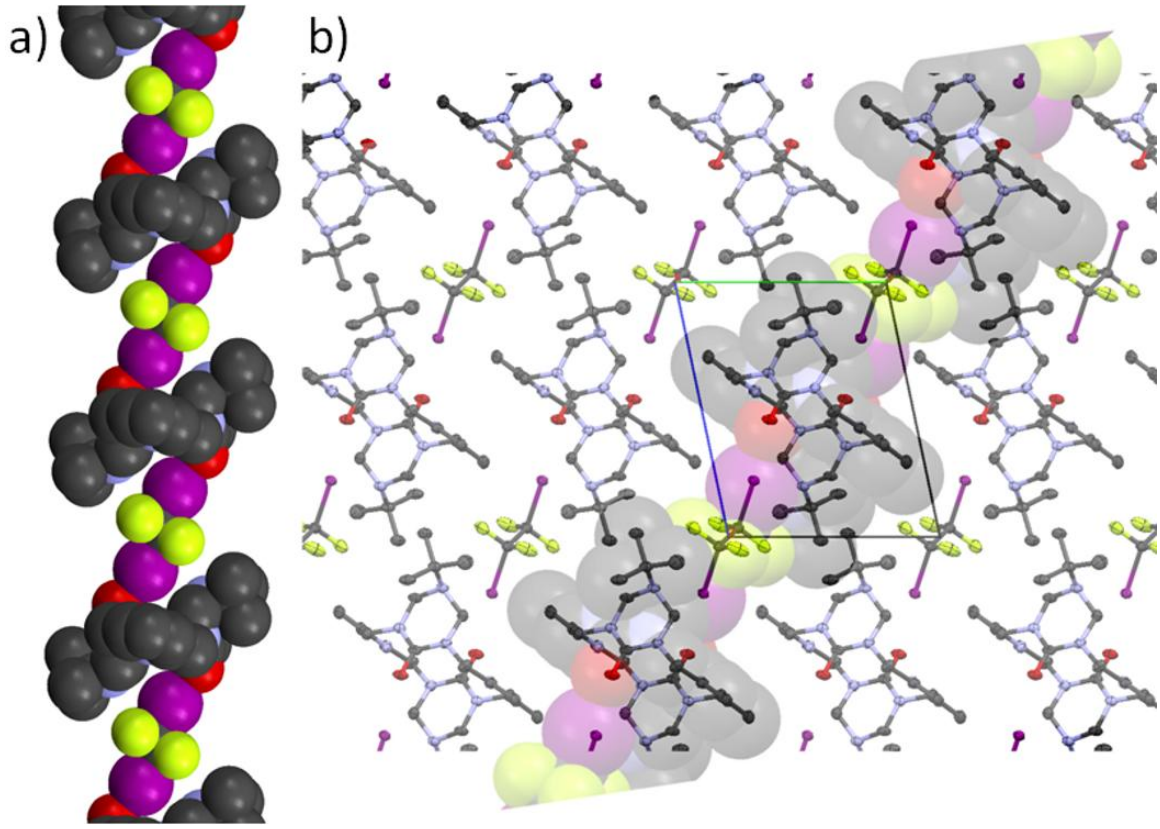

Figure 4.10. Crystal structure of macrocycle **4.1**•diiodotetrafluoroethane. a) A space filling model of the linear chains formed by the halogen bonding interactions. b) The crystal packing with an overlay of the linear chain. (Ellipses drawn at the 50% probability level, C-black, O-red, N-blue, I-purple, F- yellow, Hydrogens have been removed for clarity.)

4.6 Ionic salts of pyridyl *bis*-urea macrocycle.

Macrocycle 4.1•diiodotetrafluoroethane and light $[(C_{28}H_{38}N_8O_2)(I)_2•(C_2F_4I_2)•(CDCl_3)]$.

The slow evaporation of a 1:1 mixture of macrocycle **4.1** and diiodotetrafluoroethane from chloroform (40 mM) while exposed to ambient light, resulted in colorless block crystals of $(C_{28}H_{38}N_8O_2)(I)_2•(C_2F_4I_2)•(CDCl_3)$ shown in Figure 4.11b. The crystal structure revealed a dicationic salt of macrocycle **4.1** with two iodide counter anions. The addition and elimination of iodine across a double bond is well known to be a labile and reversible reaction. This elimination can be induced by ambient light. Because the mixture was not protected from light sources, an elimination reaction likely results in the formation of tetrafluoroethene (TFE) and iodine, which further reacts. Low boiling TFE (bp = -76.3 ºC) would be lost under the ambient conditions of the crystallization. Subsequently, the iodine likely oxidizes the triazinanone resulting in the reduced iodide anion and the imine cation seen in Figure 4.11a. Iodine has been known to oxidize alcohols, sugars and imines to form ketones, glucosamines and dicationic salts.[19] For example, in dichloromethane solutions molecular iodine oxidizes 1-methyl-imidazole-2-thione at the tertiary carbon resulting in a dicationic salt that is useful in thyroid mediation.[19e] A carbon in the triazinanone shows the characteristic of an sp^2 hybridization and double bond character with the C-N bond length with the urea nitrogen of 1.29 Å and a C-N bond length with the second nitrogen of 1.34 Å. The bonding angle of the carbon is 120 º. The bond length, association with the iodine anion, and bond angles suggests that the one carbon of the triazinanone group now has positive character.

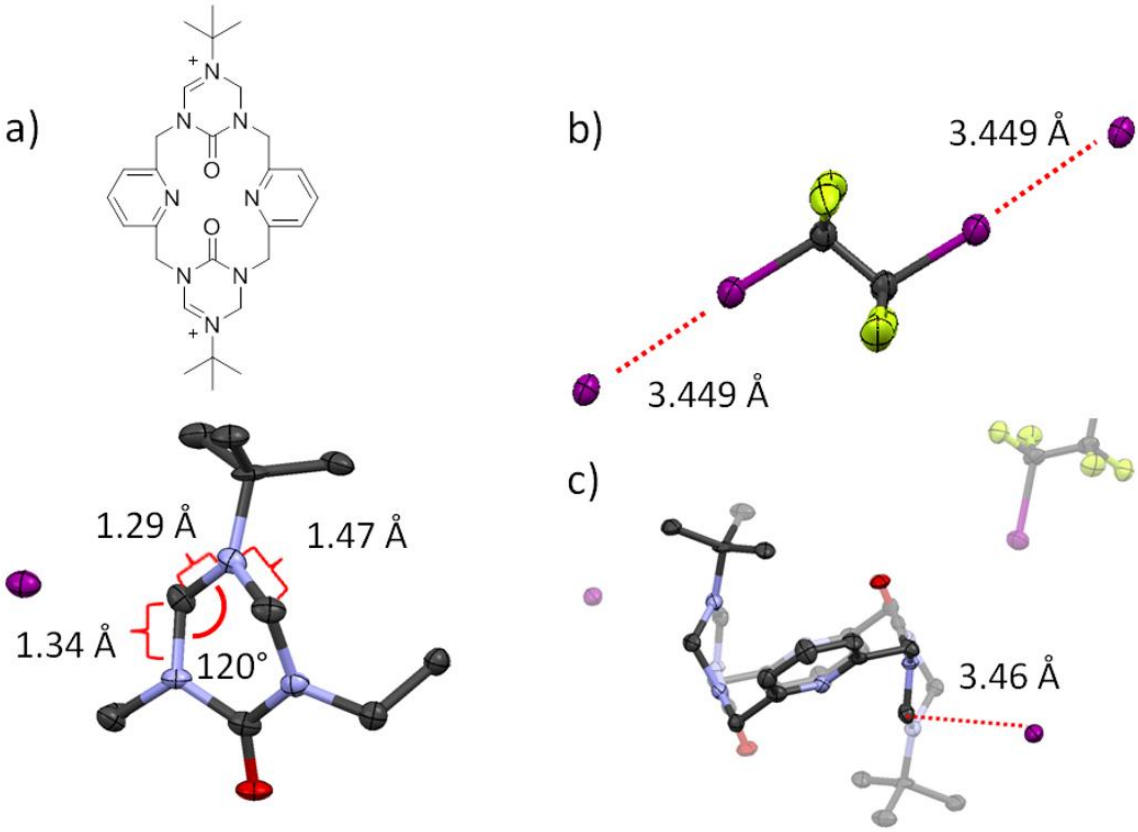

Figure 4.11. Selected crystal structure features of $[(C_{28}H_{38}N_8O_2)(I)_2 \bullet (C_2F_4I_2) \bullet (CDCl_3)]$. a) Schematic representation and crystal structure of deprotonated triazinanone group showing the double bond characteristics formed. b) The iodide anion halogen bonds formed with diiodo tetrafluoroethane with an association distance of 3.449 Å. c) The ionic bond formed by the macrocycle **4.1** dication and the iodide anion. (Ellipses drawn at the 50% probability level, C-black, O-red, N-blue, I-purple, F- yellow, Hydrogens have been removed for clarity.)

The dicationic macrocycle crystallizes in the monoclinic space group $P2_1/n$ consisting of one half of macrocycle **4.1** dication and one iodine anion and on half of diiodo tetra fluoroethane molecule. The crystal unit also contains one half of a disordered chloroform molecule with the dication and the iodo compounds on the crystallographic inversion center. The iodide anions form an ionic bond with the C in the triazinanone with a C•••I^- distance of 3.46 Å (Figure 4.11b). The two iodide anions are involved in halogen bonds with one diodotetrafluoro ethane. Figure 4.11b shows the two halogen

bonds formed between the iodine anions and the tetrafluorodiodoethane molecule with I•••I^- distance of 3.449 Å and a C-I•••I^- angle of 173.80 º. This is 87.3% of the sum of the Vander Waal's distance of the iodine and iodide anion (3.96 Å). Figure 4.12 shows the crystal packing which has the macrocycles in a body centered cubic orientation interspersed with the chloroform, diiodoethane and iodide anions.

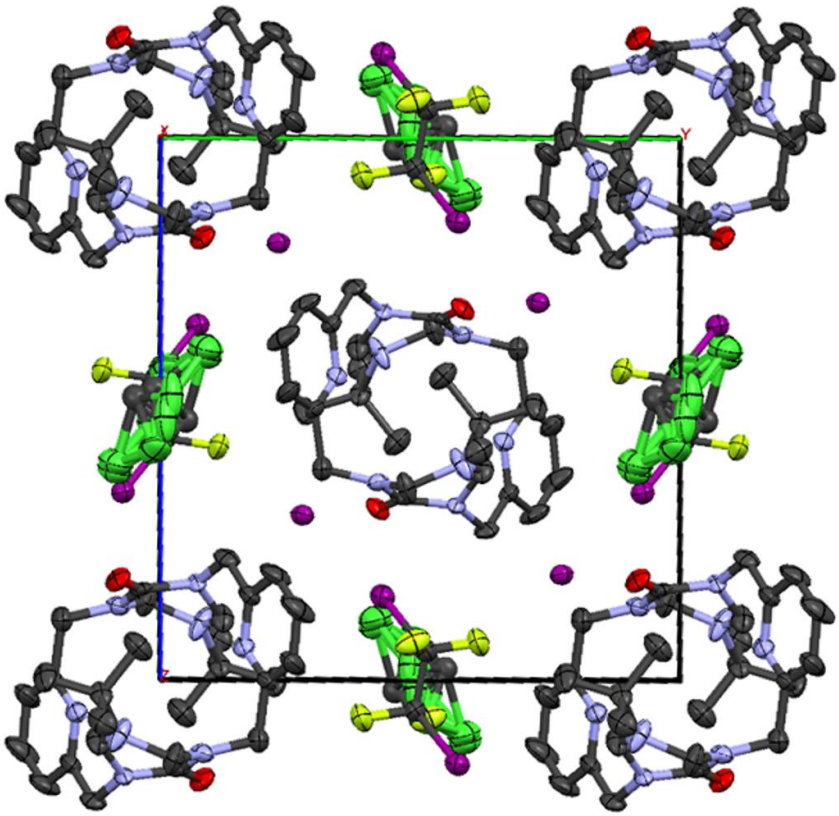

Figure 4.11. Crystal packing of $[(C_{28}H_{38}N_8O_2)(I)_2(C_2F_4I_2)\cdot(CDCl_3)]$ showing the dicationic salt, $[C_{28}H_{38}N_4O_2]^{2+}$ $[I_2]^{2-}$, oriented in a body centered cubic orientation interspersed with diiodo tetrafluoroethane and disordered chloroform. (Ellipses drawn at the 50% probability level, C-black, O-red, N-blue, I-purple, F- yellow, Hydrogens have been removed for clarity.)

Macrocycle 4.1•Diiodotetrafluorobenzene [($C_{28}H_{42}N_8O_2$)(Cl_2)].

Finally with the slow evaporation of a mixture of macrocycle **4.**1 and diiodo tetrafluorobenzene (1:1) in a chloroform solution (40 mM) resulted in a doubly protonated form of macrocycle **4.1**. with the *t*-butyl nitrogen of the triazinanone protecting group bonding the acidic proton. Figure 4.13 shows the ionic bond formed between the protonated macrocycle **4.1** and the chloride anion with a $Cl^{-}\bullet\bullet\bullet N^{+}$ distance of 3.03 Å. The chloride anion is also involved in hydrogen bonding with two chloroform solvent molecules. Interestingly, there was no iodo compound involved in the crystal structure and no halogen bonding apparent. The resulting crystal packing shows a layered orientation of the chloroform molecules and the ionic compounds.

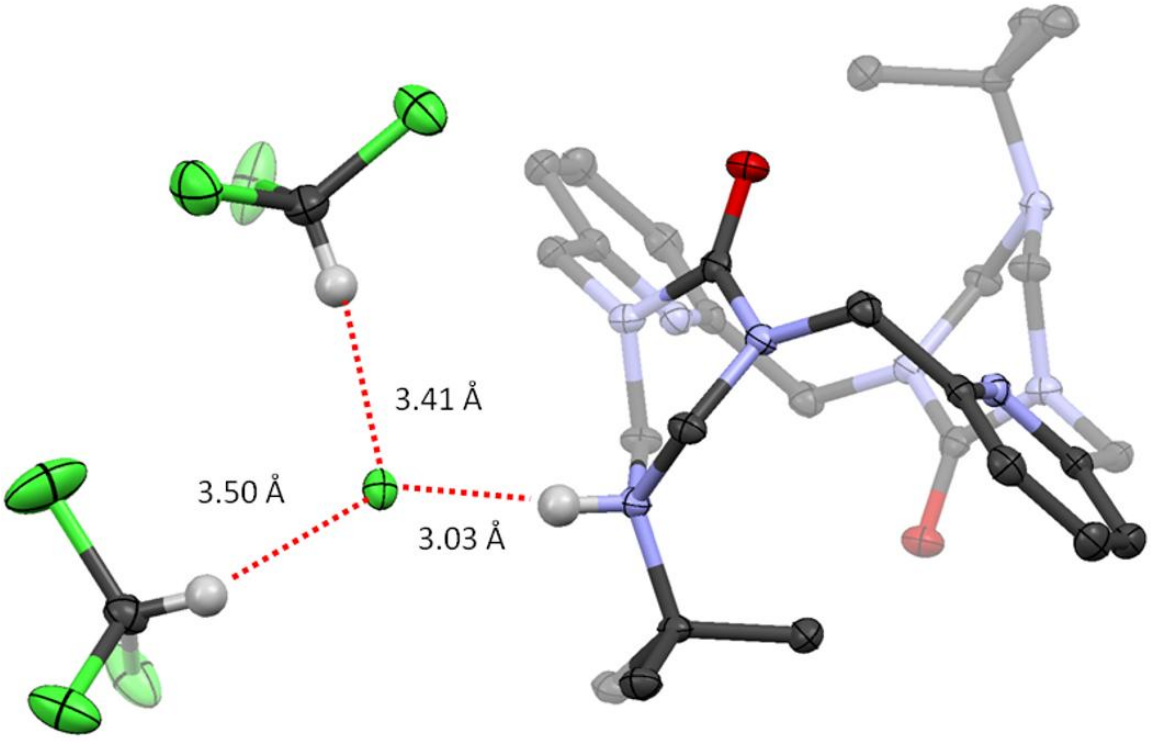

Figure 4.13. Shows the protonated pyridyl macrocycle with ionic bonding of the macrocycle and the hydrogen bonding of the chloroform solvent molecules with the chloride anion $[C_{28}H_{42}N_8O_2]^{2+}[Cl_2]^{2-}$. (Ellipses drawn at the 50% probability level, C-black, O-red, N-blue, I-purple, F- yellow, Hydrogens have been removed for clarity.)

4.7 Computational examination of halogen bonds.

In order to examine the strengths of the halogen bonding, we uploaded the crystal structure coordinates for the macrocycle and halogenated compounds onto Q-chem version 4.0.1. The single point energy calculations were performed using the PBE exchange-correlation functional with the LANL2DZ effective core potential and accompanying basis set. The bond energies were calculated by systematically removing one group at a time and recalculating the single point energy.

The first calculation were performed on the macrocycle **4.1•4.5** complex and by systematically removing each of the three iodine molecules. Figure 4.14 shows the assignment of the groups as G1 and G2 as they were for the calculations.

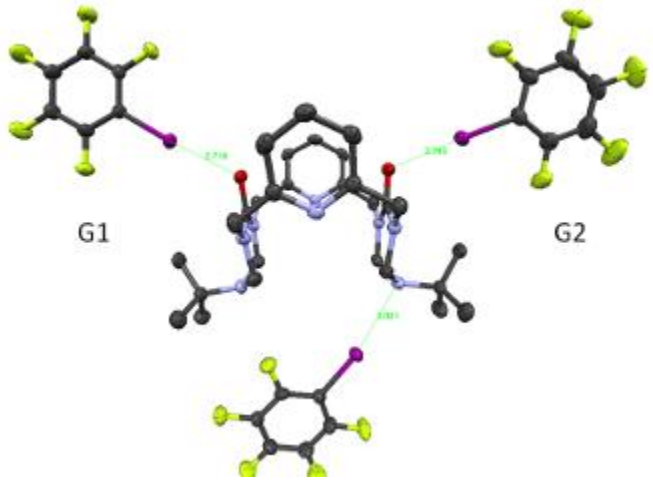

Figure 4.14. Assignment of the groups for systematic calculation of the bond energies.

How much is the interaction between the halide and the macrocycle worth? In order to assess this energy, in collaboration with Jim Mazzuca, we first calculated the energy of the whole system (Table 4.2 full system) then G1 was removed and single point

calculation redone (Table 4.2 G1-). Then the same was done for G2 (Table 4.2 G2-), and with both iodo compounds removed (Table 4.2 Both removed). Then the energies for each of the fluorocompounds (**4.5**) were calculated (Table 4.2 G1 and G2). Next, we estimated the energies of the individual halogen bonds by systematically examining the change in energy values listed in table 4.2. Table 4.3 shows the energies calculated for each difference. The first calculation was of the difference in energies with each group removed while the second group was present (Table 4.3 G1+ and G2+) resulting in an average energy of 7.38 kcal mol^{-1}. Then the diference in energy was calculated with each group removed while the second group was absent and recorded (Table 4.3 G1- and G2-). The resulting energies gave an average energy of 6.85 kcal mol^{-1} per halogen bond. Finally, the averages of each of the energies were analyzed to look at what the effect each had on the energy of the overall system. The single point calculations resulted in each of the halogen bonds having a stabilization energy of 7.381 kcal mol^{-1} when the other substrate is present but the removal of one lowers the energy of the other by 0.527 kcal mol^{-1}. When looking at the fully saturated system, picking any one of the I-O halogen bonds results in the energy of 7.381 kcal mol^{-1} and when looking at the halogen bonds independently they have an average energy of 6.85 kcal mol^{-1}. This suggests that each of the halogen bonds have a stabilization effect on the other of 0.527 kcal mol^{-1}.

Table 4.2 calculated energies used to calculate the bond energies of the complexes.

Structure	Total Energy (Eh)
Full system	-3872.7676075579
G1-	-3137.5220079163
G2-	-3137.5220666798
Both removed	-2402.2773059764
G1	-735.2337026538
G2	-735.2339141342

Table 4.3. calculated energy differences with systematic removal of halogen bonds.

Structure	Energy (Eh)	Energy (kcal mol^{-1})
G1+	0.0118969878	7.465
G2+	0.0116267439	7.296
G1-	0.0110580496	6.939
G2-	0.0107878057	6.769
Sum (G1, G2)	0.0226847935	14.235
Sum (G2,G1)	0.0226847935	14.235
Sum (both)	0.0226847935	14.235
Ave (G1+ and G2+)	0.0117618659	7.381
Ave (overall)	0.0113423968	7.117

The same calculations were then examined for the second halogen bonding complex, macrocycle **4.1**•diiodo tetrafluoroethane. Figure 4.15 shows the group designation for the systematic removal and calculation of the halogen bonding energies.

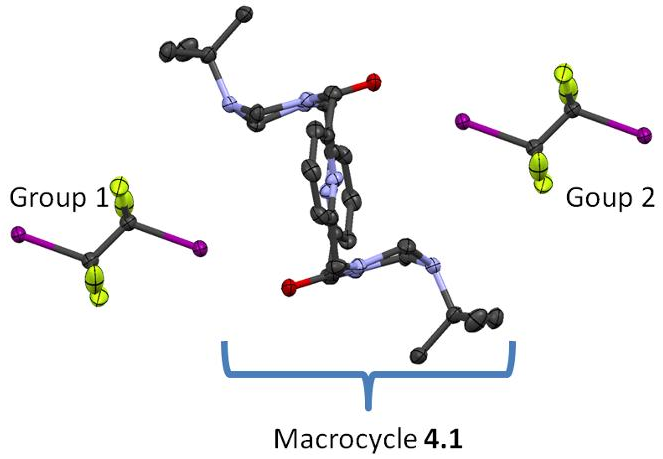

Figure 4.15 group assignment for calculation of halogen bonding energies.

The energies were calculated for the whole system from the crystal structure uploaded into Qchem version 4.0.1 using the PBE exchange-correlation functional with the LANL2DZ effective core potential and accompanying basis set. The first calculation was that of the whole structure with both iodine compounds (Table 4.4 full system). Then the

energy was calculated for the macrocycle with both iodine compounds removed (Table 4.4 both removed). Then the energies were calculated for the system with each removed one at a time (Table 4.4, G1- and G2-). Then the energies were calculated for each iodine compound by themselves (Table 4.4 G1 and G2).

Table 4.4. Calculated energies for complexes with systematic removal of halogen groups.

Structure	Energy (Eh)
Full system	-2658.2797917166
Both removed	-1667.0318424859
G1-	-2162.6554844798
G2-	-2162.6554874586
G1	-495.6077516647
G2	-495.6077516472

Then the energy of each halogen bond was calculated by looking at the change in the energies calculated in Table 4.5. First, the energies of the bonds with the other halogen present (Table 4.5 G1+ and G2+) resulting in energy of the halogen bonds of 10.33 kcal mol^{-1}. Then the energies of the halogen bonds were calculated for each with the second halogen compound removed (Table 4.5 G1-and G2-) resulting in halogen bonding energy of 9.97 kcal mol^{-1}. Finally, we checked the average and sums to analyze the validity and competency of the calculations (Table 4.5). The single-point energy calculation for the complex resulted in the average energy of 10.331 kcal mol^{-1} for each halogen bond in the presence of the second substrate and 9.972 kcal mol^{-1} in the absence of the second substrate. These results are similar to that of the first complex in that the energies are on the higher end of the halogen bonding spectrum as reported by Metrangelo *et al.* and as seen in the extremely short contact distances.[2-3] Also of interest is the stabilization effect

each substrate has on the other, each of 0.359 and 0.527 kcal mol^{-1} showing a possible inductive effect through the pyridyl macrocycle that each halogen bond has on the other.

Table 4.5. Calculated values for the halogen bonds in separate environments

Structure	Energy (Eh)	Energy (kcal mol^{-1})
G1+	0.0118969878	7.465
G2+	0.0116267439	7.296
G1-	0.0110580496	6.969
G2-	0.0107878057	6.769
Sum (G1 and G2)	0.0226847935	14.235
Sum (G2 and G1)	0.0226847935	14.235
Sum (both)	0.0226847935	14.235
Ave(G1+ and G2+)	0.0117618659	7.381
Ave (overall)	0.0113423968	7.117

4.8. Solid-to-solid transformations and analyzing the uptake of ethylene glycol.

The absorption of guest molecules by materials without pores happens in materials with flexile frameworks and has been investigated by Kitagawa *et al.* They characterize these frameworks that show structural change but retains its crystallinity as solid-to-solid transformation.[20] Dr Roy reported that the pyridyl macroycle **4.1** can absorb hydrogen bonding donors while retaining its crystallinity even though the crystal structure itself has no notable pore.[14] In order to examine the effect of the absorption of a hydrogen bond donor on the bulk crystal, empty host **4.2** crystals were loaded into a well plate and to these two drops of ethylene glycol were added. These crystals were monitored periodically over 48h under an optical microscope. Figure 4.16 shows the images that were then loaded into image manipulation software and the lengths and widths of the crystals were measured in pixels. A standard slide was used to determine the distance per pixel to be 73 pixels per 100 μm. The average lengths and widths of

selected parts of the crystals were calculated from 20 separate measurements and these were used to determine the change in the bulk crystal. Table 4.6 shows the average distances calculated over the five sample areas. After 48 h of soaking the crystals in ethylene glycol no observable change in measurements was noted. The ethylene glycol was decanted from the crystals, which were then rinsed with methanol and dissolved into δ_6-DMSO and the sample evaluated by ^{1}H-NMR. The integration of host **4.2** to ethylene glycol was ~1:1 similar to what was reported by Dr. Roy.

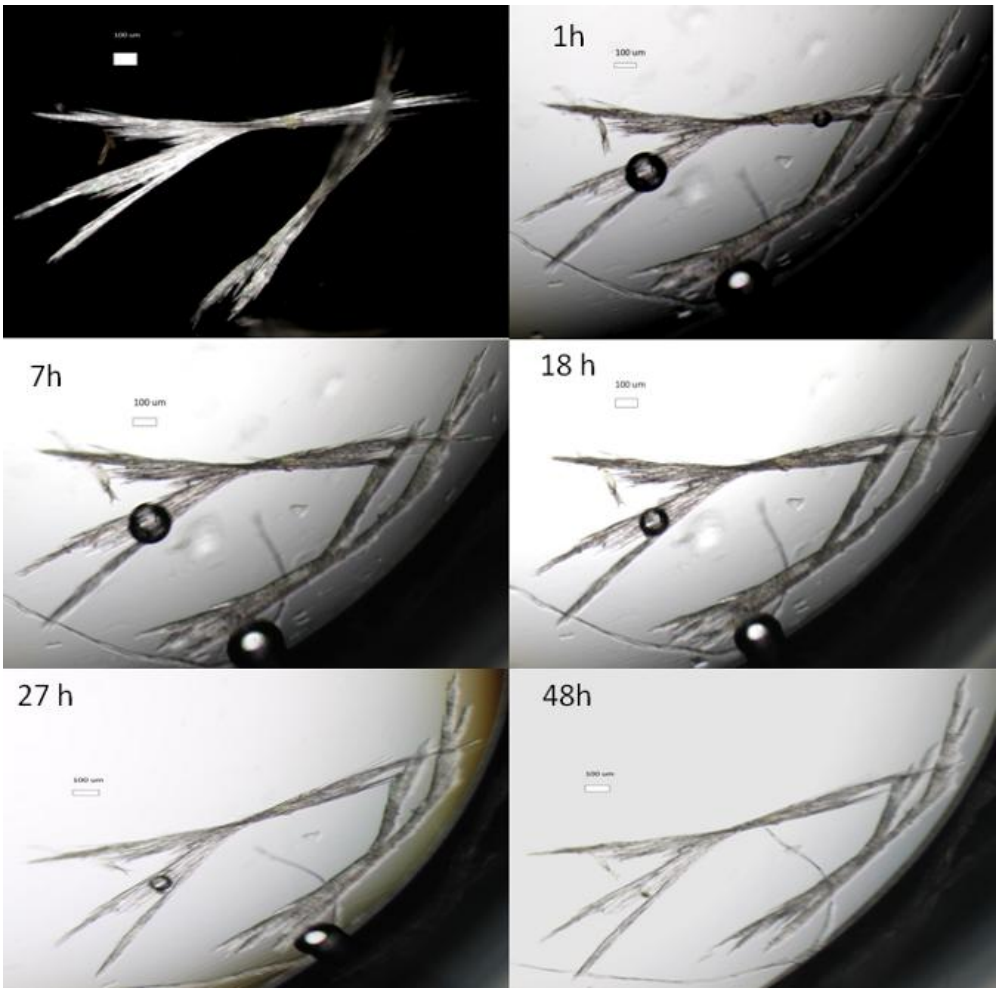

Figure 4.16. Images of the pyridyl macrocycle crystals before and during soaking in ethylene glycol (Scale bar = 100 nm).

Table 4.6. Measurements of crystals over 48 h absorption of ethylene glycol.

Measurement (μm)[a]	0h	18h	48h
A	47.8±1.9	47.9±2.6	48.0±1.4
B	49.2±1.7	48.2±1.8	47.8±1.9
C	63.5±2.5	67.6±2.7	70.8±2.8
D	1900.7±4.3	1893.1±4.4	1877.7±4.5
E	1068±11	1083±6	1073±7
F	2068.4±4.0	2072±3.2	2051±6.4

[a]measurements were an average of 20 repeat measurements of selected cross-sections and lengths of the crystals.

4.9. Future work.

The crystal structures we obtained with the protected pyridyl macrocycle **4.1** demonstrates that it can form short and strong halogen bonds. In fact, our computations suggest an even stronger electrostatic potential for the carbonyl oxygens of the deprotected macrocycle **4.2**. We will explore these same interactions with similar substrates and look for co-crystal formation with the deprotected macrocycle **4.2**. Our hypothesis is that the more electronegative potential of **4.2** will effect the length of the halogen bonds observed. We also propose to look to an expanded selection of possible halogen and hydrogen bond donor guest for absorption and organization. These will include halogen bond donors similar to diiodo tetrafluoroethane but with an extended C backbone (C_3-C_6) as well as other aryl halogens including naphthyl halides and naphthalene diimide derivatives. We are also interested in evaluating if the pyridyl nitrogen will participate in the halogen bonding once the triazinanone protecting groups are removed. The computations and preliminary results in this chapter suggest that this will not be the case. But it is known that sterics play a significant role in the limitations of halogen bonding[8] and removal of the bulky *tert*-butyl group may change the ability of the halogen bond donors to associate with the pyridyl nitrogen.

The ability of the pyridyl macrocyclic assembly unit to organize electrophilic halides or good hydrogen bond donors in co-crystals could be advantageous for controlling the order and relative geometry of guest with important optical and/or electronic properties. For example, in the field of organic semiconductors, conjugated polymers and large aryl moieties, such as naphthyl diimides, are widely used for applications such as light emitting diodes (OLED's), field effect transistors (OFET's) and photovoltaics (OPV's).[21] A common substrate in these fields are naphthyl diimides that have been shown to have excellent charge carrier mobility when arranged face-to-face.[22] Figure 4.17 shows a graphical representation of the preorganization of such guests inside the crystalline structure of macrocycle **4.2**. This could also result in ordered face-to-face assembly and control and perhaps attenuate the electronic properties of such molecules. Along with these, the incorporation of guests, such as acrylic acid, that can form hydrogen and halogen bonds can be oriented in such a way as to provide a template effect on their chemistry. This would result in stereo specific polymers with unique chemical and electronic properties.

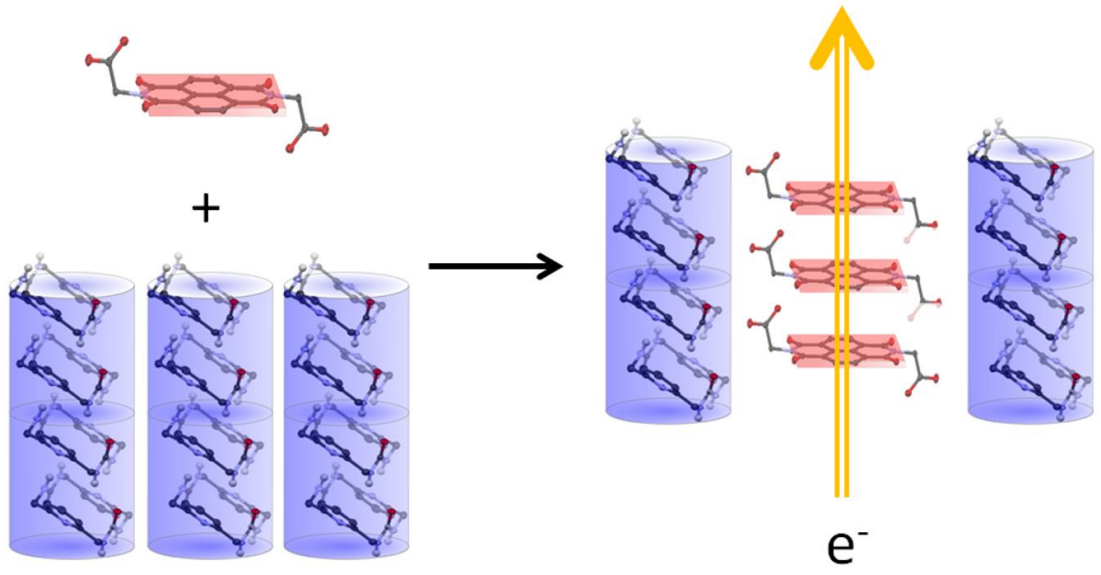

Figure 4.17. The graphic representation of macrocycle **4.2** assembled columnar structure when in the presence of a hydrogen bonding guest will absorb that guest in between the channels and preorganize the guest to increase its chemical and electrochemical properties.

Dr. Roy has also synthesized larger pyridyl macrocycles (Figure 4.18, **4.3** and **4.4**) that have the same functionality and could potentially find utility with the incorporation of guests inside the channel. To date, these larger cycles have not been crystallized into columnar structures but instead have shown a propensity to form ribbons because of the flexibility in the extended cyclic structure.[16] With the introduction of weakly hydrogen or halogen bonding guests, such as phenols, diols or diiodides, the pyridine could be masked allowing for the self-assembly of the macrocycles into columnar structures. The columnar structures of these larger macrocycles would then have the pyridyl functionality incorporated inside the column allowing for hydrogen bonding or halogen bonding associations that could template or preorganize guests for selective reactions.

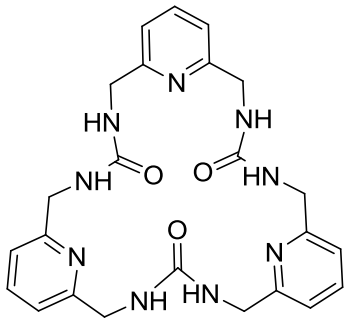

4.3

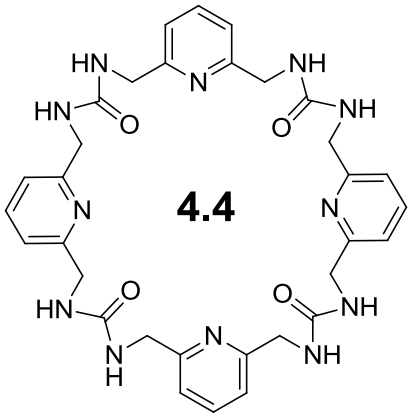

Figure 4.18. Larger *bis*-urea pyridine macrocycles synthesized by Dr. Roy[16]

4.10. Summary and Conclusions.

In summary, the crystallization of the pyridyl *bis*-urea macrocycle with two halogen bond donors, diiodotetrafluoroethane and iodopentafluorobenze, by slow evaporation from dichloride methane and resulted in very strong halogen bonds. The bonds formed with the carbonyl oxygen of the urea in host **4.1** and were an average of 78% of the Van der Waals radii for I•••O (3.50 Å). The halogen bonds formed with host **4.1** are shorter than charged analogs reported by Metrangelo and Resnati. Indeed, if we equate bond length with bond strength, co-crystal formation host **4.1** with electrophilic halides affords among the strongest halogen bonding motif surveyed by Metrangelo in the CSD.[1a] Through DFT calculation we were able to estimate these energies to be 7.381 kcal mol^{-1} for the iodopentafluorobenzene halogen bond and 10.331 kcal mol^{-1} for the iodotetrafluoro ethane halogen bond. We expect that the propensity for strong halogen bond formation will be conserved upon the deprotection of the macrocycle to **4.2**. This new assembly unit combines both hydrogen bonding donors and multiple acceptors for

hydrogen or halogen bonds and should result in cocrystalline materials that preorganize and enhance the chemical and electronic properties.

4.11. Experimental.

All chemicals were used as order without further purification. Macrocycle **4.1** and **4.2** were synthesized as previously reported.[15]

General crystallization procedures.

Macrocycle **4.1** was dissolved into methylene chloride, chloroform and THF (40 mM) in separate scintillation vials. Then, to each solution the halogenated compounds were added in either a 1:1 or a 2:1 molar ratio. The vials were then capped loosely and allowed to slow evaporate.

Purification of pyridyl *bis*-urea macrocycle.

Crude macrocycle was loaded onto silica (10:1 silica/crude product; w/w) and dry loaded onto column for purification by flash chromatography (9:1 CH_2Cl_2: ammonia sat. MeOH).

Ethylene glycol absorption:

Empty host **4.2** crystals were loaded into a well plate and to these two drops of ethylene glycol were added. These crystals were monitored periodically over 48 h under an optical microscope. The images were then loaded into image manipulation software and the lengths and widths of the crystals were measured in pixels. A standard slide was used to determine the distance per pixel to be 73 pixels per 100 μm. The average lengths and widths of selected parts of the crystals were calculated from 20 separate

measurements and these were used to determine the change in the bulk crystal. The average distances were calculated over five sample areas. After 48 h, the ethylene glycol was decanted from the crystals, which were then rinsed with methanol and dissolved into δ_6-DMSO and the sample evaluated by ^{1}H-NMR. The integration of host **4.2** to ethylene glycol was ~1:1.

4.11.1. X-ray crystal structure determination of protected pyridyl *bis*-urea macrocycle pentafluoro iodobenzene complex [$(C_{28}H_{40}N_8O_2)\bullet(C_6F_5I)_3$].

X-ray intensity data from an irregular colorless crystal were collected at 100(2) K using a Bruker SMART APEX diffractometer (Mo Kα radiation, λ = 0.71073 Å).[23] The data crystal was cleaved from an undifferentiated mass of crystalline solid. The raw area detector data frames were reduced and corrected for absorption effects with the SAINT+ and SADABS programs.[23] Final unit cell parameters were determined by least-squares refinement of 6627 reflections from the data set. Direct methods structure solution, difference Fourier calculations and full-matrix least-squares refinement against F^2 were performed with SHELXS/L[24] as implemented in OLEX2.[25]

The compound crystallizes in the triclinic system. The space group P-1 (No. 2) was confirmed by the successful solution and refinement of the structure. The asymmetric unit consists of one $C_{28}H_{40}N_8O_2$ molecule and three independent C_6F_5I molecules. All non-hydrogen atoms were refined with anisotropic displacement parameters. Hydrogen atoms were placed in geometrically idealized positions and included as riding atoms. The largest residual electron density peaks of ca. 1 $e^-/Å^3$ are located < 1 Å from the three independent iodine atoms.

Table 4.6. Crystal structure data and refinement of protected pyridyl *bis*-urea macrocycle pentafluoro iodobenzene complex [$(C_{28}H_{40}N_8O_2)$•$(C_6F_5I)_3$].

Empirical formula	$C_{46}H_{40}F_{15}I_3N_8O_2$
Formula weight	1402.56
Temperature/K	100(2)
Crystal system	triclinic
Space group	P-1
a/Å	12.787(3)
b/Å	13.339(3)
c/Å	16.139(4)
α/°	65.969(4)
β/°	83.547(4)
γ/°	85.330(4)
Volume/Å^3	2496.4(11)
Z	2
ρ_{calc}mg/mm^3	1.866
m/mm^{-1}	1.982
F(000)	1364.0
Crystal size/mm^3	0.4 × 0.25 × 0.2
2Θ range for data collection	3.2 to 53.02°
Index ranges	$-15 \leq h \leq 15$, $-16 \leq k \leq 16$, $-20 \leq l \leq 20$
Reflections collected	41108
Independent reflections	10236[R(int) = 0.0362]
Data/restraints/parameters	10236/0/673
Goodness-of-fit on F^2	1.046
Final R indexes [I>=2σ (I)]	R_1 = 0.0293, wR_2 = 0.0682

Final R indexes [all data]	$R_1 = 0.0357$, $wR_2 = 0.0713$
Largest diff. peak/hole / e Å^{-3}	1.16/-0.34

4.11.2. X-ray crystal structure determination of protected pyridyl *bis*-urea macrocycle diiodo tetrafluoro ethane complex [($C_{28}H_{40}N_8O_2$)•($C_2F_4I_2$)].

X-ray intensity data from a colorless platelike crystal were collected at 100(2) K using a Bruker SMART APEX diffractometer (Mo Kα radiation, λ = 0.71073 Å).[23] The raw area detector data frames were reduced and corrected for absorption effects with the SAINT+ and SADABS programs.[23] Final unit cell parameters were determined by least-squares refinement of 4619 reflections from the data set. Direct methods structure solution, difference Fourier calculations and full-matrix least-squares refinement against F^2 were performed with SHELXS/L[24] as implemented in OLEX2.[25]

The compound crystallizes in the triclinic system. The space group *P*-1 (No. 2) was determined by structure solution. The asymmetric unit consists of half of one $C_{28}H_{40}N_8O_2$ molecule and half of one $C_2F_2I_2$ molecule, both of which are located on crystallographic inversion centers. Non-hydrogen atoms were refined with anisotropic displacement parameters. Hydrogen atoms were placed in geometrically idealized positions and included as riding atoms. The largest residual electron density peak of 1.85 e/Å^3 in the final difference map is located 0.92 Å from the unique iodine atom I(1).

Table 4.7. Crystal structure data and refinement of protected pyridyl *bis*-urea macrocycle diiodo tetrafluoro ethane complex [($C_{28}H_{40}N_8O_2$)•($C_2F_4I_2$)].

Empirical formula	$C_{30}H_{40}N_8O_2F_4I_2$
Formula weight	874.50
Temperature/K	100(2)
Crystal system	triclinic
Space group	P-1 (No. 2)
a/Å	9.372(2)
b/Å	9.757(2)
c/Å	10.799(3)
α/°	77.105(4)
β/°	84.963(4)
γ/°	63.533(4)
Volume/Å^3	861.7(3)
Z	1
ρ_{calc}mg/mm^3	1.685
m/mm^{-1}	1.887
F(000)	434.0
Crystal size/mm^3	0.24 × 0.2 × 0.15
2Θ range for data collection	3.86 to 53.32°
Index ranges	$-11 \leq h \leq 11$, $-12 \leq k \leq 12$, $-13 \leq l \leq 13$
Reflections collected	11871
Independent reflections	3607[R(int) = 0.0407]
Data/restraints/parameters	3607/0/211
Goodness-of-fit on F^2	1.044
Final R indexes [I>=2σ (I)]	R_1 = 0.0335, wR_2 = 0.0793

Final R indexes [all data]	$R_1 = 0.0375$, $wR_2 = 0.0814$
Largest diff. peak/hole / e Å^{-3}	1.85/-0.42

4.11.3. X-ray crystal structure determination of protected pyridyl *bis*-urea macrocycle diiodo tetrafluoro ethane complex $[(C_{28}H_{38}N_4O_2)(I)_2 \cdot (C_2F_4I_2)_2]$.

X-ray intensity data from a colorless blocklike crystal were collected at 100(2) K using a Bruker SMART APEX diffractometer (Mo Kα radiation, λ = 0.71073 Å).[23] The raw area detector data frames were reduced and corrected for absorption effects with the SAINT+ and SADABS programs.[23] Final unit cell parameters were determined by least-squares refinement of 2405 reflections from the data set. Direct methods structure solution, difference Fourier calculations and full-matrix least-squares refinement against F^2 were performed with SHELXS/L[24] as implemented in OLEX2.[25]

The compound crystallizes in the triclinic system. The space group P-1 (No. 2) was confirmed by the successful solution and refinement of the structure. The asymmetric unit consists of half of one $C_{28}H_{38}N_4O_2^{2+}$ cationic cycle located on a crystallographic inversion center, one iodide anion, half of one $C_2F_4I_2$ molecule also located on a crystallographic inversion center, and an essentially continuously disordered volume of electron density running parallel to the crystallographic *a* axis direction, centered at *y* = 0.5, *z* = 0. Based on trial refinements of the strongest peaks in the region, this electron density represents one $C_2F_4I_2$ molecule per cycle. Attempts to model this density with discrete $C_2F_4I_2$ groups failed, and it was therefore modeled with a total of five fractionally occupied iodine atom positions, eight fluorine positions and three carbon

atom positions. Free refinement of the occupancy values of the five iodine positions yielded 1.94 I per cycle, supporting the reported stoichiometry. Occupancies of the C, F, and I sites were constrained to sum to one $C_2F_4I_2$ molecule per cycle, and atoms of the same kind were assigned a common isotropic displacement parameter. No restraints were applied to simulate expected molecular geometry or bond distances for these atoms. All other non-hydrogen atoms were refined with anisotropic displacement parameters. Hydrogen atoms bonded to carbon were located in difference maps before being placed in geometrically idealized positions and included as riding atoms. The largest residual electron density peak in the final difference map is located 1.0 Å from the iodide anion I(1).

Table 4.8. Crystal structure data and refinement of protected pyridyl *bis*-urea macrocycle diiodo tetrafluoro ethane complex [($C_{28}H_{40}N_8O_2$)•($C_2F_4I_2$)].

Empirical formula	$C_{32}H_{38}F_8I_6N_8O_2$
Formula weight	1480.11
Temperature/K	100(2)
Crystal system	triclinic
Space group	P-1
a/Å	8.3319(15)
b/Å	11.289(2)
c/Å	13.162(2)
α/°	84.680(4)
β/°	80.485(4)
γ/°	74.665(4)

Volume/$Å^3$	1176.0(4)
Z	1
$\rho_{calc}mg/mm^3$	2.090
m/mm^{-1}	4.031
F(000)	692.0
Crystal size/mm^3	0.1 × 0.08 × 0.06
2Θ range for data collection	3.14 to 50.06°
Index ranges	$-9 \leq h \leq 9$, $-13 \leq k \leq 13$, $-15 \leq l \leq 15$
Reflections collected	12706
Independent reflections	4154[R(int) = 0.0501]
Data/restraints/parameters	4154/3/296
Goodness-of-fit on F^2	1.091
Final R indexes [I>=2σ (I)]	R_1 = 0.0497, wR_2 = 0.1106
Final R indexes [all data]	R_1 = 0.0701, wR_2 = 0.1191
Largest diff. peak/hole / e $Å^{-3}$	1.22/-0.83

4.11.4. X-ray crystal structure determination of protected pyridyl *bis*-urea macrocycle diiodo tetrafluoro ethane complex [$(C_{28}H_{38}N_8O_2)(I)_2(C_2F_4I_2)\cdot(CDCl_3)$].

X-ray intensity data from a colorless prism were collected at 100(2) K using a Bruker SMART APEX diffractometer (Mo Kα radiation, λ = 0.71073 Å).[23] The raw area detector data frames were reduced and corrected for absorption effects with the SAINT+ and SADABS programs.[23] Final unit cell parameters were determined by least-squares refinement of 2693 reflections from the data set. Direct methods structure solution,

difference Fourier calculations and full-matrix least-squares refinement against F^2 were performed with SHELXS/L[24] as implemented in OLEX2.[25]

The compound crystallizes in the monoclinic space group $P2_1/n$ as determined by the pattern of systematic absences in the intensity data. The asymmetric unit consists of half of one $C_{28}H_{38}N_8O_2^{2+}$ cation, one unique iodide anion, half of one 1,2-diiodotetrafluoroethane molecule, and a disordered chloroform-*d* molecule. The $C_{28}H_{38}N_8O_2^{2+}$ cation and 1,2-diiodotetrafluoroethane molecule are located on crystallographic inversion centers. The chloroform-*d* molecule is disordered about an inversion center, and therefore only half of this molecule is present per asymmetric unit. It was modeled with two unique components, each with occupancy 0.25. A total of 30 C-Cl and Cl-Cl distance restraints were used to maintain chemically reasonable geometries for the disordered $CDCl_3$ components. Non-hydrogen atoms were refined with anisotropic displacement parameters except for disordered carbon atoms (isotropic). Hydrogen atoms bonded to carbon were placed in geometrically idealized positions and included as riding atoms. The largest residual electron density peak of 1.37 $e^-/Å^3$ in the final difference map is located 0.93 Å from I(1).

Table 4.9. Crystal structure data and refinement of protected pyridyl *bis*-urea macrocycle diiodo tetrafluoro ethane complex [$(C_{28}H_{38}N_8O_2)(I)_2(C_2F_4I_2)\cdot(CDCl_3)$].

Empirical formula	$C_{31}H_{38}Cl_3DF_4I_4N_8O_2$
Formula weight	1246.66
Temperature/K	100(2)

Crystal system	monoclinic
Space group	$P2_1/n$
a/Å	12.421(3)
b/Å	13.042(3)
c/Å	14.394(3)
α/°	90.00
β/°	109.437(4)
γ/°	90.00
Volume/$Å^3$	2198.9(9)
Z	2
$\rho_{calc}mg/mm^3$	1.883
m/mm^{-1}	3.071
F(000)	1192.0
Crystal size/mm^3	0.24 × 0.22 × 0.18
2Θ range for data collection	3.76 to 49.98°
Index ranges	$-14 \leq h \leq 14$, $-15 \leq k \leq 13$, $-17 \leq l \leq 17$
Reflections collected	15786
Independent reflections	3860[R(int) = 0.0641]
Data/restraints/parameters	3860/30/263
Goodness-of-fit on F^2	1.086
Final R indexes [I>=2σ (I)]	$R_1 = 0.0484$, $wR_2 = 0.1128$
Final R indexes [all data]	$R_1 = 0.0653$, $wR_2 = 0.1216$
Largest diff. peak/hole / e $Å^{-3}$	1.37/-0.68

4.11.5. X-ray crystal structure determination of protected pyridyl *bis*-urea macrocycle diiodo tetrafluoro ethane complex $(C_{28}H_{42}N_8O_2)(Cl)_2 \cdot 4(CHCl_3)$.

X-ray intensity data from a colorless rodlike crystal were collected at 100(2) K using a Bruker SMART APEX diffractometer (Mo Kα radiation, λ = 0.71073 Å).[23] The raw area detector data frames were reduced and corrected for absorption effects with the SAINT+ and SADABS programs.[23] Final unit cell parameters were determined by least-squares refinement of 6640 reflections from the data set. Direct methods structure solution, difference Fourier calculations and full-matrix least-squares refinement against F^2 were performed with SHELXS/L[24] as implemented in OLEX2.[25]

The compound crystallizes in the triclinic system. The space group P-1 (No. 2) was determined by structure solution. The asymmetric unit consists of half of one $C_{28}H_{42}N_8O_2^{2+}$ cation, which is located on a crystallographic inversion center, one crystallographically unique chloride anion and two unique chloroform molecules. All non-hydrogen atoms were refined with anisotropic displacement parameters. Hydrogen atoms bonded to carbon were located in difference maps before being placed in geometrically idealized positions and included as riding atoms. The proton H2 attached to nitrogen atom N2 was located in a difference map and refined freely.

Table 4.10. Crystal structure data and refinement of protected pyridyl *bis*-urea macrocycle diiodo tetrafluoro ethane complex [$(C_{28}H_{42}N_8O_2)(Cl)_2 \cdot 4(CHCl_3)$].

Empirical formula	$C_{32}H_{46}Cl_{14}N_8O_2$
Formula weight	1071.07
Temperature/K	100(2)
Crystal system	triclinic

Space group	P-1
a/Å	9.0531(10)
b/Å	11.4588(13)
c/Å	12.9117(15)
α/°	105.588(2)
β/°	96.332(2)
γ/°	109.439(2)
Volume/Å^3	1186.8(2)
Z	1
ρ_{calc}mg/mm^3	1.499
m/mm^{-1}	0.852
F(000)	548.0
Crystal size/mm^3	0.38 × 0.18 × 0.15
2Θ range for data collection	3.36 to 56.78°
Index ranges	$-12 \leq h \leq 12$, $-15 \leq k \leq 15$, $-17 \leq l \leq 17$
Reflections collected	21154
Independent reflections	5936[R(int) = 0.0322]
Data/restraints/parameters	5936/0/260
Goodness-of-fit on F^2	1.041
Final R indexes [I>=2σ (I)]	R_1 = 0.0425, wR_2 = 0.1014
Final R indexes [all data]	R_1 = 0.0496, wR_2 = 0.1057
Largest diff. peak/hole / e Å^{-3}	0.84/-0.57

4.12. References.

1. (a) Metrangolo, P.; Resnati, G., Halogen Bonding: Where We Are and Where We Are Going. *Cryst Growth Des* **2012**; (b) Metrangolo, P.; Resnati, G., Halogen Versus Hydrogen. *Science* **2008,** *321* (5891), 918-919.
2. Metrangolo, P.; Resnati, G., Halogen bonding: A paradigm in supramolecular chemistry. *Chemistry-a European Journal* **2001,** *7* (12), 2511-2519.
3. Metrangolo, P.; Meyer, F.; Pilati, T.; Resnati, G.; Terraneo, G., Halogen Bonding in Supramolecular Chemistry. *Angewandte Chemie International Edition* **2008,** *47* (33), 6114-6127.
4. Metrangolo, P.; Neukirch, H.; Pilati, T.; Resnati, G., Halogen Bonding Based Recognition Processes: A World Parallel to Hydrogen Bonding†. *Accounts of Chemical Research* **2005,** *38* (5), 386-395.
5. Lenoir, D.; Chiappe, C., What is the Nature of the First-Formed Intermediates in the Electrophilic Halogenation of Alkenes, Alkynes, and Allenes? *Chemistry – A European Journal* **2003,** *9* (5), 1036-1044.
6. Messina, M. T.; Metrangolo, P.; Panzeri, W.; Ragg, E.; Resnati, G., Perfluorocarbon-hydrocarbon self-assembly. Part 3. Liquid phase interactions between perfluoroalkylhalides and heteroatom containing hydrocarbons. *Tetrahedron Lett* **1998,** *39* (49), 9069-9072.
7. Burdeniuc, J.; Sanford, M.; Crabtree, R. H., Amine charge transfer complexes of perfluoroalkanes and an application to poly(tetrafluoroethylene) surface functionalization. *Journal of Fluorine Chemistry* **1998,** *91* (1), 49-54.

8. Allen, F. H.; Lommerse, J. P. M.; Hoy, V. J.; Howard, J. A. K.; Desiraju, G. R., The hydrogen-bond C-H donor and [pi]-acceptor characteristics of three-membered rings. *Acta Crystallographica Section B* **1996,** *52* (4), 734-745.

9. (a) Nguyen, H. L.; Horton, P. N.; Hursthouse, M. B.; Legon, A. C.; Bruce, D. W., Halogen Bonding: A New Interaction for Liquid Crystal Formation. *J. Am. Chem. Soc.* **2003,** *126* (1), 16-17; (b) Bruce, D. W.; Metrangolo, P.; Meyer, F.; Pilati, T.; Praesang, C.; Resnati, G.; Terraneo, G.; Wainwright, S. G.; Whitwood, A. C., Structure-Function Relationships in Liquid-Crystalline Halogen-Bonded Complexes. *Chem.--Eur. J.* **2010,** *16* (Copyright (C) 2012 American Chemical Society (ACS). All Rights Reserved.), 9511-9524, S9511/1-S9511/19; (c) Lauher, J. W.; Fowler, F. W.; Goroff, N. S., Single-Crystal-to-Single-Crystal Topochemical Polymerizations by Design. *Accounts of Chemical Research* **2008,** *41* (9), 1215-1229; (d) Cho, C. M.; Wang, X.; Li, J. J.; He, C.; Xu, J., Synthesis and self-assembly of halogen-bond donor–spacer–hydrogen-bond donor molecules: polymeric liquid crystals induced by combination of intermolecular halogen- and hydrogen-bonding interactions. *Liquid Crystals* **2012**, 1-12; (e) Priimagi, A.; Cavallo, G.; Forni, A.; Gorynsztejn-Leben, M.; Kaivola, M.; Metrangolo, P.; Milani, R.; Shishido, A.; Pilati, T.; Resnati, G.; Terraneo, G., Halogen Bonding versus Hydrogen Bonding in Driving Self-Assembly and Performance of Light-Responsive Supramolecular Polymers. *Adv Funct Mater* **2012,** *22* (12), 2572-2579; (f) Priimagi, A.; Saccone, M.; Cavallo, G.; Shishido, A.; Pilati, T.; Metrangolo, P.; Resnati, G., Photoalignment and Surface-Relief-

Grating Formation are Efficiently Combined in Low-Molecular-Weight Halogen-Bonded Complexes. *Adv Mater* **2012**, n/a-n/a.

10. Fourmigué, M.; Batail, P., Activation of Hydrogen- and Halogen-Bonding Interactions in Tetrathiafulvalene-Based Crystalline Molecular Conductors. *Chemical Reviews* **2004,** *104* (11), 5379-5418.

11. (a) Hays, F. A.; Vargason, J. M.; Ho, P. S., Effect of Sequence on the Conformation of DNA Holliday Junctions†. *Biochemistry-Us* **2003,** *42* (32), 9586-9597; (b) Muzet, N.; Guillot, B.; Jelsch, C.; Howard, E.; Lecomte, C., Electrostatic complementarity in an aldose reductase complex from ultra-high-resolution crystallography and first-principles calculations. *Proceedings of the National Academy of Sciences* **2003,** *100* (15), 8742-8747; (c) Auffinger, P.; Hays, F. A.; Westhof, E.; Ho, P. S., Halogen bonds in biological molecules. *P Natl Acad Sci USA* **2004,** *101* (48), 16789-16794; (d) Voth, A. R.; Hays, F. A.; Ho, P. S., Directing macromolecular conformation through halogen bonds. *Proceedings of the National Academy of Sciences* **2007,** *104* (15), 6188-6193.

12. Gribble, G. W., Naturally Occurring Organohalogen Compounds†. *Accounts of Chemical Research* **1998,** *31* (3), 141-152.

13. Imakubo, T.; Sawa, H.; Kato, R., Novel radical cation salts of organic π-donors containing iodine atom(s): the first application of strong intermolecular-I···X-(X = CN, halogen atom) interaction to molecular conductors. *Synthetic Metals* **1995,** *73* (2), 117-122.

14. Roy, K.; Wibowo, A. C.; Pellechia, P. J.; Ma, S.; Geer, M. F.; Shimizu, L. S., Absorption of Hydrogen Bond Donors by Pyridyl Bis-Urea Crystals. *Chemistry of Materials* **2012,** *24* (24), 4773-4781.

15. Roy, K.; Wang, C.; Smith, M. D.; Dewal, M. B.; Wibowo, A. C.; Brown, J. C.; Ma, S. G.; Shimizu, L. S., Guest induced transformations of assembled pyridyl bis-urea macrocycles. *Chem Commun* **2011,** *47* (1), 277-279.

16. Roy, K.; Wang, C.; Smith, M. D.; Pellechia, P. J.; Shimizu, L. S., Alkali Metal Ions As Probes of Structure and Recognition Properties of Macrocyclic Pyridyl Urea Hosts. *The Journal of Organic Chemistry* **2010,** *75* (16), 5453-5460.

17. Messina, M. T.; Metrangolo, P.; Panzeri, W.; Pilati, T.; Resnati, G., Intermolecular recognition between hydrocarbon oxygen-donors and perfluorocarbon iodine-acceptors: the shortest O center dot center dot center dot I non-covalent bond. *Tetrahedron* **2001,** *57* (40), 8543-8550.

18. (a) Shimizu, L. S.; Smith, M. D.; Hughes, A. D.; Shimizu, K. D., Self-assembly of a bis-urea macrocycle into a columnar nanotube. *Chem Commun* **2001,** (17), 1592-1593; (b) Shimizu, L. S.; Hughes, A. D.; Smith, M. D.; Samuel, S. A.; Ciurtin-Smith, D., Assembled columnar structures from bis-urea macrocycles. *Supramol Chem* **2005,** *17* (1-2), 27-30; (c) Shimizu, L. S.; Hughes, A. D.; Smith, M. D.; Davis, M. J.; Zhang, B. P.; zur Loye, H. C.; Shimizu, K. D., Self-assembled nanotubes that reversibly bind acetic acid guests. *J. Am. Chem. Soc.* **2003,** *125* (49), 14972-14973.

19. (a) Togo, H.; Iida, S., Synthetic use of molecular iodine for organic synthesis. *Synlett* **2006,** (Copyright (C) 2013 American Chemical Society (ACS). All Rights

Reserved.), 2159-2175; (b) Mphahlele, M. J., Molecular iodine-an expedient reagent for oxidative aromatization reactions of α,β-unsaturated cyclic compounds. *Molecules* **2009,** *14* (Copyright (C) 2013 American Chemical Society (ACS). All Rights Reserved.), 5308-5322; (c) Fusaro, M. B.; Chagnault, V.; Postel, D., Synthesis of glycosylamines and glyconamides using molecular iodine. *Tetrahedron* **2013,** *69* (2), 542-550; (d) Colombeau, L.; Traoré, T. n.; Compain, P.; Martin, O. R., Metal-Free One-Pot Oxidative Amidation of Aldoses with Functionalized Amines. *The Journal of Organic Chemistry* **2008,** *73* (21), 8647-8650; (e) Aragoni, M. C.; Arca, M.; Demartin, F.; Devillanova, F. A.; Garau, A.; Isaia, F.; Lippolis, V.; Verani, G., Anti-Thyroid Drug Methimazole: X-ray Characterization of Two Novel Ionic Disulfides Obtained from Its Chemical Oxidation by I2. *J. Am. Chem. Soc.* **2002,** *124* (17), 4538-4539.

20. Kitagawa, S.; Kitaura, R.; Noro, S.-i., Functional porous coordination polymers. *Angew. Chem., Int. Ed.* **2004,** *43* (Copyright (C) 2013 American Chemical Society (ACS). All Rights Reserved.), 2334-2375.

21. Cataldo, S.; Pignataro, B., Polymeric Thin Films for Organic Electronics: Properties and Adaptive Structures. *Materials* **2013,** *6* (3), 1159-1190.

22. Schuettfort, T.; Huettner, S.; Lilliu, S.; Macdonald, J. E.; Thomsen, L.; McNeill, C. R., Surface and Bulk Structural Characterization of a High-Mobility Electron-Transporting Polymer. *Macromolecules* **2011,** *44* (6), 1530-1539.

23. (a) *SMART* 5.630; Bruker Analytical X-ray Systems Inc.: Madison Wisconsin USA, 2003; (b) *SAINT+*, 6.45; Bruker Analytical X-ray Systems Inc.: Madison,

Wisconsin, USA, 2003; (c) *SADABS*, 2.10; Bruker Analytical X-ray Systems: Madison, Wisconsin, USA, 2003.

24. Sheldrick, G. M., A short history of SHELX. *Acta Crystallogr A* **2008,** *64*, 112-122.

25. Dolomanov, O. V.; Bourhis, L. J.; Gildea, R. J.; Howard, J. A. K.; Puschmann, H., OLEX2: a complete structure solution, refinement and analysis program. *J Appl Crystallogr* **2009,** *42*, 339-341.

BIBLIOGRAPHY

1. Zhang, M.; Wang, L.; Ji, H.; Wu, B.; Zeng, X., Cumene Liquid Oxidation to Cumene Hydroperoxide over CuO Nanoparticle with Molecular Oxygen under Mild Condition. *Journal of Natural Gas Chemistry* **2007,** *16* (4), 393-398.

2. Zhan, W.; Guo, Y.; Wang, Y.; Liu, X.; Guo, Y.; Wang, Y.; Zhang, Z.; Lu, G., Synthesis of Lanthanum-Doped MCM-48 Molecular Sieves and Its Catalytic Performance for the Oxidation of Styrene. *The Journal of Physical Chemistry B* **2007,** *111* (42), 12103-12110.

3. You, K. Y.; Yin, D. L.; Mao, L. Q.; Liu, P. L.; Luo, H. A., Selective photosensitized oxidation and its catalytic regulation of monoterpene with molecular oxygen in different reaction media. *Journal of Photochemistry and Photobiology a-Chemistry* **2011,** *217* (2-3), 321-325.

4. Yang, J.; Dewal, M. B.; Sobransingh, D.; Smith, M. D.; Xu, Y. W.; Shimizu, L. S., Examination of the Structural Features That Favor the Columnar Self-Assembly of Bis-urea Macrocycles. *Journal of Organic Chemistry* **2009,** *74* (1), 102-110.

5. Yang, J.; Dewal, M. B.; Shimizu, L. S., Self-assembling bisurea macrocycles used as an organic zeolite for a highly stereoselective photodimerization of 2-cyclohexenone. *J. Am. Chem. Soc.* **2006,** *128* (25), 8122-8123.

6. Yang, J.; Dewal, M. B.; Profeta, S.; Smith, M. D.; Li, Y. Y.; Shimizu, L. S., Origins of selectivity for the 2+2 cycloaddition of alpha,beta-unsaturated ketones within a porous self-assembled organic framework. *J. Am. Chem. Soc.* **2008,** *130* (2), 612-621.

7. Xu, Y. W.; Smith, M. D.; Krause, J. A.; Shimizu, L. S., Control of the Intramolecular 2+2 Photocycloaddition in a Bis-Stilbene Macrocycle. *Journal of Organic Chemistry* **2009,** *74* (13), 4874-4877.

8. Xu, Y. W.; Smith, M. D.; Geer, M. F.; Pellechia, P. J.; Brown, J. C.; Wibowo, A. C.; Shimizu, L. S., Thermal Reaction of a Columnar Assembled Diacetylene Macrocycle. *J. Am. Chem. Soc.* **2010,** *132* (15), 5334-+.

9. Xu, Y. W.; Smith, M. D.; Geer, M. F.; Pellechia, P. J.; Brown, J. C.; Wibowo, A. C.; Shimizu, L. S., Thermal Reaction of a Columnar Assembled Diacetylene Macrocycle. *J. Am. Chem. Soc.* **2010,** *132* (15), 5334-+.

10. Woodward, J. R.; Lin, T.-S.; Sakaguchi, Y.; Hayashi, H., Biphotonic photochemistry of benzophenones in dimethylsulphoxide: a flash photolysis EPR study. *Mol Phys* **2002,** *100* (8), 1235-1244.

11. Wheeler, S. E., Understanding Substituent Effects in Noncovalent Interactions Involving Aromatic Rings. *Accounts of Chemical Research* **2012**.

12. Weiss, R. G.; Ramamurthy, V.; Hammond, G. S., Photochemistry in organized and confining media: a model. *Accounts of Chemical Research* **1993,** *26* (10), 530-536.

13. Wasserman, H. H.; Lipshutz, B. H., REACTIONS OF LITHIUM ENOLATES WITH MOLECULAR-OXYGEN ALPHA-HYDROXYLATION OF AMIDES AND OTHER CARBOXYLATE DERIVATIVES. *Tetrahedron Lett* **1975,** (21), 1731-1734.

14. Wash, P. L.; Ma, S.; Obst, U.; Rebek, J., Nitrogen−Halogen Intermolecular Forces in Solution. *J. Am. Chem. Soc.* **1999,** *121* (34), 7973-7974.

15. Wang, W.; Zhang, Y.; Wang, Y.-B., The π···π Stacking Interactions between Homogeneous Dimers of C6FxI(6–x) (x = 0, 1, 2, 3, 4, and 5): A Comparative Study with the Halogen Bond. *The Journal of Physical Chemistry A* **2012,** *116* (51), 12486-12491.

16. Wang, H.; Zhao, X. R.; Jin, W. J., The C-IX- halogen bonding of tetraiodoethylene with halide anions in solution and cocrystals investigated by experiment and calculation. *Phys Chem Chem Phys* **2013,** *15* (12), 4320-4328.

17. Wang, H.; Shi, Y.; Wei, J.; Jiang, X.; Yin, J., ESR and kinetic study of a novel polymerizable photoinitiator comprising the structure of N-phenylmaleimide and benzophenone for photopolymerization. *J Appl Polym Sci* **2006,** *101* (4), 2347-2354.

18. Wang, C.; Wei, L.; Lai, G.; Zhong, T.; Shen, Y., Synthesis and photopolymerization kinetics of lower odor benzophenone derivative photoinitiators. *Polymers for Advanced Technologies* **2010,** *21* (1), 72-76.

19. Walter, S. M.; Kniep, F.; Rout, L.; Schmidtchen, F. P.; Herdtweck, E.; Huber, S. M., Isothermal Calorimetric Titrations on Charge-Assisted Halogen Bonds: Role of Entropy, Counterions, Solvent, and Temperature. *J. Am. Chem. Soc.* **2012,** *134* (20), 8507-8512.

20. Voth, A. R.; Hays, F. A.; Ho, P. S., Directing macromolecular conformation through halogen bonds. *Proceedings of the National Academy of Sciences* **2007,** *104* (15), 6188-6193.

21. Valerio, G.; Raos, G.; Meille, S. V.; Metrangolo, P.; Resnati, G., Halogen Bonding in Fluoroalkylhalides: A Quantum Chemical Study of Increasing Fluorine Substitution. *The Journal of Physical Chemistry A* **2000,** *104* (8), 1617-1620.

22. Uemura, T.; Horike, S.; Kitagawa, K.; Mizuno, M.; Endo, K.; Bracco, S.; Comotti, A.; Sozzani, P.; Nagaoka, M.; Kitagawa, S., Conformation and Molecular Dynamics of Single Polystyrene Chain Confined in Coordination Nanospace. *J. Am. Chem. Soc.* **2008,** *130* (21), 6781-6788.

23. Udachin, K. A.; Ripmeester, J. A., A Polymer Guest Transforms Clathrate Cages into Channels: The Single-Crystal X-Ray Structure of Tetra-n-butylammonium Polyacrylate Hydrate, nBu4NPA·40 H2O. *Angewandte Chemie International Edition* **1999,** *38* (13-14), 1983-1984.

24. Turro, N. J., *Modern Molecular Photochemistry*. 1 ed.; University Science Books: CA, 1991; p 628.

25. Tsierkezos, N. G.; Ritter, U., Application of electrochemical impedance spectroscopy for characterisation of the reduction of benzophenone in acetonitrile solutions. *Physics and Chemistry of Liquids* **2011,** *49* (6), 729-742.

26. Trachtenberg, E. N.; Nelson, C. H.; Carver, J. R., Mechanism of selenium dioxide oxidation of olefins. *The Journal of Organic Chemistry* **1970,** *35* (5), 1653-1658.

27. Trachtenberg, E. N.; Carver, J. R., Stereochemistry of selenium dioxide oxidation of cyclohexenyl systems. *The Journal of Organic Chemistry* **1970,** *35* (5), 1646-1653.

28. Togo, H.; Iida, S., Synthetic use of molecular iodine for organic synthesis. *Synlett* **2006,** (Copyright (C) 2013 American Chemical Society (ACS). All Rights Reserved.), 2159-2175.

29. Tian, L.-l.; Wang, C.; Dawn, S.; Smith, M. D.; Krause, J. A.; Shimizu, L. S., Macrocycles with Switchable exo/endo Metal Binding Sites. *J. Am. Chem. Soc.* **2009,** *131* (48), 17620-17629.

30. Thomas, J. R.; Tolman, C. A., Inhibition of Cumene Oxidation by Tetralin Hydroperoxide. *J. Am. Chem. Soc.* **1962,** *84* (11), 2079-2080.

31. Thomas, J. R., Stability of Cumylperoxy Radical-Pyridine Charge-Transfer Complex. *J. Am. Chem. Soc.* **1963,** *85* (5), 591-593.

32. ten Brink, G.-J.; Vis, J. M.; Arends, I. W. C. E.; Sheldon, R. A., Selenium catalysed oxidations with aqueous hydrogen peroxide. Part 3: Oxidation of carbonyl compounds under mono/bi/triphasic conditions. *Tetrahedron* **2002,** *58* (20), 3977-3983.

33. Tehfe, M.-A.; Dumur, F.; Graff, B.; Morlet-Savary, F.; Fouassier, J.-P.; Gigmes, D.; Lalevée, J., Trifunctional Photoinitiators Based on a Triazine Skeleton for Visible Light Source and UV LED Induced Polymerizations. *Macromolecules* **2012,** *45* (21), 8639-8647.

34. Tanner, D. D.; Blackburn, E. V.; Diaz, G. E., A free-radical chain reaction involving electron transfer. The replacement of the nitro group by hydrogen using trialkyltin hydride, a variation of the Kornblum reaction. *J. Am. Chem. Soc.* **1981,** *103* (6), 1557-1559.

35. Tamao, K.; Ishida, N.; Tanaka, T.; Kumada, M., Silafunctional compounds in organic synthesis. Part 20. Hydrogen peroxide oxidation of the silicon-carbon bond in organoalkoxysilanes. *Organometallics* **1983,** *2* (11), 1694-1696.

36. Tagmatarchis, N.; Shinohara, H.; Fujitsuka, M.; Ito, O., Photooxidation of Olefins Sensitized by Bisazafullerene (C59N)2 and Hydroazafullerene C59HN: Product

Analysis, Emission of Singlet Oxygen, and Transient Absorption Spectroscopy. *The Journal of Organic Chemistry* **2001,** *66* (24), 8026-8029.

37. Syssa-Magale, J.-L.; Boubekeur, K.; Palvadeau, P.; Meerschaut, A.; Schollhorn, B., The tailoring of crystal structures via the self-assembly of organic coordination compounds by NI non-covalent halogen bonds: co-crystals of sterically hindered N-heterocycles and 1,4-diiodo-tetrafluorobenzene. *Crystengcomm* **2005,** *7* (50), 302-308.

38. Svoboda, J.; König, B., Templated Photochemistry: Toward Catalysts Enhancing the Efficiency and Selectivity of Photoreactions in Homogeneous Solutions. *Chemical Reviews* **2006,** *106* (12), 5413-5430.

39. Suresh, A. K.; Sharma, M. M.; Sridhar, T., Engineering Aspects of Industrial Liquid-Phase Air Oxidation of Hydrocarbons. *Ind Eng Chem Res* **2000,** *39* (11), 3958-3997.

40. Sunderhaus, J. D.; Lam, H.; Dudley, G. B., Oxidation of Carbon−Silicon Bonds: The Dramatic Advantage of Strained Siletanes. *Organic Letters* **2003,** *5* (24), 4571-4573.

41. Stephenson, L. M.; Speth, D. R., Mechanism of allylic hydroxylation by selenium dioxide. *The Journal of Organic Chemistry* **1979,** *44* (25), 4683-4689.

42. Solomon, M. R.; Sivaguru, J.; Jockusch, S.; Adam, W.; Turro, N. J., Decoding Stereocontrol During the Photooxygenation of Oxazolidinone-Functionalized Enecarbamates. *Organic Letters* **2010,** *12* (9), 2142-2145.

43. Soldatov, D. V.; Tinnemans, P.; Enright, G. D.; Ratcliffe, C. I.; Diamente, P. R.; Ripmeester, J. A., Modified Metal Dibenzoylmethanates for Soft Supramolecular Materials: Extension to Oligomeric and Polymeric Host Receptors with Nanosized Void Spaces†. *Chemistry of Materials* **2003,** *15* (20), 3826-3840.

44. Soldatov, D. V.; Ripmeester, J. A.; Shergina, S. I.; Sokolov, I. E.; Zanina, A. S.; Gromilov, S. A.; Dyadin, Y. A., α- and β-Bis(1,1,1-trifluoro-5,5-dimethyl-5-methoxyacetylacetonato)copper(II): Transforming the Dense Polymorph into a Versatile New Microporous Framework†. *J. Am. Chem. Soc.* **1999,** *121* (17), 4179-4188.

45. Sobransingh, D.; Dewal, M. B.; Hiller, J.; Smith, M. D.; Shimizu, L. S., Inclusion of electrochemically active guests by novel oxacalixarene hosts. *New Journal of Chemistry* **2008,** *32* (1), 24-27.

46. Sivaguru, J.; Solomon, M. R.; Poon, T.; Jockusch, S.; Bosio, S. G.; Adam, W.; Turro, N. J., The reaction of singlet oxygen with enecarbamates: A mechanistic playground for investigating chemoselectivity, stereoselectivity, and vibratioselectivity of photooxidations. *Accounts of Chemical Research* **2008,** *41* (3), 387-400.

47. Sivaguru, J.; Poon, T.; Franz, R.; Jockusch, S.; Adam, W.; Turro, N. J., Stereocontrol within Confined Spaces: Enantioselective Photooxidation of Enecarbamates Inside Zeolite Supercages. *J. Am. Chem. Soc.* **2004,** *126* (35), 10816-10817.

48. Simon, J. D.; Peters, K. S., Solvent effects on the picosecond dynamics of the photoreduction of benzophenone by aromatic amines. *J. Am. Chem. Soc.* **1981,** *103* (21), 6403-6406.

49. Silverman, S. K.; Foote, C. S., Singlet oxygen and electron-transfer mechanisms in the dicyanoanthracene-sensitized photooxidation of 2,3-diphenyl-1,4-dioxene. *J. Am. Chem. Soc.* **1991,** *113* (20), 7672-7675.

50. Sijbesma, R. P.; Beijer, F. H.; Brunsveld, L.; Folmer, B. J. B.; Hirschberg, J. H. K. K.; Lange, R. F. M.; Lowe, J. K. L.; Meijer, E. W., Reversible polymers formed from

self-complementary monomers using quadruple hydrogen bonding. *Science* **1997,** *278* (5343), 1601-1604.

51. Shimizu, N.; Bartlett, P. D., Photooxidation of olefins sensitized by .alpha.-diketones and by benzophenone. A practical epoxidation method with biacetyl. *J. Am. Chem. Soc.* **1976,** *98* (14), 4193-4200.

52. Shimizu, L. S.; Smith, M. D.; Hughes, A. D.; Shimizu, K. D., Self-assembly of a bis-urea macrocycle into a columnar nanotube. *Chem Commun* **2001,** (17), 1592-1593.

53. Shimizu, L. S.; Smith, M. D.; Hughes, A. D.; Shimizu, K. D., Self-assembly of a bis-urea macrocycle into a columnar nanotube. *Chem Commun* **2001,** (17), 1592-1593.

54. Shimizu, L. S.; Hughes, A. D.; Smith, M. D.; Samuel, S. A.; Ciurtin-Smith, D., Assembled columnar structures from bis-urea macrocycles. *Supramol Chem* **2005,** *17* (1-2), 27-30.

55. Shimizu, L. S.; Hughes, A. D.; Smith, M. D.; Davis, M. J.; Zhang, B. P.; zur Loye, H. C.; Shimizu, K. D., Self-assembled nanotubes that reversibly bind acetic acid guests. *J. Am. Chem. Soc.* **2003,** *125* (49), 14972-14973.

56. Shimizu, L. S., Cyclic bis-ureas: Applications as hosts for molecular recognition and as reliable supramolecular assembly units. *Abstracts of Papers of the American Chemical Society* **2009,** *238*.

57. Sherrill, C. D., Energy Component Analysis of π Interactions. *Accounts of Chemical Research* **2012,** *46* (4), 1020-1028.

58. Sherrill, C. D., Energy Component Analysis of π Interactions. *Accounts of Chemical Research* **2012**.

59. Sheldrick, G. M., A short history of SHELX. *Acta Crystallogr A* **2008,** *64*, 112-122.

60. Sharpless, K. B.; Lauer, R. F., Selenium dioxide oxidation of olefins. Evidence for the intermediacy of allylseleninic acids. *J. Am. Chem. Soc.* **1972,** *94* (20), 7154-7155.

61. Sharnoff, M., Radiative and radiationless triplet exciton decay in benzophenone. *Chem. Phys. Lett.* **1972,** *17* (Copyright (C) 2012 American Chemical Society (ACS). All Rights Reserved.), 355-8.

62. Sharma, S.; Sinha, S.; Chand, S., Polymer Anchored Catalysts for Oxidation of Styrene Using TBHP and Molecular Oxygen. *Ind Eng Chem Res* **2012,** *51* (26), 8806-8814.

63. Shao, Y.; Molnar, L. F.; Jung, Y.; Kussmann, J.; Ochsenfeld, C.; Brown, S. T.; Gilbert, A. T. B.; Slipchenko, L. V.; Levchenko, S. V.; O'Neill, D. P.; DiStasio Jr, R. A.; Lochan, R. C.; Wang, T.; Beran, G. J. O.; Besley, N. A.; Herbert, J. M.; Yeh Lin, C.; Van Voorhis, T.; Hung Chien, S.; Sodt, A.; Steele, R. P.; Rassolov, V. A.; Maslen, P. E.; Korambath, P. P.; Adamson, R. D.; Austin, B.; Baker, J.; Byrd, E. F. C.; Dachsel, H.; Doerksen, R. J.; Dreuw, A.; Dunietz, B. D.; Dutoi, A. D.; Furlani, T. R.; Gwaltney, S. R.; Heyden, A.; Hirata, S.; Hsu, C.-P.; Kedziora, G.; Khalliulin, R. Z.; Klunzinger, P.; Lee, A. M.; Lee, M. S.; Liang, W.; Lotan, I.; Nair, N.; Peters, B.; Proynov, E. I.; Pieniazek, P. A.; Min Rhee, Y.; Ritchie, J.; Rosta, E.; David Sherrill, C.; Simmonett, A. C.; Subotnik, J. E.; Lee Woodcock Iii, H.; Zhang, W.; Bell, A. T.; Chakraborty, A. K.; Chipman, D. M.; Keil, F. J.; Warshel, A.; Hehre, W. J.; Schaefer Iii, H. F.; Kong, J.; Krylov, A. I.; Gill, P. M. W.; Head-Gordon, M., Advances in methods and algorithms in a modern quantum chemistry program package. *Phys Chem Chem Phys* **2006,** *8* (27), 3172-3191.

64. Shailaja, J.; Sivaguru, J.; Robbins, R. J.; Ramamurthy, V.; Sunoj, R. B.; Chandrasekhar, J., Singlet Oxygen Mediated Oxidation of Olefins within Zeolites: Selectivity and Complexities. *Tetrahedron* **2000,** *56* (36), 6927-6943.

65. Sereda, G.; Rajpara, V., Benzylic oxidation and photooxidation by air in the presence of graphite and cyclohexene. *Tetrahedron Lett* **2007,** *48* (19), 3417-3421.

66. Schuettfort, T.; Huettner, S.; Lilliu, S.; Macdonald, J. E.; Thomsen, L.; McNeill, C. R., Surface and Bulk Structural Characterization of a High-Mobility Electron-Transporting Polymer. *Macromolecules* **2011,** *44* (6), 1530-1539.

67. Schneider, H.-J., Binding Mechanisms in Supramolecular Complexes. *Angewandte Chemie International Edition* **2009,** *48* (22), 3924-3977.

68. Schmidt, R., Photosensitized generation of singlet oxygen. *Photochemistry and Photobiology* **2006,** *82* (5), 1161-1177.

69. Sakamoto, M.; Cai, X.; Fujitsuka, M.; Majima, T., Solvent Effect on the Deactivation Processes of Benzophenone Ketyl Radicals in the Excited State. *The Journal of Physical Chemistry A* **2006,** *110* (42), 11800-11808.

70. Roy, K.; Wibowo, A. C.; Pellechia, P. J.; Ma, S.; Geer, M. F.; Shimizu, L. S., Absorption of Hydrogen Bond Donors by Pyridyl Bis-Urea Crystals. *Chemistry of Materials* **2012,** *24* (24), 4773-4781.

71. Roy, K.; Wang, C.; Smith, M. D.; Pellechia, P. J.; Shimizu, L. S., Alkali Metal Ions As Probes of Structure and Recognition Properties of Macrocyclic Pyridyl Urea Hosts. *The Journal of Organic Chemistry* **2010,** *75* (16), 5453-5460.

72. Roy, K.; Wang, C.; Smith, M. D.; Dewal, M. B.; Wibowo, A. C.; Brown, J. C.; Ma, S. G.; Shimizu, L. S., Guest induced transformations of assembled pyridyl bis-urea macrocycles. *Chem Commun* **2011,** *47* (1), 277-279.

73. Roy, K.; Smith, M. D.; Shimizu, L. S., 1D coordination network formed by a cadmium based pyridyl urea helical monomer. *Inorganica Chimica Acta* **2011,** *376* (1), 598-604.

74. Rosas, N.; Sharma, P.; Alvarez, C.; Gómez, E.; Gutiérrez, Y.; Méndez, M.; Toscano, R. A.; Maldonado, L. A., A novel method for the synthesis of 5,6-dihydro-4H-oxocin-4-ones: 6-endo-dig versus 8-endo-dig cyclizations. *Tetrahedron Lett* **2003,** *44* (43), 8019-8022.

75. Robbins, R. J.; Ramamurthy, V., Generation and reactivity of singlet oxygen within zeolites: Remarkable control of hydroperoxidation of alkenes. *Chem Commun* **1997,** (11), 1071-1072.

76. Riley, K. E.; Hobza, P., On the Importance and Origin of Aromatic Interactions in Chemistry and Biodisciplines. *Accounts of Chemical Research* **2012,** *46* (4), 927-936.

77. Riley, K.; Murray, J.; Fanfrlík, J.; Řezáč, J.; Solá, R.; Concha, M.; Ramos, F.; Politzer, P., Halogen bond tunability I: the effects of aromatic fluorine substitution on the strengths of halogen-bonding interactions involving chlorine, bromine, and iodine. *Journal of Molecular Modeling* **2011,** *17* (12), 3309-3318.

78. Ricks, H. L.; Shimizu, L. S.; Smith, M. D.; Bunz, U. H. F.; Shimizu, K. D., An N,N '-diaryl urea based conjugated polymer model system. *Tetrahedron Lett* **2004,** *45* (16), 3229-3232.

79. Reijerse, E., High-Frequency EPR Instrumentation. *Appl Magn Reson* **2010,** *37* (1-4), 795-818.

80. Rawson, J. M.; Alberola, A.; Whalley, A. E., *J. Mater. Chem.* **2006,** *16*, 2560-2575.

81. Ramamurthy, V.; Parthasarathy, A., Chemistry in Restricted Spaces: Select Photodimerizations in Cages, Cavities, and Capsules. *Israel Journal of Chemistry* **2011,** *51* (7), 817-829.

82. Rajca, A., *Chem. Rev.* **1994,** *94*, 871-893.

83. Qu, B.; Hawthorn, G.; Mau, A. W. H.; Dai, L., Photochemical Generation of Polymeric Alkyl-C60 Radicals: ESR Detection and Identification. *The Journal of Physical Chemistry B* **2001,** *105* (11), 2129-2134.

84. Qi, X.-J.; Liu, L.; Fu, Y.; Guo, Q.-X., Hydrogen Bonding Interactions of Radicals. *Struct Chem* **2005,** *16* (3), 347-353.

85. Priimagi, A.; Saccone, M.; Cavallo, G.; Shishido, A.; Pilati, T.; Metrangolo, P.; Resnati, G., Photoalignment and Surface-Relief-Grating Formation are Efficiently Combined in Low-Molecular-Weight Halogen-Bonded Complexes. *Adv Mater* **2012**, n/a-n/a.

86. Priimagi, A.; Cavallo, G.; Forni, A.; Gorynsztejn-Leben, M.; Kaivola, M.; Metrangolo, P.; Milani, R.; Shishido, A.; Pilati, T.; Resnati, G.; Terraneo, G., Halogen Bonding versus Hydrogen Bonding in Driving Self-Assembly and Performance of Light-Responsive Supramolecular Polymers. *Adv Funct Mater* **2012,** *22* (12), 2572-2579.

87. Polyakov, N. E.; Okazaki, M.; Toriyama, K.; Leshina, T. V.; Fujiwara, Y.; Tanimoto, Y., Product Yield Detected ESR Study on the Dynamic Behavior of Radical

Pairs Generated in Photoreduction of Acetylenic Ketones in SDS Micellar Solution. *The Journal of Physical Chemistry* **1994,** *98* (41), 10563-10567.

88. Politzer, P.; Murray, J. S.; Clark, T., Halogen bonding: an electrostatically-driven highly directional noncovalent interaction. *Phys Chem Chem Phys* **2010,** *12* (28), 7748-7757.

89. Pearson, R. G., Hard and Soft Acids and Bases. *J. Am. Chem. Soc.* **1963,** *85* (22), 3533-3539.

90. Parker, C. A.; Joyce, T. A., Phosphorescence of benzophenone in fluid solution. *Chemical Communications (London)* **1968,** (13), 749-750.

91. Palacin, S.; Chin, D. N.; Simanek, E. E.; MacDonald, J. C.; Whitesides, G. M.; McBride, M. T.; Palmore, G. T. R., Hydrogen-bonded tapes based on symmetrically substituted diketopiperazines: A robust structural motif for the engineering of molecular solids. *J. Am. Chem. Soc.* **1997,** *119* (49), 11807-11816.

92. Pace, A.; Clennan, E. L., A New Experimental Protocol for Intrazeolite Photooxidations. The First Product-Based Estimate of an Upper Limit for the Intrazeolite Singlet Oxygen Lifetime. *J. Am. Chem. Soc.* **2002,** *124* (38), 11236-11237.

93. Opeida, I. A.; Zalevskaya, N. M.; Skichko, Y. I.; Voloshkin, R. A., Simulation of cumene oxidation in the presence of a binary mixture of initiators. *Pet. Chem.* **2011,** *51* (3), 226-229.

94. Oliveira, B. G., Interplay between dihydrogen and alkali–halogen bonds: Is there some covalency upon complexation of ternary systems? *Computational and Theoretical Chemistry* **2012,** *998* (0), 173-182.

95. Oh, S. Y.; Nickels, C. W.; Garcia, F.; Jones, W.; Friscic, T., Switching between halogen- and hydrogen-bonding in stoichiometric variations of a cocrystal of a phosphine oxide. *Crystengcomm* **2012,** *14* (19), 6110-6114.

96. Ogilby, P. R.; Foote, C. S., Chemistry of singlet oxygen. 36. Singlet molecular oxygen (1.DELTA.g) luminescence in solution following pulsed laser excitation. Solvent deuterium isotope effects on the lifetime of singlet oxygen. *J. Am. Chem. Soc.* **1982,** *104* (7), 2069-2070.

97. Ogilby, P. R., Singlet oxygen: there is still something new under the sun, and it is better than ever. *Photochemical & Photobiological Sciences* **2010,** *9* (12), 1543-1560.

98. Ogilby, P. R., Singlet oxygen: there is indeed something new under the sun. *Chemical Society Reviews* **2010,** *39* (8), 3181-3209.

99. Ochiai, M.; Miyamoto, K.; Shiro, M.; Ozawa, T.; Yamaguchi, K., Isolation, characterization, and reaction of activated iodosylbenzene monomer hydroxy(phenyl)iodonium ion with hypervalent bonding: Supramolecular complex PhI+OH center dot 18-Crown-6 with secondary I center dot center dot center dot O interactions. *J. Am. Chem. Soc.* **2003,** *125* (43), 13006-13007.

100. Nilson, M. G.; Funk, R. L., Total Synthesis of (−)-Nakadomarin A. *Organic Letters* **2010,** *12* (21), 4912-4915.

101. Nguyen, H. L.; Horton, P. N.; Hursthouse, M. B.; Legon, A. C.; Bruce, D. W., Halogen Bonding: A New Interaction for Liquid Crystal Formation. *J. Am. Chem. Soc.* **2003,** *126* (1), 16-17.

102. Nawghare, B. R.; Lokhande, P. D., First Iodine-Catalyzed Deallylation of Reactive Allyl Methylene Esters. *Synthetic Commun* **2013,** *43* (14), 1955-1963.

103. Natarajan, A.; Kaanumalle, L. S.; Jockusch, S.; Gibb, C. L. D.; Gibb, B. C.; Turro, N. J.; Ramamurthy, V., Controlling Photoreactions with Restricted Spaces and Weak Intermolecular Forces: Exquisite Selectivity during Oxidation of Olefins by Singlet Oxygen. *J. Am. Chem. Soc.* **2007,** *129* (14), 4132-4133.

104. Nakatsuji, S.; Anzai, H., *J. Mater. Chem.* **1997,** *7*, 2161-2174.

105. Muzet, N.; Guillot, B.; Jelsch, C.; Howard, E.; Lecomte, C., Electrostatic complementarity in an aldose reductase complex from ultra-high-resolution crystallography and first-principles calculations. *Proceedings of the National Academy of Sciences* **2003,** *100* (15), 8742-8747.

106. Murai, H.; Imamura, T.; Obi, K., Time-resolved ESR detection of benzophenone nπ* triplet state in glassy matrixes at 77 K. *Chem. Phys. Lett.* **1982,** *87* (Copyright (C) 2013 American Chemical Society (ACS). All Rights Reserved.), 295-8.

107. Mucha, J. A.; Pratt, D. W., Optically detected magnetic resonance spectra of the lowest triplet states of benzophenone, [sup 13]C-benzophenone, and three 4,4[prime]-dihalobenzophenones. *The Journal of Chemical Physics* **1977,** *66* (12), 5339-5355.

108. Mphahlele, M. J., Molecular iodine-an expedient reagent for oxidative aromatization reactions of α,β-unsaturated cyclic compounds. *Molecules* **2009,** *14* (Copyright (C) 2013 American Chemical Society (ACS). All Rights Reserved.), 5308-5322.

109. Moreau, J. J. E.; Vellutini, L.; Man, M. W. C.; Bied, C., New hybrid organic-inorganic solids with helical morphology via H-bond mediated sol-gel hydrolysis of silyl derivatives of chiral (R,R)- or (S,S)-diureidocyclohexane. *J. Am. Chem. Soc.* **2001,** *123* (7), 1509-1510.

110. Monti, S.; Flamigni, L.; Martelli, A.; Bortolus, P., Photochemistry of benzophenone-cyclodextrin inclusion complexes. *The Journal of Physical Chemistry* **1988,** *92* (15), 4447-4451.

111. Miyagawa, K.; Murai, H.; I'Haya, Y. J., Spin-polarized radical pairs transiently produced by the photochemical reaction of benzophenone with aromatic amines. *Chem. Phys. Lett.* **1984,** *109* (Copyright (C) 2013 American Chemical Society (ACS). All Rights Reserved.), 97-100.

112. Mitchell, A. R.; Pagoria, P. F.; Coon, C. L.; Jessop, E. S.; Poco, J. F.; Tarver, C. M.; Breithaupt, R. D.; Moody, G. L., Nitroureas .1. Synthesis, Scale-up and Characterization of K-6. *Propell Explos Pyrot* **1994,** *19* (5), 232-239.

113. Metrangolo, P.; Resnati, G., Halogen Bonding: Where We Are and Where We Are Going. *Cryst Growth Des* **2012**.

114. Metrangolo, P.; Resnati, G., Halogen Versus Hydrogen. *Science* **2008,** *321* (5891), 918-919.

115. Metrangolo, P.; Resnati, G., Halogen bonding: A paradigm in supramolecular chemistry. *Chemistry-a European Journal* **2001,** *7* (12), 2511-2519.

116. Metrangolo, P.; Neukirch, H.; Pilati, T.; Resnati, G., Halogen Bonding Based Recognition Processes: A World Parallel to Hydrogen Bonding†. *Accounts of Chemical Research* **2005,** *38* (5), 386-395.

117. Metrangolo, P.; Neukirch, H.; Pilati, T.; Resnati, G., Halogen Bonding Based Recognition Processes: A World Parallel to Hydrogen Bonding†. *Accounts of Chemical Research* **2005,** *38* (5), 386-395.

118. Metrangolo, P.; Meyer, F.; Pilati, T.; Resnati, G.; Terraneo, G., Halogen Bonding in Supramolecular Chemistry. *Angewandte Chemie International Edition* **2008,** *47* (33), 6114-6127.

119. Messina, M. T.; Metrangolo, P.; Panzeri, W.; Ragg, E.; Resnati, G., Perfluorocarbon-hydrocarbon self-assembly. Part 3. Liquid phase interactions between perfluoroalkylhalides and heteroatom containing hydrocarbons. *Tetrahedron Lett* **1998,** *39* (49), 9069-9072.

120. Messina, M. T.; Metrangolo, P.; Panzeri, W.; Pilati, T.; Resnati, G., Intermolecular recognition between hydrocarbon oxygen-donors and perfluorocarbon iodine-acceptors: the shortest O center dot center dot center dot I non-covalent bond. *Tetrahedron* **2001,** *57* (40), 8543-8550.

121. Merkel, P. B.; Kearns, D. R., Remarkable solvent effects on the lifetime of 1.DELTA.g oxygen. *J. Am. Chem. Soc.* **1972,** *94* (3), 1029-1030.

122. Melville, H. W.; Richards, S., The photochemical autoxidation of isopropylbenzene. *Journal of the Chemical Society (Resumed)* **1954,** *0* (0), 944-952.

123. Matsushita, Y.; Kajii, Y.; Obi, K., Photochemical reaction of excited benzophenone in the gas phase. *The Journal of Physical Chemistry* **1992,** *96* (11), 4455-4458.

124. Marshall, J. A.; Jenson, T. M.; DeHoff, B. S., Synthesis of cembrane natural products via [2,3] Wittig ring contraction of propargylic ethers. *The Journal of Organic Chemistry* **1987,** *52* (17), 3860-3866.

125. Marin, M. L.; Santos-Juanes, L.; Arques, A.; Amat, A. M.; Miranda, M. A., Organic Photocatalysts for the Oxidation of Pollutants and Model Compounds. *Chemical Reviews* **2011,** *112* (3), 1710-1750.

126. Maksimov, Y. V.; Suzdalev, I. P.; Tsodikov, M. V.; Kugel, V. Y.; Bukhtenko, O. V.; Slivinsky, E. V.; Navio, J. A., Study of cumene oxidation over zirconia-, titania- and alumina-based complex oxides obtained by sol-gel methods: activity-structure relationships. *Journal of Molecular Catalysis A: Chemical* **1996,** *105* (3), 167-173.

127. Macias, A. T.; Norton, J. E.; Evanseck, J. D., Impact of Multiple Cation−π Interactions upon Calix[4]arene Substrate Binding and Specificity. *J. Am. Chem. Soc.* **2003,** *125* (8), 2351-2360.

128. Lucarini, M.; Mezzina, E., EPR investigations of organic non-covalent assemblies with spin labels and spin probes. *Electron Paramagn. Reson.* **2011,** *22* (Copyright (C) 2013 American Chemical Society (ACS). All Rights Reserved.), 41-70.

129. Lovinger, A. J.; Nuckolls, C.; Katz, T. J., Structure and morphology of helicene fibers. *J. Am. Chem. Soc.* **1998,** *120* (2), 264-268.

130. Long, C. A.; Kearns, D. R., Radiationless decay of singlet molecular oxygen in solution. II. Temperature dependence and solvent effects. *J. Am. Chem. Soc.* **1975,** *97* (8), 2018-2020.

131. Lommerse, J. P. M.; Stone, A. J.; Taylor, R.; Allen, F. H., The Nature and Geometry of Intermolecular Interactions between Halogens and Oxygen or Nitrogen. *J. Am. Chem. Soc.* **1996,** *118* (13), 3108-3116.

132. Lommerse, J. P. M.; Stone, A. J.; Taylor, R.; Allen, F. H., The Nature and Geometry of Intermolecular Interactions between Halogens and Oxygen or Nitrogen. *J. Am. Chem. Soc.* **1996,** *118* (13), 3108-3116.

133. Lissi, E. A.; Encinas, M. V.; Lemp, E.; Rubio, M. A., Singlet oxygen O2(1.DELTA.g) bimolecular processes. Solvent and compartmentalization effects. *Chemical Reviews* **1993,** *93* (2), 699-723.

134. Lin, T.-S., EPR study of diphenylnitroxide in benzophenone. *J. Chem. Phys.* **1972,** *57* (Copyright (C) 2013 American Chemical Society (ACS). All Rights Reserved.), 2260-4.

135. Lim, K. S.; Oh, K. W.; Kim, S. H., Antimicrobial activity of organic photosensitizers embedded in electrospun nylon 6 nanofibers. *Polym. Int.* **2012,** *61* (Copyright (C) 2013 American Chemical Society (ACS). All Rights Reserved.), 1519-1524.

136. Lim, K. S.; Oh, K. W.; Kim, S. H., Antimicrobial activity of organic photosensitizers embedded in electrospun nylon 6 nanofibers. *Polym. Int.* **2012,** *61* (Copyright (C) 2013 American Chemical Society (ACS). All Rights Reserved.), 1519-1524.

137. Li, X.; Ramamurthy, V., Selective Oxidation of Olefins within Organic Dye Cation-Exchanged Zeolites. *J. Am. Chem. Soc.* **1996,** *118* (43), 10666-10667.

138. Lewandowska-Andralojc, A.; Kazmierczak, F.; Hug, G. L.; Horner, G.; Marciniak, B., Photoinduced CC-coupling reactions of rigid diastereomeric benzophenone-methionine dyads. *Photochem. Photobiol.* **2013,** *89* (Copyright (C) 2013 American Chemical Society (ACS). All Rights Reserved.), 14-23.

139. Lenoir, D.; Chiappe, C., What is the Nature of the First-Formed Intermediates in the Electrophilic Halogenation of Alkenes, Alkynes, and Allenes? *Chemistry – A European Journal* **2003,** *9* (5), 1036-1044.

140. Legon, A. C., The halogen bond: an interim perspective. *Phys Chem Chem Phys* **2010,** *12* (28), 7736-7747.

141. Legon, A. C., Prereactive Complexes of Dihalogens XY with Lewis Bases B in the Gas Phase: A Systematic Case for the Halogen Analogue B···XY of the Hydrogen Bond B···HX. *Angewandte Chemie International Edition* **1999,** *38* (18), 2686-2714.

142. Lauher, J. W.; Fowler, F. W.; Goroff, N. S., Single-Crystal-to-Single-Crystal Topochemical Polymerizations by Design. *Accounts of Chemical Research* **2008,** *41* (9), 1215-1229.

143. Lacombe, S.; Pigot, T., New materials for sensitized photooxygenation. *Photochemistry* **2010,** *38* (Copyright (C) 2013 American Chemical Society (ACS). All Rights Reserved.), 307-329.

144. Kyle, A. F.; Jakubec, P.; Cockfield, D. M.; Cleator, E.; Skidmore, J.; Dixon, D. J., Total synthesis of (-)-nakadomarin A. *Chem Commun* **2011,** *47* (36), 10037-10039.

145. Kuzmanich, G.; Simoncelli, S.; Gard, M. N.; Spanig, F.; Henderson, B. L.; Gudi, D. M.; Garcia-Garibay, M. A., Excited State Kinetics in Crystalline Solids: Self-Quenching in Nanocrystals of 4,4 '-Disubstituted Benzophenone Triplets Occurs by a Reductive Quenching Mechanism. *J. Am. Chem. Soc.* **2011,** *133* (43), 17296-17306.

146. Kolar, M.; Hobza, P.; Bronowska, A. K., Plugging the explicit [sigma]-holes in molecular docking. *Chem Commun* **2012**.

147. Kobayashi, J. i.; Watanabe, D.; Kawasaki, N.; Tsuda, M., Nakadomarin A, a Novel Hexacyclic Manzamine-Related Alkaloid from Amphimedon Sponge. *The Journal of Organic Chemistry* **1997,** *62* (26), 9236-9239.

148. Kleiner, G.; Tarnopolsky, A.; Hoz, S., Reduction of Benzophenone by SmI2: The Role of Proton Donors in Determining Product Distribution. *Organic Letters* **2005,** *7* (19), 4197-4200.

149. Klärner, F.-G.; Schrader, T., Aromatic Interactions by Molecular Tweezers and Clips in Chemical and Biological Systems. *Accounts of Chemical Research* **2012**.

150. Kitagawa, S.; Kitaura, R.; Noro, S.-i., Functional porous coordination polymers. *Angew. Chem., Int. Ed.* **2004,** *43* (Copyright (C) 2013 American Chemical Society (ACS). All Rights Reserved.), 2334-2375.

151. Kim, E.; Paliwal, S.; Wilcox, C. S., Measurements of molecular electrostatic field effects in edge-to-face aromatic interactions and CH-pi interactions with implications for protein folding and molecular recognition. *J. Am. Chem. Soc.* **1998,** *120* (43), 11192-11193.

152. Kihara, N.; Ollivier, C.; Renaud, P., Efficient Radical Oxygenation of α-Iodocarboxylic Acid Derivatives. *Organic Letters* **1999,** *1* (9), 1419-1422.

153. Kessel, D.; Reiners, J., Light-Activated Pharmaceuticals: Mechanisms and Detection. *Israel Journal of Chemistry* **2012,** *52* (8-9), 674-680.

154. Kearns, D. R., Physical and chemical properties of singlet molecular oxygen. *Chemical Reviews* **1971,** *71* (4), 395-427.

155. Kawai, A.; Hirakawa, M.; Abe, T.; Obi, K.; Shibuya, K., Specific Solvent Effects on the Structure and Reaction Dynamics of Benzophenone Ketyl Radical. *The Journal of Physical Chemistry A* **2001,** *105* (42), 9628-9636.

156. Katz, H. E.; Lovinger, A. J.; Kloc, C.; Siegrist, T.; Li, W.; Lin, Y.-Y.; Dodabalapur, A., *Nature* **2000,** *404* (478-481).

157. Kato, Y.; Okamoto, Y.; Nagasawa, S.; Ishihara, I., Relationship between polymorphism and bioavailability of drugs. IV. New polymorphic forms of phenobarbital. *Chem. Pharm. Bull.* **1984,** *32* (Copyright (C) 2013 American Chemical Society (ACS). All Rights Reserved.), 4170-4.

158. Karpfen, A., The intermolecular interaction in the charge-transfer complexes between amines and halogens: A theoretical characterization of the trends in halogen bonding. *Theor Chem Acc* **2003,** *110* (1), 1-9.

159. Jin, C.; Zhang, L.; Su, W. K., Direct Benzylic Oxidation with Sodium Hypochlorite Using a New Efficient Catalytic System: TEMPO/Co(OAc)(2). *Synlett* **2011,** (10), 1435-1438.

160. Jin, C.; Zhang, L.; Su, W., Direct Benzylic Oxidation with Sodium Hypochlorite Using a New Efficient Catalytic System: TEMPO/Co(OAc)2. *Synlett* **2011,** *2011* (EFirst), 1435-1438.

161. Jeong, H. A.; Cho, E. J.; Yeo, H. M.; Ryu, B. J.; Nam, K. C., Naphthalene urea derivatives for anion receptor: effects of substituents on benzoate binding. *Bull. Korean Chem. Soc.* **2007,** *28* (Copyright (C) 2013 American Chemical Society (ACS). All Rights Reserved.), 851-854.

162. Jensen, R. L.; Arnbjerg, J.; Ogilby, P. R., Temperature Effects on the Solvent-Dependent Deactivation of Singlet Oxygen. *J. Am. Chem. Soc.* **2010,** *132* (23), 8098-8105.

163. Jensen, R. L.; Arnbjerg, J.; Ogilby, P. R., Temperature Effects on the Solvent-Dependent Deactivation of Singlet Oxygen. *J. Am. Chem. Soc.* **2010,** *132* (23), 8098-8105.

164. Jakubec, P.; Cockfield, D. M.; Dixon, D. J., Total Synthesis of (−)-Nakadomarin A. *J. Am. Chem. Soc.* **2009,** *131* (46), 16632-16633.

165. Inokuma, Y.; Kawano, M.; Fujita, M., Crystalline molecular flasks. *Nature Chemistry* **2011,** *3* (5), 349-358.

166. Imakubo, T.; Sawa, H.; Kato, R., Novel radical cation salts of organic π-donors containing iodine atom(s): the first application of strong intermolecular-I···X-(X = CN, halogen atom) interaction to molecular conductors. *Synthetic Metals* **1995,** *73* (2), 117-122.

167. Ikeda, T.; Higuchi, M., Electrochromic Properties of Polythiophene Polyrotaxane Film. *Langmuir* **2011,** *27* (7), 4184-4189.

168. Ibrahim, M., Molecular mechanical perspective on halogen bonding. *Journal of Molecular Modeling* **2012,** *18* (10), 4625-4638.

169. Hunter, C. A., Quantifying Intermolecular Interactions: Guidelines for the Molecular Recognition Toolbox. *Angewandte Chemie International Edition* **2004,** *43* (40), 5310-5324.

170. Hoshino, M.; Shizuka, H., Photochemistry of benzophenone in aliphatic amines studied by laser photolysis in the temperature range 300-77 K. *The Journal of Physical Chemistry* **1987,** *91* (3), 714-718.

171. Hoffmann, N., Photochemical reactions as key steps in organic synthesis. *Chemical Reviews* **2008,** *108* (3), 1052-1103.

172. Hikcks, R. G., *Org. Biomol. Chem.* **2007,** *5*, 1321-1338.

173. Hendry, D. G., Rate constants for oxidation of cumene. *J. Am. Chem. Soc.* **1967,** *89* (21), 5433-5438.

174. Heinze, J.; Frontana-Uribe, B. A.; Ludwigs, S., Electrochemistry of Conducting Polymers—Persistent Models and New Concepts†. *Chemical Reviews* **2010,** *110* (8), 4724-4771.

175. Hays, F. A.; Vargason, J. M.; Ho, P. S., Effect of Sequence on the Conformation of DNA Holliday Junctions†. *Biochemistry-Us* **2003,** *42* (32), 9586-9597.

176. Harada, T.; Rudzinski, J. M.; Shinkai, S., Relative stabilities of teramethoxycalix[4]arenes: combined NMR spectroscopy and molecular mechanics studies. *Journal of the Chemical Society, Perkin Transactions 2* **1992,** *0* (12), 2109-2115.

177. Hajimohammadi, M.; Safari, N.; Mofakham, H.; Deyhimi, F., Highly selective, economical and efficient oxidation of alcohols to aldehydes and ketones by air and sunlight or visible light in the presence of porphyrins sensitizers. *Green Chemistry* **2011,** *13* (4), 991-997.

178. Gunnlaugsson, T.; Davis, A. P.; O'Brien, J. E.; Glynn, M., Fluorescent Sensing of Pyrophosphate and Bis-carboxylates with Charge Neutral PET Chemosensors†. *Organic Letters* **2002,** *4* (15), 2449-2452.

179. Grimme, S., Do special noncovalent pi-pi stacking interactions really exist? *Angew Chem Int Edit* **2008,** *47* (18), 3430-3434.

180. Griesser, M.; Rosspeintner, A.; Dworak, C.; Höfer, M.; Grabner, G.; Liska, R.; Gescheidt, G., Initiators Based on Benzaldoximes: Bimolecular and Covalently Bound Systems. *Macromolecules* **2012,** *45* (21), 8648-8657.

181. Griesbeck, A. G.; Reckenthaler, M.; Uhlig, J., Photoinduced azidohydroperoxidation of myrtenyl hydroperoxide with semiconductor particles and lucigenin as PET-catalysts. *Photochemical & Photobiological Sciences* **2010,** *9* (6), 775-778.

182. Griesbeck, A. G.; Cho, M., Singlet oxygen addition to homoallylic substrates in solution and microemulsion: novel secondary reactions. *Tetrahedron Lett* **2009,** *50* (1), 121-123.

183. Griesbeck, A. G.; Adam, W.; Bartoschek, A.; El-Idreesy, T. T., Photooxygenation of allylic alcohols: kinetic comparison of unfunctionalized alkenes with prenol-type allylic alcohols, ethers and acetates. *Photochemical & Photobiological Sciences* **2003,** *2* (8), 877-881.

184. Gribble, G. W., Naturally Occurring Organohalogen Compounds†. *Accounts of Chemical Research* **1998,** *31* (3), 141-152.

185. González-Béjar, M. a.; Montes-Navajas, P.; García, H.; Scaiano, J. C., Methylene Blue Encapsulation in Cucurbit[7]uril: Laser Flash Photolysis and Near-IR Luminescence Studies of the Interaction with Oxygen. *Langmuir* **2009,** *25* (18), 10490-10494.

186. Geer, M. F.; Walla, M. D.; Solntsev, K. S.; Strassert, C. A.; Shimizu, L. S., Self-assembled benzophenone *bis*-urea macrocycles facilitate selective oxidations by singlet oxygen. *J. Org. Chem* **2013,** *Submitted: jo-2013-00685u*.

187. Geer, M. F.; Smith, M. D.; Shimizu, L. S., A bis-urea naphthalene macrocycle displaying two crystal structures with parallel ureas. *Crystengcomm* **2011,** *13* (11), 3665-3669.

188. Geer, M. F.; Smith, M. D.; Shimizu, L. S., A bis-urea naphthalene macrocycle displaying two crystal structures with parallel ureas. *Crystengcomm* **2011**.

189. Gassensmith, J. J.; Barr, L.; Baumes, J. M.; Paek, A.; Nguyen, A.; Smith, B. D., Synthesis and Photophysical Investigation of Squaraine Rotaxanes by "Clicked Capping". *Organic Letters* **2008,** *10* (15), 3343-3346.

190. Gale, P. A., Anion and ion-pair receptor chemistry: highlights from 2000 and 2001. *Coordination Chemistry Reviews* **2003,** *240* (1–2), 191-221.

191. Galcera, J.; Friscic, T.; Hejczyk, K. E.; Fabian, L.; Clarke, S. M.; Day, G. M.; Molins, E.; Jones, W., Isostructural organic binary-host frameworks with tuneable and diversely decorated inclusion cavities. *Crystengcomm* **2012,** *14* (23), 7898-7906.

192. Fusaro, M. B.; Chagnault, V.; Postel, D., Synthesis of glycosylamines and glyconamides using molecular iodine. *Tetrahedron* **2013,** *69* (2), 542-550.

193. Fürstner, A.; Guth, O.; Rumbo, A.; Seidel, G., Ring Closing Alkyne Metathesis. Comparative Investigation of Two Different Catalyst Systems and Application to the Stereoselective Synthesis of Olfactory Lactones, Azamacrolides, and the Macrocyclic Perimeter of the Marine Alkaloid Nakadomarin A. *J. Am. Chem. Soc.* **1999,** *121* (48), 11108-11113.

194. Fung, Y.-S.; Yan, S.-C.; Wong, M.-K., Selective oxidation of unactivated C-H bonds by supramolecular control. *Org Biomol Chem* **2012,** *10* (15), 3122-3130.

195. Fujiwara, Y.; Ozawa, R.; Onuma, D.; Suzuki, K.; Yoza, K.; Kobayashi, K., Double Alkylene-Strapped Diphenylanthracene as a Photostable and Intense Solid-State Blue-Emitting Material. *The Journal of Organic Chemistry* **2013**.

196. Fourmigué, M.; Batail, P., Activation of Hydrogen- and Halogen-Bonding Interactions in Tetrathiafulvalene-Based Crystalline Molecular Conductors. *Chemical Reviews* **2004,** *104* (11), 5379-5418.

197. Fourmigué, M., Halogen bonding: Recent advances. *Current Opinion in Solid State and Materials Science* **2009,** *13* (3–4), 36-45.

198. Forni, A.; Rendine, S.; Pieraccini, S.; Sironi, M., Solvent effect on halogen bonding: The case of the I···O interaction. *Journal of Molecular Graphics and Modelling* **2012,** *38* (0), 31-39.

199. Foote, C. S.; Wexler, S.; Ando, W.; Higgins, R., Chemistry of Singlet Oxygen .4. Oxygenations with Hypochlorite-Hydrogen Peroxide. *J. Am. Chem. Soc.* **1968,** *90* (4), 975-&.

200. Foote, C. S., Definition of type I and type II photosensitized oxidation. *Photochem. Photobiol.* **1991,** *54* (Copyright (C) 2013 American Chemical Society (ACS). All Rights Reserved.), 659.

201. Foote, C. S., Photosensitized Oxygenations and Role of Singlet Oxygen. *Accounts of Chemical Research* **1968,** *1* (4), 104-&.

202. Fisher, T. H.; Meierhoefer, A. W., A kinetic study of the N-bromosuccinimide bromination of some 4-substituted 3-cyanotoluenes. *The Journal of Organic Chemistry* **1978,** *43* (2), 220-224.

203. Etter, M. C.; Urbanczyklipkowska, Z.; Ziaebrahimi, M.; Panunto, T. W., Hydrogen-Bond Directed Cocrystallization and Molecular Recognition Properties of Diarylureas. *J. Am. Chem. Soc.* **1990,** *112* (23), 8415-8426.

204. Etter, M. C., Encoding and Decoding Hydrogen-Bond Patterns of Organic-Compounds. *Accounts of Chemical Research* **1990,** *23* (4), 120-126.

205. Espeau, P.; Négrier, P.; Corvis, Y., A Crystallographic and Pressure-Temperature State Diagram Approach for the Phase Behavior and Polymorphism Study of Glutaric Acid. *Cryst Growth Des* **2013**.

206. Erdelyi, M., Halogen bonding in solution. *Chemical Society Reviews* **2012,** *41* (9), 3547-3557.

207. Duarte, D. J. R.; Angelina, E. L.; Peruchena, N. M., On the strength of the halogen bonds: Mutual penetration, atomic quadrupole moment and Laplacian distribution of the charge density analyses. *Computational and Theoretical Chemistry* **2012,** *998* (0), 164-172.

208. Dolomanov, O. V.; Bourhis, L. J.; Gildea, R. J.; Howard, J. A. K.; Puschmann, H., OLEX2: a complete structure solution, refinement and analysis program. *J Appl Crystallogr* **2009,** *42*, 339-341.

209. Dhende, V. P.; Samanta, S.; Jones, D. M.; Hardin, I. R.; Locklin, J., One-Step Photochemical Synthesis of Permanent, Nonleaching, Ultrathin Antimicrobial Coatings for Textiles and Plastics. *ACS Applied Materials & Interfaces* **2011,** *3* (8), 2830-2837.

210. Dewal, M. B.; Xu, Y. W.; Yang, J.; Mohammed, F.; Smith, M. D.; Shimizu, L. S., Manipulating the cavity of a porous material changes the photoreactivity of included guests. *Chem Commun* **2008,** (33), 3909-3911.

211. Dewal, M. B.; Lufaso, M. W.; Hughes, A. D.; Samuel, S. A.; Pellechia, P.; Shimizu, L. S., Absorption properties of a porous organic crystalline apohost formed by a self-assembled bis-urea macrocycle. *Chemistry of Materials* **2006,** *18* (20), 4855-4864.

212. Desiraju, G. R., *Crystal Engineering: The Design of Organic Solids*. Elsevier: New York, 1989.

213. Della Pina, C.; Falletta, E.; Rossi, M., Update on selective oxidation using gold. *Chemical Society Reviews* **2012,** *41* (1), 350-369.

214. Dawn, S.; Dewal, M. B.; Sobransingh, D.; Paderes, M. C.; Wibowo, A. C.; Smith, M. D.; Krause, J. A.; Pellechia, P. J.; Shimize, L. S., Self-Assembled Phenylethynylene Bis-urea Macrocycles Facilitate the Selective Photodimerization of Coumarin. *J. Am. Chem. Soc.* **2011,** *133* (18), 7025-7032.

215. Davis, R.; Berger, R.; Zentel, R., Two-dimensional aggregation of organogelators induced by biaxial hydrogen-bonding gives supramolecular nanosheets. *Adv Mater* **2007,** *19* (22), 3878-+.

216. Davey, R. J., Pizzas, polymorphs and pills. *Chem Commun* **2003,** (13), 1463-1467.

217. Custelcean, R.; Remy, P., Selective Crystallization of Urea-Functionalized Capsules with Tunable Anion-Binding Cavities. *Cryst Growth Des* **2009,** *9* (4), 1985-1989.

218. Cuquerella, M. C.; Lhiaubet-Vallet, V.; Cadet, J.; Miranda, M. A., Benzophenone Photosensitized DNA Damage. *Accounts of Chemical Research* **2012,** *45* (9), 1558-1570.

219. Cuquerella, M. C.; Lhiaubet-Vallet, V.; Cadet, J.; Miranda, M. A., Benzophenone Photosensitized DNA Damage. *Accounts of Chemical Research* **2012**.

220. Colombeau, L.; Traoré, T. n.; Compain, P.; Martin, O. R., Metal-Free One-Pot Oxidative Amidation of Aldoses with Functionalized Amines. *The Journal of Organic Chemistry* **2008,** *73* (21), 8647-8650.

221. Clennan, E. L.; Pace, A., Advances in singlet oxygen chemistry. *Tetrahedron* **2005,** *61* (28), 6665-6691.

222. Clennan, E. L., Mechanisms of oxygenations in zeolites. In *Advances in Physical Organic Chemistry*, Richard, J. P., Ed. 2008; Vol. 42, pp 225-269.

223. Chow, T. W. S.; Chen, G. Q.; Liu, Y. G.; Zhou, C. Y.; Che, C. M., Practical iron-catalyzed atom/group transfer and insertion reactions. *Pure Appl Chem* **2012,** *84* (8), 1685-1704.

224. Chong, Y. S.; Carroll, W. R.; Burns, W. G.; Smith, M. D.; Shimizu, K. D., A High-Barrier Molecular Balance for Studying Face-to-Face Arene-Arene Interactions in the Solid State and in Solution. *Chemistry-a European Journal* **2009,** *15* (36), 9117-9126.

225. Cho, C. M.; Wang, X.; Li, J. J.; He, C.; Xu, J., Synthesis and self-assembly of halogen-bond donor–spacer–hydrogen-bond donor molecules: polymeric liquid crystals induced by combination of intermolecular halogen- and hydrogen-bonding interactions. *Liquid Crystals* **2012**, 1-12.

226. Chin, K. K.; Natarajan, A.; Gard, M. N.; Campos, L. M.; Shepherd, H.; Johansson, E.; Garcia-Garibay, M. A., Pump-probe spectroscopy and circular dichroism

of nanocrystalline benzophenone - towards absolute kinetic measurements in solid state photochemical reactions. *Chem Commun* **2007,** (41), 4266-4268.

227. Cheney, M. L.; Shan, N.; Healey, E. R.; Hanna, M.; Wojtas, L.; Zaworotko, M. J.; Sava, V.; Song, S. J.; Sanchez-Ramos, J. R., Effects of Crystal Form on Solubility and Pharmacokinetics: A Crystal Engineering Case Study of Lamotrigine. *Cryst Growth Des* **2010,** *10* (1), 394-405.

228. Chen, Y.-Z.; Wu, L.-Z.; Zhang, L.-P.; Tung, C.-H., Confined Space-Controlled Hydroperoxidation of Trisubstituted Alkenes Adsorbed on Pentasil Zeolites. *The Journal of Organic Chemistry* **2005,** *70* (12), 4676-4681.

229. Cataldo, S.; Pignataro, B., Polymeric Thin Films for Organic Electronics: Properties and Adaptive Structures. *Materials* **2013,** *6* (3), 1159-1190.

230. Castellano, R. K.; Nuckolls, C.; Eichhorn, S. H.; Wood, M. R.; Lovinger, A. J.; Rebek, J., Hierarchy of order in liquid crystalline polycaps. *Angew Chem Int Edit* **1999,** *38* (17), 2603-2606.

231. Campbell, A. N.; Stahl, S. S., Overcoming the "Oxidant Problem": Strategies to Use O-2 as the Oxidant in Organometallic C-H Oxidation Reactions Catalyzed by Pd (and Cu). *Accounts of Chemical Research* **2012,** *45* (6), 851-863.

232. Burns, D. H.; Calderon-Kawasaki, K.; Kularatne, S., Buried Solvent Determines Both Anion-Binding Selectivity and Binding Stoichiometry with Hydrogen-Bonding Receptors. *The Journal of Organic Chemistry* **2005,** *70* (7), 2803-2807.

233. Burdeniuc, J.; Sanford, M.; Crabtree, R. H., Amine charge transfer complexes of perfluoroalkanes and an application to poly(tetrafluoroethylene) surface functionalization. *Journal of Fluorine Chemistry* **1998,** *91* (1), 49-54.

234. Bryant, J. R.; Matsuo, T.; Mayer, J. M., Cumene Oxidation by cis-[RuIV(bpy)2(py)(O)]2+, Revisited. *Inorg Chem* **2004,** *43* (4), 1587-1592.

235. Bryant, J. R.; Matsuo, T.; Mayer, J. M., Cumene Oxidation by cis-[RuIV(bpy)2(py)(O)]2+, Revisited. *Inorg Chem* **2004,** *43* (4), 1587-1592.

236. Bruce, D. W.; Metrangolo, P.; Meyer, F.; Pilati, T.; Praesang, C.; Resnati, G.; Terraneo, G.; Wainwright, S. G.; Whitwood, A. C., Structure-Function Relationships in Liquid-Crystalline Halogen-Bonded Complexes. *Chem.--Eur. J.* **2010,** *16* (Copyright (C) 2012 American Chemical Society (ACS). All Rights Reserved.), 9511-9524, S9511/1-S9511/19.

237. Bregeault, J. M., Transition-metal complexes for liquid-phase catalytic oxidation: some aspects of industrial reactions and of emerging technologies. *Dalton Transactions* **2003,** (17), 3289-3302.

238. Brammer, L.; Minguez Espallargas, G.; Libri, S., Combining metals with halogen bonds. *Crystengcomm* **2008,** *10* (12), 1712-1727.

239. Blanchard, H. S., A Study of the Mechanism of Cumene Autoxidation. Mechanism of the Interaction of t-Peroxy Radicals1. *J. Am. Chem. Soc.* **1959,** *81* (17), 4548-4552.

240. Blagden, N.; de Matas, M.; Gavan, P. T.; York, P., Crystal engineering of active pharmaceutical ingredients to improve solubility and dissolution rates. *Adv Drug Deliver Rev* **2007,** *59* (7), 617-630.

241. Bhosale, S. V.; Jani, C. H.; Langford, S. J., *Chem. Soc. Rev.* **2008,** *37*, 331-342.

242. Bertani, R.; Sgarbossa, P.; Venzo, A.; Lelj, F.; Amati, M.; Resnati, G.; Pilati, T.; Metrangolo, P.; Terraneo, G., Halogen bonding in metal–organic–supramolecular networks. *Coordination Chemistry Reviews* **2010,** *254* (5–6), 677-695.

243. Bartusik, D.; Aebisher, D.; Lyons, A. M.; Greer, A., Bacterial Inactivation by a Singlet Oxygen Bubbler: Identifying Factors Controlling the Toxicity of 1O2 Bubbles. *Environ Sci Technol* **2012,** *46* (21), 12098-12104.

244. Barash, L.; Wasserman, E.; Yager, W. A., Generation of methylenes from germinal diazides via excited nitrenes. *J. Am. Chem. Soc.* **1967,** *89* (15), 3931-3932.

245. Auffinger, P.; Hays, F. A.; Westhof, E.; Ho, P. S., Halogen bonds in biological molecules. *P Natl Acad Sci USA* **2004,** *101* (48), 16789-16794.

246. Arunkumar, E.; Fu, N.; Smith, B. D., Squaraine-Derived Rotaxanes: Highly Stable, Fluorescent Near-IR Dyes. *Chemistry – A European Journal* **2006,** *12* (17), 4684-4690.

247. Arumugam, S., Alkali metal cation exchanged Nafion as an efficient micro-environment for oxidation of olefins by singlet oxygen. *Journal of Photochemistry and Photobiology A: Chemistry* **2008,** *199* (2–3), 242-249.

248. Araki, Y.; Dobrowolski, D. C.; Goyne, T. E.; Hanson, D. C.; Jiang, Z. Q.; Lee, K. J.; Foote, C. S., Chemistry of singlet oxygen. 47. 9,10-Dicyanoanthracene-sensitized photooxygenation of alkyl-substituted olefins. *J. Am. Chem. Soc.* **1984,** *106* (16), 4570-4575.

249. Aragoni, M. C.; Arca, M.; Devillanova, F. A.; Isaia, F.; Lippolis, V., Adducts of S/Se Donors with Dihalogens as a Source of Information for Categorizing the Halogen Bonding. *Cryst Growth Des* **2012,** *12* (6), 2769-2779.

250. Allen, F. H.; Lommerse, J. P. M.; Hoy, V. J.; Howard, J. A. K.; Desiraju, G. R., The hydrogen-bond C-H donor and [pi]-acceptor characteristics of three-membered rings. *Acta Crystallographica Section B* **1996,** *52* (4), 734-745.

251. Alberti, M. N.; Vougioukalakis, G. C.; Orfanopoulos, M., Photosensitized Oxidations of Substituted Pyrroles: Unanticipated Radical-Derived Oxygenated Products. *Journal of Organic Chemistry* **2009,** *74* (19), 7274-7282.

252. Alberti, M. N.; Orfanopoulos, M., Unraveling the Mechanism of the Singlet Oxygen Ene Reaction: Recent Computational and Experimental Approaches. *Chemistry-a European Journal* **2010,** *16* (31), 9414-9421.

253. Alberti, M. N.; Orfanopoulos, M., The Cyclopropyl Group as a Hypersensitive Probe in the Singlet Oxygen Ene Reaction Mechanism. *Organic Letters* **2008,** *10* (12), 2465-2468.

254. Akiyama, K.; Sekiguchi, S.; Tero-Kubota, S., Origin of an Absorptive Electron Spin Polarization Observed in Photochemical Hydrogen Abstraction Reaction by Benzophenone Derivatives. CW and Pulsed EPR Studies. *The Journal of Physical Chemistry* **1996,** *100* (1), 180-183.

255. Adam, W.; Prein, M., π-Facial Diastereoselectivity in the [4+2] Cycloaddition of Singlet Oxygen as a Mechanistic Probe. *Accounts of Chemical Research* **1996,** *29* (6), 275-283.

256. Adam, W.; Prein, M., π-Facial Diastereoselectivity in the [4+2] Cycloaddition of Singlet Oxygen as a Mechanistic Probe. *Accounts of Chemical Research* **1996,** *29* (6), 275-283.

257. *SADABS*, 2.10; Bruker Analytical X-ray Systems: Madison, Wisconsin, USA, 2003.

258. *SAINT*+, 6.45; Bruker Analytical X-ray Systems Inc.: Madison, Wisconsin, USA, 2003.

259. *SMART* 5.630; Bruker Analytical X-ray Systems Inc.: Madison Wisconsin USA, 2003.